Cloning, expression, purification and characterization of tryptophan hydroxylase variants

Boesen, Jane; Christensen, Hans Erik Mølager

Publication date:
2010

Document Version
Publisher's PDF, also known as Version of record

Cloning, expression, purification and characterization of tryptophan hydroxylase variants

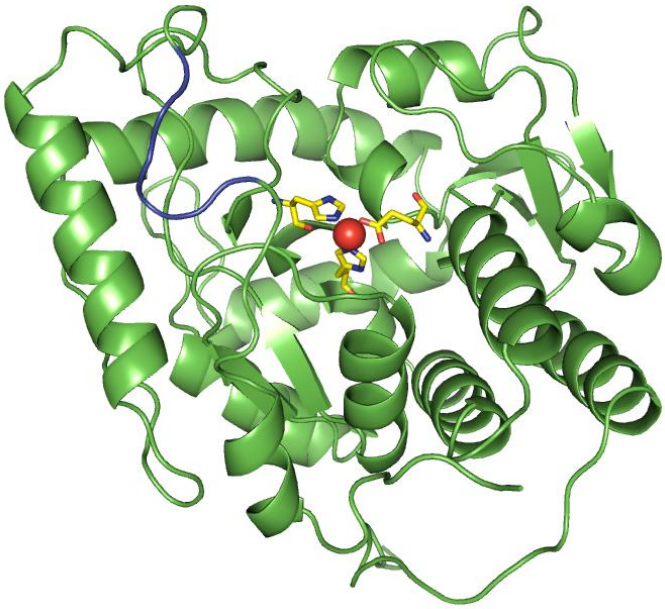

Jane Boesen

Metalloprotein Chemistry and Engineering Group
Department of Chemistry
Technical University of Denmark
June 2010

Cloning, expression, purification and characterization of tryptophan hydroxylase variants

Ph.D. project by

Jane Boesen

Supervisor:

Hans Erik Mølager Christensen

Metalloprotein Chemistry and Engineering Group

Department of Chemistry

Technical University of Denmark

2010

Front cover figure: Structure of the catalytic domain of human tryptophan hydroxylase isoform 1

Preface and acknowledgement

This Ph.D. project, entitled “Cloning, expression, purification and characterization of tryptophan hydroxylase variants”, was performed in the Metalloprotein Chemistry and Engineering Group, Department of Chemistry, Technical University of Denmark (DTU). The Ph.D. scholarship was founded by DTU. The project was supervised by Associate Professor Hans E. M. Christensen.

First of all I would like to thank my supervisor Associate Professor Hans E. M. Christensen for his help and guidance during this project. Also thanks to the Technical University of Denmark who provided me with financial means to complete this project. I would also like to thanks members of the research group here at DTU who helped me in my work: Ph.D. student Lærke T. Haahr, Ph.D. student Trine V. Vendelboe, Laboratory Technicians Lise-Lotte Jespersen, Martin H. Pedersen and Stefanie Boy, Ph.D. student Maja Martic and other members of the group for providing a pleasant atmosphere. Also thanks to Ph.D. Michael S. Windahl for his previous work on tryptophan hydroxylase.

I would also like to thank Professor Carol V. Robinson, for letting me do the mass spectrometric characterization in her mass spectrometry group, Department of Chemistry, University of Cambridge, UK. I would especially like to thank Dr. Elisabetta Boeri Erba for her great advice and enthusiasm in this project. I would also like to thanks Dr. Min Zou and the other members of the group. Financial support for my stay in UK was provided by Otto Mønsteds Foundation (13.000 kr) and the Danish Chemical Society (5000 kr). I would like to thank both of these foundations for supporting my work.

Finally, I would like to thank Associate Professor Ole Kristensen, Department of Medicinal Chemistry, Faculty of Pharmaceutical Sciences, University of Copenhagen for helping me with the crystallization part (data collection, structure solution and refinement) and Associate Professor Lars Hellgreen, Department of Systems Biology, Technical University of Denmark for letting me use their ultracentrifuge.

_____

Jane Boesen

Kgs. Lyngby, June 2010

Abstract

Tryptophan hydroxylase (TPH) catalyzes the first and rate-limiting step in the biosynthesis of the neurotransmitter and hormone serotonin (5-hydroxytryptamine). Serotonin is involved in many physiological functions, such as appetite and sleep rhythm, as well as a wide range of psychiatric disorders such as depression and obsessive-compulsive disorder (OCD). Characterization of TPH and elucidation of the enzymes regulation and catalytic mechanism is therefore vital to our understanding of the serotonin balance.

This study concerns variants of both human TPH isoform 1 (*h*TPH1) and human TPH isoform 2 (*h*TPH2). The main goal was to purify full-length *h*TPH1. Based on earlier results, *h*TPH1 was purified using detergent in the purification methods. After incubation of the *h*TPH1 sample with 0.1 % of n-dodecyl-β-D-maltopyranoside (DDM) the protein binds to the anion exchange column and elutes over a large area in the anion exchange, indicating that the protein still exists in different oligomer forms. This was also observed in the gel filtration. Variants of both *h*TPH1 and *h*TPH2 containing the regulatory domain or parts of it were constructed and tested for expression in *Escherichia coli* as well as solubility. It was observed that changes in the amino acid sequence of the regulatory domain by point mutations or truncations in the N-terminal had a huge impact on the solubility of the protein and caused the protein to be insoluble.

The regulatory domain of human TPH1 (r*h*TPH1), and two fusion proteins of r*h*TPH1 fused to the green fluorescent protein (GFP) in the C-terminal and the glutathione S-transferase (GST) in the N-terminal, respectively, were expressed in a soluble form. The purification trials of the variants containing the regulatory domain showed that a high salt concentration was necessary to stabilize the variant. The GST-r*h*TPH1 variant could be purified using affinity chromatography followed by gel filtration with high purity and a yield of 40 mg/l culture. The purified GST-r*h*TPH1 exists as a dimer in solution due to dimerization of GST. The GST could be cleaved successfully from the fusion protein using Factor Xa and r*h*TPH1 was successfully purified from GST after cleavage.

Characterization was performed on the three *h*TPH variants: The catalytic domain of both *h*TPH1 (c*h*TPH1) and *h*TPH2 (c*h*TPH2) as well as the catalytic and tetramerization domain of *h*TPH2 (ct*h*TPH2). The kinetic parameters of c*h*TPH1 was determined and compared with parameters of

c*h*TPH2. Large differences were observed between the two isoforms and tryptophan inhibition was observed for c*h*TPH1 but not for c*h*TPH2.

Mass spectrometric analysis of c*h*TPH1 shows that the sample contains two species: c*h*TPH1 and another species, which could not be seen during purification or electrophoresis of the c*h*TPH1 sample. Additionally, c*h*TPH1 shows to be fully loaded with iron, whereas c*h*TPH2 showed to be heterogeneous with respect to Fe. c*h*TPH2 binds both tryptophan and tetrahydrobiopterin individually. Also characterization of ct*h*TPH2 by tandem mass spectrometry shows that the variant is a tetramer.

Crystallization of c*h*TPH1 was achieved both without substrate and with bound substrate (tryptophan and pterin) but resulted in very small crystals. A data set of the variant without bound substrate was collected to 4 Å and the structure was solved by molecular replacement. The structure was refined to an R_{free} of 33.5 % and the overall structure is compared to the overall structure of the catalytic domain of *h*TPH1 co-crystallized with BH_2. A structural change in the residues 125 to 130 is observed. This is the first structure of c*h*TPH1 without any substrates or inhibitors.

Dansk resumé

Tryptophanhydroxylase (TPH) katalyserer det første og hastighedsbestemmende trin i biosyntesen af serotonin (5-hydroxytryptamin). Serotonin er involveret i mange fysiologiske funktioner, såsom appetit og søvnrytme, samt en lang række af psykiske sygdomme, som depression og obsessiv-kompulsiv lidelse (OCD). Karakterisering af TPH og bestemmelse af enzymets regulering og katalytiske mekanisme er derfor vigtig for forståelsen af serotonin.

I dette projekt er varianter af human TPH isoform 1 (*h*TPH1) and human TPH isoform 2 (*h*TPH2) blevet studeret. Det overordnede mål var at oprense fuldlængde *h*TPH1. På baggrund af tidligere resultater blev *h*TPH1 oprenset med anvendelse af detergent i oprensningsmetoden. Efter inkubering af *h*TPH1 prøven med 0.1 % of n-dodecyl-β-D-maltopyranosid (DDM) kan proteinet binde til anionbytterkolonnen. Den del af *h*TPH1 som binder til kolonnen eluerer over et stort område i anionbytningen, hvilket understreger at protein stadig findes på forskellige oligomere former. Dette ses også i gelfiltreringen. Varianter af både *h*TPH1 og *h*TPH2 indeholdende det regulatoriske domæne eller dele af dette blev fremstillet og testet for udtrykkelse i *Escherichia coli* samt opløselighed. Fra disse resultater blev det observeret at en ændring af aminosyre-sekvensen i det regulatoriske domæne, enten i form af punktmutation eller ved trunkering i den N-terminale ende, gør at proteinet er uopløseligt.

Det regulatoriske domæne af human TPH1 (r*h*TPH1) samt to fusionsproteiner af r*h*TPH1 fusioneret til henholdsvis det grønt-fluorescerende-protein (GFP) i den C-terminale ende og glutathione S-transferase (GST) i den N-terminale ende blev udtrykt i opløselig form. Fra oprensningsforsøg blev det observeret at en høj salt-koncentration er nødvendig for stabilisering af proteinet. GST-r*h*TPH1 varianten blev oprenset ved anvendelse af affinitetskromatografi efterfulgt af gelfiltrering til høj renhed og et udbytte på 40 mg/l kultur. Den oprensede GST-r*h*TPH1 variant eksisterer som en dimer i opløsning på grund af dimerisering af GST. GST blev succesfuldt kløvet fra fusionsproteinet med Faktor Xa og r*h*TPH1 adskilt fra GST efter kløvning.

Dette studie omhandler også karakterisering af tre *h*TPH varianter; Det katalytiske domæne af både *h*TPH1 (c*h*TPH1) og *h*TPH2 (c*h*TPH2) samt det katalytiske og tetrameriseringsdomænet af *h*TPH2 (ct*h*TPH2). De kinetiske parametre for c*h*TPH1 blev bestemt og sammenlignet med værdier for c*h*TPH2. Der ses en stor forskel mellem de to isoformer og substratinhibering af tryptophan observeres for c*h*TPH1, men ikke for c*h*TPH2.

Massespektrometrisk analyse af c*h*TPH1 viste at prøven indeholder to proteiner: c*h*TPH1 samt et andet protein, som ikke kunne observeres i hverken oprensningen af proteinet eller ved elektroforese. Yderligere ses c*h*TPH1 at være mættet med Fe, mens c*h*TPH2 er heterogen med hensyn til Fe. c*h*TPH2 binder tryptophan og tetrahydrobiopterin. Tandem-massespektrometrisk karakterisering af ct*h*TPH2 viser at varianten er en tetramer.

Krystallisationsforsøg af c*h*TPH1 blev udført til bestemmelse af krystallisationsbetingelser for c*h*TPH1 med og uden ligander. Krystallionsbetingelserne blev fundet, men resulterede i meget små krystaller. Der blev opsamlet et datasæt til 4 Å af c*h*TPH1 uden ligander og strukturen blev løst. Strukturen blev forfinet og sammenlignet med strukturen af det katalytiske domæne af *h*TPH1 krystalliseret med BH_2. En strukturændring ses fra aminosyrerest 125 til 130. Dette er den første struktur af c*h*TPH1 uden tilstedeværelsen af substrater eller inhibitorer.

List of abbreviations

AAAH	Aromatic amino acid hydroxylase
ACN	Acetonitrile
Amp	Ampicillin
BH_4	(6R)-5,6,7,8-tetrahydro-L-biopterin
BH_2	(6R)-7,8-dihydro-L-bioterin
Cam	Chloramphenicol
CID	Collision-induced-dissociation
CIP	Calf intestinal phosphatase
CMC	Critical micelle concentration
exCMC	Experimental critical micelle concentration
CRM	Charged residue model
CV	Column volume
DC	Direct current
DDM	n-dodecyl-β-D-maltopyranoside
DP	Declustering potential
DoF	Degrees of freedom
DOPA	3,4-dihydroxyphenylalanine
E. coli	*Escherichia coli*
EDTA	Ethylenediamine tetraacetate
ESI	Electrospray ionization
FP	Focusing potential
GST	Glutathione S-transferase
GFP	Green fluorescent protein
frGFP	Green fluorescent protein folding reporter
HEPES	4-(2-hydroxyethyl)-piperazine-1-ethanesulfonic acid
IEM	Ion evaporation model
IPTG	Isopropyl-β-D-thiogalactopyranoside
Kan	Kanamycin sulfate
LAF	Laminar air flow
LB	Luria Bertani
n/a	Non applicable

MALDI	Matrix-assisted laser desorption ionization
MBP	Maltose-binding protein
MCP	Microchannel plate
m/z	Mass-to-charge
MS	Mass spectrometry
nanoESI	Nanoelectrospray ionization
NIH	National Institutes of Health
OCD	Obsessive compulsive disorder
OD_{600}	Optical density at 600 nm
PAH	Phenylalanine hydroxylase
*h*PAH	Human phenylalanine hydroxylase
PCR	Polymerase chain reaction
PEG	Polyethylene glycol
PTM	Photomultiplicator tube
RF	Radio frequency
SDS-Page	Sodium dodecyl sulfate polyamide gel electrophoresis
SS	Sum of squares
TPH	Tryptophan hydroxylase
TPH1	Tryptophan hydroxylase isoform 1
TPH2	Tryptophan hydroxylase isoform 2
*h*TPH1	Human tryptophan hydroxylase isoform 1
*h*TPH2	Human tryptophan hydroxylase isoform 2
*gg*TPH	Gallus gallus (chicken) TPH
cTPH	Catalytic domain of TPH
rTPH	Regulatory domain of TPH
tTPH	Tetramerization domain of TPH
TH	Tyrosine hydroxylase
*h*TH4	Human tyrosine hydroxylase isoform 4
TIR	Translation initiation region
TOF	Time-of-flight
Tris	Tris(hydroxymethyl)-aminomethane

Contents

1 Introduction

Tryptophan hydroxylase (TPH) is an iron containing enzyme that catalyzes the hydroxylation of tryptophan to 5-hydroxytryptophan. This is the first and rate-limiting step in the biosynthesis of serotonin [1], and the initial step in the biosynthesis of the hormone melatonin [2], as shown in figure 1.1.

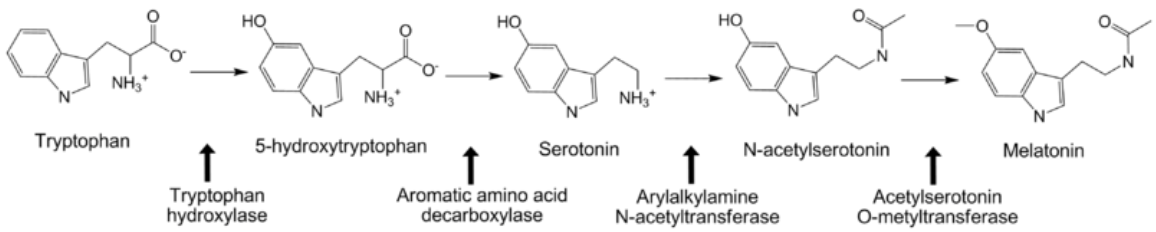

Figure 1.1. The biosynthesis of 5-hydroxytryptophan, serotonin and melatonin. Tryptophan hydroxylase catalyzes the rate-limiting step in the biosynthesis of serotonin.

Serotonin is involved in a many physiological functions such as appetite and regulation of body temperature [3] as well as a wide range of psychiatric disorders such as depression and obsessive-compulsive disorders (OCD) [1]. These psychiatric disorders have a massive impact on the patients suffering from them and they account for large direct and indirect social expenses of which in Denmark alone corresponds to approximately 30 billion Danish kroner a year [4]. Therefore, knowledge of serotonin and its implication has lead to a huge interest in TPH and the enzyme has been studied for several years. Despite the great interest, the knowledge on TPH is limited and many issues such as the three-dimensional structure of the full-length TPH and determination of the exact catalytic mechanism remains to be determined.

There are two isoforms of human TPH: Human TPH isoform 1 (*h*TPH1), which is expressed mainly in the peripheral part of the body and human TPH isoform 2 (*h*TPH2), which is expressed in the central nervous system. Both isoforms consist of three domains: A regulatory domain (r), a catalytic domain (c) and a tetramerization domain (t) [1,2]. The Metalloprotein Chemistry and Engineering Group has worked with TPH for several years and the initial work was done with a truncated version of *Gallus gallus* (chicken) TPH1 (*gg*TPH1) [5]. Methods for expression and purification were developed [6,7,8,9,10,11,12] and lead to a structural determination of c*gg*TPH1 [13]. Different strains for expression of truncated variants of *h*TPH have also been constructed in the group and purification methods for purifying these have been developed [6,7,9]. During my master project I worked on construction, expression and purification of both the full-length and the catalytic domain of *h*TPH1 (c*h*TPH1) [14]. Methods for expression and purification of c*h*TPH1 were successfully developed and therefore, it was chosen to continue with characterization of this variant. The purification of the full-length *h*TPH1 was unsuccessful and because neither the full-length nor a variant containing the regulatory domain of TPH had been characterized thoroughly it was also decided to work on this.

The initial goal was to purify full-length *h*TPH1 but due to difficulties with purification observed both in this project and in my master project; variants of *h*TPH containing the regulatory domain or parts of it were constructed. This was done to elucidate the properties of the different domains of *h*TPH, especially the regulatory domain, in order to understand the behavior of full-length *h*TPH. Characterization of truncated variants of *h*TPH was also done.

1.1 Outline of the thesis

In chapter 2 an introduction to TPH is given as well as the important functions and the related disorders of serotonin. Chapter 3 presents the project background and describes the experimental strategies that my Ph.D. project is based on. Chapter 4 presents the results from the purification of full-length *h*TPH1. Chapter 5 describes the strategies for construction of various *h*TPH expression strains with the expression and solubility results of these variants given in chapter 6. Chapter 7 presents the results from the purification of r*h*TPH1 variants. In chapter 8 the assay used for determination of the c*h*TPH1 kinetic parameters is described as well as the results obtained and discussion of these. Chapter 9 presents theory of mass spectrometry of non-covalent protein complexes. Because this is a new technique used in the group a detailed description of the theory is given. Also, mass spectrometric characterization of three *h*TPH variants is presented and discussed. Chapter 10 gives a short introduction to crystallization of proteins and crystallization of c*h*TPH1. Chapter 11 is the final chapter and serves to summarize the work done in this project.

2 Tryptophan hydroxylase

In this chapter an introduction to tryptophan hydroxylase (TPH, EC 1.14.16.4) is given and the most important properties of and knowledge on TPH are summarized. Also, serotonin is introduced together with the disorders related to its function and the important role of TPH in these disorders. Information on the two other members of the aromatic amino acid hydroxylase (AAAH) family, phenylalanine hydroxylase (PAH) and tyrosine hydroxylase (TH), is also presented because they are closely related to TPH and are characterized to a much greater extent.

2.1 The aromatic amino acid hydroxylases

TPH, also known as tryptophan 5-monooxygenase, is a non-heme iron-containing enzyme which catalyzes the hydroxylation of tryptophan to 5-hydroxy-tryptophan in the presence of Fe(II), dioxygen and 5,6,7,8-tetrahydrobiopterin (BH_4) [15], as seen in figure 2.1. This is the first and rate-limiting step in the biosynthesis of serotonin [15].

Together with PAH and TH, TPH forms the family of AAAHs [16,17]. All three enzymes are non-heme iron monooxygenases which require BH_4 for hydroxylation of their respective aromatic amino acid and show substantial similarities in structure and catalytic mechanism [16]. The eukaryotic enzymes all forms homotetramers and each monomer of between 444 and 528 amino acid residues consists of three distinct domains; The N-terminal regulatory domain (100-190 residues), the catalytic domain (approximately 315 residues) and the C-terminal tetramerization domain (approximately 25-40 residues) [15,18,19,20].

PAH is found in the liver [21] and catalyzes the hydroxylation of phenylalanine to tyrosine which is the rate-limiting step in the catabolism of phenylalanine [22]. Deficiency in PAH results in the disease phenylketonuria, where phenylalanine is converted to phenylpuryvate instead of

tyrosine. If this condition is not treated, which can be done through a low phenylalanine diet, it can lead to mental retardation [17,22]. TH is found in the central nervous system and adrenal gland [22,23] and catalyzes the hydroxylation of tyrosine to 3,4-dihydroxyphenylalanine (DOPA), which is the first step in the biosynthesis of the catecholamines dopamine, norepinephrine and epinephrine [17]. Mutation in the TH gene is related to the genetic disease L-DOPA responsive dystonia and juvenile Parkinson [24,25].

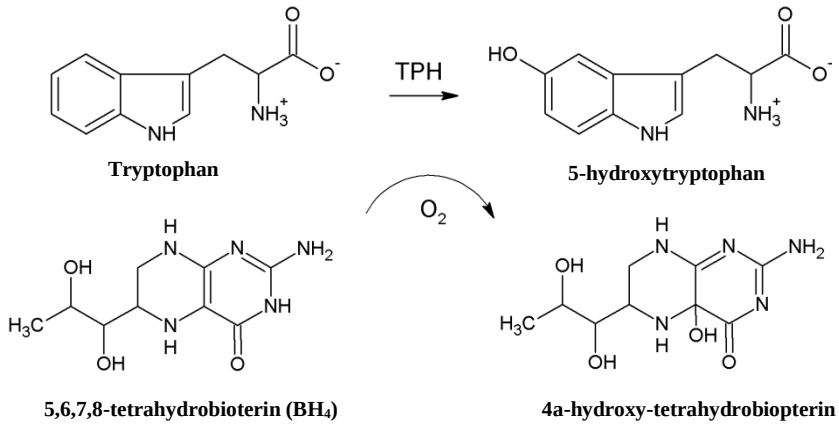

Figure 2.1. Hydroxylation of tryptophan to 5-hydroxytryptophan catalyzed by TPH in the presence of dioxygen and BH_4.

2.2 The two isoforms of tryptophan hydroxylase

Until recently the hydroxylation of tryptophan to 5-hydroxytryptophan was believed to be catalyzed by only one TPH enzyme, but the presence of another isoform was determined in 2003 when Walther *et al.* [26] identified a second gene encoding TPH. The two isoforms are named: TPH isoform 1 (TPH1) and TPH isoform 2 (TPH2).

TPH1 is mainly expressed in the pineal gland [27,28] and in peripheral parts of the body such as skin cells [29], cancer cells [27], intestinal mucosa and in enterochromaffin cells [30]. It controls the serotonin synthesis in the periphery [31]. TPH2 on the other hand is primarily expressed in serotonergic neurons of the brain and gut, and is responsible for synthesis of serotonin in the central nervous system [26,28,31,32].

The two human isoforms consist of 444 (*h*TPH1) and 490 (*h*TPH2) amino acids, respectively (see figure 2.3) and have a sequence identity of 71 %, see table 2.2. The most pronounced difference between the isoforms is seen in the regulatory domains which are 46 residues longer for *h*TPH2 (see figure 2.3) [33].

2.3 Structure of tryptophan hydroxylase

The structure of a full-length AAAH has not yet been determined. However, several structures of truncated variants of all three AAAHs have been determined by X-ray crystallography. TH and especially PAH are more structurally characterized than TPH and only structures of the catalytic

domain of TPH have been solved. Therefore, knowledge of TPH is mostly built on studies of the other two AAAHs. In this section the main features in the structures of the AAAHs are described.

2.3.1 Sequence alignment of the aromatic amino acid hydroxylases

The structure of the AAAHs consists of three domains, as mentioned in section 2.1. The domains of *h*TPH1 and *h*TPH2 are divided according to figure 2.2 and the nomenclature of the domains is given in table 2.1.

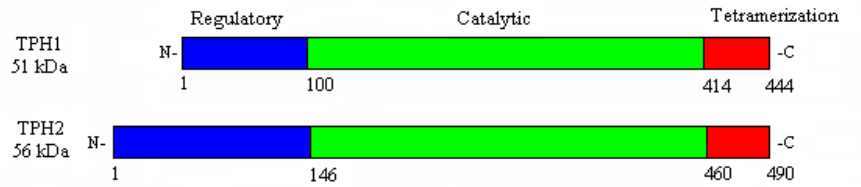

Figure 2.2. The division of the three domains of human TPH1 (*h*TPH1) and human TPH2 (*h*TPH2).

Table 2.1. Nomenclature of the three domains of TPH.

Abbreviation	Explanation
rTPH	The regulatory domain of TPH
cTPH	The catalytic domain of TPH
tTPH	The tetramerization domain of TPH

All three AAAHs have a high sequence identity of approximately 50 %, as seen from the alignment of *h*TPH1, *h*TPH2, human PAH (*h*PAH) and human TH isoform 4 (*h*TH4) shown in figure 2.3 and given in table 2.2. It is especially in the catalytic domain the sequence identity is high with 60-65 % between the AAAHs and 81 % between the two TPH isoform, whereas the regulatory domains are more different both in length and amino acid sequence.

Table 2.2. Sequence identity of human TPH1 (*h*TPH1), human TPH2 (*h*TPH2), human PAH (*h*PAH) and human TH isoform 4 (*h*TH4). The sequence identity was determined by the program Vektor NTI Advance 11 [34].

	***h*TPH2**	***h*PAH**	***h*TH4**
***h*TPH1**	71 %	56 %	49 %
***h*TPH2**		54 %	46 %
***h*PAH**			50 %

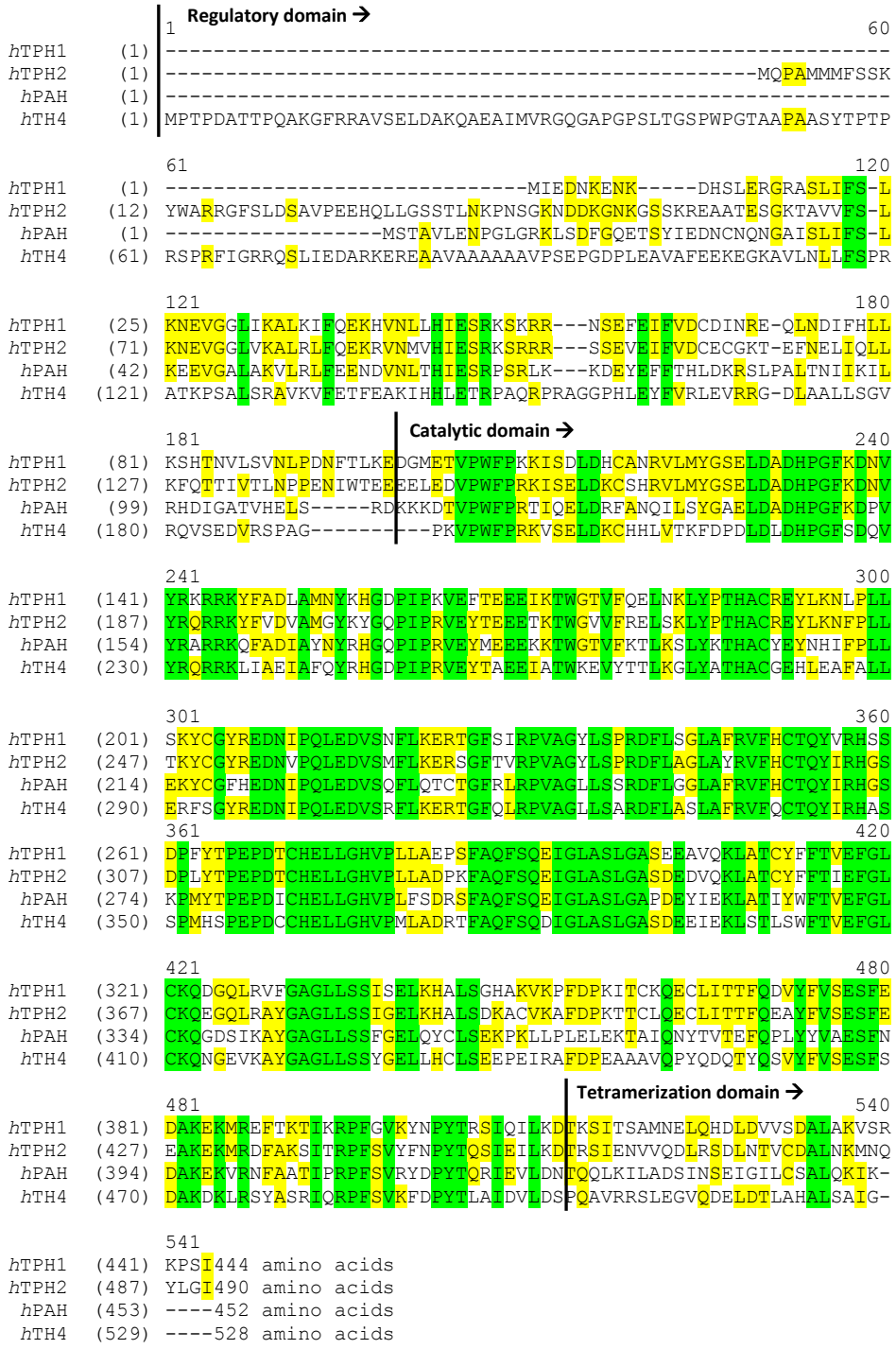

Figure 2.3. Amino acid sequence alignment of human TPH1 (*h*TPH1), human TPH2 (*h*TPH2), human PAH (*h*PAH) and human TH isoform 4 (*h*TH4). The sequences are obtained from the ExPaSy server [35] with the primary accession numbers P17752 (*h*TPH1), Q8IWU9 (*h*TPH2), P00439 (*h*PAH) and P07101 (*h*TH4). The alignment was done using Vektor NTI Advance 11 [34]. Green background indicates conserved residues in all sequences and yellow background indicates conserved residues in some of the sequences. The domain boundaries as used in this project are marked by black vertical lines.

2.3.2 Three-dimensional structures of the catalytic domain

Only structures of the catalytic domain of TPH1 (cTPH1) have been determined, and in 2002 the first crystal structure of c*h*TPH1 with Fe(III) and 7,8-dihydrobipterin (BH_2), a competitive inhibitor and analog to BH_4, was determined by Wang *et al.* to 1.7 Å resolution [36]. The overall structure, shown in figure 2.4A (PDB entry 1MLW), is very similar to the structure of the catalytic domain of PAH (PDB entry 1PAH) and TH (PDB entry 1TOH) [36]. The active site of c*h*TPH1, shown in figure 2.4B, consists of a 9 Å deep and 10 Å wide cavity where iron is located and octahedrally coordinated to His272, His277 and Glu317 (*h*TPH1 numbering) and three water molecules [36]. The coordination of iron by two histidines and one glutamate is also seen for PAH and TH [37,38], and is known as the facial triad [39,40]. The BH_2 bound in the active site is sandwiched between Tyr235 and Phe241 and forms hydrogen bonds to Glu273 and Leu236. Furthermore, BH_2 is hydrogen bonded through bridging water molecules to Glu273 and Glu317 [36].

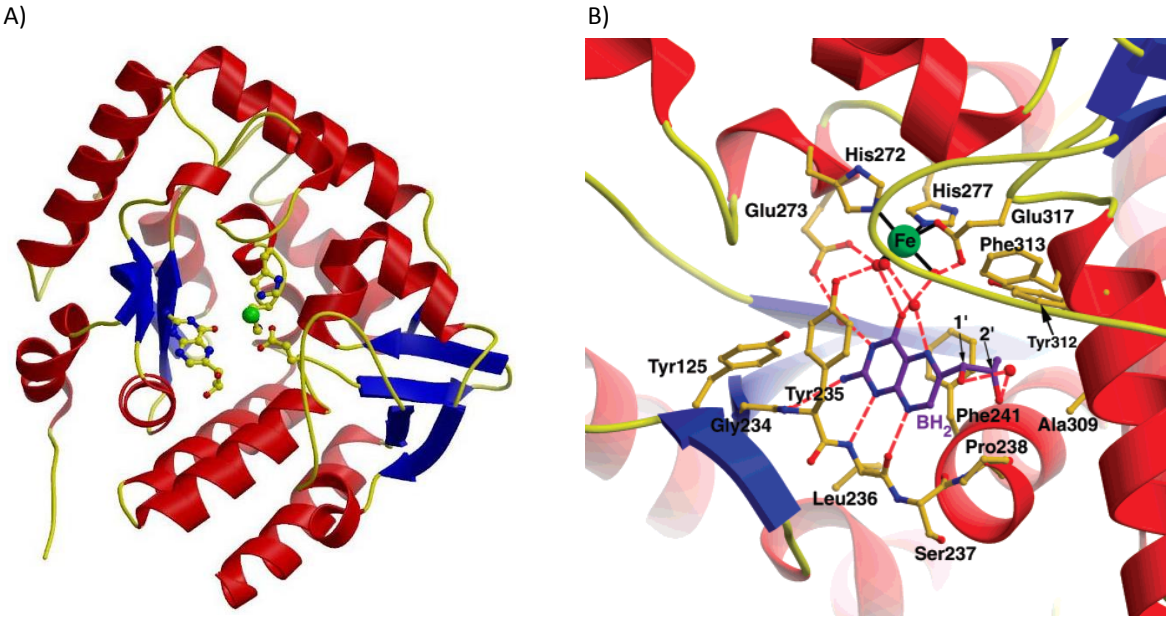

Figure 2.4. A) The overall structure of the catalytic domain of *h*TPH1 (PDB entry 1MLW) with bound ferric iron and 7,8-dihydrobiopterin (BH_2). B) The active site with the iron shown in green coordinated to His272, His277, Glu317 and three water molecules which are shown in red. The BH_2 cofactor is shown as a ball-and-stick model with carbon atoms in purple, oxygen atoms in red, and nitrogen atoms in blue. The interaction between BH_2 and c*h*TPH1 is indicated with dashed lines [36]. Reproduced with permission from the American Chemical Society.

The second structure of TPH is c*gg*TPH1 with bound Fe(III), tryptophan and imidazole, and was the first structure of any AAAH with its natural amino acid substrate. It was determined by Windahl *et al.* in 2007 to 1.9 Å resolution and published in 2008 [13]. The iron is described as being distorted trigonal bipyramidal with coordination to His273, His278, Glu318 (*gg*TPH1 numbering) and an imidazole, as shown in figure 2.5. No water molecules are coordinated to the iron and the coordination by glutamate to iron is partially bidentate [13]. The tryptophan substrate is bound close to the iron in a binding pocket with the hydrophobic part lined by residues Tyr236, Thr266, Pro267, Glu268, Pro269, His273, Phe314, Phe319 and Ile367. The polar interactions of the tryptophan are with Thr266, Ile367, and Ser337 and a salt bridge to Arg258.

Imidazole does not interact directly with c*gg*TPH1 but interacts through two bridging water molecules with Gly235, Leu237, His252 and Glu274 and is believed to mimic the BH_4 binding in the active site [13].

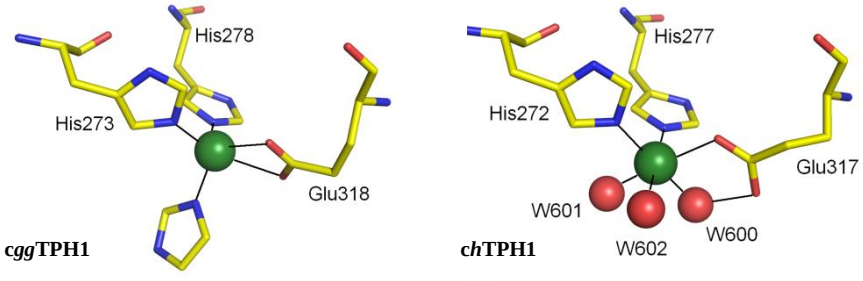

Figure 2.5. Coordination of Fe(III) (green sphere) by His273, His278, Glu318 and an imidazole in c*gg*TPH1 and coordination of Fe(III) (green sphere) by His272, His277, Glu317 and three water molecules in c*h*TPH1 [13]. Reproduced with permission from the American Chemical Society.

By comparing the two structures of cTPH1 (see figure 2.6), the structure of c*gg*TPH1 is more compact than the structure of c*h*TPH1, because the loops of residues Leu124-Asp139 and Ile367-Thr369 are closing around the active site in what appears to be a substrate triggered induced fit [13]. This large loop movement is also seen in the structure of the ternary PAH complex with a bound substrate analog [41,42]. The structure of c*gg*TPH1 resembles the structure of the ternary PAH complex [41,42] more than the c*h*TPH1 structure [36] with only BH_2 bound. This suggests either that the substrate alone rather that the substrate and the pterin together causes the large structural changes or that the imidazole mimics BH_4 and therefore, the structural change is caused by both binding of substrate and pterin (imidazole) [13].

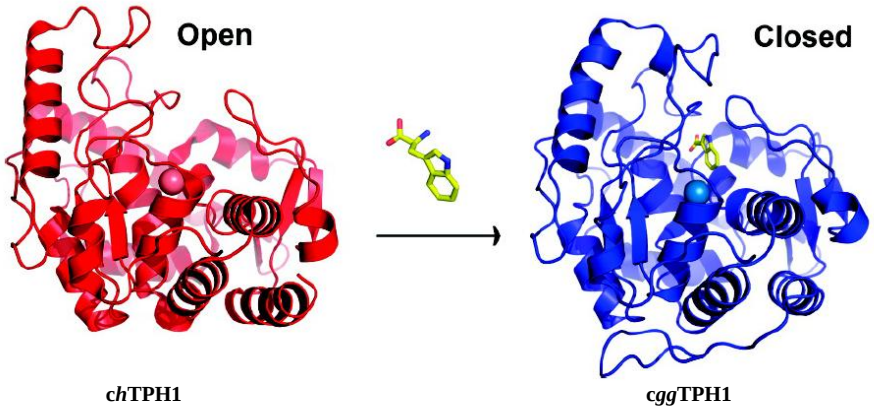

Figure 2.6. The substrate triggered induced fit, which gives rise to a more compact structure (c*gg*TPH1) compared to the structure without bound substrate (c*h*TPH1) [13]. Reproduced with permission from the American Chemical Society.

Additionally, three other structures of the catalytic domain of TPH1 crystallized with three different inhibitors have recently been determined. These were determined by Cianchetta *et al.* to resolution of 1.80, 1.85 and 1.9 Å, respectively [43]. All three inhibitors have a phenylalanine moiety which occupies the tryptophan binding site of the enzyme [43].

2.3.2.1 Coordination of iron

The two structures of *ch*TPH1 and c*gg*TPH1 [13,36] show different coordination of iron where a change in coordination from six to five upon incorporation of the substrate is observed. This is due to loss of two water ligands and a change in coordination geometry of glutamate from monodentate to bidentate, also shown in figure 2.5. Spectroscopic studies of rat PAH [44] and rat TH [45] reveal a similar change in iron (II) coordination from six to five.

2.3.3 The regulatory domain

The regulatory domain has the largest differences both in length and in amino acid sequence for the two isoforms of TPH and the AAAHs, as mentioned in section 2.3.1. No structure of the regulatory domain of TPH (rTPH) has been solved but the structure of the regulatory and catalytic domain of PAH was determined in 1998 [46], and is shown in figure 2.7. The first 18 residues are not visible in the structure. The structure contains an N-terminal sequence from residue 19 to 33, which extends across the catalytic domain blocking the entrance to the active site. Movement of this sequence is believed to be involved in the regulation of PAH by binding of phenylalanine [46].

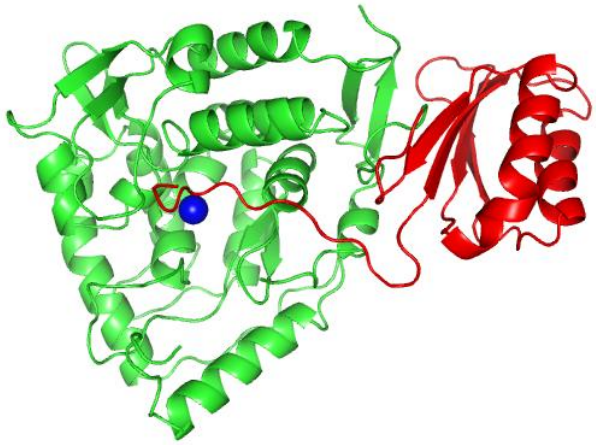

Figure 2.7. The crystal structure of the regulatory (shown in red) and catalytic (shown in green) domain of PAH (PDB entry 1PHZ). Iron is shown in blue. The figure was made using Pymol [47].

2.3.3.1 The regulatory domain of TPH

From the primary structure of rTPH it is seen that the domain contains a 3,4-hydrophobic repeat from amino acid 21 to 41 (see figure 2.8A). This sequence is believed to have an α-helix structure and this coiled-coil structure creates a hydrophobic face [48], as shown in figure 2.8B.

The regulation of TPH1 and TPH2 is not well understood. Both isoforms are believed to be regulated by phosphorylation and TPH1 has been reported to be phosphorylated *in vitro* by protein kinase A (PKA) at Ser58 [49] and by calmodulin-dependent kinase at Ser260 [50]. TPH2 on the other hand has been reported to be phosphorylated *in vitro* at Ser19 both by PKA [49,51,52] and by calmodulin-dependent protein kinase II [53]. PKA also phosphorylate Ser104 in TPH2 *in vitro*, which corresponds to the Ser58 in *h*TPH1 [52]. Phosphorylation in the regulatory domain is presumed to regulate enzyme activity [50] and phosphorylated TPH has been reported *in vitro* to

interact with 14-3-3 protein in the regulatory domain increasing the activity of the enzyme and preventing dephosphorylation [52,54,55]. Therefore, the differences in phosphorylation sites in the two isoforms and differences in their regulatory domains may allow for differentiated regulations, but this still remain to be proven [33].

A)

```
                    3,4-hydrophibic repeat
                      ┌  ┬  ┬  ┬  ┬  ┬  ┐
1                     *  *  *  *  *  *  *          50
MIEDNKENKDHSLERGRASLIFSLKNEVGGLIKALKIFQEKHVNLLHIES
51                                                99
RKSKRRNSEFEIFVDCDINREQLNDIFHLLKSHTNVLSVNLPDNFTLKE
```

B)

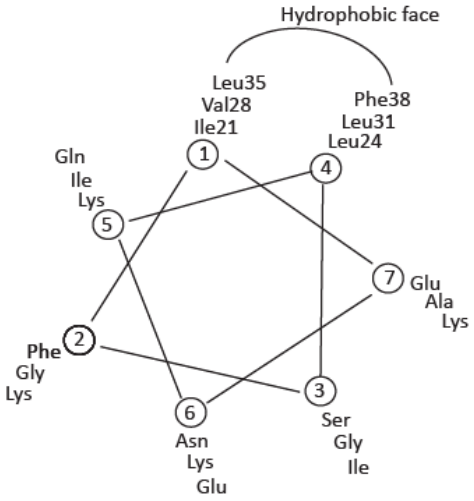

Figure 2.8. A) Amino acid sequence of the regulatory domain of TPH1 showing the hydrophobic amino acids from residue 21 to 41 in red as well as the 3,4-hydrophobic repeat. B) The coiled-coil structure of amino acid 21 to 41 showing how the 3,4-hydrophobic repeat creates a hydrophobic face in the structure.

2.3.4 The tetramerization domain

A structure of the tetramerization domain of TPH (tTPH) has not been solved but structures of the tetrameric form of both TH and PAH has been determined [38,56] and in figure 2.9 the structure of tetrameric TH containing both the catalytic and tetramerization domain is shown.

The tetramerization domains of four monomers of TH interact through hydrophobic interactions in a coiled-coil motif due to the presence of a 3,4-hydrophobic repeat in the domain [38]. This repeat is also present in the tetramerization domain of TPH (see figure 2.3) and from studies of ct*h*TPH2 it was determined to form a tetramer [57].

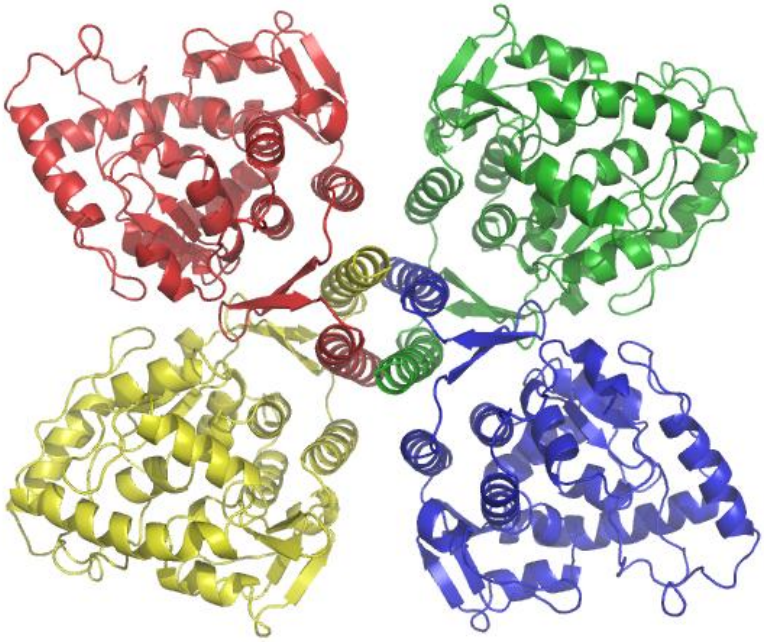

Figure 2.9. The crystal structure of the catalytic and tetramerization domains of tetrameric TH (PDB entry 1TOH) [38]. The coiled-coil motif is seen in the center of the structure. The figure was made using Pymol [47].

2.4 The enzymatic mechanism

Due to TPH's instability *in vitro*, studies on the catalytic mechanism are limited. Because of high sequence homology and structural similarity between the catalytic domains of the AAAHs it is believed that they share a common catalytic mechanism [15,58], thus results obtained from TH and PAH as well as TPH are described in this section.

The active form of iron in AAAHs is ferrous iron, Fe(II) [59], and the hydroxylation of the aromatic amino acid is coupled to a two electron oxidation of BH_4 by using molecular oxygen as oxygendonor for both hydroxylation of the amino acid and BH_4 [15,60]. The mechanism can be divided into two partial reactions: The formation of the hydroxylating intermediate, believed to be Fe(IV)=O, and oxygen transfer to the aromatic amino acid which corresponds to the hydroxylation of the aromatic amino acid [15].

2.4.1 Formation of hydroxylating intermediate and oxygen activation

Different hydroxylating intermediates have been proposed, but theoretical investigations have shown that a ferryl oxo species (Fe(IV)=O) is a likely candidate [61,62,63], and recently evidence for a high-spin Fe(IV) intermediate, presumably Fe(IV)=O, was found for TH using Mössbauer spectroscopy [64]. Additionally, this ferryl oxo species is expected to be an intermediate in several mononuclear iron enzymes having facial triad coordination [62,65]. How the Fe(IV)=O is formed is not known, but is believed to be formed from cleavage of the O-O bond in Fe-peroxybiopterin [15]. The formation of this Fe-peroxybioterin is consistent with theoretical

studies [61] and the distance between iron and the reactive carbon atom (C4a) of pterin is compatible with a peroxy bridge in the crystal structure of the ternary complex of PAH [15,42]. The proposed mechanism is illustrated in figure 2.10.

Disagreements exist on whether or not O_2 forms a peroxo species with Fe or BH_4. Theoretical investigations have suggested that Fe(II), upon binding of O_2, is converted into a peroxo-iron-complex which then attacks the C4a of BH_4 forming Fe(II)-peroxybioterin [61,62]. From the two structures of the catalytic domain of TPH1, described in section 2.3.2 (c*h*TPH1 and c*gg*TPH1), a shift in iron coordination from six to five gives a free coordination site for oxygen which indicates that oxygen forms a peroxo species with Fe. However, spectroscopic and kinetic studies on PAH mutants suggest that O_2 first reacts with pterin to form a peroxy-pterin [66].

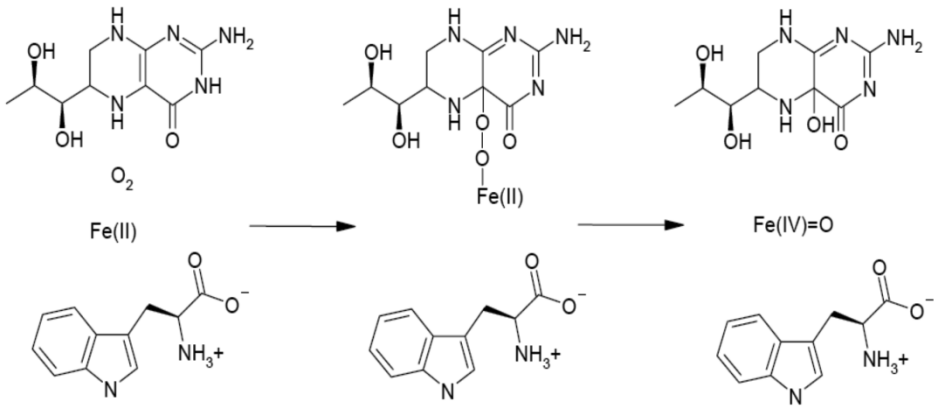

Figure 2.10. Proposed mechanism for formation of the hydroxylating intermediate, Fe(IV)=O.

2.4.2 Mechanism of hydroxylation

The first step in the hydroxylation of the aromatic amino acid is believed to be an electrophilic attack of the Fe(IV)=O on the aromatic C atom making an arenium cation intermediate [15], as shown in figure 2.11. Formation of the cationic intermediate is consistent with observation of a NIH-shift from carbon 5 to 4 upon hydroxylation of the aromatic amino acid which is observed for all three AAAHs [67,68,69,70]. Kinetic isotope effect studies on TPH also support this mechanism [71,72].

2.4.3 Regeneration of tetrahydrobiopterin

BH_4 is synthesized in the body and functions as a substrate in the catalytic mechanism of TPH, as shown in figure 2.10. During formation of the intermediate, Fe(IV)=O, BH_4 is oxidized to 4a-hydroxy-BH_4, also called BH_4-carbinolamin, and released by the enzyme. *In vivo* 4a-hydroxy-BH_4 is then regenerated by dehydration and reduction by the enzymes pterin-4a-carbinolamin dehydratase and dihydropterin reductase**.** This regeneration of BH_4 is important for continuous supply of reduced substrate to the catalytic mechanism [73]. *In vitro* 4a-hydroxy-BH_4 spontaneously decomposes to quinonoid-7,8-dihydro-L-bioterin (q-BH_2) [74].

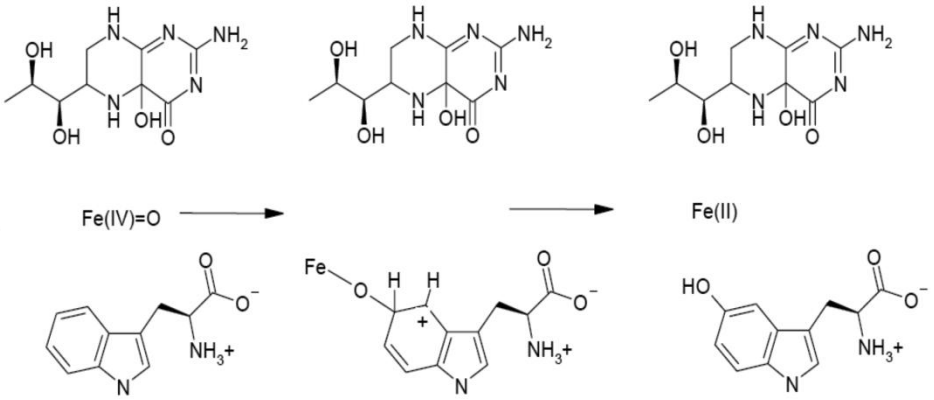

Figure 2.11. Mechanism of the hydroxylation of tryptophan to 5-hydroxytryptophan.

2.4.4 Order of substrate binding

Studies on the catalytic mechanism and the order of substrate binding have been done for all three AAAHs by steady-state kinetics. From these results it is suggested that all substrates are bound in the active site before any reaction can occur, but disagreement in the binding order and whether or not it is partially or fully ordered is observed in these studies [6,18,75,76].

From the structures of c*h*TPH1 with bound BH_2 and c*gg*TPH1 with bound tryptophan and imidazole, described in section 2.3.2, a change from six- to five-coordinate iron site is seen upon binding of tryptophan and imidazole. This change gives an open site for O_2, which is also supported by structure determination of human PAH with bound BH_2 and a substrate analog [41,42]. Spectroscopic studies of the active site of rat PAH [44] and rat TH [45] shows the same five-coordination geometry of iron with a bidentate glutamate. Additionally, a large conformational change is observed in substrate analog and BH_2 binding in PAH and upon binding of tryptophan in c*gg*TPH1 (see figure 2.6). This structural change is likely to reduce the affinity of iron for water, thus yielding an open coordinate site [13]. From the structures of AAAHs with bound BH_2 and spectroscopic studies, it is seen that binding of pterin alone does not change the conformation of the active site nor change the iron-coordination geometry but upon binding of both the aromatic amino acid and pterin a change is observed [13,36,44,45]. Due to these observations, it is now believed that the mechanism is a substrate triggered induced fit mechanism where the enzyme-iron-tryptophan-BH_4 complex reacts with dioxygen.

2.5 Serotonin and its related disorders

5-hydroxytryptamine, better known as serotonin, is a hormone and neurotransmitter and it is synthesized in several tissues such as the enterochromaffin cells in the intestine (periphery) and in the serotonergic neurons in the brain and gut [3,77,78].

The peripheral and the central serotonergic system which are regulated by *h*TPH1 and *h*TPH2, respectively, are coupled to different physiological functions in the body such as cardiac function

[79], body temperature regulation and appetite [3]. In the pineal gland serotonin serves as a precursor of the hormone melatonin, which is involved in circadian rhythm control [80].

Serotonin is implicated in a wide range of disorders. In the peripheral part of the body it is believed to be involved in ulcerative colitis and irritable bowel syndrome [81] and recently, interest has been turned toward designing inhibitors for TPH1 in the gastrointestinal tract which could be used in the treatment of these disorders [82]. In the central serotonergic system serotonin plays a role in psychiatric disorders such as depression, obsessive–compulsive disorder (OCD), anxiety and schizophrenia [83]. These disorders are caused by dysfunctions of the serotonergic system and major depression is believed to be due to deficiency of available serotonin in the brain [84]. Therefore, the central serotonergic system is a major target in the treatment of these disorders. Different treatment strategies such as the use of selective serotonin re-uptake inhibitors, which increases the extracellular concentration of serotonin in the synapse, and the use of monoamine oxidase inhibitors to prevent degradation of serotonin in the synapse have been tried [85,86]. The problem with these antidepressant drug therapies is the variability among patients in treatment response as well as the many side effects [86].

3 Project background

TPH catalyzes the rate-limiting step in the biosynthesis of serotonin and the possibility to specifically influence TPH instead of serotonin, constitute a promising new target for treatment of for example depression and OCD (mentioned in section 2.5). In order to fully understand the functions of the two serotonergic systems and to elucidate the possibility of isoform-specific inhibitors it is necessary to understand the biochemistry of both *h*TPH1 and *h*TPH2. Knowledge of the three-dimensional structure of the enzymes as well as their regulatory and catalytic mechanisms may lead to identification of compounds that regulates the activity of TPH. Also, knowledge of the differences between the two isoforms, especially in their regulatory domains, can give information regarding the design of drugs or compounds that could individually target to either the central or the peripheral serotonergic system.

It is therefore of great importance to characterize TPH and determine the catalytic properties of the isoforms as well as to understand the regulation of the enzymes. The main goal of this project is to purify full-length TPH in a soluble and stable form in order to characterize the enzyme. The experimental strategies used in this project are described in the next section. The expression and purification methods are mainly based on results obtained in my master project and these are therefore summarized first.

3.1 Experimental strategies

The most dominant host organism for expression of recombinant TPH is *Escherichia coli* (*E. coli*) [6] which is also the organism used in the Metalloprotein Chemistry and Engineering Group. In my master project a method for expression of soluble and active recombinant c*h*TPH1 and *h*TPH1 was developed. It was also observed that the solubility of *h*TPH1 decreased with decreasing pH and therefore a pH value of 8.5 should be used (pI value of *h*TPH1 is 6.8) [14]. For purification of

*h*TPH variants a simple and fast method has been developed in the Metalloprotein Chemistry and Engineering Group. The purification procedure consists of two steps: An anion exchange followed by a gel filtration from which a high yield of >20 mg protein can be purified in only 6-8 hours to a purity suitable for crystallization [6,7,12]. This method was used in my master project for the purification of both c*h*TPH1 and *h*TPH1 where c*h*TPH1 was successfully purified to high purity. *h*TPH1 on the other hand was more difficult to purify and it did not bind to any of the ion exchange columns applied. It was concluded that this was most probably due to interactions of *h*TPH1 with other components present in the raw extract such as membrane fragments or DNA [14].

Due to the problems observed during purification of *h*TPH1 in my master project another purification method needed to be developed. Different methods for purification of full-length TPH have been published, but in general it is difficult to verify the quality of the results obtained from the purifications due to lack of experimental evidence and short described procedures without any explanation of the steps involved. For example Liu *et al.* [87] purified human full-length TPH1 and TPH2 using pterin-based affinity chromatography. From the article no results or no detailed explanation on how the proteins are purified are given. It is therefore very difficult to be convinced that they purified full-length TPH. McKinney *et al.* [88] purified different TPH fusion proteins by affinity tag chromatography, and concluded that the fusion proteins had a strong tendency to aggregate and precipitate during purification. Kowlessur and Kaufman [89] on the other hand published a strategy for purifying TPH using pterin-agarose columns where they describe the experimental procedures and show the purified product from the different steps on a SDS-Page. They obtain a very pure and active product. This purification method was tried in the Metalloprotein Chemistry and Engineering Group, but with no success [90]. This could be due to the fact that pterin is attached to the column material at nitrogen 5 (N5) [91], see figure 3.1, which, according to structural analysis, is involved in the interaction between TPH and pterin, as described in chapter 2. Additionally, the pterin ring is bound in the active site and sandwiched between Tyr235 and Phe241. Due to this it is speculated that binding of N5 in the pterin ring to the column material would make it difficult for TPH to interact with pterin. This is also consistent with the fact that this method has shown not to be a success in the group. Another method is therefore applied for purifying full-length *h*TPH1 without the use of pterin-based affinity chromatography. This method is based on the use of detergent to eliminate the association with other compounds thereby decreasing the size of *h*TPH1 (further described in chapter 4).

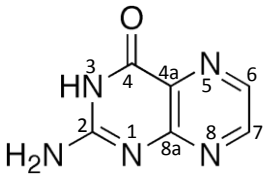

Figure 3.1. Numbering of the atoms in the pterin ring.

Additionally, as expression and purification methods for c*h*TPH1 [14], c*h*TPH2 and ct*h*TPH2 [6,57] already have been developed prior to my Ph.D. project, characterization of these variants were also performed and is described in chapter 8, 9 and 10.

4 Purification of full-length *h*TPH1 using detergent

The full-length *h*TPH1 (named *h*TPH1 in this chapter) is difficult to purify and in my master project [14] purification trials showed that *h*TPH1 does not bind to either cation or anion exchange columns in the pH range 4-10, but that the *h*TPH1 present in the flow-through was enzymatic active. It is speculated that *h*TPH1 associates to other components, such as membrane fragments or DNA, present in the raw extract which causes the size of the *h*TPH1-complex to be higher than the columns exclusion limit (3 x 10^7 Da). These associations with *h*TPH1 could be at the 3,4-hydrophobic repeat present in both the regulatory and tetramerization domains (see chapter 2). A method to overcome this problem is to add detergent to the protein solution and thereby reduce the hydrophobic associations between *h*TPH1 and other components, thus decreasing the size of the variant and allowing *h*TPH1 to be purified. The theoretical pI value of *h*TPH is 6.8.

In this chapter the use of detergent in the purification strategy is introduced followed by description of the experimental procedures as well as a result and discussion section.

4.1 Purification using detergent

4.1.1 Solubilization and isolation using detergent

Detergents are, among other things, used as solubilizing agents for membrane proteins. Membrane proteins are embedded by lipids, which interact with the hydrophobic surfaces of the proteins. By addition of detergents, the hydrophobic surface of the protein is shielded, thereby preventing the protein from interacting with the membrane causing the membrane protein to be solubilized and extracted from the membrane [92]. The solubilization is a three stage process that

depends on the detergent-protein ratio. At low concentration of detergent, the detergent monomers slowly penetrate into the membrane. By increasing the concentration of detergent the membrane bilayer is disrupted and gives rise to lipid-protein-detergent mixed micelles. By further increase in detergent concentration heterogeneous complexes of detergent, lipid and protein begin to form resulting in mixed micelles of lipid/detergent and protein/detergent [93,94]. One problem in solubilization of membrane proteins is that too high concentration of detergent can cause the protein to lose its activity. Therefore, there is a balance between sufficient solubilization and preservation of the activity [92,93,94].

Using this strategy for membrane-associated proteins, proteins can be released by penetration of the detergent into the complex and thereby disruption of the association. The concentration of detergent used in solubilization is typically guided by the critical micelle concentration (CMC) of the detergent. Two CMC's need to be distinguished: The theoretical CMC and the effective CMC. The theoretical CMC is the one determined in pure water, whereas the effective CMC is the one obtained under the actual experimental conditions and depends on lipids, proteins, pH and salts.

4.1.1.1 Release of *h*TPH1 using detergent

Addition of detergent to the *h*TPH1 sample could possibly prevent some of the associations of *h*TPH1 with other molecules in the raw extract such as membrane fragments or DNA. This would then decrease the size of *h*TPH1 causing it to bind to the ion exchange column.

The detergent used in this project is n-dodecyl-β-D-maltopyranoside (DDM). It is a commonly used non-ionic detergent [92,93] which is mild and only breaks lipid-lipid and lipid-protein interactions. Therefore, it could be possible to isolate the protein in its biologically active form [95]. Another advantage of using non-ionic detergents in ion exchange purification is that the detergent itself does not bind to the columns.

4.2 Experimental procedures

4.2.1 Materials

DDM was obtained from Anatrace and (6R)-5,6,7,8-tetrahydro-L-bioterin dihydrochloride (BH_4) was from Schircks Laboratories. Luria Bertani (LB) media and all other chemicals were obtained from Sigma-Aldrich. The chemicals were of analytical grade. All solutions were prepared using 18.2 MΩ cm water from a Milli-Q synthesis A10 Q-Gard system (Millipore). All work with bacteria was carried out in a sterile environment. Materials were handled in a laminar air flow (LAF) bench and sterilization of growth media, antibiotics and water were done by autoclaving or filter sterilization.

4.2.2 Expression

Cells from a frozen glycerol stock containing *E. coli* BL21(DE3)pLysS expressing *h*TPH1 (HC1100) were streaked into single colonies on a LB agar plate containing 30 μg/ml kanamycin sulfate (30kan) and 34 μg/ml chloramphenicol (34cam). The plate was incubated overnight at 37^{o}C. A single colony was inoculated in 50 ml LB/30kan/34cam media in a 250 ml shake flask and

incubated at 37°C and 250 rpm for approximately 4 hours until an optical density at 600 nm (OD_{600}) of 0.6-1.0 was reached. The cells were transferred to a 50 ml polypropylene tube and sedimented by centrifugation at +4°C and 3000 x g for 10 min. The cells were resuspended in 50 ml fresh LB/30kan/34cam media and 6.5 ml of the resuspended cells were used to inoculate 650 ml LB/30kan/34cam media in a 2 L shake flask. The cultures were incubated at 30°C and 250 rpm. After approximately 3½ hour the temperature was lowered to 20°C. When OD_{600} of 0.4-0.6 was attained the expression of *h*TPH1 was induced by adding isopropyl-β-D-thiogalactopyranoside (IPTG) to a final concentration of 0.1 mM. After induction at 20°C and 250 rpm for 18 hours, the cells were harvested by centrifugation at +4°C and 3000 x g for 15 min. The cells were resuspended in ice cold 20 mM Tris/H_2SO_4 pH 8.5, transferred to 50 ml polypropylene tubes and centrifuged again at +4°C and 3000 x g for 15 min. The supernatant was discarded and the cells stored at -80°C until further use.

4.2.3 Release of membrane-associated *h*TPH1

4.2.3.1 Preparation of raw extract

Cells from one 650 ml culture (HC1100) were resuspended in 20 mM Tris/H_2SO_4 pH 8.5 to a total volume of 40 ml and lysed on ice by sonication for 3 x 30 sec. The cell extract were centrifuged in high-speed centrifuge tubes at 18,000 x g and +4°C for 20 min. The supernatant was recovered and centrifuged again as above. Then the supernatant (S) was collected and filtered through a 0.45 µm GHP Acrodisc GF syringe filter.

4.2.3.2 Ultracentrifugation

The strategy for ultracentrifugation is described in [96] and is used to determine whether or not *h*TPH1 can be solubilized from its associated molecules. 20 ml of the supernatant (S) from section 4.2.3.1 was centrifuged at 150,000 x g and +4°C for 45 min. The high speed supernatant ($S_{1.u}$) was discarded and the pellet ($P_{1.u}$) was resuspended in the same volume of 20 mM Tris/H_2SO_4 pH 8.5. The protein concentration in the resuspended pellet was estimated by spectrophotometric measurements in the UV region taking into account nucleic acids as described in [97]. The resuspension was centrifuged again as above. The new supernatant ($S_{2.u}$) was discarded and the pellet ($P_{2.u}$) resuspended in 20 mM Tris/H_2SO_4 pH 8.5 to a concentration of approximately 3 mg protein/ml. DDM was added to a final concentration of 1 % (w/v) to 5 ml of this resuspension and the protein solubilized by incubating the suspension for 1 hour at +4°C under mild agitation (S_{DDM}). Non-solubilized material (M_{non}) was removed from solubilized protein (M_s) by centrifugation at 150,000 x g and +4°C for 45 min or 90 min, respectively. Samples for activity measurements (section 4.2.6) and SDS-Page analysis (section 4.2.7) were collected from the supernatants S, $S_{1.u}$, $S_{2.u}$, S_{DDM} and M_s and from the resuspended pellets $P_{1.u}$, $P_{2.u}$ and M_{non}. In table 4.1 the definitions of the collected samples are given.

4.2.3.3 Ultracentrifugation using different detergent concentrations

To see if it was possible to lower the concentration of DDM while keeping the solubilizing effect of the detergent the sample was incubated with different concentrations of DDM. Centrifugation was done as described in section 4.2.3.2, where final concentrations of 1 %, 0.2 % or 0.05 % (w/v)

DDM were added. The centrifugation time used was 45 min. Samples were analyzed by SDS-Page (see section 4.2.7).

Table 4.1. Definition of the collected samples from the ultracentrifugation of *h*TPH1.

Sample	Definition
S	Supernatant before ultracentrifugation
$S_{1.u}$	Supernatant after 1. Ultracentrifugation
$P_{1.u}$	Resuspended pellet after 1. Ultracentrifugation
$S_{2.u}$	Supernatant after 2. ultracentrifugation
$P_{2.u}$	Resuspended pellet after 2. ultracentrifugation (3 mg protein/ml)
S_{DDM}	DDM extraction of protein (protein suspension incubated with DDM)
M_S	DDM solubilized proteins
M_{non}	Non-solubilized fraction

4.2.4 Purification of membrane-associated *h*TPH1

Once it was established that DDM has a solubilizing effect an alternative strategy was employed since ultracentrifugation is not easy to "scale up". In this strategy the flow-through from the anion exchange column containing the active membrane-associated *h*TPH1 is used. *h*TPH1 was then released by incubation with DDM followed by purification of the DDM protein extraction.

4.2.4.1 Purification tests

Cells from one 650 ml culture, containing *h*TPH1, were prepared as described in section 4.2.3.1. The filtered supernatant was loaded onto a Q Sepharose Fast Flow 16/10 column, which was equilibrated in 20 mM Tris/H_2SO_4 pH 8.5. During loading the flow-through was collected and pooled and DDM was added to a final concentration of 0.05 %. The sample was divided in two portions and incubated for 1½ hour and overnight, respectively at +4^{o}C under mild agitation.

After incubation the solution was filtered through a 0.45 µm filter and loaded onto the Q Sepharose Fast Flow 16/10 column, which was equilibrated in 20 mM Tris/H_2SO_4 pH 8.5, 0.02 % DDM. A linear gradient of 0-20 % of 20 mM Tris/NaOH, 0.8M $(NH_4)_2SO_4$ pH 8.5, 0.02 % DDM (buffer B) over 6 CV followed by a linear gradient of 20-100 % of buffer B over 2 CV was applied to the column. From the supernatant loaded onto the column, the flow-through and each peak in the chromatogram samples were analyzed by SDS-Page (see section 4.2.7).

4.2.4.2 Anion exchange with DDM at the CMC

Cells from three times 650 ml cultures, containing *h*TPH1, were prepared as described in section 4.2.3.1. The filtered supernatant was loaded onto a Q Sepharose High Performance 26/10 column, which where equilibrated with 20 mM Tris/H_2SO_4 pH 8.5. During loading the flow-through was collected and pooled.

DDM was added to a concentration corresponding to the experimental CMC (exCMC). The exCMC was determined as described in section 4.2.5. The solution was incubated at +4^{o}C overnight under mild agitation. After incubation the solution was filtered through a 0.45 µm filter and purified as described in section 4.2.4.1 but on a Q Sepharose High Performance 26/10 column with the stepwise gradient given in table 4.2 and with a concentration of DDM in the buffer system corresponding to the exCMC. From each peak in the chromatogram, the supernatant loaded onto the column and the flow-through samples were analyzed by SDS-Page and western blotting (see section 4.2.7).

Table 4.2. Stepwise gradient used in the anion exchange of *h*TPH1 on a Q Sepharose HP 26/10 column.

Buffer B	Column volume	Fraction volume
0-5%	0	n/a
5-14%	2	3 ml
14-35%	0	n/a
35-35%	2	3 ml
35-100%	2	Not collected

4.2.4.3 Gel filtration

Fractions containing *h*TPH1 from the anion exchange (section 4.2.4.2) was collected and pooled. $(NH_4)_2SO_4$ was added to a final concentration of 200 mM from a 20 mM Tris/NaOH, 2M $(NH_4)_2SO_4$ pH 8.5 stock solution. The solution was then concentrated by ultrafiltration in an Amicon stirred pressure cell with an Ultracel PL-3 membrane. After concentration the sample was filtered through a 0.45 µm filter and loaded onto a HiLoad Superdex 200 26/60 prep grade column. Prior to use the column was equilibrated with 20 mM Tris/NaOH, 200 mM $(NH_4)_2SO_4$ pH 8.5, 0.1 % DDM. Samples were taken from the supernatant loaded onto the column and from each peak in the chromatogram and analyzed by SDS-Page (see section 4.2.7).

4.2.5 Determination of the critical micelle concentration

The exCMC was determined as described by J. H. Kleinschmidt, M. C. Wiener and L. K. Tamm [98] where the maximum absorption of Coomassie Brilliant Blue R-250 shift from 555 nm in the absence to 595 nm in the presence of detergent micelles. The only difference from [98] is that the concentration of Coomassie Blue was lowered from 10 mM to 2 mM due to too high absorbance. A solution of 2 mM Coomassie blue in 5 mM borax buffer was used. As blank the same buffer without Coomassie blue was used (blank buffer). Different DDM concentrations were added to the flow-through from the first anion exchange (section 4.2.4.2) and two 1 ml samples of each DDM concentration were prepared. One with 10 µl of the blank buffer and one with 10 µl of the borax buffer containing Coomassie blue. The absorption spectrum was measured in the range 500-700 nm in order to detect the Coomassie blue shift for each concentration. This was done until a shift in maximum absorption was observed indicating that the concentration of DDM was at the exCMC.

4.2.6 Activity measurements

Samples of 400 µl collected during ultracentrifugation of *h*TPH1 (section 4.2.3.2) were tested for activity. The activity measurements were done as described in section 8.3.3 using 70 µM tryptophan, 300 µM BH_4 and 500 µM O_2. Because the samples were only tested for activity the oxygen level in the samples were not controlled and the concentration of *h*TPH1 was not determined. Additionally, the measured values are given in intensity/min.

4.2.7 SDS-page and Western blotting analysis

Tris-HCl gels from Bio-Rad were used and 7.5 % were chosen for optimal separation region corresponding to the size of *h*TPH1. The gels were prepared as described in the standard protocol from Bio-Rad [99]. The marker contained 0.5 µl protein-standard (161-0304) and 19.5 µl water. All samples were mixed with 5 µl sample buffer and heated in a water-bath at 80^{o}C for 10 min. The samples were loaded into the wells and the proteins were separated at 100 V for approximately 90 min with running buffer. After electrophoresis the gels were transferred to a fixing solution and soaked for 30 min. Afterwards they were stained for 1 hour in a staining solution, followed by overnight de-staining. The composition of the buffers and solutions are given in table 4.3.

Table 4.3. Composition of the buffers and solutions used for SDS-Page analysis.

Buffer	Composition
Running buffer	3.0 g Tris base, 14.4 g glycine and 5 ml 20 % SDS diluted to 1 L water
Sample buffer	2.0 ml water, 2.0 ml 1.0 M Tris/HCl pH 6.8, 4.0 ml 100 % glycerol, 2.0 ml 10 % SDS, 4 mg Coomassie Blue G-250 Before use 28 µl β-mercaptoethanol was mixed with 190 µl of sample buffer
Fixation solution	500 ml water, 400 ml 96% ethanol, 100 ml glacial acetic acid
Staining solution	900 ml water, 100 ml glacial acetic acid, 0.25g Coomassie blue G-250
De-staining solution	900 ml water, 100 ml glacial acetic acid

Western blotting analysis was done using PVDF membranes and chemicals (Immun-blot kit 170-6461) from Bio-Rad. The primary antibody was the murine monoclonal PH8 antibody against TPH, TH and PAH which binds to *h*TPH1 at amino acid 125-142 [100], from Chemicon, Victoria, Australia. 50 µl of the PH8 antibody was added to 5 ml 20 mM Tris, 500 mM NaCl, 0.05 % (vol/vol) Tween-20, 1 % (w/vol) gelatine, pH 7.5. The secondary antibody was goat anti-mouse alkaline phosphatase (GAM-AP). 3.3 µl GAM-AP was added to 10 ml 20 mM Tris, 500 mM NaCl, 0.05 % (vol/vol) Tween-20, 1 % (w/vol) gelatine, pH 7.5. The blotting and the colour development were done as described in the instruction manual for the Immun-blot kit [101].

4.2.8 Protein identification by mass spectrometry

Samples collected during purification of *h*TPH1 were identified by removing bands from the SDS-Page gels and digesting the proteins in the gel pieces with trypsin. The analysis of the tryptic digested peptides was done by tandem mass spectrometry and the protein was identified and

characterized using the Mascot database. The digestion, tandem mass spectrometric analysis and identification were done by the Company Pick'n Post [102] or by the Department of Systems Biology at the Technical University of Denmark [103].

4.3 Results

4.3.1 Release of membrane-associated TPH1

4.3.1.1 Ultracentrifugation

Membrane-associated *h*TPH1 was harvested by ultracentrifugation as described in section 4.2.3.2. During centrifugation samples were collected from the different supernatants and resuspended pellets. In figure 4.1 a flow chart of the steps in ultracentrifugation is given together with an overview of the samples collected. From the S_{DDM} solution (DDM extract) only 5 ml were used further and centrifuged, whereas the solution volume in the two first ultracentrifugations was 20 ml. The samples were analyzed by SDS-Page and activity measurements. On figure 4.2 the SDS-Page analysis is shown and the activities of the samples are given.

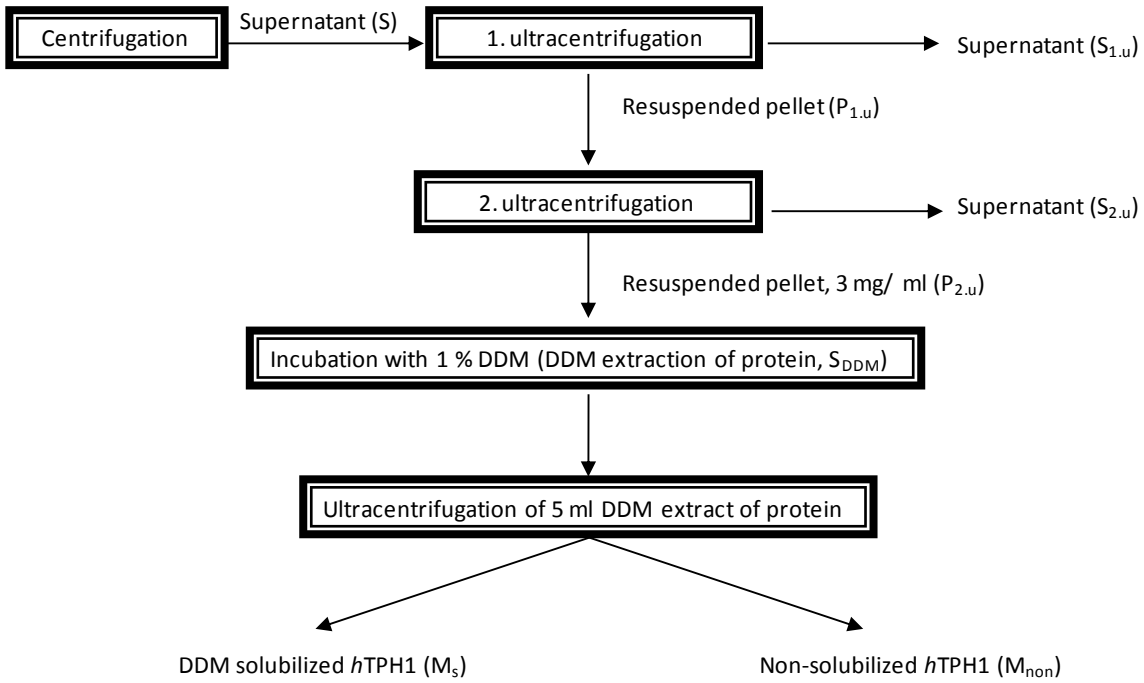

Figure 4.1. Flow chart of the steps involved in ultracentrifugation and overview of the samples collected.

After ultracentrifugation of the *h*TPH1 raw extract, a large amount of *h*TPH1 is present in the pellet ($P_{1.u}$) and *h*TPH1 can therefore be "harvested". This is also consistent with the fact that *h*TPH1 was present in the flow-through during ion exchange indicating that the protein-complex is larger than the ion exchange columns exclusion limit (3×10^7 Da) [14]. Comparing the amount of *h*TPH1 present in the supernatant, M_s, and the resuspended pellet, M_{non}, after incubation with DDM almost all *h*TPH1 is seen in a soluble form. This indicates that *h*TPH1 is membrane-associated and that the association can be disrupted by incubation with 1 % DDM.

After each round of ultracentrifugation, *h*TPH1 is present in equilibrium between the supernatant and resuspended pellet (see lane $S_{1.u}$, $P_{1.u}$, $S_{2.u}$, $P_{2.u}$, M_s and M_{non} on figure 4.2). This could be due to too short centrifugation times giving rise to insufficient harvesting of the membrane-associated *h*TPH1. It was tried to increase the centrifugation time from 45 min to 90 min, but the same pattern was observed (data not shown). The activity measurements follow the same pattern as what is observed on the SDS-Page analysis (see figure 4.2). If the protein suspension contained 2/3 non-membrane-associated and 1/3 membrane-associated *h*TPH1 (as seen on figure 4.2, lane $S_{1.u}$ and lane $P_{1.u}$), then the harvested membrane-associated *h*TPH1 present in $P_{1.u}$ after first ultracentrifugation, would only be present in $P_{2.u}$ after the second ultracentrifugation. From the SDS-Page analysis it seems that the amount of *h*TPH1 present in the supernatant of sample $S_{1.u}$ and $S_{2.u}$ is the same corresponding to approximately 2/3 of the total amount of *h*TPH1. This means that for every centrifugation 2/3 of the *h*TPH1 exist in the "non-membrane-associated" fraction whereas the rest exists as "membrane-associated". This pattern could be due to a weak interaction between *h*TPH1 and the membrane.

The SDS-Page analysis also shows an intensive band at 35 kDa in both sample $P_{1.u}$ and $P_{2.u}$ (membrane-associated fractions) but not in sample $S_{1.u}$ and $S_{2.u}$ (non-membrane-associated fractions, see also figure 4.3). In the supernatant after the addition of detergent (sample M_s), this band is seen indicating that the membrane-associated protein has been solubilized with DDM. The intensity between the 35 kDa protein and *h*TPH1 is approximately 1:1 and is elaborated in the next sections.

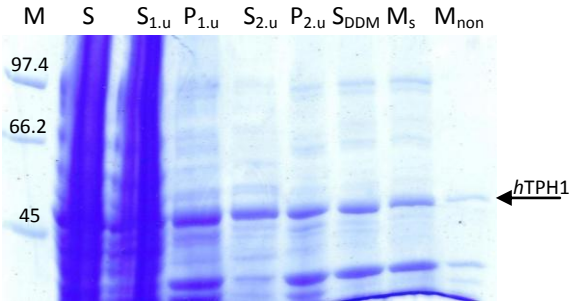

Sample	Activity (int/min)	Volume (ml)
S	1030	20
$S_{1.u}$	780	20
$P_{1.u}$	390	20
$S_{2.u}$	233	20
$P_{2.u}$	117	30 (3 mg/ml)
S_{DDM}	105	30 (3 mg/ml)
M_S	70	5
M_{non}	10	5

Figure 4.2. SDS-Page analysis and activity of each sample collected during ultracentrifugation of *h*TPH1. M is the molecular weight standard given in kDa and S, $S_{1.u}$, $P_{1.u}$, $S_{2.u}$, $P_{2.u}$, S_{DDM}, M_s and M_{non} are the samples collected during ultracentrifugation. The definition of these samples is given in table 4.1 and figure 4.1.

4.3.1.2 Ultracentrifugation using different detergent concentrations

Ultracentrifugation of *h*TPH1 using lower concentrations of detergent was done as described in section 4.2.3.3. This was done in order to see if it was possible to lower the concentration of DDM while keeping the solubilizing effect.

On figure 4.3 the SDS-Page analysis of the samples collected during ultracentrifugation at different DDM concentration is shown. *h*TPH1 is observed in every sample and again approximately 2/3 of the *h*TPH1 is present in the supernatant (sample $S_{1.u}$ and $S_{2.u}$). It is also seen that lowering the DDM concentration does not affect the amount of solubilized *h*TPH1 (S_{DDM}, M_S and M_{non}). These results could indicate that there is equilibrium between solubilized *h*TPH1 and the membrane-associated *h*TPH1. The only difference is the intensity of the 35 kDa protein which increases with increasing concentration of DDM. A more "clean" sample of *h*TPH1 is therefore obtained at low DDM concentrations. Therefore, it was chosen to use a concentration of 0.05 % in a solution with 3 mg protein/ml.

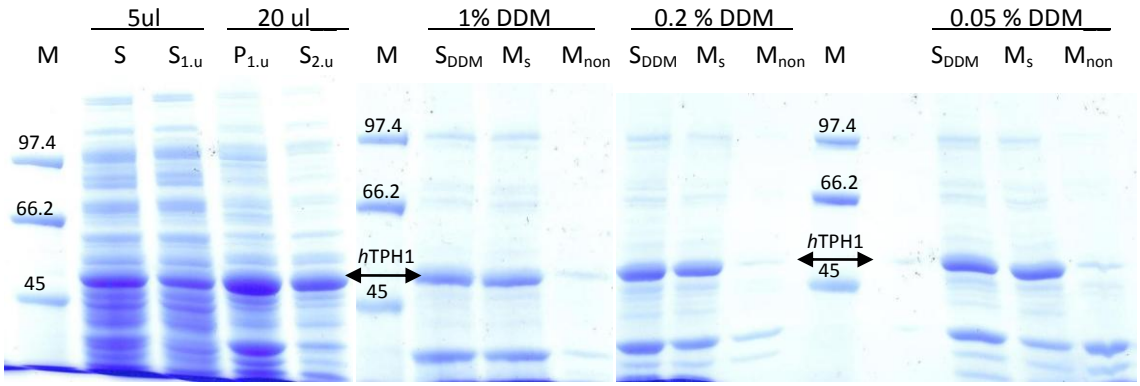

Figure 4.3. SDS-Page analysis of sample S to M_{non} collected during ultracentrifugation. M is the molecular weight standard given in kDa and S, $S_{1.u}$, $P_{1.u}$, $S_{2.u}$, $P_{2.u}$, S_{DDM}, M_s and M_{non} are the samples collected during ultracentrifugation. The definition of these samples is given in figure 4.1 and in table 4.1.

4.3.1.3 Summary

Ultracentrifugation was done to determine whether *h*TPH1 could be solubilized from its associated molecules and approximate the amount of DDM required to solubilize *h*TPH1 from its membrane-associated components. From the results obtained during ultracentrifugation of the *h*TPH1 sample it was observed that the *h*TPH1 membrane-associated complex could be "harvested" and solubilized using detergent and that 0.05 % DDM would be a good concentration to go further with.

4.3.2 Purification of membrane-associated *h*TPH1

Ultracentrifugation requires low working sample volumes and is therefore not a sensible strategy for large sample volumes. Therefore an alternative strategy was employed using the flow-through from the anion exchange column containing the membrane-associated *h*TPH1. *h*TPH1 was then isolated by incubation with DDM followed by purification of the DDM protein extraction, as described in the following section.

4.3.2.1 Purification test

The supernatant prepared as described in section 4.2.3.1 was loaded onto a Q Sepharose Fast Flow 16/10 column and *h*TPH1 was passed through the column as described in section 4.2.4.1. The flow-through was collected, DDM was added to a final concentration of 0.05 % and the sample was incubated for 1½ hour or overnight, as described in section 4.2.4.1. After incubation

the protein solution was purified on an anion exchange column. During purification samples were collected and analyzed by SDS-Page. In figure 4.4 the chromatograms from the second anion exchange of each sample are shown together with the SDS-Page analysis of the samples.

A) 0.05 % DDM for 1½ hour

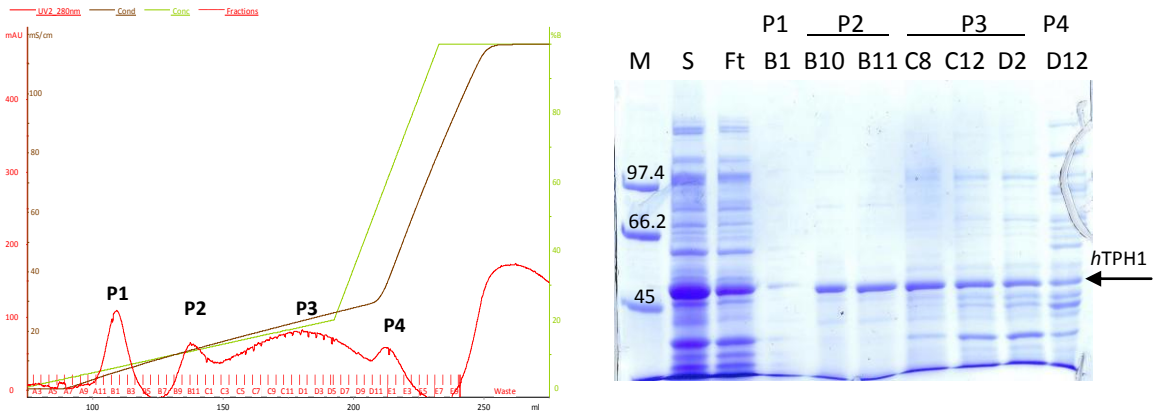

B) 0.05 % DDM and overnight

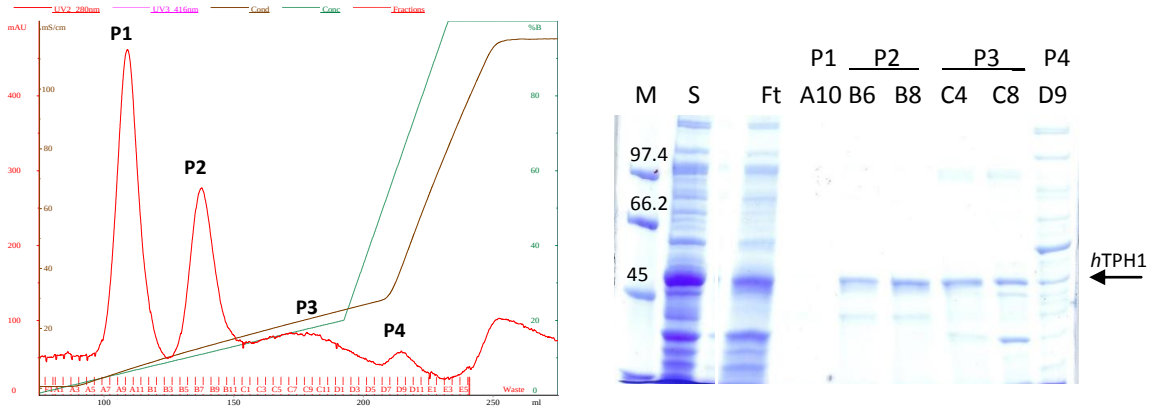

Figure 4.4. Chromatogram and SDS-Page analysis of the anion exchange of the DDM solubilized *h*TPH1 using 0.05 % DDM and different incubation times where A) is incubation for 1½ hour and B) is incubation overnight. The red curve is absorbance at 280 nm, the brown curve is the conductivity in mS/cm, the green curve is the concentration of buffer B in %. Fractions are shown with red lines. M is the molecular weight standard given in kDa, S is the supernatant loaded onto the column, Ft is the flow-through and A10, B1, B6, B8, B10, B11, C4, C8, D2, D9 and D12 are fractions collected during purification.

The chromatograms from both purifications are very alike with the observation of four peaks: Two major ones (P1 and P2), a broad peak (P3) and a smaller one (P4). On the SDS-Page analysis a band with the same size as *h*TPH1 (51 kDa) is seen in the fractions corresponding to the last three peaks (P2, P3 and P4), showing that *h*TPH1 might bind to the column. The presence of *h*TPH1 in the last peak is most likely due to a poor resolution between P3 and P4 and by decreasing the slope of the gradient a better resolution between P3 and P4 can be achieved.

The main differences between the two chromatograms are the absorbance ratio between P1, P2 and P3. The absorbance of P1 is much higher for the anion exchange of the sample incubated with DDM overnight (figure 4.4B), compared to the other two. From the SDS-Page analysis no band is observed and the absorbance is most probably due to DNA. Additionally, the absorbance ratio between P2 and P3 (P2/P3) is much higher for the anion exchange of the sample incubated with 0.05 % DDM overnight. From the SDS-Pages the intensity of *h*TPH1 in P2 and P3 is the same indicating that for example DNA could be present in the sample giving rise to this higher absorbance. From the SDS-Page-analysis the *h*TPH1 sample is much cleaner in P2 compared to P3. Also the 35 kDa protein mentioned in section 4.3.1 is present in P3.

Comparing the amount of *h*TPH1 present in the supernatant loaded onto the column with the amount seen in the flow-through from the two purifications there is still some *h*TPH1 present in the flow-through, but with a lower amount observed for the sample incubated overnight (has a higher supernatant/flow-through ratio). It was therefore chosen to use overnight incubation with DDM. To increase the yield of solubilized *h*TPH1, thus decreasing the amount of *h*TPH1 in the flow-through a higher concentration of DDM could be the answer.

From these results it is observed that *h*TPH1 could be released from the *h*TPH1-complex by DDM and that the released *h*TPH1 binds to the column. It was therefore chosen to optimize the purification method in order to increase the yield of purified *h*TPH1.

4.3.2.2 Anion exchange with DDM at the exCMC

To optimize the yield of purified *h*TPH1, cells from 3 times 650 ml cultures were prepared as described in section 4.2.3.1 and the purification was performed on a Q Sepharose High Performance 26/10 column. To obtain a higher amount of solubilized *h*TPH1, thus increasing the amount of *h*TPH1 binding to the column the concentration of DDM was increased until the exCMC of DDM was reached. This was done to ensure, that the amount of DDM was high enough to get all membrane-associated *h*TPH1 solubilized (see section 4.1). The concentration of DDM in the anion exchange buffer system was also changed so the concentration corresponded to the exCMC of DDM in the sample that was used. The gradient was changed to a stepwise gradient in order to decrease the elution volume of P3.

*h*TPH1 was purified as described in section 4.2.4.2. The flow-through from the first anion exchange was collected and the exCMC of DDM was determined. This was done by using Coomassie Blue as described in section 4.2.5. In figure 4.5 the UV-Vis spectra of the exCMC assay are shown. From the series of spectra a shift in absorbance from 555 nm to 595 nm is seen at a DDM concentration of 0.1 % and above, indicating the presence of detergent micelles. It was therefore chosen to add DDM to a total concentration of 0.1 % to the flow-through.

After incubation the flow-through was loaded onto an anion exchange and eluted as described in section 4.2.4.2. The chromatogram from the anion exchange is shown in figure 4.6. Again three peaks with absorbance at 280 nm are seen in the chromatogram eluting at 5 mS/cm, 13 mS/cm and 30 mS/cm, respectively. Samples from the supernatant loaded onto the column, the flow-

through and from each peak (fraction B6, C3, C4, C5 E4) were analyzed by SDS-Page and western blotting shown in figure 4.7 and 4.8, respectively. A sample from P5 (absorbance at 416 nm) was also collected and analyzed.

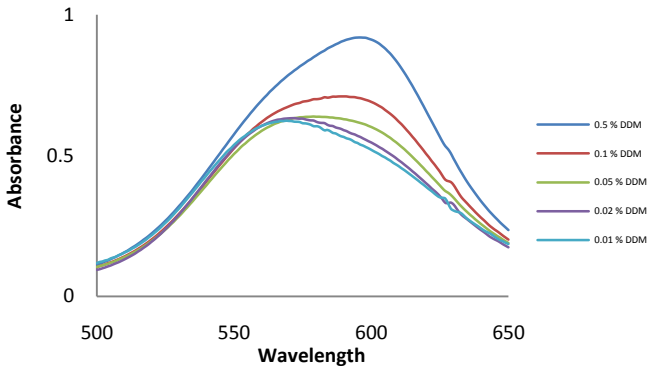

Figure 4.5. UV-Vis spectra of the flow-through with different concentrations of DDM. A shift in absorbance is seen at concentrations of DDM at 0.1 % and above.

Comparing the chromatogram in figure 4.6 with the chromatogram in figure 4.4B they are very similar, but a better resolution between P2 and P3 is seen due to a change in gradient. A higher absorbance intensity is also seen for P2 in figure 4.6 which is due to a higher amount of proteins and DNA (increased amount of cell culture).

Comparing the amount of *h*TPH1 in the supernatant with the amount in the flow-through almost all *h*TPH1 binds to the column which indicates that at higher concentration of DDM more *h*TPH1 is solubilized from the *h*TPH1-complex. Combining the results from the SDS-Page analysis and western blotting analysis with the chromatogram, *h*TPH1 is observed both in P2 and P5 with the same intensity but the absorbance of P2 is much higher than the absorbance of P5. Therefore, the absorbance in P2 is most probably due to DNA or a protein smaller than the separation region of the SDS-Page, which was also observed in the purification test (see section 4.3.2.1). Additionally, the band corresponding to the size of *h*TPH1 in P3 on the SDS-Page analysis does not show a band on the western blot and is therefore not *h*TPH1. The 35 kDa protein is present in P3.

The ratio between *h*TPH1 and the 35 kDa protein are approximately 1:1 in the supernatant. The *h*TPH1 present in the flow-through is also in a 1:1 ratio with this protein. It could therefore be speculated that *h*TPH1 associates with this protein and in the presence of DDM they dissociates and bind to the column due to decrease in size. From the results of the anion exchange and SDS-Page analysis it is seen that they are separated.

From these results it can be concluded that by incubating the *h*TPH1-complex with 0.1 % DDM, *h*TPH1 can be released and for the first time it is able to bind to the anion exchange column. The bound *h*TPH1 showed to elute in several peaks (over a large area) which could indicate that *h*TPH1 still exists in different oligomer forms just smaller in size. Despite this and because a huge

amount of *h*TPH1 is observed in the fraction eluting at P2 (see figure 4.9) the fractions were collected and pooled, and used in the further purification of *h*TPH1.

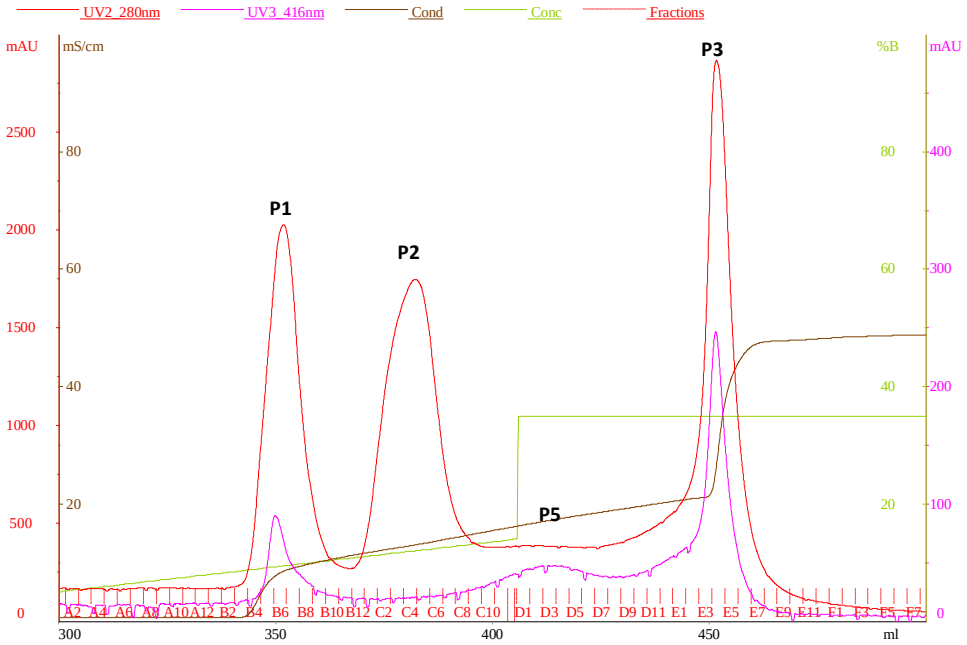

Figure 4.6. Chromatogram of the anion exchange of *h*TPH1 with 0.1 % DDM on a Q sepharose High Performance 26/10 column. The red curve is absorbance at 280 nm, the brown curve is the conductivity in mS/cm, the green curve is concentration of buffer B in % and the pink curve is absorbance at 416 nm. Fractions are shown with red lines.

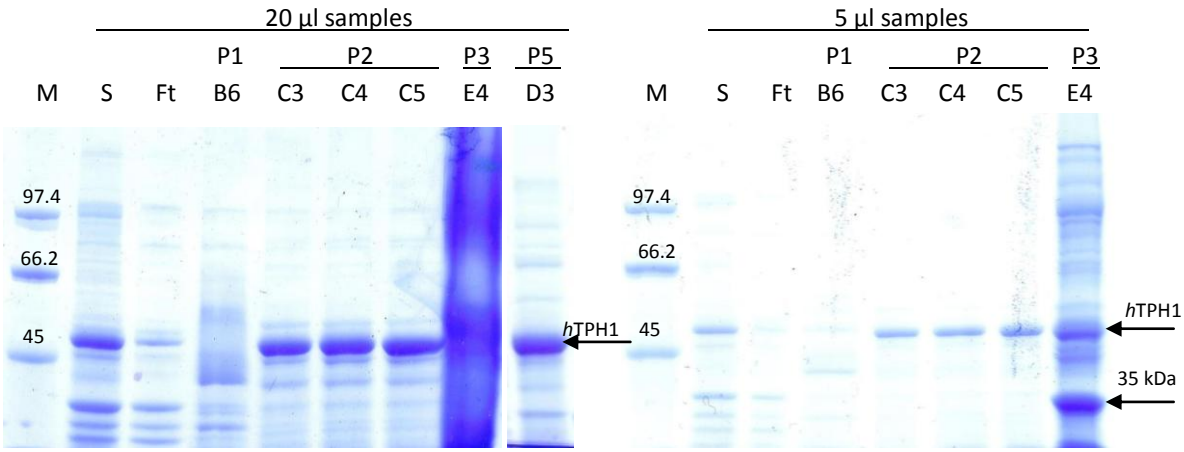

Figure 4.7. SDS-Page analysis of the samples collected during anion exchange of TPH1 with 0.1 % DDM. M is the molecular weight standard in kDa, S is the supernatant loaded onto the column, Ft is the flow-through and B6, C3, C4, C5, D3 and E4 are fractions from the anion exchange.

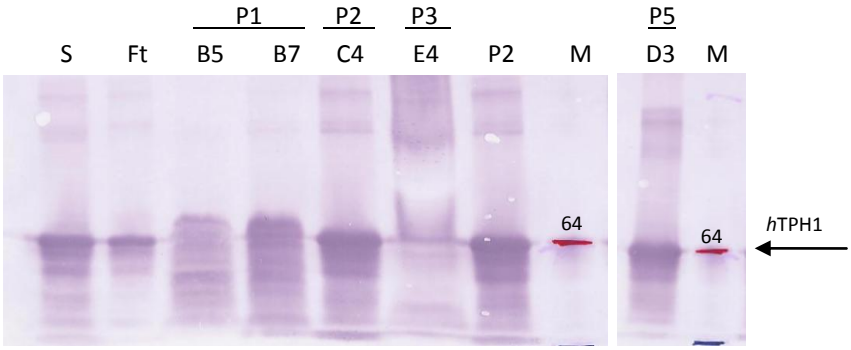

Figure 4.8. Western blotting analysis of samples collected during anion exchange of *h*TPH1 with 0.1 % DDM. M is the molecular weight standard given in kDa, S is the supernatant loaded onto the column, Ft is the flow-through and B5, B6, C4, D3 and E4 are fractions from the anion exchange. P2 is a sample from all fractions from peak 2 (P2) in the anion exchange.

4.3.2.3 Gel filtration

The fraction B12-C8 (P2) from the anion exchange were collected and pooled, ammonium sulfate was added to a total concentration of 200 mM and the solution concentrated to approximately 9 ml. The protein solution was loaded onto a Superdex200 26/60 column as described in section 4.2.4.3 and the chromatogram from the purification is shown in figure 4.9. Samples from each peak were analyzed by SDS-Page and western blotting and the analysis is shown in figure 4.10.

From the gel filtration two peaks are seen: One at 140 ml and one at 158 ml. From the SDS-Page a band corresponding to the size of *h*TPH1 is seen in all fractions but with a higher amount in the first peak. From the western blotting analysis it can be concluded that these bands correspond to *h*TPH1. It can therefore be concluded that the size of the *h*TPH1-complex has been decreased by DDM and that the size is within the gel filtration column separation region ($1 \times 10^4 - 6 \times 10^5$ Da). *h*TPH1 does not elute in the void volume. From a calibration curve constructed for this column [57] the elution volumes correspond to a size of 280 kDa and 154 kDa, respectively. It can therefore be concluded that *h*TPH1 can be purified in two oligomer forms (monomer 51 kDa). These oligomer forms could either be by formation of a 5mer or a 3mer or by association to other molecules. From the bottom of the SDS-Page a blue line is observed which is most probably due to the presence of smaller molecules which cannot be separated on the gel used (7.5 %).

4.3.3 Protein identification

The bands from the SDS-Page analysis corresponding to *h*TPH1 from the anion exchange (fraction C4 and D3) and from the gel filtration (fraction B5 and B12) were subjected to protein identification by mass spectrometry (described in section 4.2.8). The identification confirmed that the protein was *h*TPH1. Additionally, the band corresponding to the 35 kDa was also analyzed and it showed to be an outer membrane protein F (OmpF) from *E. coli* with a molecular weight of 39330 Da. The OmpF is a membrane protein and therefore, it also gets solubilized by DDM followed by binding to the column.

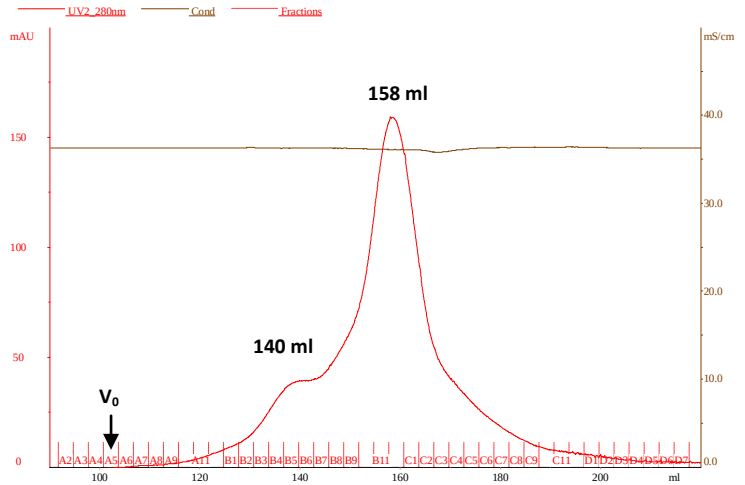

Figure 4.9. Chromatogram of the gel filtration of the fractions B12-C8 corresponding to P2 from the anion exchange of *h*TPH1 solubilized with DDM . The red curve is absorbance at 280 nm and the brown curve is the conductivity in mS/cm. Fractions are shown with red lines.

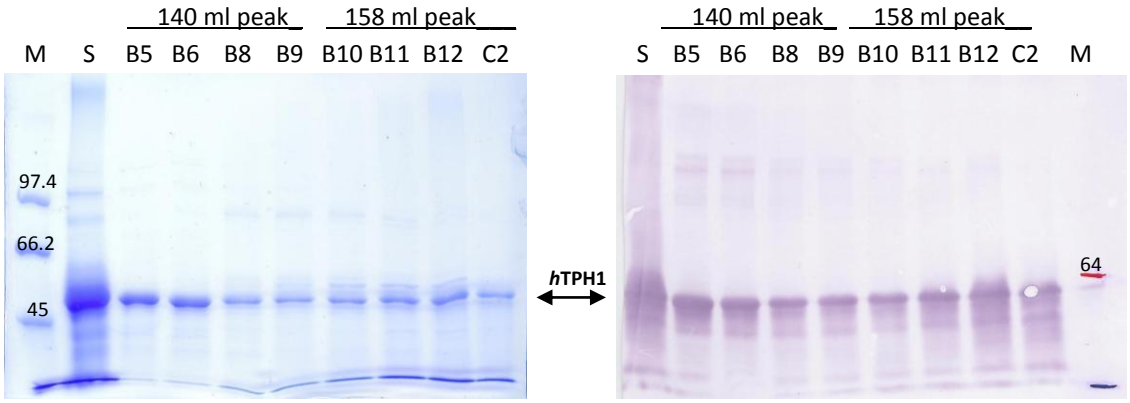

Figure 4.10. SDS-Page and western blotting analysis of the gel filtration of *h*TPH1 solubilized with DDM where M is the molecular weight standard given in kDa, S is the supernatant loaded onto the column and B5, B6, B8, B9, B10, B11, B12 and C2 are fractions collected during the gel filtration.

4.3.4 Summary and overall discussion

Membrane-associated *h*TPH1 can be released by DDM using a concentration of 0.05 – 0.1 % (see figure 4.4 and figure 4.6). The DDM released *h*TPH1 binds to the anion exchange column and it can be concluded that the size of the *h*TPH1-complex has been decreased by DDM and that the size is below the columns exclusion limit. The *h*TPH1 which binds to the column elutes over a large volume in the anion exchange, as observed from figure 4.6, 4.7 and 4.8, indicating that the protein still exists in different oligomer forms, either as intermolecular association or as a protein-complex with other components, which are now smaller in size. This is the first time in the Metalloprotein Chemistry and Engineering Group that full-length of *h*TPH1 can bind to the

anion exchange column applied. The *h*TPH1 sample, from the anion exchange that was loaded onto the gel filtration column, also showed to exists in two oligomer forms.

Additionally, from the anion exchange an OmpF protein is present in P3. This membrane protein is also observed to be isolated by ultracentrifugation and solubilized by DDM. The ratio between this and *h*TPH1 in the supernatant before loading on the anion exchange column is approximately 1:1. Due to this and the elution pattern of *h*TPH1 in the anion exchange it could be speculated that *h*TPH1 associates with this protein. This also point towards that *h*TPH1 can be solubilized and purified using DDM and that the protein stabilizes *h*TPH1 in solution by association. When the association is interrupted *h*TPH1 elutes in the anion exchange over a large volume.

From these results it can be concluded that the effect of DDM is most probably to stabilize the protein so the interaction of *h*TPH1 with other components is decreased. However, it is still difficult to understand the behavior of *h*TPH1 during purification. From expression and solubility test done on c*h*TPH2, ct*h*TPH2 and *h*TPH2, respectively [6,57,104] it was observed that the presence of the regulatory domain caused the protein to be insoluble. Because of this and the fact that c*h*TPH1, c*h*TPH2 and ct*h*TPH2 can be purified the problems of purifying *h*TPH1 was speculated to be due to the regulatory domain. Therefore in order to understand the behavior of *h*TPH1, a “divide-and-conquer” strategy was applied. Variants of both *h*TPH1 and *h*TPH2 containing the regulatory domain or parts of it were constructed as described in chapter 5 and 6.

4.4 Conclusion

*h*TPH1 has been released from its membrane-associations by DDM. After incubation *h*TPH1 can successfully bind to the anion exchange column indicating that the size of the protein has been decreased. This is the first time the full-length of *h*TPH1 binds to an anion exchange column. The bound *h*TPH1 elutes over a large volume which is most probably due to oligomerization of the protein which is also observed in the gel filtration. It can be concluded that DDM stabilizes the protein and eliminates the interaction to other molecules. This is the first simple procedure that has been developed for purification of *h*TPH1. However, it still needs some optimization regarding stability and elution of the protein in one oligomeric form.

5 Construction of *E. coli* strains for expression of *h*TPH variants

*h*TPH is very difficult to work with due to insolubility and precipitation, and the behavior of full-length *h*TPH1 during purification, as described in chapter 4, is still not understood. Therefore, to better examine the properties of *h*TPH a "divide-and-conquer" strategy has been applied where both isoforms were truncated to fewer domains or shorter sequences. Expression strains were constructed for expression of these variants. The expression strategy was not fully established from the beginning of this project but has evolved and changed on the way based on the results obtained from both expression and purification of the constructed variants (see chapter 6 and 7).

In this chapter a detailed description of the strategy used for construction of the expression strains using *E. coli* as an expression host is presented, together with experimental procedures and a summary of the results.

5.1 Strategies used for construction of expression strains

Construction of an expression strain can be divided into three parts: Production of the gene of interest, construction of the expression vector containing the gene of interest and construction of the expression strain for expression of the gene of interest.

The gene of interest is produced by polymerase chain reaction (PCR) amplification using a template and a set of primers designed specifically for the gene. When the gene fragment has been amplified by PCR it is cloned into the PCR-Script cloning vector and transferred into *E. coli* DH5α cells. The gene is then removed from the cloning vector, ligated into an expression vector

and propagated by transformation of the vector into DH5α cells. The expression vector is then transferred into *E. coli* BL21(DE3) cells and an expression strain has been constructed. In figure 5.1 a schematic presentation of the steps involved is given.

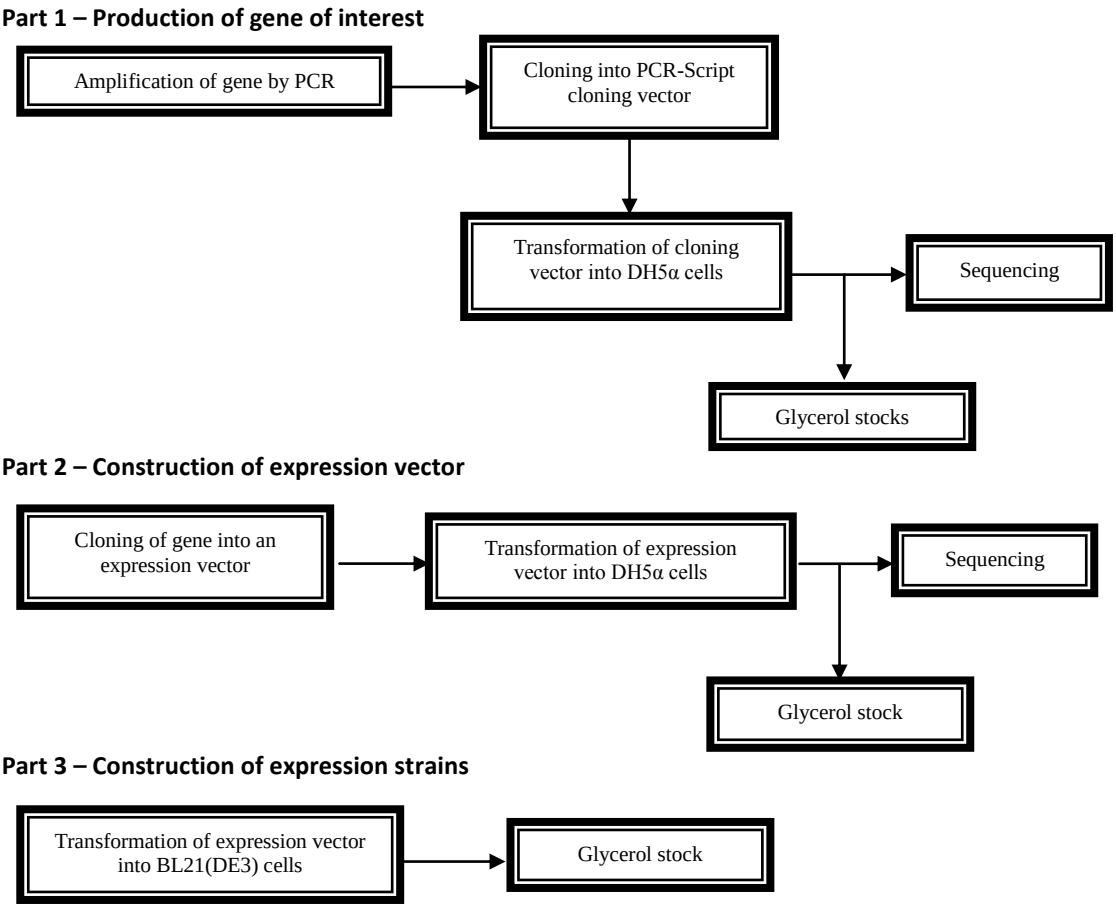

Figure 5.1. A schematic presentation of the steps involved in construction of genes, expression vectors and expression strains.

5.2 Construction of *h*TPH1 strains

5.2.1 Production of gene of interest

5.2.1.1 Gene design

The sequences of the different constructs were chosen from alignment of the amino acid sequence of full-length *h*TPH1 with c*gg*TPH1 and c*h*TPH2 both produced in the Metalloprotein Chemistry and Engineering Group. In figure 5.2 this alignment is shown. From the alignment the sequence of the regulatory domain (r) was chosen from amino acid 1 to 99 corresponding to bp 1 to 297, the catalytic domain (c) from amino acid 100 to 413 corresponding to bp 298 to 1239, and the tetramerization domain (t) from amino acid 414 to 444 corresponding to bp 1240 to 1332.

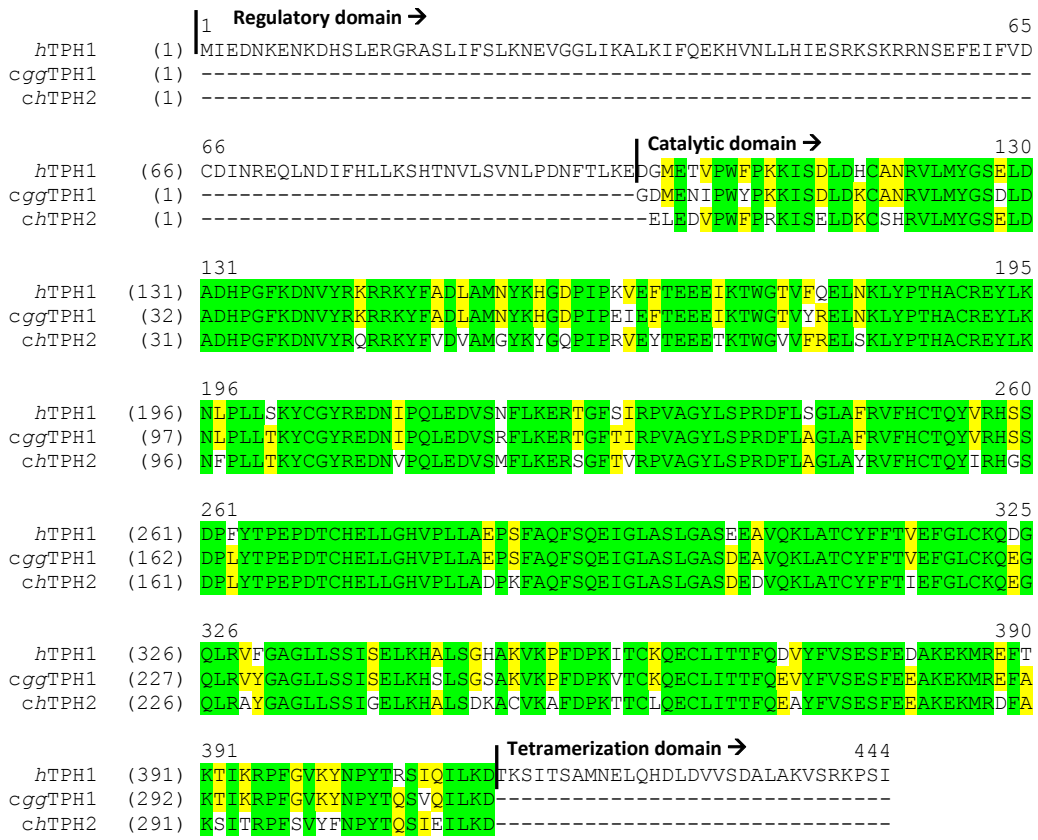

Figure 5.2. Alignment of full-length human TPH1 (*h*TPH1) with *gallus gallus* cTPH1 (c*gg*TPH1) and human cTPH2 (c*h*TPH2). The program Vector NTI Advance 10 from Invitrogen was used for alignment [34]. Green background indicates conserved residues in all sequences and yellow background indicates conserved residues in two of the sequences. The domain boundaries as used in this project are marked by black vertical lines.

5.2.1.2 Gene amplification

The codon optimized full-length *h*TPH1 gene sequence for expression in *E. coli* and inserted in a pUC57 cloning vector was obtained from Genscript Corporation, USA. The gene was flanked with two unique restriction enzyme sites, *Nde*I in the N-terminal and *Xho*I in the C-terminal and termed *h*TPH1/*Nde*I/*Xho*I. The Met-codon (ATG), required for translation initiation, is part of the *Nde*I site (CATATG) and a stop codon (TAA) was placed directly before the *Xho*I site.

Each gene was produced by PCR amplification with the full-length *h*TPH1 gene as template and a specific set of primers given in table A1.1, appendix A.1. After amplification of each gene they were cloned into the PCR-script cloning vector (Stratagene), propagated and the gene fragments were sequenced by Eurofins MWG Operon, Germany.

5.2.2 Construction of expression vectors

5.2.2.1 pET-expression vector system

The pET-expression vector system developed by Studier *et al.* [105,106] was used in this project. This system was chosen due to its tightly regulated promoter as well as the ability to express target proteins of up to 50 % of the total cell protein. The system uses a highly specific T7 RNA polymerase that expresses target genes under the control of T7 transcription and translation signals. It typically contains a T7*lac* promoter consisting of a *lac* operator sequence downstream of the T7 promoter and a *lac*I gene coding for a *lac* repressor which blocks the T7 promoter, thus blocking transcription of the gene of interest under non-inducible conditions. The promoter is an IPTG inducible T7 promoter [107].

5.2.2.2 Construction of *h*TPH1 pET-expression vectors

The produced *h*TPH1/*Nde*I/*Xho*I gene fragments (section 5.2.1.2) were removed from the cloning vectors and ligated into a pET-expression vector (pET26b) between the *Nde*I and *Xho*I sites in the cloning region. A pET26-expression vector for expression of a *h*TPH1 variant was constructed.

5.2.3 Construction of expression strains

The constructed expression vectors (section 5.2.2.2) were transferred into *E. coli* BL21(DE3) expression host strains. These host strains are DE3 lysogens and the genome contains coding regions for T7 RNA polymerase, a *lac*I gene and a *lacUV*5 promoter with a *lac* operator sequence. T7 RNA polymerase is transcribed from the host genome when *E. coli* RNA polymerase binds to the *lacUV*5 promoter sequence and thereby initiate transcription. With the absence of inducer the transcription, of both T7 RNA polymerase and the gene of interest, is blocked by binding of the *lac* repressor to the *lac* operator sequence, also mentioned in section 5.2.2.1. T7 RNA polymerase and the gene of interest are therefore tightly regulated by the *lac* operator so no basal expression of target protein is present in the absence of inducer [105,106].

5.3 Construction of fusion tag expression strains

The fusion tag strategy offers several advantages such as increased expression levels, correct folding, thus enhanced solubility and simple purification procedures. Different kinds of fusion tags exist and the most often used are the solubility-enhancing tags that increase the recovery of functional proteins and the affinity tags that reduce the number of purification steps [108].

Purification of *h*TPH variants containing the regulatory domain showed to be more difficult than first expected as described both in chapter 4 and 7. To better understand the property of *h*TPH and to achieve a soluble and purified variant containing the regulatory domain of *h*TPH, strategies using the green fluorescent protein (GFP) or glutathione S-transferase (GST) as fusion tags were applied as described in section 5.3.1 and 5.3.2. The GFP was used to visualize the r*h*TPH1 variant during expression and purification (see chapter 6 and 7), whereas GST is used because of stabilization of r*h*TPH1 by salt in the raw extract, as described in chapter 7.

5.3.1 GFP fusion tag

TPH is a colorless enzyme and by fusion of the GFP folding reporter (frGFP) to TPH, it is possible to use frGFP as a visual marker for both gene expression and purification [109,110,111]. The frGFP is a modified soluble variant that folds well in *E. coli* and contains six mutations compared to the wild type GFP (wtGFP) from *Aequorea victoria*. One mutation (Q80R) is due to a PCR error [109], 3 mutations increase the fluorescence signal of the protein (F99S, M153T, V163A) [109], one mutation is a red-shifted mutation (S65T) [110] and the final mutation is a folding mutation which increases the amount of soluble protein (F64L) [110,111].

To visualize the folding of a protein the frGFP is fused to the C-terminal of the target protein. By a correct folding of the target protein, frGFP will be folded correctly and only by correct folding of frGFP the protein will be fluorescent (colored green) [111,112]. The fluorescence of GFP can therefore be used to estimate the yield of correctly folded upstream protein.

Due to this visualization effect it was chosen to fuse the frGFP to the C-terminal of r*h*TPH1 for two reasons. Firstly, because it was difficult to follow the purification of r*h*TPH1 due to an extinction coefficient of zero at 280 nm and because western blotting analysis is impossible since no antibody against rTPH exists and secondly, to determine the expression level as well as the yield of correctly folded mutants of r*h*TPH1.

5.3.1.1 Waldo-GFP expression vector

The pWaldo-GFP vector used in this project was kindly provided by Jan-Willem de Gier [112]. It is a pET28(a+) expression vector containing the *Bgl*II/*Xho*I fragment of pET21(a+). The DNA sequence for the recombinant tobacco etch virus (TEV) protease cleavage site (protease recognition site: ENLYFQ/G (/: cleavage site)) followed by the DNA sequence of the frGFP gene is inserted in the *Bam*HI/*Hind*III site of the vector [111,113], as shown in figure 5.3. The pET-expression vector system is described in section 5.2.2.

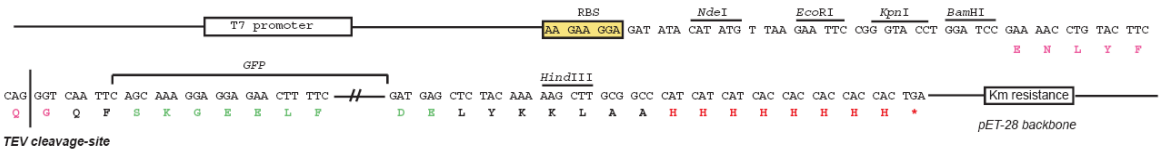

Figure 5.3. Overview of the pWaldo-GFPd expression vector that shows the translation initiation region (TIR), the TEV protease cleavage site and the frGFP sequence [113, supplementary figure 1]. Reproduced with permission from the Nature Publishing Group.

5.3.1.2 Construction of the r*h*TPH1-frGFP expression strain

The r*h*TPH1 gene was constructed with a *Nde*I site in the N-terminal and a *Bam*HI site in the C-terminal due to cloning into the *Nde*I/*Bam*HI site of the pWaldo-GFPd vector. The gene is produced by PCR amplification with the full-length *h*TPH1 gene as template and a specific set of primers given in table A1.2, appendix A1. After amplification the gene was cloned into the PCR-script cloning vector, propagated and the PCR-product was analyzed by DNA sequencing. The

produced r*h*TPH1/*Nde*I/*Bam*HI gene fragment was removed from the cloning vector and ligated into the *Nde*I/*Bam*HI site of the pWaldo-GFPd expression vector. The constructed vector was then transferred into *E. coli* BL21(DE3) cells.

As a positive control the frGFP protein is expressed alone to compare the intensity of the fluorescence of fusion protein with the intensity of correctly folded frGFP. The frGFP expression vector contains an additional nucleotide between the *Nde*I and *Bam*HI (see figure 5.3), which does not have any influence when the frGFP is used as a fusion partner, due to insertion of the gene of interest in the vectors *Nde*I and *Bam*HI restrictions sites. This is only relevant when frGFP itself is used as positive control. This nucleotide was removed by PCR-based site-directed mutagenesis.

5.3.1.3 Constructions of mutation in the 3,4-hydrophobic face of r*h*TPH1

As described in chapter 4 it is difficult to purify full-length *h*TPH. From previous purification of *h*TPH1 done in my master project [14] it was concluded that *h*TPH1 interacts with other molecules such as membrane fragments or lipid molecules through hydrophobic interaction. This results in formation of large oligomers that could not bind to the applied columns. From purification of *h*TPH1 using DDM the *h*TPH1 protein elutes in several fractions indicating that the protein still exists in different oligomer forms. This is also observed from purification of r*h*TPH1 (see chapter 7).

The secondary structure of the regulatory domain of TPH is predicted to make an α-helix structure and due to a 3,4-hydrophobic repeat placed from amino acid 21 to 41 in *h*TPH1 a coiled-coil structure in the regulatory domain is possibly creating a hydrophobic face, as mentioned in section 2.3.3. If this hydrophobic face is located at the outer surface of the native protein the protein can oligomerize either by intermolecular associations or by interaction to other hydrophobic molecules. By mutation in the hydrophobic face these interactions could be decreased, and therefore formation of different oligomers could be eliminated causing the protein to be present in hopefully one oligomer form. Mutations in this repeat is therefore performed to see which, if any, of the amino acids in the hydrophobic face that are involved in oligomer formation as well as to elucidate the function of this repeat.

Three different mutants are constructed each containing two mutations. The hydrophobic amino acids are changed to arginine to create more charges. The following mutants of r*h*TPH1 were constructed: L24R and V28R (L24R/V28R-r*h*TPH1), L31R and L35R (L31R/L35R-r*h*TPH1) and finally V28R and L31R (V28R/L31R-r*h*TPH1). The mutants were constructed as described for the *h*TPH variants in section 5.2, but the production of genes was done by PCR-based site-directed mutagenesis with the r*h*TPH1/*Nde*I/*Bam*HI gene fragment inserted in the PCR-script vector (section 5.3.1.2) as template and a specific set of primers containing the desired base changes to generate the different mutations. The primer sets are given in table A1.2, appendix A1. In the PCR-based site-directed mutagenesis the whole plasmid containing the gene of interest is used as template. The mutant gene was removed from the cloning vector, inserted into the pWaldo-GFPd vector and the expression vector was then transferred into *E. coli* BL21(DE3) expression strains.

The fluorescence intensity of the three mutants was compared to the r*h*TPH1-frGFP from section 5.3.1.1 to see whether or not these mutations had any influence on the folding and solubility of the enzyme.

5.3.2 GST fusion tag

During purification of r*h*TPH1 it was observed that a high content of salt in the raw extract stabilized the r*h*TPH1 (see chapter 7). Therefore, it was decided to construct a variant which can be purified with a high content of salt. This was done by using GST as an affinity tag. The vector used is a pGEX-5X-1 vector.

5.3.2.1 pGEX-5X-1 fusion vector system

The pGEX fusion vector system contains the GST gene from *Schistosoma japonicum* [114]. The target gene is cloned into the multiple cloning site positioned downstream from the GST gene. Expression of the fusion protein is under control of a *tac* promoter, which is induced by IPTG [115]. The pGEX-5X-1 also encodes the recognition region for the site-specific protease Factor Xa located between the GST domain and the multiple cloning site. Proteins can therefore be separated from GST by cleavage with Factor Xa [116,115]. In figure 5.4 a schematic representation of the multiple cloning site of pGEX-5X-1 is given.

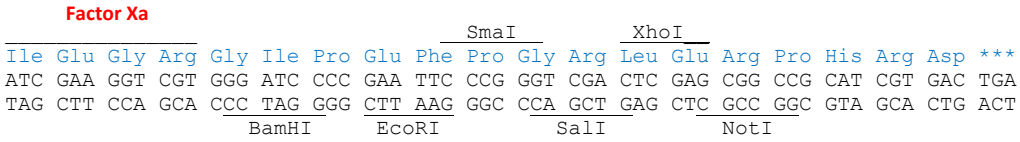

Figure 5.4. Multiple cloning site of the pGEX-5X-1 vector [116].

5.3.2.2 Construction of the GST-r*h*TPH1 expression strain

r*h*TPH1 was fused to the C-terminal of GST by cloning the r*h*TPH1 gene into the *Bam*HI/*Xho*I site in the multiple cloning site. The gene was therefore flanked with a *Bam*HI site in the N-terminal and a stop codon followed by a *Xho*I site in the C-terminal. The use of the *Bam*HI site gives rise to an extra nucleotide between the Factor Xa recognition site and the *Bam*HI which alters the reading frame, also shown in figure 5.4. For correction two additional nucleotides, CC, is inserted between the *Bam*HI site and the r*h*TPH1 gene. These additional nucleotides give the following codons after Factor Xa; GGG ATC CCC encoding for Gly, Ile and Pro. The expression strain for expression of the fusion protein GST-r*h*TPH1 is constructed as described in section 5.2, where the gene is first constructed using PCR amplification, a specific set of primers (given in table A1.3, appendix A1) and *h*TPH1 as template.

5.4 Construction of *h*TPH2 expression strains

5.4.1 Gene design

In the Metalloprotein Chemistry and Engineering Group both c*h*TPH2 and ct*h*TPH2 have been expressed and purified with high purity, but the full-length variant of *h*TPH2 has almost

exclusively been expressed in an insoluble form [6,57,104]. Considering this, the regulatory domain must play a certain role in the proteins solubility and from structure prediction done by Michael S. Windahl [6] it is seen that a region from amino acid 42-55 in the regulatory domain is predicted disordered and may give problems with solubility, purification and characterization. Due to this, an expression strain expressing a variant of *h*TPH2 lacking the first 58 amino acids was constructed (*h*TPH2$_{59\text{-}490}$).

By alignment of the sequence of full-length *h*TPH1 and *h*TPH2, given in figure 5.5, it is seen that *h*TPH2 also contains a 3,4-hydrophobic repeat in the regulatory domain from amino acid 67 to 84. Due to this a construct lacking the 3,4-hydrophobic repeat was constructed. The construct was chosen to begin at amino acid 90 due to higher content of adenine in the gene sequence resulting in a higher content of adenine in translation initiation region (TIR) [117,118,119]. This A/U enrichment presumably decreases the possibility of secondary structure formation in mRNA facilitating the entry of the ribosome to enhance translation initiation and subsequent high-level protein expression [117,119]. The construct was termed *h*TPH2$_{90\text{-}490}$.

The reason why these construct were made with *h*TPH2 and not *h*TPH1 was due to already developed purification methods for both c*h*TPH2 and ct*h*TPH2 [6,57].

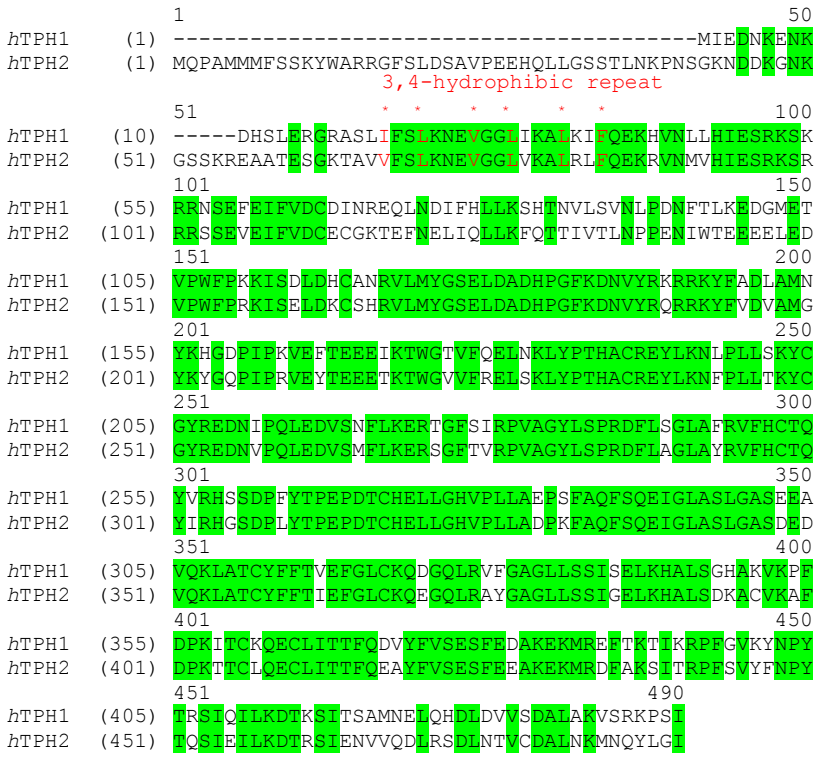

Figure 5.5. Amino acid sequence for the two isoforms of tryptophan hydroxylase, *h*TPH1 and *h*TPH2. The program Vector NTI Advance 10 from Invitrogen was used for alignment [34]. Green background indicates conserved residues in all sequences. The amino acid residues highlighted in red are the residues involved in the 3,4-hydrophobic repeat.

5.4.2 Constructions of *h*TPH2 expression strains

The two variants: One without the first 58 amino acids (*h*TPH2$_{59-490}$) and one which lacks the 3,4-hydrophobic repeat (TPH2$_{90-490}$) were constructed as described in section 5.2.1. Each gene was produced by PCR amplification with the full-length *h*TPH2 gene as template and a set of primers specific for each gene (given in table A1.3, appendix A1). Because the *h*TPH2 gene contains a unique *Dra*I site in the gene sequence, the gene fragments were constructed with an *Nde*I site in the N-terminal and a *Dra*I site in the C-terminal for ligation into the pET expression vector. After amplification of each gene they were cloned into the PCR-script cloning vector, propagated and the PCR-product sequenced by Eurofins MWG Operon, Germany. The produced *h*TPH2/*Nde*I/*Dra*I gene fragments were removed from the cloning vector and ligated into the pET26b expression vector using the *Nde*I site in the vectors cloning region and the *Dra*I site in the *h*TPH2 sequence. A pET26-*h*TPH2$_{59-490}$ and pET26-*h*TPH2$_{90-490}$ expression vectors were constructed and transferred into *E. coli* BL21(DE3) expression strains for expression of *h*TPH2$_{59-490}$ or *h*TPH2$_{90-490}$, respectively.

5.5 Experimental procedures

This section describes the experimental procedures used for construction of the *h*TPH expression strains, described in section 5.2, 5.3 and 5.4. Most of the procedures are described in general with important issues highlighted for the specific *h*TPH gene variants. Protocols, alike or with minor adjustment from the standard protocol of the supplier, are not given in full but only referred to.

5.5.1 Materials and chemicals

All work with bacteria was carried out in a sterile environment. Materials were handled under a LAF bench and sterilization of growth media, antibiotics and water were done by autoclaving or filter sterilization. All solutions were prepared with 18.2 MΩ cm water from a Milli-Q synthesis A10 Q-Gard system (Millipore).

5.5.2 Production of genes

The TPH gene variants were produced by amplification using PCR or by PCR-based site-directed mutagenesis. In the following sections the experimental procedures for production of the gene variants are described.

5.5.2.1 Primer design for amplification with PCR

For each gene a specific set of primers were designed. Each primer set was constructed according to the strategies described in section 5.2 (*h*TPH1 gene variants), section 5.3 (r*h*TPH1-frGFP gene and GST-r*h*TPH1 gene) and section 5.4 (*h*TPH2 gene variants) where the forward primer contained a *Nde*I or a *Bam*HI site and the reverse primer contained a stop codon followed by a *Xho*I site or a *Bam*HI site without the upstream stop codon (only the r*h*TPH1-GFP). The annealing part of each primer was chosen according to equation 5.1 with an annealing temperature of either 53^{o}C or 55^{o}C. The full-length *h*TPH1 gene or full-length *h*TPH2 gene, ordered from Genscript Corporation with a sequence optimized for expression in *E. coli*, were used as templates.

$$T_{annealing} = [2^{o}C (\#Adenine + \#Thymine) + 4^{o}C (\#Guanine + \#Cytosine)] - 5^{o}C \quad (5.1)$$

In table A1.1 to A1.3 in appendix A1 the sequences of the primer sets are given. They were all obtained from TAG Copenhagen A/S with four A's in the 5'-end to avoid loss of effective primer sequence during PCR because of exonuclease activity.

5.5.2.2 Primer design for PCR-based site-directed mutagenesis

The mutations in the 3,4-hydrophobic repeat of r*h*TPH1, described in section 5.3.1.3, were produced by PCR based site-directed mutagenesis. A set of primer for each mutant was designed, where each primer set consisted of two mutations surrounded by annealing sequences. In table A1.2, appendix A1 the sequences of the primer sets are given. They were all ordered from TAG Copenhagen A/S.

5.5.2.3 PCR amplification and PCR-based site-directed mutagenesis

The PCR reactions were carried out with the primer sets given in table 5.1. A Platinum *Pfx* DNA polymerase kit from Invitrogen was used for both the PCR amplification and the PCR-based site-directed mutagenesis.

For the PCR amplification reactions the following reagents were mixed in the given order. Water to a final volume of 50 µl, 1x Pfx amplication buffer, 0.3 mM dNTP, 1 mM $MgSO_4$ and 1 unit Platinum ® *Pfx* plus 0.5 µl of template (miniprep DNA) and 0.3 µM of each primer. The PCR amplifications were executed on a Perkin Elmer GeneAmp PCR system 2400 and programmed as described in table 5.1. The extension time was determined according to 1 minute per 1 kbp. After PCR amplification the PCR-product is separated from the template by preparative gel electrophoresis as described in section 5.5.2.4 and 5.5.2.5 and cloned into the PCR-script vector (section 5.5.2.7) before transformation into *E. coli* DH5α cells.

Table 5.1. PCR amplification parameters.

Variant	Primer set	Template	Cycles	Denaturation	Annealing	Extension
ct*h*TPH1/*Nde*I/*Xho*I ~1100 bp	HCP596 HCP655	*h*TPH1	25	94°C for 15 sec	55°C for 30 sec	68°C for 1 min
r*h*TPH1/*Nde*I/*Xho*I ~300 bp	HCP641 HCP643	*h*TPH1	25	94°C for 15 sec	53°C for 30 sec	68°C for 30 sec
rc*h*TPH1/*Nde*I/*Xho*I ~1200 bp	HCP641 HCP593	*h*TPH1	25	94°C for 15 sec	55°C for 30 sec	68°C for 1 min
r*h*TPH1/*Nde*I/*Bam*HI (frGFP fusion) ~300 bp	HCP641 HCP642	*h*TPH1	25	94°C for 15 sec	53°C for 30 sec	68°C for 30 sec
r*h*TPH1-*Bam*HI/*Xho*I (GST-fusion) ~300 bp	HCP702 HCP643	*h*TPH1	25	94°C for 15 sec	53°C for 30 sec	68°C for 30 sec
***h*TPH2$_{59-490}$/*Nde*I/*Xho*I ~1300 bp**	HCP631 HCP632	*h*TPH2	25	94°C for 15 sec	55°C for 30 sec	68°C for 1 min
***h*TPH2$_{90-490}$/*Nde*I/*Xho*I ~1200 bp**	HCP632 HCP697	*h*TPH2	25	94°C for 15 sec	55°C for 30 sec	68°C for 1 min

For the PCR-based site-directed mutagenesis reactions the following reagents were mixed in the given order. Water to a final volume of 50 µl, 1x Pfx amplication buffer, 1 µl of template, 0.3 µM of each primer (see table 5.2), 0.2 mM dNTP mix, 1 mM $MgSO_4$ and 1.0 µl *Pfx* polymerase. The program settings were: Denaturation at 94°C for 30 sec, annealing at 55°C for 30 sec and extension at 68°C for 7 min for a total of 25 cycles. The extension time was determined according to the size of the plasmid template. After mutagenesis 1 µl of the *Dpn*I restriction enzyme (U/µl) were added to each reaction and they were incubated for 1 hour at 37°C to digest the parental methylated dsDNA (the template). The products were directly transferred to *E. coli* DH5α cells as described in section 5.5.2.8.

Table 5.2. Primer set for the site-directed mutagenesis reactions of each of the three r*h*TPH1 mutant genes.

Variant	Primer set
L24R/V28R-r*h*TPH1-frGFP	HCP683
	HCP684
L31R/L35R-r*h*TPH1-rGFP	HCP685
	HCP686
V28R/L31R-r*h*TPH1-frGFP	HCP687
	HCP688

5.5.2.4 Preparation of agarose gels

Agarose gel electrophoresis is used to separate linear DNA fragments according to size. The gels were prepared depending on the size of the fragments. An amount of agarose powder determined from table 5.3 was weighed in a 100 ml PYREX conical flask and mixed with 25 ml TBE buffer (10.8 g Tris, 5.5 g boric acid and 0.93 g EDTA in 1L of water). The mixture was heated in a microwave oven until the gel was completely melted and dissolved. The gel solution was cooled to 50-60°C and 0.2 µl 10 mg/ml ethidium bromide (EtBr) was added using an aerosol-resistant pipet tip. Afterwards the gel solution was poured to a casting tray, where an appropriate comb was chosen depending on which kind of electrophoresis that was being used (analytical - 10 wells 12 µl, or preparative - 2 wells of 24 µl and 120 µl, respectively). The gel was solidified and moved to a running vessel containing electrophoresis buffer (TBE buffer with 12.5 µl EtBr pr. liter).

Table 5.3. Amount of agarose powder used in preparation of gels.

Size of DNA fragment	Recommended % for gel	Per gel (per 25ml TBE)
> 4000bp	0.8 %	0.20 g
800-4000bp	1.0 %	0.25 g
400-800bp	1.2 %	0.30 g
< 400bp	1.5 %	0.37 g

5.5.2.5 Separation of DNA by preparative gel electrophoresis

The PCR product from section 5.5.2.3 was separated from the template using preparative gel electrophoresis. The gel was prepared as described in section 5.5.2.4. 1/5 volume of loading dye (0.25 % bromphenol blue, 30 % glycerol and 50 mM EDTA) was added to the PCR sample. For preparation of the marker 1 µl 1 kbp DNA standard, 4 µl loading dye and 19 µl of sterilized MQ water were used. Marker and sample were loaded in the wells and the gels subjected to electrophoresis at 100 V constant voltages for approximately 30 min. The DNA was visualized using UV light and the band removed with a scalpel. The mass of the gel slice was determined.

5.5.2.6 Purification of DNA from agarose gels

After separation of the DNA fragments and isolation of the desired gel slice (section 5.5.2.5), the DNA fragments were extracted and purified from the agarose gel. This was performed with Gel *Advanced*™ Gel Extraction Miniprep System from Viogene [120] and the standard protocol from the kit was followed with the exception that the sample was eluted using 30 µl of MQ water.

5.5.2.7 Cloning of PCR-products into the PCR-Script cloning vector

The gel purified PCR-products (section 5.5.2.6) was inserted into the PCR-Script cloning vector with the PCR Script™ Amp Cloning kit from Stratagene [121].

5.5.2.8 Transformation of cloning vector into *E. coli* DH5α cells

After ligation of the PCR product into the PCR-script cloning vector (section 5.5.2.7) or after digestion with *Dpn*I (section 5.5.2.3) the vector products were transferred into plasmid propagating cells. Max efficiency competent *E. coli* DH5α cells from Invitrogen were thawed on ice and 100 µl was transferred to a cooled 15 ml polypropylene tube. 1 µl plasmid solution was mixed with the cells and the solution was kept on ice for 30 min. The tube was transferred to a water-bath at 42°C for precisely 45 sec followed by 2 min on ice. 450 µl LB media without antibiotic was added.

5.5.2.9 Propagation of cells and glycerol stocks

Cells from the transformation (section 5.5.2.8) were streaked on two LB agar plates containing 100 µg/ml ampicillin (100amp): One with 55 µl (1/10) and one with 440 µl (8/10) of the culture. The plates were incubated overnight at 37°C. From the plates a single colony was transferred to a 15 ml polypropylene tube containing 3 ml LB/100amp media. The cultures were incubated overnight at 37°C and 250 rpm.

From each 3 ml culture a glycerol stock was made. 500 µl of the culture was mixed with 116 µl 80 % glycerol in an Eppendorf tube and stored at -80°C.

5.5.2.10 Plasmid purification

The plasmid from the remaining 2.5 ml of overnight culture was isolated with a GenElute™ Plasmid MiniPrep kit from Sigma-Aldrich [122]. Water was used for elution.

5.5.2.11 Restriction enzyme analysis and gel electrophoresis

The gene products were analyzed, and estimation of size was done using analytical restriction enzyme analysis and gel electrophoresis. The purified plasmids (section 5.5.2.10) were digested with a set of restriction enzymes depending on the variant being analyzed. In table 5.4 the enzymes used for each variant are given. In an Eppendorf tube 8.4 µl of purified plasmid, 1.0 µl of NEBuffer, chosen for optimal digestion condition [123], and 0.3 µl of each enzyme was added, mixed and incubated for 2 hours at 37°C. The digested DNA was analyzed by analytical gel electrophoresis. The gels were prepared as described in section 5.5.1.4. 2 µl of loading dye was mixed with the 10 µl sample from the digestion. The electrophoresis was performed as described in section 5.5.1.5.

Table 5.4. *h*TPH variant, enzymes and NEBuffer used for restriction enzyme analysis.

***h*TPH gene variant**	**Enzymes**	**NEBuffer**
ct*h*TPH1/*Nde*I / *Xho*I	*Nde*I / *Xho*I	4
r*h*TPH1/*Nde*I/*Xho*I	*Nde*I / *Xho*I	4
rc*h*TPH1/*Nde*I/*Xho*I	*Nde*I / *Xho*I	4
r*h*TPH1/*Nde*I/*Bam*HI (frGFP fusion)	*Nde*I / *Bam*HI	*Bam*HI
L24R/V28R-r*h*TPH1-frGFP	*Nde*I / *Bam*HI	*Bam*HI
L31R/L35R-r*h*TPH1-frGFP	*Nde*I / *Bam*HI	*Bam*HI
V28R/L31R-r*h*TPH1-frGFP	*Nde*I / *Bam*HI	*Bam*HI
r*h*TPH1/*Bam*HI/*Xho*I (GST fusion)	*Bam*HI / *Xho*I	*Bam*HI
***h*TPH2$_{59\text{-}490}$/*Nde*I/*Dra*I**	*Nde*I / *Dra*I	4
***h*TPH2$_{90\text{-}490}$/*Nde*I/*Dra*I**	*Nde*I / *Dra*I	4

5.5.2.12 Sequencing

The plasmid containing the desired DNA fragments was sequenced. The concentration of purified plasmid was determined by spectrophotometry at 260 nm and the required sample volume for sequence analysis was calculated from the simplified equation 5.2.

$$X\ \mu l\ = \frac{5\ \mu l}{A_{260} - A_{850}} \tag{5.2}$$

The estimated volume was diluted to 50 µl with MQ water, mixed with a mixture of 165 µl 96 % ethanol and 5 µl 3 M Na-acetate pH 4.6 and left at room temperature for 15 min. The plasmids were then pelleted by centrifugation for 20 min at 13,000 rpm and the supernatant discarded. The plasmid sediment was washed with 250 µl freshly made 70 % ethanol and the solution was centrifugated for 5 min at 13,000 rpm. This was done three times. The plasmid was then left to dry for more than 30 min at room temperature.

Due to the large size of some of the genes (more than 900 bp), these were sequenced from both ends. The primers used for sequencing were T7 and T3. The primers were designed and synthesized by the MWG-Biotech AG Sequencing service, which also performed the sequencing.

5.5.3 Construction of expression vectors

After production of the gene of interest (section 5.5.2) an expression vector containing this gene was constructed. This was done by ligation of the gene into the expression vector. The experimental procedures involved are described in the following sections.

5.5.3.1 Restriction enzyme digestion

In order to ligate the expression vector with the gene insert from the PCR-script vector (section 5.5.2), both vectors were digested with the same restriction enzymes, given in table 5.4. Before digestion *E. coli* DH5α strains containing the cloning vector with the gene of interest were streaked on LB/100amp agar plates. The expression vector, see table 5.5, was either streaked on LB/30kan agar plates or LB/100amp agar plates. The plates were incubated overnight at 37^{o}C. One colony from each plate was inoculated in 3 ml LB media with appropriate antibiotic in a 15 ml polypropylene tube. The 3 ml cultures were then incubated overnight at 37^{o}C and 250 rpm and the plasmids were purified as described in section 5.5.2.11.

After plasmid purification 84 µl purified plasmid sample, 10 µl appropriate NEBuffer and 3 µl of each enzyme were incubated for 4 hours at 37^{o}C. In table 5.4 the restriction enzyme and NEBuffer are given for each variant. The digested expression vectors (pET vector, pwaldo-dGFP and pGEX-5X-1) were incubated for another hour after addition of 1 µl Calf intestinal phosphatase (CIP) to prevent inter- or self ligation.

5.5.3.2 Separation af DNA fragments

The digested DNA fragments were separated using preparative gel electrophoresis as described in section 5.5.2.4 and 5.5.2.5. The correct bands on the gel indicating insert or vector were cut out and the DNA fragments were purified as described in section 5.5.2.6.

5.5.3.3 Ligation and transformation into *E. coli* DH5α cells

Ligation of the vector and insert was done using a Ligate-IT^{TM} Rapid kit from USB Corporation [124] and carried out according to their standard protocol. After ligation the products were transferred into *E. coli* DH5α cells as described in section 5.5.2.8 and if the expression vectors contained a kanamycin resistance gene these cultures were incubated for 1 hour at 37^{o}C and 250 rpm after addition of LB media without antibiotic. After transformation the cells were plated and propagated as described in section 5.5.2.9. From each 3 ml culture, glycerol stocks were prepared as described in section 5.5.2.9.

5.5.3.4 Analysis of ligation product

The plasmid from the remaining 2.5 ml of each overnight culture was isolated as described in section 5.5.2.10 and the ligation product was analyzed by restriction enzyme analysis and gel electrophoresis as described in section 5.5.2.11. The plasmid containing the wanted DNA fragment was sequenced as described in section 5.5.2.12.

Table 5.5. Expression vector and antibiotic for each *h*TPH variant.

	Expression vector	Antibiotic
ct*h*TPH1/*Nde*I / *Xho*I	pET26	30kan
r*h*TPH1/*Nde*I/*Xho*I	pET26	30kan
rc*h*TPH1/*Nde*I/*Xho*I	pET26	30kan
r*h*TPH1/*Nde*I/*Bam*HI (frGFP fusion)	pWaldo-GFPd	30kan
L24R/V28R-r*h*TPH1-frGFP	pWaldo-GFPd	30kan
L31R/L35R-r*h*TPH1-frGFP	pWaldo-GFPd	30kan
V28R/L31R-r*h*TPH1-frGFP	pWaldo-GFPd	30kan
r*h*TPH1/*Bam*HI/*Xho*I (GST fusion)	pGEX-5X-1	100amp
***h*TPH2$_{59\text{-}490}$/*Nde*I/*Dra*I**	pET26	30kan
***h*TPH2$_{90\text{-}490}$/*Nde*I/*Dra*I**	pET26	30kan

5.5.4 Construction of expression strains

Constructions of expression strains were carried out by transformation of the constructed expression vectors (section 5.5.3) into *E. coli* BL21(DE3) expression cells. 100 µl of $CaCl_2$ competent cells were thawed on ice and transferred to a 15 ml polypropylene tube. 1 µl of purified plasmid (section 5.5.3.1) was mixed with the cells and the solution was kept on ice for 20 min. The tube was transferred to a water-bath at 37^{o}C for precisely 45 sec followed by 2 min on ice. 450 µl LB media without antibiotic was added and the culture was incubated for one hour at 37^{o}C and 250 rpm. The cells were propagated as described in section 5.5.2.9 with 30kan or 100amp as selective marker, and glycerol stocks were prepared as described in section 5.5.2.9.

5.6 Summary of results

The strategies and theoretical background for development of *h*TPH variants are given in section 5.2 to 5.4. In the following sections a summary of the results from construction of the expression strains for expression of *h*TPH variants are presented.

5.6.1 Production of *h*TPH gene variants

All *h*TPH gene variants were produced by either PCR amplification or PCR-based site-directed mutagenesis as described in section 5.5.2.3 using the primer sets given in table A1.1, A1.2 and A1.3 in appendix A1 and the full-length *h*TPH1 gene, full-length *h*TPH2 gene or the r*h*TPH1-PCR-script vector as template, depending on the variant. This gives rise to products with either a *Nde*I or a *Bam*HI restriction site in the N-terminal and a stop codon followed by a *Xho*I site or a *Bam*HI site in the C-terminal, as given in table 5.6. The experimental steps in the production of the gene variants is shown in figure 5.1 and described in section 5.5.2. In table 5.6 the stock number for each produced gene is given as well as the type of PCR, template used in the PCR reaction and the restriction enzyme sites in the N-terminal and C-terminal.

Table 5.6. Gene with type of PCR, template used in the PCR reaction, the restriction enzyme sites in the N-terminal and C-terminal, the size of the gene and glycerol stock numbers.

Gene	Type of PCR	Template	N-terminal	C-terminal	Size (bp)	Stock number
ct*h*TPH1/*Nde*I / *Xho*I	PCR amplification	TPH1	*Nde*I	Stop codon + *Xho*I	300	HC1717
r*h*TPH1/*Nde*I/*Xho*I	PCR amplification	TPH1	*Nde*I	Stop codon + *Xho*I	1200	HC1966
rc*h*TPH1/*Nde*I/*Xho*I	PCR amplification	TPH1	*Nde*I	Stop codon + *Xho*I		HC1938
r*h*TPH1/*Nde*I/*Bam*HI (frGFP fusion)	PCR amplification	TPH1	*Nde*I	*Bam*HI	300	HC1710
L24R/V28R-r*h*TPH1-GFP	PCR-based site-directed mutagenesis	rTPH1-PCR script vector	*Nde*I	*Bam*HI	300	HC2288
L31R/L35R-r*h*TPH1-GFP	PCR-based site-directed mutagenesis	rTPH1-PCR script vector	*Nde*I	*Bam*HI	300	HC2330
V28R/L31R-r*h*TPH1-GFP	PCR-based site-directed mutagenesis	rTPH1-PCR script vector	*Nde*I	*Bam*HI	300	HC2298
r*h*TPH1/*Bam*HI/*Xho*I (GST fusion)	PCR amplification	TPH1	*Bam*HI	Stop codon + *Xho*I	300	HC2467
***h*TPH2$_{59-490}$/*Nde*I/*Dra*I**	PCR amplification	TPH2	*Nde*I	*Dra*I	1300	HC1588
***h*TPH2$_{90-490}$/*Nde*I/*Dra*I**	PCR amplification	TPH2	*Nde*I	*Dra*I	1200	HC2446

5.6.2 Construction of expression vectors

The expression vectors for production of the *h*TPH variants were constructed by insertion of the genes from section 5.6.1 into the pET26+, the pWaldo-dGFP or the pGEX-5X-1 expression vector. This was done as given in figure 5.1 and described in section 5.5.3.

In table 5.7 the stock number of each constructed expression vector containing the gene of interest is given as well as the antibiotic marker and restriction enzymes.

Table 5.7. Glycerol stock numbers with description of vector, gene fragment and antibiotic marker.

Gene	Expression vector	Restriction enzymes	Stock number	Antibiotic marker
ct*h*TPH1/*Nde*I / *Xho*I	pET26	*Nde*I / *Xho*I	HC1803	30kan
r*h*TPH1/*Nde*I/*Xho*I	pET26	*Nde*I / *Xho*I	HC1983	30kan
rc*h*TPH1/*Nde*I/*Xho*I	pET26	*Nde*I / *Xho*I	HC1949	30kan
r*h*TPH1/*Nde*I/*Bam*HI (GFP fusion)	pWaldo-dGFP	*Nde*I / *Bam*HI	HC1747	30kan
L24R/V28R-r*h*TPH1-GFP	pWaldo-dGFP	*Nde*I / *Bam*HI	HC2241	30kan
L31R/L35R-r*h*TPH1-GFP	pWaldo-dGFP	*Nde*I / *Bam*HI	HC2353	30kan
V28R/L31R-r*h*TPH1-GFP	pWaldo-dGFP	*Nde*I / *Bam*HI	HC2338	30kan
r*h*TPH1/*Bam*HI/*Xho*I (GST fusion)	pGEX-5X-1	*Bam*HI / *Xho*I	HC2472	100amp
***h*TPH2$_{59-490}$/*Nde*I/*Dra*I**	pET26	*Nde*I / *Dra*I	HC1640	30kan
***h*TPH2$_{90-490}$/*Nde*I/*Dra*I**	pET26	*Nde*I / *Dra*I	HC2454	30kan

5.6.3 Construction of expression strains

By transformation of the produced expression vectors from section 5.6.2 into *E. coli* BL21(DE3) cells, as described in section 5.5.4, expression strains for expression of r*h*TPH1, rc*h*TPH1, ct*h*TPH1, r*h*TPH1-GFP, L24R/V28R-r*h*TPH1-GFP, L31R/L35R-r*h*TPH1-GFP, V28R/L31R-r*h*TPH1-GFP, GST-r*h*TPH1, *h*TPH2$_{59-490}$ and *h*TPH2$_{90-490}$, respectively were achieved. After propagation of the BL21(DE3) cells glycerol stocks were produced. These are numbered according to table 5.8.

Table 5.8. Glycerol stock numbers with description of vector, gene fragment and antibiotic marker.

Gene product	Expression vector	Stock number	Antibiotic marker
ct*h*TPH1/*Nde*I / *Xho*I	pET26	HC1869	30kan
r*h*TPH1/*Nde*I/*Xho*I	pET26	HC1986	30kan
rc*h*TPH1/*Nde*I/*Xho*I	pET26	HC1964	30kan
r*h*TPH1/*Nde*I/*Bam*HI (frGFP fusion)	pWaldo-dGFP	HC1785	30kan
L24R/V28R-r*h*TPH1-frGFP	pWaldo-dGFP	HC2346	30kan
L31R/L35R-r*h*TPH1-frGFP	pWaldo-dGFP	HC2373	30kan
V28R/L31R-r*h*TPH1-frGFP	pWaldo-dGFP	HC2344	30kan
r*h*TPH1/*Bam*HI/*Xho*I (GST fusion)	pGEX-5X-1	HC2477	100amp
***h*TPH2$_{59-490}$/*Nde*I/*Dra*I**	pET26	HC1659	30kan
***h*TPH2$_{90-490}$/*Nde*I/*Dra*I**	pET26	HC2462	30kan

5.7 Summary and conclusion

Construction of the *h*TPH expression strains for expression of the 10 *h*TPH variants was successfully accomplished. These strains are tested for expression and solubility as described in chapter 6.

Table 5.9 summarizes all constructed cloning and expression strains with the latter highlighted in red.

Table 5.9. Summary of all constructed cloning and expression strains with the latter highlighted in red.

Gene	Cloning and expression vectors	Glycerol stock number	*E. coli* host cells	Antibiotic marker
r*h*TPH1	PCR-script-r*h*TPH1	HC1717	DH5α	100amp
	pET26-r*h*TPH1	HC1803	DH5α	100amp
	pET26-r*h*TPH1	HC1869	BL21(DE3)	30kan
rc*h*TPH1	PCR-script-rc*h*TPH1	HC1966	DH5α	100amp
	pET26-rc*h*TPH1	HC1983	DH5α	100amp
	pET26-rcTPH1	HC1986	BL21(DE3)	30kan
ct*h*TPH1	PCR-script-ctTPH1	HC1938	DH5α	100amp
	pET-ctTPH1	HC1949	DH5α	100amp
	pET26-ctTPH1	HC1964	BL21(DE3)	30kan
r*h*TPH1-frGFP	PCR-script-rTPH1	HC1710	DH5α	100amp
	pWaldo-rTPH1-GFP	HC1747	DH5α	100amp
	pWaldo-rTPH1-GFP	HC1785	BL21(DE3)	30kan
L24R/V28R-r*h*TPH1-GFP	PCR-script-m1-rTPH1	HC2288	DH5α	100amp
	pWaldo-m1-rTPH1-GFP	HC2241	DH5α	100amp
	pWaldo-m1-rTPH1-GFP	HC2346	BL21(DE3)	30kan
L31R/L35R-r*h*TPH1-GFP	PCR-script-m2-rTPH1	HC2330	DH5α	100amp
	pWaldo-m2-rTPH1-GFP	HC2353	DH5α	100amp
	pWaldo-m2-rTPH1-GFP	HC2373	BL21(DE3)	30kan
V28R/L31R-r*h*TPH1-GFP	PCR-script-m3-rTPH1	HC2298	DH5α	100amp
	pWaldo-m3-rTPH1-GFP	HC2338	DH5α	100amp
	pWaldo-m3-rTPH1-GFP	HC2344	BL21(DE3)	30kan
GST-r*h*TPH1	PCR-script-rTPH1	HC2467	DH5α	100amp
	pGEX-5X-1-GST-rTPH1	HC2472	DH5α	100amp
	pGEX-5X-1-GST-rTPH1	HC2477	BL21(DE3)	100amp
***h*TPH2$_{59-490}$**	PCR-script-TPH2$_{59-490}$	HC1588	DH5α	100amp
	pET26-TPH2$_{59-490}$	HC1640	DH5α	100amp
	pET26-TPH2$_{59-490}$	HC1659	BL21(DE3)	30kan
***h*TPH2$_{90-490}$**	PCR-script-TPH2$_{90-490}$	HC2446	DH5α	100amp
	pET26-TPH2$_{90-490}$	HC2454	DH5α	100amp
	pET26-TPH2$_{90-490}$	HC2462	BL21(DE3)	30kan

6 Expression and solubility test

Expression and solubility test are conducted in order to analyze the expression level as a function of time as well as the solubility of each *h*TPH variant constructed in chapter 5. This chapter describes the experimental procedures for expression and solubility test of the *h*TPH expression strains, followed by a result and discussion section.

6.1 Experimental procedures

Most of the procedures are described in general with important points highlighted for the specific *h*TPH gene variants. Protocols, alike or with only minor adjustment from the standard protocols obtained from the supplier, are not given in full but only referred to.

6.1.1 Materials and chemicals

All work with bacteria was carried out in a sterile environment. Materials were handled under a LAF bench and sterilization of growth media, antibiotics and water were done by autoclaving or filter sterilization. All solutions were prepared with 18.2 MΩ cm water from a Milli-Q synthesis A10 Q-Gard system (Millipore).

6.1.2 Expression and solubility test

6.1.2.1 Test expression and solubility test

The constructed expression strains were tested for expression of the recombinant protein at both 30^{o}C and 20^{o}C. The cells were streaked on agar plates with appropriate antibiotic and incubated overnight at 37^{o}C. A single colony was transferred to a 250 ml flask with 50 ml LB media with appropriate antibiotic (given in table 6.1) and incubated with shaking at 250 rpm and 30^{o}C. After approximately 3½ hour the temperature, for the cultures to be induced at 20^{o}C, was set to 20^{o}C.

When the OD_{600} was between 0.4 and 0.6, 25 µl 200 mM IPTG was added to a final concentration of 0.1 mM. To estimate the expression level as a function of time samples were collected prior to induction (50 µl samples) and during induction (25 µl samples). The samples were centrifuged at 13,000 rpm for 1 min, the supernatant removed and the pellet was kept at -20°C until further analysis (described in section 6.1.2.3). After overnight induction the cells were harvested by centrifugation at +4°C and 3000 x g for 15 min. The cells were resuspended in appropriate ice cold buffer, transferred to 50 ml polypropylene tubes and centrifuged at +4°C and 3000 x g for 15 min. The supernatant was discarded. The cells were resuspended in 40 ml buffer and sonicated 3 x 30 sec on ice using a labsonic ultrasonic homogenizer (Satorius AG). The cell extract was centrifuged for 20 min at 18,000 x g and +4°C. The supernatant and pellet were separated and the pellet was resuspended in 40 ml buffer. 20 µl samples were taken from the cell extract, supernatant and resuspended pellet and kept at -20°C for SDS-Page analysis.

6.1.2.2 Solubility test on large scale expression

After test expression and solubility test on small scale cultures and determination of induction time and temperature (section 6.1.2.1) the solubility was tested on large scale cultures (650 ml). The same volume of buffer (40 ml) was used in the sonication process for both small scale and large scale cultures. Therefore, large scale solubility test was performed to see if there was any change in solubility when the ratio between the amount of cells and buffer volume was increased.

From a frozen glycerol stock containing *E. coli* BL21(DE3) cells expressing the *h*TPH variants were streaked into single colonies on agar plates with appropriate antibiotic and incubated overnight at 37°C. A single colony was transferred to a 250 ml flask with 50 ml LB media with appropriate antibiotic and incubated at 37°C and 250 rpm for approximately 4 hours until an OD_{600} of 0.6-1.0 was reached. The cells were transferred to a 50 ml polypropylene tube and sedimented by centrifugation at +4°C and 3000 x g for 10 min. The cells were resuspended in 50 ml fresh LB media with appropriate antibiotic and 6.5 ml of the resuspended cells were used to inoculate 650 ml LB media with appropriate antibiotic in a 2 L shake flask. The cultures were incubated at 30°C and 250 rpm. After approximately 3½ hour the temperature was lowered to 20°C for the cultures to be induced at 20°C. In table 6.1 the induction temperature and induction time for each strain are given. When OD_{600} was between 0.4-0.6 the expression was induced by adding IPTG to a final concentration of 0.1 mM. After induction the cells were harvested by centrifugation at +4°C and 3000 x g for 15 min. The cells were resuspended in ice cold appropriate buffer, transferred to 50 ml polypropylene tubes and centrifuged again at 4°C and 3000 x g for 15 min. The supernatant was discarded and the cells stored at -80°C until further use.

Cells from a 650 ml culture was thawed on ice and resuspended in 40 ml buffer. The cells were sonicated 3 x 30 sec on ice. The cell extract was centrifuged for 20 min at 18,000 x g and 4°C. The supernatant and pellet were separated and the pellet was resuspended in 40 ml buffer. 20 µl samples were taken from the cell extract, supernatant and resuspended pellet and kept at -20 °C for SDS-Page analysis.

Table 6.1. Stock number, induction temperature and induction time for each *h*TPH variant.

Variant	Stock number	Antibiotic marker	Induction temperature	Induction time
***h*TPH1**	HC1083	30kan	20°C	18 hours
rc*h*TPH1	HC1986	30kan	20°C	18 hours
r*h*TPH1	HC1869	30kan	20°C	18 hours
c*h*TPH1	HC1962	30kan	30°C	4 hours
ct*h*TPH1	HC1964	30kan	30°C	4 hours
r*h*TPH1-frGFP	HC1785	30kan	20°C	18 hours
L24R/V28R-r*h*TPH1-frGFP	HC2346	30kan	20°C	18 hours
L31R/L35R-r*h*TPH1-frGFP	HC2373	30kan	20°C	18 hours
V28R/L31R-r*h*TPH1-frGFP	HC2344	30kan	20°C	18 hours
GST-r*h*TPH1	HC2477	100amp	20°C	18 hours
***h*TPH2$_{59-490}$**	HC1659	30kan	20°C	18 hours
***h*TPH2$_{90-490}$**	HC2462	30kan	20°C	18 hours

6.1.2.3 SDS-Page analysis

The collected samples from section 6.1.2.1 and section 6.1.2.2 were analyzed by SDS-Page. Tris-HCl gels from Bio-Rad were used and 7.5 %, 12 % or 18 % were chosen for optimal separation region corresponding to the size of the protein of interest. The analysis was done as described in section 4.2.7.

6.2 Results and discussion

Each of the 10 expression strains described in chapter 5 was tested for expression of target protein and the expression level was analyzed as a function of time. The solubility of each variant was also tested. This was done as described in section 6.2.1. The results obtained are described in the following sections.

6.2.1 *h*TPH1 variants

The three expression strains, HC1869, HC1986 and HC1964 constructed as described in chapter 5 were tested for expression of r*h*TPH1, rc*h*TPh1 and ct*h*TPH1, respectively and the solubility from small scale cultures examined in 20 mM Tris/H_2SO_4 pH 8.5. A pH value of 8.5 was chosen due to the theoretical pI value of the three variants of 7.15, 6.64 and 6.78, respectively, and because full-length has shown to be more soluble at high pH and because c*h*TPH1 is purified at this pH [14]. The expression and solubility test was done as described in section 6.1.2.1.

6.2.1.1 r*h*TPH1

The SDS-Page analysis of the expression level of r*h*TPH1 (11 kDa) is shown as a function of time at 20°C and 30°C in figure 6.1 as well as the result from solubility test from small scale cultures (50 ml). From the increased intensity of the marked band corresponding to the size of r*h*TPH1 (11 kDa) in figure 6.1 it is seen that r*h*TPH1 can be expressed with almost the same expression level at 30°C and at 20°C. Furthermore, the intensity of the bands has reached a stabile level after 19 hours for expression at 20°C and after 4 hours for expression at 30°C. By comparing the solubility

of r*h*TPH1 expressed at 20°C and 30°C it is seen that r*h*TPH1 is expressed in a soluble form at 20°C and that almost all r*h*TPH1 is soluble by expression at 30°C. Therefore, for further studies of r*h*TPH1 it was chosen to use an induction time of approximately 19 hours at 20°C.

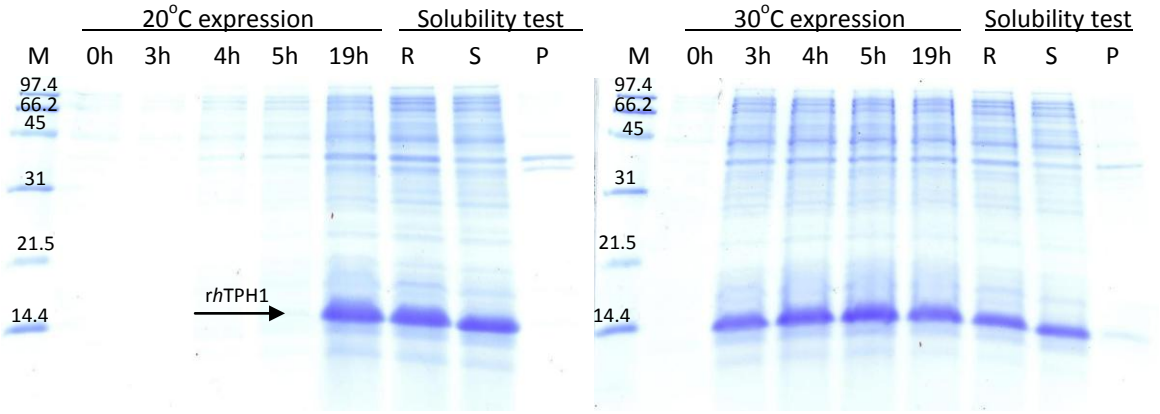

Figure 6.1. SDS-Page analysis of the expression level as a function of time and small scale solubility test of r*h*TPH1 for the expression strain HC1869 at both 20°C and 30°C. During test expression samples were collected after 0, 3, 4, 5 and 19 hours (h). M is the molecular weight standard given in kDa, R is the raw extract (total amount of expressed protein), S is the supernatant (soluble fraction) and P is pellet (insoluble fraction).

6.2.1.2 rc*h*TPH1

The SDS-Page analysis of the expression level of rc*h*TPH1 (47 kDa) is shown as a function of time expressed at 20°C and 30°C in figure 6.2. Also the result from the solubility test from small scale cultures is shown on the SDS-Page analysis in figure 6.2. From the increased intensity of the marked band corresponding to the size of rc*h*TPH1 (47 kDa) in figure 6.2 it is seen that rc*h*TPH1 can be expressed with almost the same expression level at 30°C and at 20°C. Furthermore, the intensity of the band has reached a stabile level after 18 hours for expression at both 20°C and 30°C. By comparing the solubility of rc*h*TPH1 at 20°C and 30°C ¾ of rc*h*TPH1 is expressed in a soluble form at 20°C whereas only half of the rc*h*TPH1 is expressed in a soluble form at 30°C. Therefore, for further studies of rc*h*TPH1 it was chosen to use an induction time of approximately 18 hours at 20°C.

6.2.1.3 ct*h*TPH1

The SDS-Page analysis of the expression level of ct*h*TPH1 (39.4 kDa) as a function of time expressed at 20°C and 30°C is given in figure 6.3 together with the results from the solubility test from small scale cultures. From the increased intensity of the marked band corresponding to the size of ct*h*TPH1 (39.4 kDa) in figure 6.3 it is seen that ct*h*TPH1 can be expressed with almost the same expression level at 30°C and at 20°C. Furthermore, the intensity of the band has reached a stabile level after 18 hours for expression at 20°C and after 4 hours for expression at 30°C. Approximately half of ct*h*TPH1 is soluble at both 20°C and 30°C. For further studies of ct*h*TPH1 expression at 30°C with an induction time of approximately 4 hours was chosen. The expression level is also observed to be much lower for this variant compared to r*h*TPH1 in figure 6.1 and rc*h*TPH1 in figure 6.2 (further explained in section 6.2.1.4).

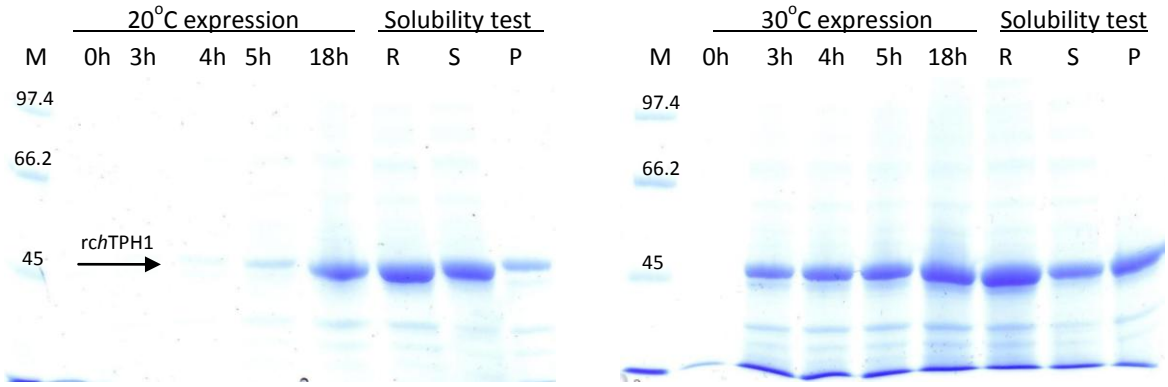

Figure 6.2. SDS-Page analysis of the expression level as a function of time and small scale solubility test of rc*h*TPH1 for the expression strain HC1986 at both 20°C and 30°C. During test expression of the strain samples were collected after 0, 3, 4, 5 and 18 hours (h). M is the molecular weight standard given in kDa, R is the raw extract (total amount of expressed protein), S is the supernatant (soluble fraction) and P is pellet (insoluble fraction).

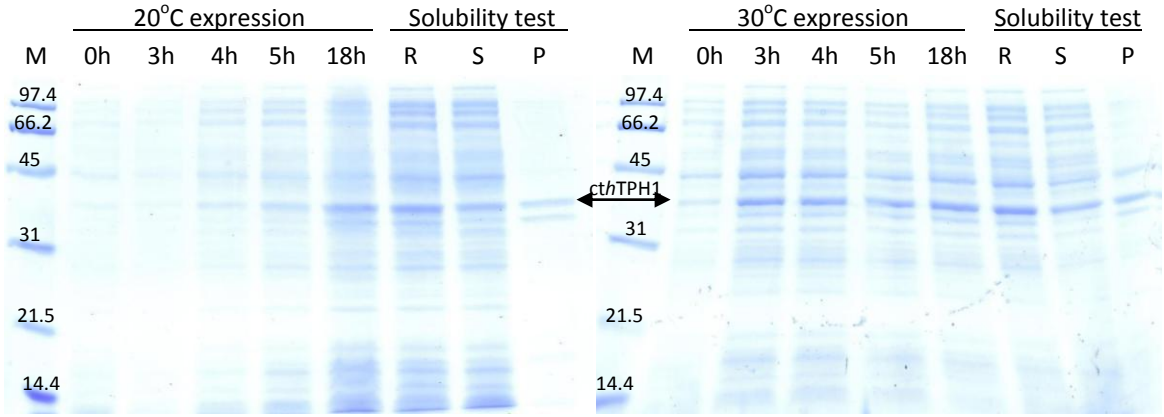

Figure 6.3. SDS-Page analysis of the expression level as a function of time and small scale solubility of ct*h*TPH1 for the expression strain HC1964 at both 20°C and 30°C. During test expression of the strain samples were collected after 0, 3, 4, 5 and 18 hours (h). M is the molecular weight standard given in kDa, R is the raw extract (total amount of expressed protein), S is the supernatant (soluble fraction) and P is pellet (insoluble fraction).

6.2.1.4 Summary and overall discussion

All three variants can be expressed in a soluble form. Solubility test on large scale cultures did not show any change in solubility (data not shown). Comparing the three variants constructed in this project a higher expression level is seen for the three variants containing the regulatory domain. By comparing the total amount of expressed protein (R) it is seen that the two variants containing the regulatory domain all expresses more protein than ct*h*TPH1 (as mentioned in section 6.2.1.3). This pattern is also observed between full-length *h*TPH1 and c*h*TPH1 [14]. All five genes are cloned in a pET26 expression vector as *Nde*I/*Xho*I fragments and expressed using *E. coli* BL21(DE3) expression strains. The difference in expression level could be due to differences in the AT content in the TIR of the variants [117,118,119]. Comparing the first 12 nucleotides in the regulatory domain with the first 12 in the catalytic domain it is seen that the regulatory domain has 8 A and T's whereas the catalytic domain only has 6, see table 6.2. This could mean that an

increased amount of A and T in the first 12 nucleotides of both c*h*TPH1 and ct*h*TPH1 can increase the expression level of c*h*TPH1 and ct*h*TPH1. It was tried to increase the AT content in c*h*TPH1 by changing the first nine nucleotides to the same nucleotides that exist in the N-terminal of *h*TPH1. This project was a part of our laboratory technician Kathrine's project [125]. I planned the strategy and helped her with the construction of the three strains. It indeed showed an increase in the expression level (data not shown) [125].

Table 6.2. The first 12 nucleotides from the TIR, the amount of expressed protein and the A/T content for each of the five *h*TPH1 variants

Variant	First 12 bases	Amount of expressed protein	AT content
r*h*TPH1			
rc*h*TPH1	ATT GAA GAC AAC	++++	8
***h*TPH1**			
c*h*TPH1			
ct*h*TPH1	GAT GGC ATG GAA	+	6

The amount of soluble protein increases from rc*h*TPH1 to r*h*TPH1. This pattern could be due to the interaction with other molecules, which increases the size of the protein and thereby decreasing the solubility, also given in table 6.3. In order to understand the behavior of the regulatory domain and because the r*h*TPH1 showed to be more soluble it was chosen to continue with this variant for further purifications attempt (see chapter 7).

Table 6.3. List of the three variants of *h*TPH1 with the amount of expressed and soluble protein.

Variant	Expressed protein	Solubility
rc*h*TPH1	++++	++
r*h*TPH1	++++	++++
ct*h*TPH1	+	++

6.2.2 r*h*TPH1-frGFP variants

6.2.2.1 r*h*TPH1-frGFP

In order to understand the behavior of r*h*TPH1 during purification (see chapter 7) it was chosen to construct a fusion protein of r*h*TPH1 fused to frGFP as explained in chapter 5. This was done because it was difficult to follow r*h*TPH1 during purification. The r*h*TPH1-frGFP expression strain (HC1785) was tested for expression as a function of time and the solubility was tested on small scale cultures as described in section 6.1.2.1. The result is shown on the SDS-Page analysis in figure 6.4. From the increased intensity of the marked band (r*h*TPH1-frGFP – 41 kDa) it is seen that r*h*TPH1-frGFP can be expressed at a higher level at 30°C than at 20°C. Furthermore, the intensity of the band has reached a stabile level after 19 hours for expression at 20°C and after 4 hours for expression at 30°C. Comparing the solubility of r*h*TPH1-frGFP at 20°C and 30°C it is seen that approximately 75 % of r*h*TPH1-frGFP is soluble when expressed at 20°C and that almost all rTPH1-frGFP is insoluble when expressed at 30°C. The high amount of insoluble r*h*TPH1fr-GFP at

30°C is mainly due to frGFP and not r*h*TPH1, as seen in figure 6.5 and 6.1, where the expression level as a function of time and the solubility of frGFP and r*h*TPH1 is shown. Therefore, for further studies of r*h*TPH1-GFP expression at 20°C is used with an induction time of approximately 19 hours.

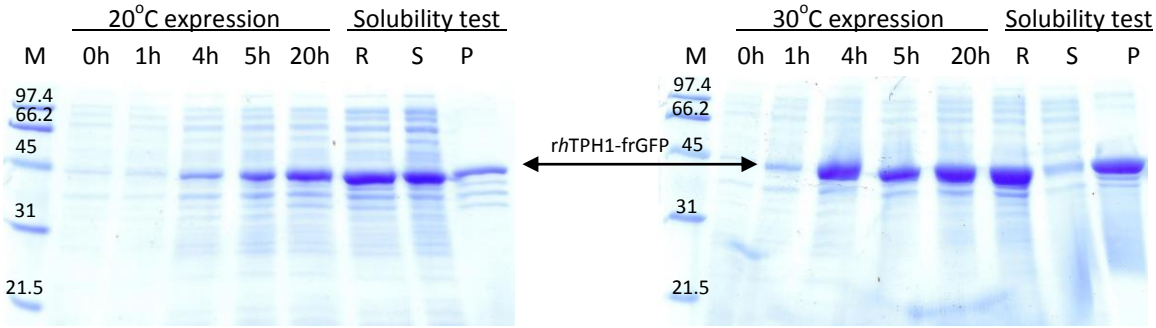

Figure 6.4. SDS-Page analysis of the expression level as a function of time and small scale solubility test of r*h*TPH1-frGFP for the expression strains HC1785 at both 20°C and 30°C. During test expression of the strain samples were collected after 0, 3, 4, 5 and 20 hours (h). M is the molecular weight standard given in kDa, R is the raw extract (total amount of expressed protein), S is the supernatant (soluble fraction) and P is pellet (insoluble fraction).

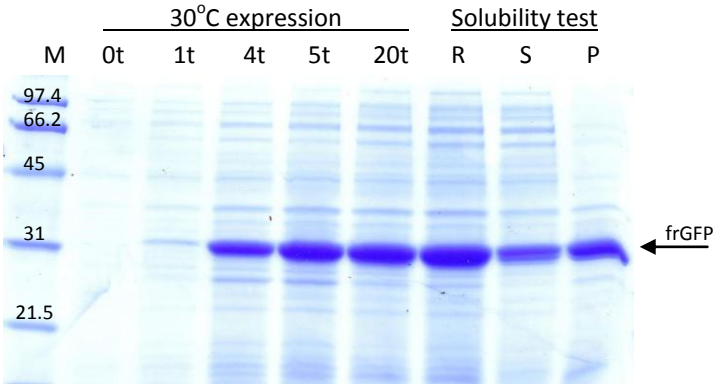

Figure 6.5. SDS-Page analysis of the expression level as a function of time and small scale solubility test of frGFP at 30°C. During test expression of the strain samples were collected after 0, 1, 4, 5 and 20 hours (h). M is the molecular weight standard given in kDa, R is the raw extract (total amount of expressed protein), S is the supernatant (soluble fraction) and P is pellet (insoluble fraction).

6.2.2.2 Mutation in the 3,4-hydrophobic repeat in r*h*TPH1

Purification of r*h*TPH1-GFP (chapter 7) shows a broad elution pattern in the anion exchange, which is also observed in the purification of *h*TPH1 (see chapter 4). This can be a result of hydrophobic interaction of the 3,4-hydrophibic face with other hydrophobic molecules in different oligomer forms as mentioned in chapter 5 and discussed in my master project [14]. By mutations in the hydrophobic face these interactions could be decreased and therefore

formation of large oligomer forms could to some extent be eliminated. The mutants are constructed in order to "disrupt" the hydrophobic surface and to see which, if any, of the amino acids that are involved in the hydrophobic interactions. The hydrophobic residues are mutated to the positive residue arginine.

Three different expression strains for expression of mutants of r*h*TPH1-frGFP were constructed, each containing two mutations in the hydrophobic repeat. The three expression strains HC2346, HC2373 and HC2344 were tested for expression of L24R/V28R-r*h*TPH1-frGFP, L31R/L35R-r*h*TPH1-frGFP and V28R/L31R-r*h*TPH1-frGFP, respectively as a function of time (data not shown). The optimal induction time were determined to approximately 19 hours at 20°C. The expression level and the solubility from large scale expression in 20 mM Tris/H_2SO_4 pH 8.5 were tested as described in section 6.1.2.2 for each mutant and compared with r*h*TPH1-frGFP. The SDS-Page analysis is shown in figure 6.6 and on the pictures shown in figure 6.7.

By comparing the total amount of expressed protein (R) it is seen that all four variants expresses the same amount of protein, but by comparing the raw extract (R) with the supernatant (S) and pellet (P) the three mutant of r*h*TPH1-frGFP shows that all the expressed protein is insoluble. From figure 6.7 it is also seen that the intensity of the green fluorescence of L24R/V28R-r*h*TPH1-frGFP, L31R/L35R-r*h*TPH1-frGFP and V28R/L31R-r*h*TPH1-frGFP is less intensive than r*h*TPH1-frGFP. By incorrectly folding of the target protein frGFP is not correctly folded and thereby it cannot be fluorescent (described in section 5.3.1). From these results it can be concluded that the mutants are not folded correctly and it shows that the 3,4-hydrophobic domain of r*h*TPH1 must be important for correct folding of the full-length protein. No further work is done with the mutants.

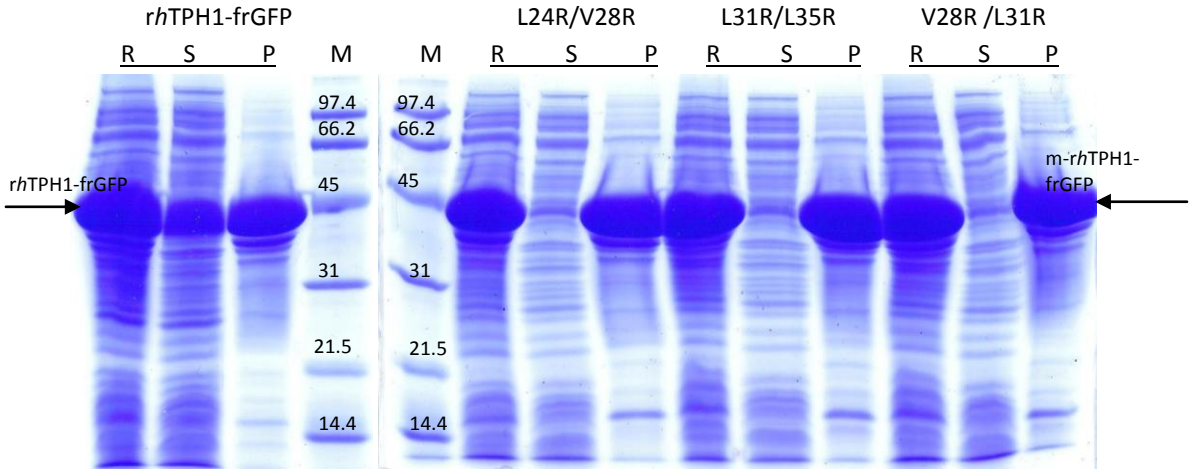

Figure 6.6. SDS-Page analysis of the expression level and solubility of r*h*TPH1-frGFP (HC1785), L24R/V28R-r*h*TPH1-frGFP (HC2346), L31R/L35R-r*h*TPH1-frGFP (HC2373) and V28R/L31R-r*h*TPH1-frGFP (HC2344) at 20°C from large scale expression. M is the molecular weight standard given in kDa, R is the raw extract (total amount of expressed protein), S is the supernatant (soluble fraction) and P is pellet (insoluble fraction).

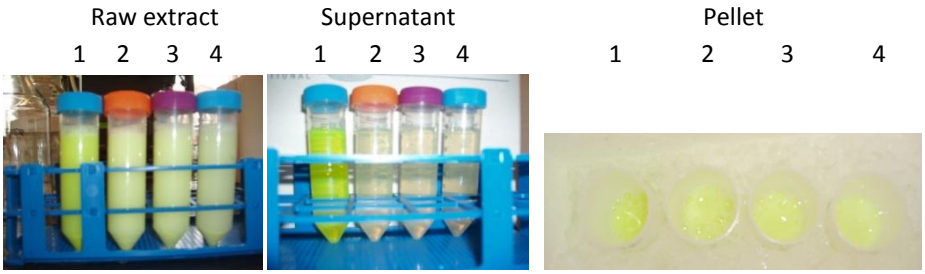

Figure 6.7. Expression test showing the intensity in the raw extract (R), supernatant (S) and resuspended pellet (P) of the four r*h*TPH1-GFP variants, where 1 is r*h*TPH1-frGFP, 2 is L24R/V28R-r*h*TPH1-frGFP, 3 is L31R/L35R-r*h*TPH1-frGFP and 4 is V28R/L31R-r*h*TPH1-frGFP.

6.2.2.3 Summary

r*h*TPH1 was fused to frGFP in order to visualize the protein during purification. The variant could be expressed in a soluble form and with the soluble form colored green indicating that the protein was correctly folded, see chapter 5.1.3. Three mutants of the regulatory domain were constructed and fused to frGFP. They could be expressed but in an insoluble form. From the intensity of the color it is observed that these variants are not correctly folded. Therefore only the r*h*TPH1-frGFP without mutation is used for further work in this project.

6.2.3 GST-r*h*TPH1

Anion exchange of r*h*TPH1 and r*h*TPH1-GFP showed that the variants binds throughout the column and elutes over a large volume indicating that they exist in different forms either by intersubunit interactions or interactions with other compounds present in the raw extract (see chapter 7). Based on this result it was decided to construct a variant which can be purified with a high content of salt in the first purification step. It was chosen to construct a fusion protein of r*h*TPH1 fused to GST in the N-terminal end, as described in section 5.1.4.

The expression strain HC2477 (chapter 5) was tested for expression of GST-r*h*TPH1 as described in section 6.2.1.2 at 20^{o}C. The result is shown on the SDS-Page analysis on figure 6.8 where the expression level of GST-r*h*TPH1 (37 kDa) is shown as a function of time. From the increased intensity of the marked band on figure 6.8 it is seen that GST-r*h*TPH1 is expressed. Furthermore, the intensity of the band reaches a stabile level after 18 to 19 hours. A band corresponding to the size of 26 kDa is also seen on the SDS-Page analysis with an increased intensity over time, but has not been identified. It corresponds to the size of GST (26 kDa). The solubility from large scale cultures was also tested as described in section 6.2.1.2 using 1xPBS, 300 mM $(NH_4)_2SO_4$ pH 8.0 and shown in figure 6.8. It is seen that almost all of the GST-r*h*TPH1 fusion protein is expressed in a soluble form.

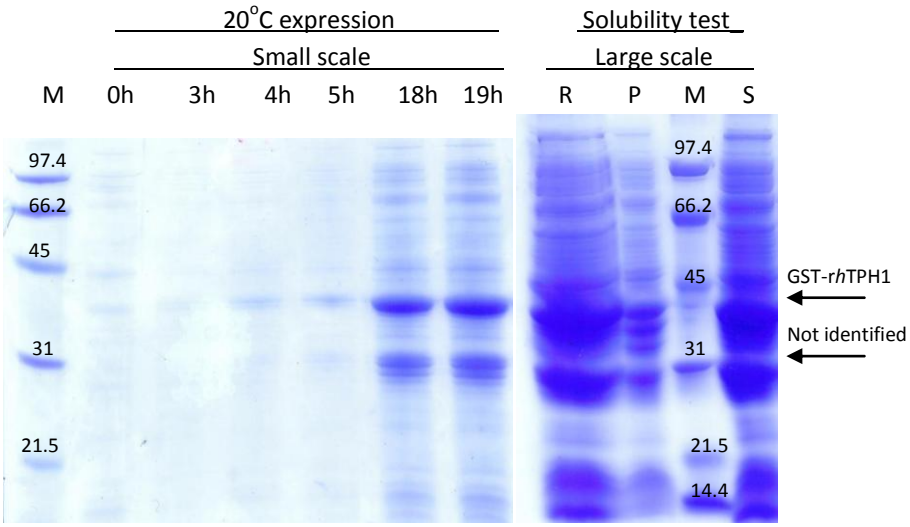

Figure 6.8. SDS-Page analysis of the expression level as a function of time and small scale solubility of GST-r*h*TPH1 for the expression strain HC2477 at 20°C. During test expression of the strain samples were collected after 0, 3, 4, 5 and 18 or 19 hours (h). M is the molecular weight standard given in kDa, R is the raw extract (total amount of expressed protein), S is the supernatant (soluble fraction) and P is pellet (insoluble fraction). 20 µl was loaded from the expression test, whereas 5 µl was loaded from the solubility test.

6.2.4 *h*TPH2 variants

Two different expression strains were constructed for expression of *h*TPH2$_{59\text{-}490}$ (HC1659) and *h*TPH2$_{90\text{-}490}$ (HC2462), as described in chapter 5, and tested for expression as described in section 6.2.1.2. From small scale expression it was concluded that optimal expression conditions were 20°C for approximately 19 hours (data not shown).

The expression level and the solubility of both variants from large scale expression were examined, as described in section 6.2.1.2, and compared with *h*TPH2 (56 kDa) and ct*h*TPH2 (39.8 kDa). ct*h*TPH2 and *h*TPH2 were expressed at 20°C for approximately 19 hours. The solubility of *h*TPH2$_{59\text{-}490}$ (49.7 kDa) and *h*TPH2$_{90\text{-}490}$ (46.3 kDa) were examined in 20 mM BisTris/H_2SO_4 pH 7.2 and 20 mM Tris/H_2SO_4 pH 8.5 and compared with the solubility of ct*h*TPH2 and *h*TPH2 in 20 mM BisTris/H_2SO_4 pH 7.2. The solubility was tested at two different pH values because both c*h*TPH2 and ct*h*TPH2 is purified at pH 7.2, whereas c*h*TPH1 is purified in the anion exchange at pH 8.5. The theoretical pI value is 5.68 for *h*TPH2$_{59\text{-}490}$ and 5.39 for *h*TPH2$_{90\text{-}490}$.

Results of the solubility test are shown in figure 6.9. By comparing the amount of soluble protein of each *h*TPH2 variant it is seen that 50 % of ct*h*TPH2 is expressed in a soluble form, whereas almost all of the other three variants are expressed in an insoluble form. This means that the residues from 90 to 146 (part of the regulatory domain, se figure 2.2) is important for the solubility of the variants. It could therefore be interesting to construct variants of *h*TPH2 which is truncated different places in the regulatory domain from residue 90 to 146 in order to determine which residues that causes the change of the protein from being insoluble to soluble.

No further work is done with these two variants.

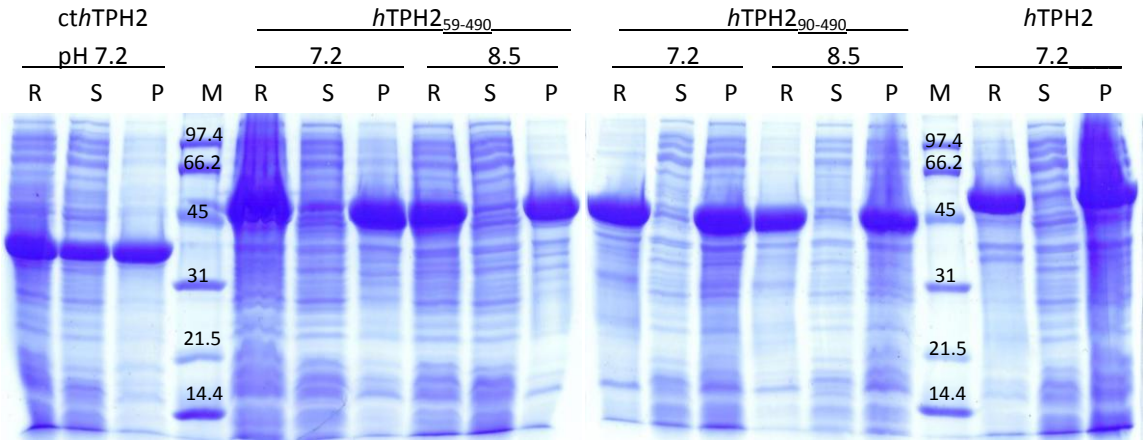

Figure 6.9. SDS-Page analysis of the expression level and solubility of *h*TPH2$_{59-490}$ (HC1659), *h*TPH2$_{90-490}$ (HC2462), *h*TPH2 and ct*h*TPH2 at 20°C for approximately 19 hours from large scale expression. The solubility was examined at pH 7.2 for c*h*TPH2 and *h*TPH2 and at 7.2 and 8.5 for *h*TPH2$_{59-490}$ (HC1659), *h*TPH2$_{90-490}$ (HC2462). M is the molecular weight standard given in kDa, R is the raw extract (total amount of expressed protein), S is the supernatant (soluble fraction) and P is pellet (insoluble fraction).

6.3 Summary and conclusion

All *h*TPH variants constructed in chapter 5 were tested for expression and solubility and all variant could be expressed at both 20°C and 30°C. The r*h*TPH1, rc*h*TPH1, ct*h*TPH1, r*h*TPH1-GFP an GST-r*h*TPH1 could be expressed in a soluble form whereas the three mutants of r*h*TPH1 and the two *h*TPH2 variants could not be expressed in a soluble form. These results showed that point mutations in the regulatory domain as well as truncations in the N-terminal have a negative influence on the solubility. It was chosen not to continue with these 5 insoluble variants.

For the further work in this project and to understand the behavior of the regulatory domain the three variants; r*h*TPH1, r*h*TPH1-frGFP and GST-r*h*TPH1 are used and the purification of these are described in chapter 7. In table 6.4 the variants used further in this project is given including their stock number, expression temperature and induction time as well as antibiotic selective marker.

Table 6.4. The three variants which is used further for purification (chapter 7) including their stock number, expression temperature and induction time as well as antibiotic marker.

Variant	Stock number	Expression temperature	Induction time	Antibiotic
r*h*TPH1	HC1869	20°C	19 hours	30 kan
r*h*TPH1-frGFP	HC1785	20°C	19 hours	30 kan
GST-r*h*TPH1	HC2477	20°C	19 hours	100 Amp

7 Purification of r*h*TPH1 variants

To understand the properties of *h*TPH1, a "divide-and-conquer" strategy was applied and different truncated variants of *h*TPH were constructed. The variants were exposed to solubility test and from these results it was chosen to use the regulatory domain of *h*TPH1 (r*h*TPH1) for further investigations due to its high solubility of the variant and because elucidating the properties of this domain could help understanding full-length TPH.

The purification strategy has evolved throughout this project based on results obtained. In this chapter the strategies behind purification of r*h*TPH1 are presented as well as the experimental procedures followed by a result and discussion section.

7.1 Introduction to the variants

The purification trials of r*h*TPH1 were based on the purification strategy of c*h*TPH1 developed in my master project [14]. It is a two step procedure consisting of an anion exchange followed by gel filtration.

Three different constructs of the regulatory domain are used: The r*h*TPH1 variant as well as two fusions proteins, r*h*TPH1-frGFP and GST-r*h*TPH1, respectively. These were constructed as described in chapter 5 and tested for expression and solubility as described in chapter 6. Table 7.1 lists the molecular mass, theoretical pI value and extinction coefficients for each variant. r*h*TPH does not contain tryptophan or tyrosine residues and therefore the extinction coefficient at 280 nm is zero (see table 7.1). Despite this, comparing the absorbance at 280 nm and 236 nm (peptide backbone) it is expected to be possible to follow the elution of r*h*TPH1.

Table 7.1. List of the monomer molecular mass of the three r*h*TPH1 variants as well as their theoretical pI value, extinction coefficients and stock numbers used in the experimental part.

Variant	Description	Stock number	Molecular mass	Theoretical pI value	Extinction coefficients at 280 nm*
r*h*TPH1	Regulatory domain of tryptophan hydroxylase isoform 1	HC1869	11599.86 Da	7.15	0
r*h*TPH1-frGFP	Fusion protein: Regulatory domain of tryptophan hydroxylase isoform 1 fused to the green fluorescence protein in the C-terminal	HC1785	40976.52 Da	6.37	23380
GST-r*h*TPH1	Fusion protein: Regulatory domain of tryptophan hydroxylase isoform 1 fused to glutathione S-transferase in the N-terminal	HC2477	38116.37 Da	6.30	42860

*Calculated from the equation given in [126] without taking into account the cystine residues.

7.2 Experimental procedures

7.2.1 Materials

Factor Xa was obtained from Qiagen. LB media and all other chemicals were obtained from Sigma-Aldrich. The chemicals were analytical grade. All solutions were prepared using 18.2 MΩ cm water from a Milli-Q synthesis A10 Q-Gard system (Millipore). All work with bacteria was carried out in a sterile environment. Materials were handled in a LAF bench and sterilization of growth media, antibiotics and water were done by autoclaving or filter sterilization.

7.2.2 Expression

Cells from a frozen glycerol stock containing *E. coli* BL21(DE3) expressing either r*h*TPH1, r*h*TPH1-GFP or GST-r*h*TPH1 were streaked into single colonies on LB agar plates with appropriate antibiotic (see table 7.2) and incubated overnight at 37°C. A single colony was inoculated in 50 ml LB media with appropriate antibiotic in a 250 ml shake flask and incubated at 37°C, 250 rpm until an OD_{600} of 0.6-1.0 was reached. The cells were transferred to a 50 ml polypropylene tube and sedimented by centrifugation at +4°C and 3000 x g for 10 min. The cells were resuspended in 50 ml fresh LB media with appropriate antibiotic and 6.5 ml of the resuspended cells were used to inoculate 650 ml LB media containing appropriate antibiotic in a 2 L shake flask. The cultures were incubated at 30°C and 250 rpm. After approximately 3½ hour the temperature was lowered to 20°C. When OD_{600} of 0.4-0.6 was attained r*h*TPH1 expressions was induced by addition of IPTG to a final concentration of 0.1 mM. After induction at 20°C and 250 rpm for 18 hours, the cells were harvested by centrifugation at +4°C and 3000 x g for 15 min. The cells were resuspended in ice cold 20 mM Tris/H_2SO_4 pH 8.5, transferred to 50 ml polypropylene tubes and centrifuged

again at +4°C and 3000 x g for 15 min. The supernatant was discarded and the cells stored at -80°C until further use.

In table 7.2 the induction temperature and time as well as appropriate antibiotic for each strain are given.

Table 7.2. Expression condition for each of the three r*h*TPH1 variants.

Strain	Induction time	Induction temperature	Antibiotic
r*h*TPH1	18 hours	20°C	30 kan
r*h*TPH1-frGFP	18 hours	20°C	30 kan
GST-r*h*TPH1	18 hours	20°C	100 amp

7.2.3 Preparation of raw extract

7.2.3.1 Preparation of r*h*TPH1 and r*h*TPH1-frGFP

Cells from a 650 ml culture containing either r*h*TPH1 or r*h*TPH1-frGFP (section 7.2.2) were resuspended in 20 mM Tris/H_2SO_4 pH 8.5 (buffer A) to a total volume of 40 ml and lysed on ice by sonication for 3 x 30 sec. The cell extract was centrifuged in a high-speed centrifuge tube at 18000 x g and +4°C for 20 min. The supernatant was recovered and centrifuged again as above. The supernatant was collected and filtered through a 0.45 µm filter and diluted to conductivity less than 1 mS/cm.

7.2.3.2 Preparation of GST-r*h*TPH1

Cells from a 650 ml culture containing GST-r*h*TPH1 (section 7.2.2) were resuspended in 1xPBS, 300 mM $(NH_4)_2SO_4$ pH 8.0 (buffer A) to a total volume of 40 ml and lysed on ice by sonication for 3 x 30 sec. The cell extract was centrifuged in a high-speed centrifuge tube at 18000 x g and +4°C for 20 min. The supernatant was recovered and centrifuged again as above. After the second centrifugation the supernatant was collected and filtered through a 0.45 µm.

7.2.4 Purification of r*h*TPH1

7.2.4.1 Anion exchange

Cells from a 650 ml culture were prepared as described in section 7.2.3.1. The filtered and diluted supernatant was loaded onto a Q Sepharose High Performance 16/10 column, which was equilibrated in 20 mM Tris/H_2SO_4 pH 8.5. A linear gradient of 0-10 % of 20 mM Tris/NaOH, 0.8 M $(NH_4)_2SO_4$ pH 8.5 (buffer B) over 12 CV followed by a linear gradient of 20-100 % of buffer B over 2 CV was applied to the column. From the supernatant loaded onto the column, the flow-through and each top in the chromatogram samples were analyzed by SDS-Page.

7.2.4.2 Gel filtration

Fractions from the anion exchange containing r*h*TPH1 was collected and pooled. 2 M $(NH_4)_2SO_4$ was added to a final concentration of 100 mM and the solution was concentrated by ultrafiltration on an Amicon stirred pressure cell with an Ultracel PL-3 membrane to approximately 5 ml. The concentrated sample was then filtered through a 0.45 µm filter and

loaded onto a HiLoad Superdex75 16/60 prep grade column. From the supernatant loaded onto the column and each peak in the chromatogram samples were analyzed by SDS-Page.

The approximately size of r*h*TPH1 was determined from the calibration curve constructed for the the HiLoad Superdex75 16/60 prep grade. 5 proteins of known sizes (Ribonuclease A, Chymotrypsinogen, Ovalalbumin, Albumin, Blue Dextran 2000) from the Gel Filtration Calibration Kit, Low Molecular Weight from Amersham Biosciences [127] were used for calibration. The result is a linear trend line of the gel-phase distribution coefficient, K_{av}, as a function of the logarithm of the molecular weight. K_{av} is defined as given in equation 7.1,

$$K_{av} = \frac{V_e - V_o}{V_c - V_o} \tag{7.1}$$

where V_e is the elution volume, V_o is the void volume and V_c is the geometric column volume. The calibration equation is given in equation 7.2, with a void volume of 44 ml and a total geometric column volume of 120 ml.

$$K_{av} = -0.4688Log(MW) + 2.4686 \tag{7.2}$$

7.2.5 Purification of r*h*TPH1-frGFP

7.2.5.1 Anion exchange

Cells from a 650 ml culture containing r*h*TPH1-frGFP were prepared as described in section 7.2.3.1. The filtered and diluted supernatant was loaded onto a Q Sepharose High Performance 16/10 column, which was equilibrated in 20 mM Tris/H_2SO_4 pH 8.5 (buffer A). A linear gradient of 0-10 % of 20 mM Tris/NaOH, 0.8 M $(NH_4)_2SO_4$ pH 8.5 (buffer B) over 12 CV followed by a linear gradient of 20-100 % of buffer B over 2 CV was applied to the column. From the supernatant loaded onto the column, the flow-through and each peak in the chromatogram samples were analyzed by SDS-Page.

7.2.5.2 Stabilization by salt

To determine the stabilization effect by salt cells from a 650 ml culture containing r*h*TPH1-frGFP were prepared as described in section 7.2.3.1 using 40 ml 20 mM Tris/NaOH, 200 mM $(NH_4)_2SO_4$ pH 8.5 as buffer but without dilution of the supernatant. 5 ml of the filtered supernatant was directly loaded onto a HiLoad Superdex75 16/60 prep grade column which was equilibrated with the buffer. From the supernatant loaded onto the column and each peak in the chromatogram samples were analyzed by SDS-Page.

7.2.6 Purification of GST-r*h*TPH1

7.2.6.1 GST affinity purification

Cells from a 650 ml culture containing GST-r*h*TPH1 were prepared as described in section 7.2.3.2 using 40 ml 20 mM 1xPBS, 300 mM $(NH_4)_2SO_4$ pH 8.0 as binding buffer (buffer A). The filtered

supernatant was loaded onto a 20 ml GSTPrep FF 16/10 which was equilibrated in buffer A. The sample was eluted using 100 % of 50 mM Tris/H_2SO_4, 300 mM $(NH_4)_2SO_4$, pH 8.0, 10 mM reduced glutathione (buffer B). Buffer B was freshly prepared due to the reduced glutathione. Samples from the supernatant, flow-through and from each peak in the chromatogram were analyzed by SDS-Page.

7.2.6.2 Gel filtration

Fractions from section 7.2.6.1 containing GST-r*h*TPH1 were collected and pooled. The sample was filtered through a 0.45 µm filter and loaded onto a HiLoad Superdex200 26/60 prep grade column which was equilibrated in 20 mM Tris/H_2SO_4, 300 mM $(NH_4)_2SO_4$ pH 8.0. From the supernatant loaded onto the column and each peak in the chromatogram samples were analyzed by SDS-Page.

7.2.6.3 Cleavage with Factor Xa

Fractions from the gel filtration (section 7.2.6.2) containing GST-r*h*TPH1 was collected and pooled. The sample was analyzed using mass spectrometric analysis as described in section 7.2.6.4. The concentration of the sample was determined by UV-Vis spectrophotometry at 280 nm. The extinction coefficient is given in table 7.1. Four 1 ml solutions of the GST-r*h*TPH1 fusion protein were prepared with 2.5 unit/50 µg GST-r*h*TPH1, 1.5 unit/50 µg GST-r*h*TPH1, 0.7 unit/50 µg GST-r*h*TPH1 and 0.3 unit/50 µg GST-r*h*TPH1, respectively. 200 mM $CaCl_2$ was also added to each sample to a concentration of 5 mM. The samples were incubated at room temperature overnight and samples were collected after 2 hours (2h), 4 hours (4h), 6 hours (6h) and 21 hours (21h). The samples were analyzed by SDS-Page.

The sample which was not subjected to cleavage by Factor Xa was frozen in aliquots of 200 µl using liquid nitrogen and stored at -80^{o}C.

7.2.6.4 Affinity removal of GST tag

The r*h*TPH1 is isolated from the cleavad GST by affinity removal of the GST tag. This is done using a 1 ml GSTrap Fast Flow column and a peristaltic pump P-1 from Pharmacia. The column was equilibrated with buffer A. After loading of the sample, the column was washed with 5 CV of buffer A and eluted with 5 CV of buffer B taking into account the volume of the tubes (approximately 1.5 ml). Samples were collected during loading, wash and elution and the fraction sizes are given in table 7.3.

Table 7.3. Fraction name and volume of fraction collected during purification of GST-r*h*TPH1 on a small 1 ml GSTrap Fast Flow column.

	Fraction name	Volume
Load	Ft1	1.5 ml
	Ft2	1.0 ml
	Ft3	0.5 ml
Wash	W1, W2, W3, W4	1.5 ml
Elution	E1, E2, E3, E4	1.5 ml

7.2.6.5 Mass spectrometric analysis on the LCT premier

The fractions collected and pooled from the gel filtration (section 7.2.6.3) were buffer exchanged into 600 mM CH_3COONH_4/NH_3 pH 8.5. This was done using Biospin devices (Bio-Rad). The columns were washed 4 times with 500 µl MQ water followed by two times with 500 µl 600 mM CH_3COONH_4 pH 8.5. 100 µl of purified GST-r*h*TPH1 was loaded onto the column and centrifuged. The flow-through was again loaded onto another column and centrifuged. The sample was diluted to approximately 2-4 µM and 3-5 µl of sample was immediately loaded into a nano-spray capillary from Proxeon and introduced to the mass spectrometer.

The spectrum was recorded in positive ion mode using a LCT premier instrument equipped with a nano electrospray ionization (nanoESI) source, under conditions optimized for the transmission of high-mass non-covalent complexes, as described in chapter 9. The following instrumental parameters were used: Capillary voltage up to 1.8 kV and ion guide voltage 100-130 V. The instrument was calibrated externally by using a solution of cesium iodide (100 mg/ml) in 50 % iso-propanol.

7.2.7 SDS-Page analysis and protein identification by MS

For SDS-Page analysis of the samples collected during purification 18 % or 12 % Tris-HCl gels from Bio-Rad were used depending on the size of the variants being analyzed. The gels were prepared and the electrophoresis was done as described in section 4.2.7.

The protein identification of samples collected during purification of r*h*TPH1 variants was done as described in section 4.2.8.

7.3 Results and discussion

7.3.1 Purification of r*h*TPH1

7.3.1.1 Anion exchange

The soluble fraction of r*h*TPH1 from one 650 ml cell culture was loaded onto a Q Sepharose High Performance column as described in section 7.2.4.1. As mentioned in section 7.1, r*h*TPH1 does not contain any tryptophan or tyrosine residues and therefore the elution of r*h*TPH1 is followed at 236 nm (peptide backbone) and compared with the absorbance at 280 nm.

In figure 7.1 the chromatogram of the anion exchange is shown. Five major peaks (P1, P2, P3, P4, P5) and some smaller ones (P6, P7 and P8) are seen. From each peak as well as from the supernatant and the flow-through samples were analyzed by SDS-Page. The analysis is shown in figure 7.2. From the SDS-Page it is observed, by comparing the amount of r*h*TPH1 (11.6 kDa) in the supernatant (S) with the amount present in the flow-through (Ft), that approximately 80-90 % of r*h*TPH1 binds to the column. Combining the results from the SDS-Page with the chromatogram it is seen that r*h*TPH1 elutes in each collected fraction indicating that r*h*TPH1 exists in different oligomer forms. The regulatory domain consists of a 3,4-hydrophobic repeat, which most probably creates a hydrophobic face. Formations of these oligomer forms could therefore be due

to interaction between r*h*TPH1 and other hydrophobic molecules or due to intermolecular association, as mentioned in chapter 2 and 5.

Additionally, by comparing the absorbance at 236 nm and at 280 nm no major differences between these two curves are observed, which would have been expected if r*h*TPH1 was eluting in one peak. Therefore, the absorbance at 236 nm must also be due to the presence of other peptides in all peaks. The band from fraction C3 were subjected to protein identification by mass spectrometry (described in section 4.2.8). The identification confirmed that the protein was r*h*TPH1.

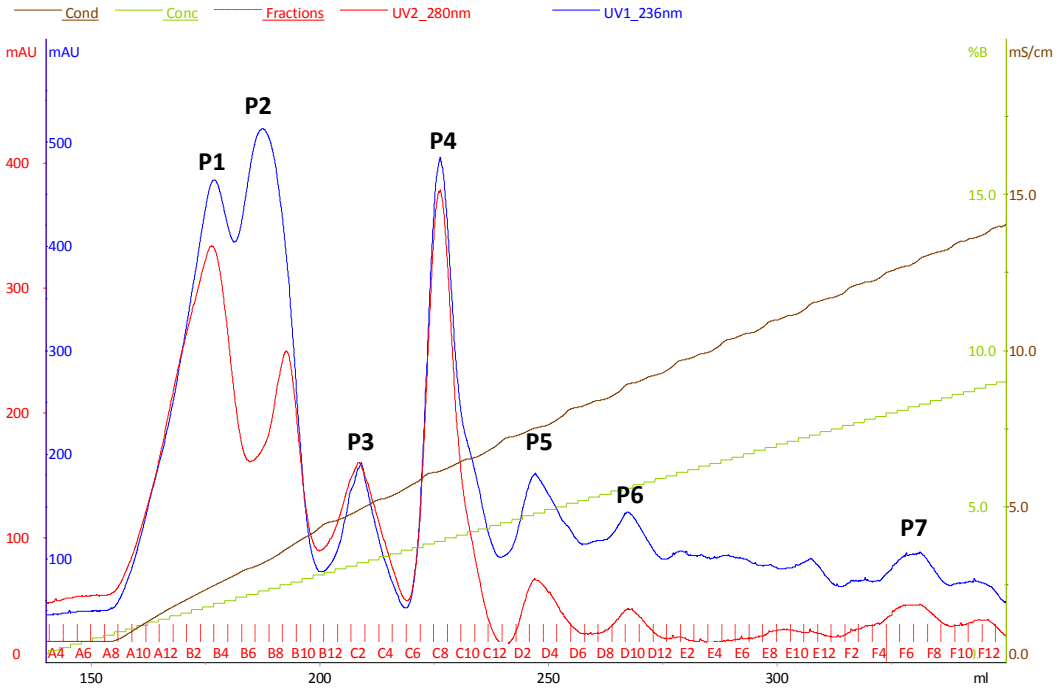

Figure 7.1. Chromatogram from the anion exchange of r*h*TPH1 on a HiLoad Q Sepharose High Performance 16/10 column. The red curve is the absorbance at 280 nm, the blue curve is absorbance at 236 nm, the brown curve is the conductivity in mS/cm and the green curve is concentration of buffer B in %. Fractions are shown with red lines on the x-axis.

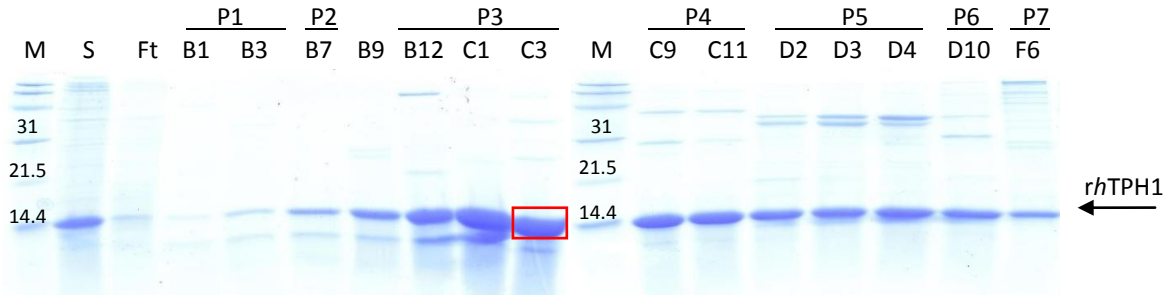

Figure 7.2. SDS-Page analysis of samples collected during purification of r*h*TPH1 on a HiLoad Q Sepharose HP 16/10 column. S is the supernatant loaded onto the column and peak number and fraction number refers to the chromatogram in figure 7.1. M is the molecular weight standard given in kDa. The red box indicates the band that was subjected to protein identification by mass spectrometry.

7.3.1.2 Gel filtration

Even though r*h*TPH1 eluted in all collected fractions in the anion exchange, a gel filtration was carried out. Fractions containing r*h*TPH1 were therefore collected, divided into three samples according to their purities (P3 (C1-C2), P4 (C9-C10) and P5 (D2-D4), respectively) and loaded onto a Superdex75 16/60 as described in section 7.2.4.2. The chromatograms from the three purifications are combined and shown in figure 7.3. Only one peak is observed for all three purifications at approximately 70 ml and samples from this as well as from the supernatant were collected and analyzed by SDS-Page. The analysis is given in figure 7.4.

Combining the results from the SDS-Page with the chromatogram it is seen that r*h*TPH1 elutes in the peak at around 70 ml. From the calibration equation (see section 7.2.4.2) of the column this elution volume corresponds to approximately 34 kDa, indicating that r*h*TPH1 exists as a trimer. No absorbance at 280 nm is seen in the chromatogram, which could indicate that the sample is pure and only contains r*h*TPH1. This is also seen from the SDS-Page analysis.

Despite the elution behavior of r*h*TPH1 in the anion exchange the protein elutes in a nice chromatographic peak in the gel filtration. The differences between these two purifications are the concentration of salt, which is much higher in the gel filtration (100 mM $(NH_4)_2SO_4$). It is therefore speculated that a high salt concentration stabilizes the protein. It could also mean that the hypothetical r*h*TPH1-association complex disassociates during gel filtration.

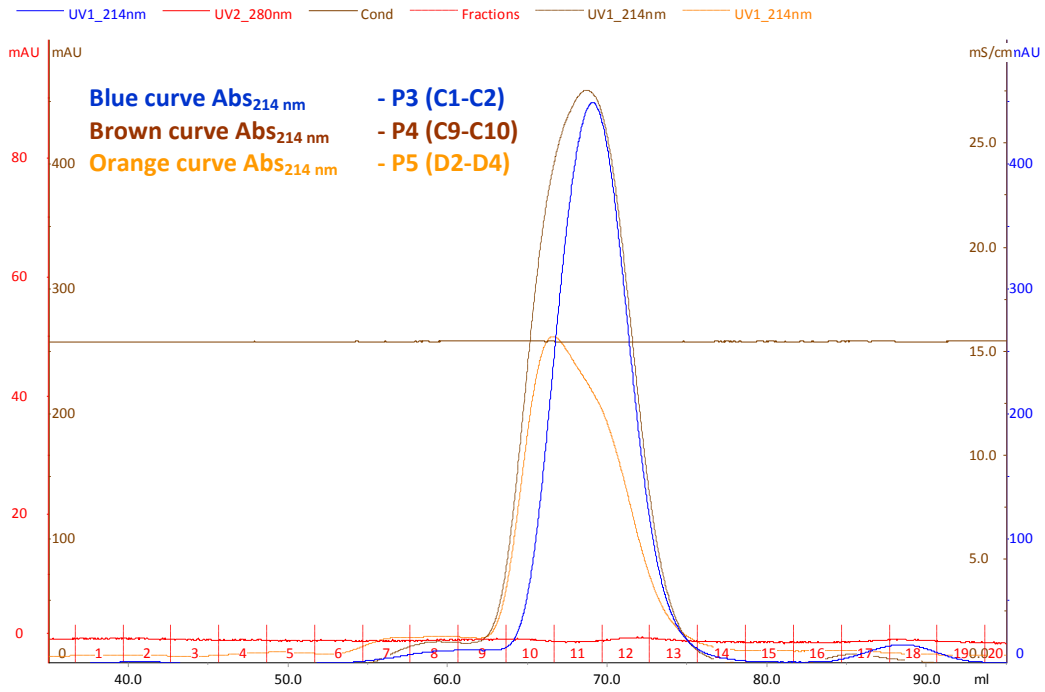

Figure 7.3. Chromatogram from the three gel filtrations on a Superdex75 16/60 column of fractions collected during anion exchange of r*h*TPH1 (figure 7.1). The fractions were divided in three parts; fraction C1-C2 (P3), fraction C9-C10 (P4) and fraction D2-D4 (P5). The blue, brown and orange curves are the absorbance at 214 nm, the red curves is the absorbance at 280 nm, the horizontal curves are the conductivity in mS/cm. Fractions are shown with red lines on the x-axis.

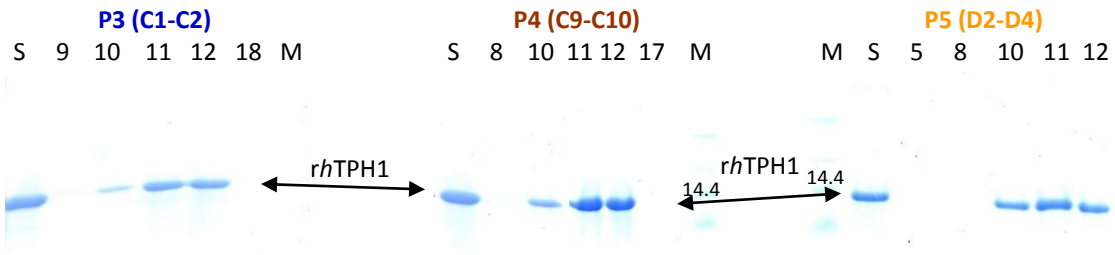

Figure 7.4. SDS-Page analysis of the three gel filtrations of fractions collected during anion exchange of r*h*TPH1. The fractions were divided into three parts; fraction C1-C2 (P3), fraction C9-C10 (P4) and fraction D2-D4 (P5). S is the supernatant loaded onto the column and 5, 8, 9, 10, 11, 12, 17 and 18 refers to fractions collected during gel filtration. M is the molecular weight standard given in kDa.

7.3.1.3 Summary and overall discussion

Approximately 80 % of the soluble r*h*TPH1 binds to the anion exchange column. The r*h*TPH1 that binds elutes in all collected fractions, which could be due to oligomerization of the protein by intermolecular interaction or due to association to other components. The fractions containing the highest amount of r*h*TPH were collected and purified on the gel filtration column. r*h*TPH1 eluted in one chromatographic peak, which is speculated to be due to the higher salt concentration in the gel filtration (100 mM $(NH_4)_2SO_4$). It could also be due to dissociation of the r*h*TPH1-complex during gel filtration.

Comparing the purification of r*h*TPH1 with *h*TPH1 the elution pattern of the variants is very similar. The difference between the two variants is the size, where r*h*TPH1 is much smaller and is therefore able to bind to the anion exchange column, despite the fact that it exists in different oligomer forms. The *h*TPH1-complex needs to be decreased by detergent in order to get it to bind to the anion exchange column (see chapter 4). This also indicates that the regulatory domain is responsible for this behavior during purification.

From these results it is seen that the elution of r*h*TPH1 is not as straight forward to follow as first expected and the elution behavior of r*h*TPH1 is very difficult to understand. In order to optimize the purification the behavior of the protein should be elucidated. Therefore, in order to visualize the protein during purification and make the elution of the protein easier to follow, frGFP is fused to the C-terminal of r*h*TPH1 as described in chapter 5. The purification is described in next section.

7.3.2 Purification of rTPH1-frGFP fusion

As mentioned in section 7.3.1.3, r*h*TPH1 was fused to the N-terminal of frGFP. This is done in order to visualize the protein during purification.

7.3.2.1 Anion exchange

r*h*TPH1-frGFP was purified on a Q Sepharose HP 16/10 column as described in section 7.2.5.1. During purification pictures were taking to visualize the elution pattern of r*h*TPH1-frGFP on the anion exchange column. The chromatogram of the ion exchange is shown on figure 7.5. Several

peaks are seen and samples from the supernatant, flow-through and from each peak in the chromatogram were analyzed by SDS-Page and shown on figure 7.6.

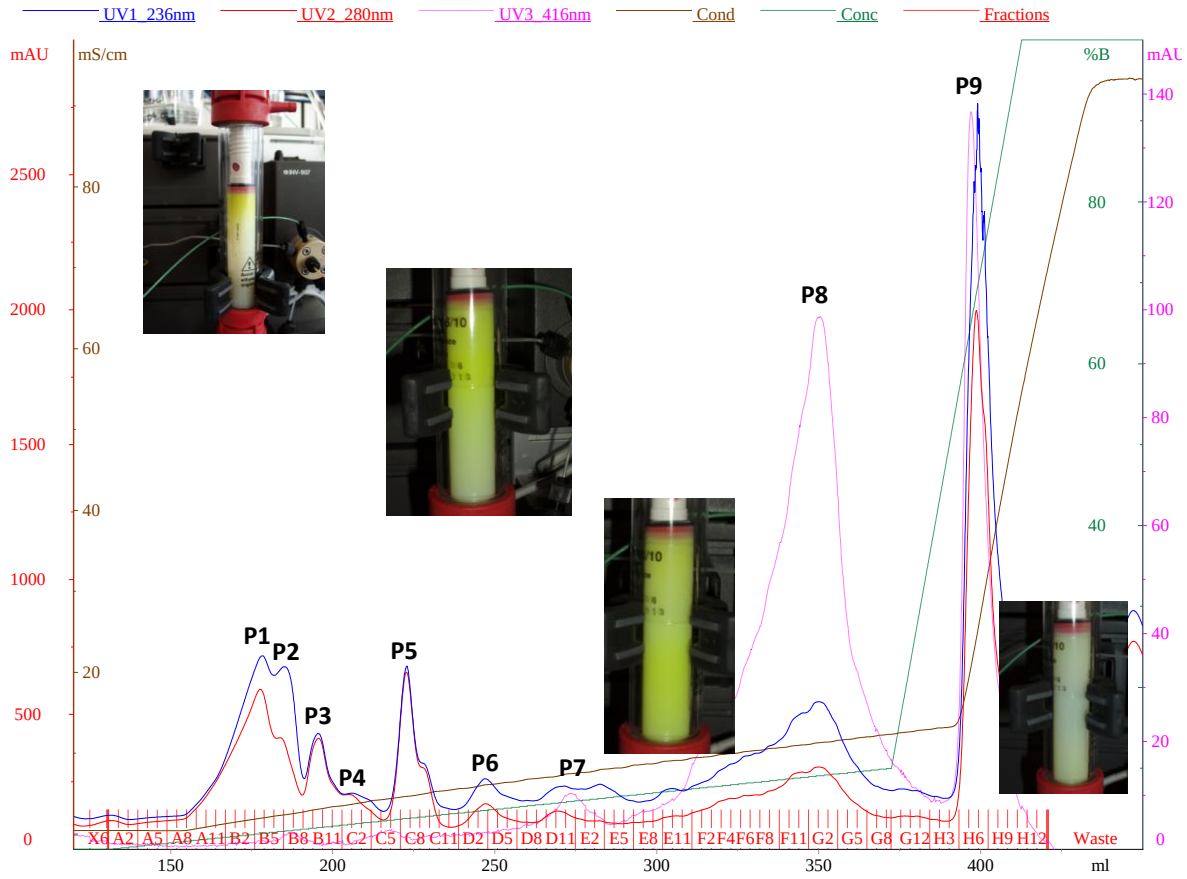

Figure 7.5. Chromatogram from the anion exchange of r*h*TPH1-frGFP using glycerol on a HiLoad Q Sepharose High Performance 16/10 column. The blue curve is absorbance at 236 nm, the red curve is the absorbance at 280 nm, the pink curve is the absorbance at 416 nm, the brown curve is the conductivity in mS/cm and the green curve is concentration of buffer B. Fractions are shown with red lines on the x-axis. Pictures taking during purification are also shown.

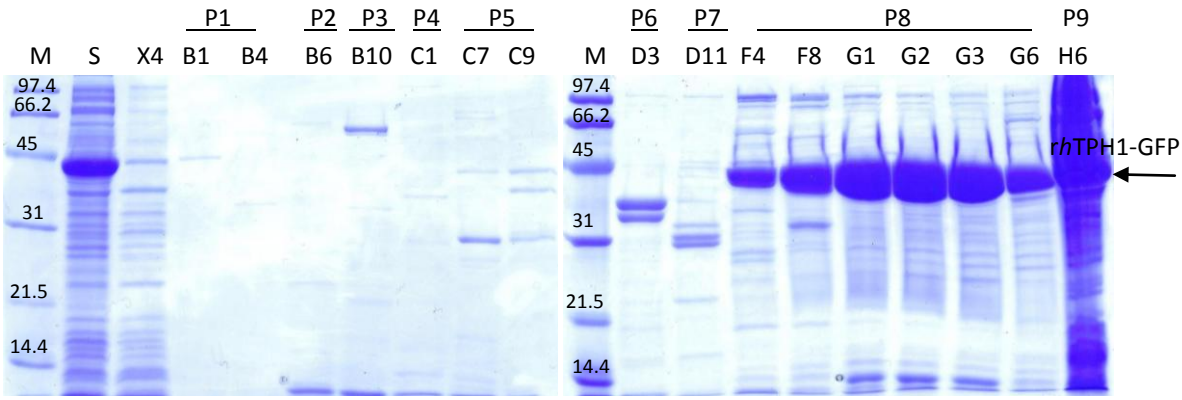

Figure 7.6. SDS-Page analysis of samples collected during anion exchange of r*h*TPH1-frGFP. S is the supernatant loaded onto the column and peak numbers and fraction numbers refers to the chromatogram in figure 7.5. M is the molecular weight standard given in kDa.

Combining the SDS-Page with the chromatogram it is seen that r*h*TPH1-frGFP elutes over a large volume with the highest intensity in fraction G1 (P8). From pictures taken during purification (see figure 7.5) r*h*TPH1-frGFP is bound throughout the column volume indicating that the fusion protein exists in different oligomers or associated forms. This is consistent with the results from the purification of r*h*TPH1 (see section 7.3.1).

Comparing the chromatograms from the purification of r*h*TPH1 with r*h*TPH1-frGFP they are very alike. The only differences are the maximum absorption of P8, which is much higher at both 280 nm and 236 nm. Absorbance at 416 nm is also observed at P8. This absorbance peak is due to GFP [109] and therefore corresponds to the presence of r*h*TPH1-frGFP (see on the SDS-Page analysis). The elution pattern of r*h*TPH1-frGFP is the same as for the previous purification of r*h*TPH1, but due to a higher negative charge, r*h*TPH1-frGFP elutes later in the chromatogram than r*h*TPH1. The high absorbance and amount of r*h*TPH1-frGFP present in P9 corresponds to a high increase in the conductivity due to change in the slope of the linear gradient. If the slope was the same during the whole purification the amount of r*h*TPH1-frGFP would have been spread over a large volume with a decreased concentration.

7.3.2.2 Stabilization by salt

From anion exchange of both r*h*TPH1 and r*h*TPH1-frGFP the variants elute in different oligomer forms and from gel filtration of samples collected during anion exchange the r*h*TPH1 variant elutes in a nice chromatographic peak with the size of a trimer. It is speculated that salt stabilizes the protein.

Therefore, to see whether or not salt stabilize and eliminate oligomerization of the regulatory domain, the r*h*TPH1-frGFP variant was loaded directly onto the Superdex75 column as described in section 7.2.5.2 where 5 ml of the prepared raw extract with 200 mM $(NH_4)_2SO_4$ was loaded. In figure 7.7 the chromatogram from the purification is shown. The chromatogram shows three peaks: One corresponding to the void volume, V_o, one eluting at 53 ml (P1) and one eluting at 67 ml (P2). From the supernatant loaded onto the column and from the three peaks, samples were analyzed by SDS-Page and shown on figure 7.8. In figure 7.7 a picture of these fractions are given.

Combining the results from the SDS-Page analysis with the chromatogram it is seen that r*h*TPH1-frGFP (41 kDa) exists in P1 with an elution volume of 53 ml corresponding to a size of 76.2 kDa determined using the calibration equation (see section 7.2.4.2) indicating that r*h*TPH1 exists as a dimer. The dimerization of the fusion protein could either be due to r*h*TPH1 or frGFP, but since GFP has shown to crystallize as a dimer, the dimerization is most probably due to frGFP [128].

Comparing the chromatogram in figure 7.3 with the chromatogram in figure 7.7 the r*h*TPH1 elutes as a trimer, whereas r*h*TPH1-frGFP elutes as a dimer. The differences between these two purifications is that a salt concentration of 200 mM $(NH_4)_2SO_4$ is present at the beginning of the purification of r*h*TPH1-frGFP, whereas salt is first added to the r*h*TPH1 sample after anion exchange to a concentration of 100 mM. Therefore, the presence of salt already in the

preparation of the raw extract stabilizes the protein causing it to elute in a nice chromatographic peak.

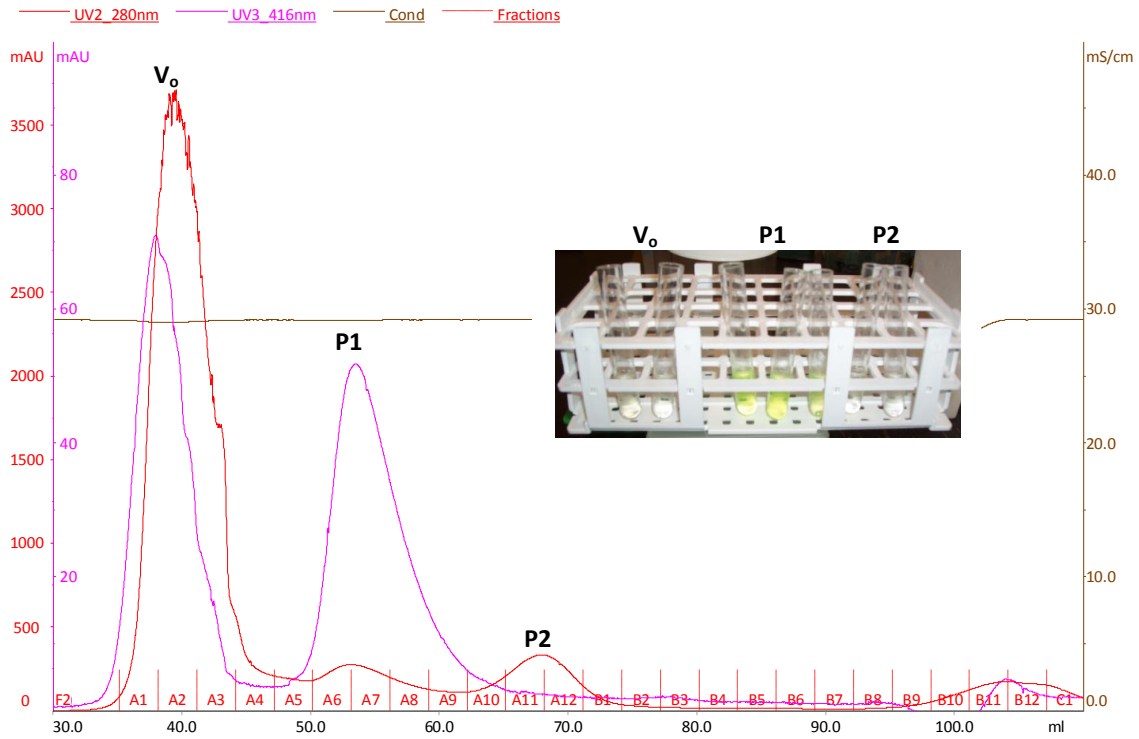

Figure 7.7. Chromatogram from the gel filtration on a Superdex75 16/60 column of *rh*TPH1-GFP using gel filtration as the first step. The red curve is the absorbance at 280 nm, the pink curve is the absorbance at 416 nm and the brown curve is the conductivity in mS/cm. Fractions are shown with red lines on the x-axis. A picture of the sample collected during purification is also shown.

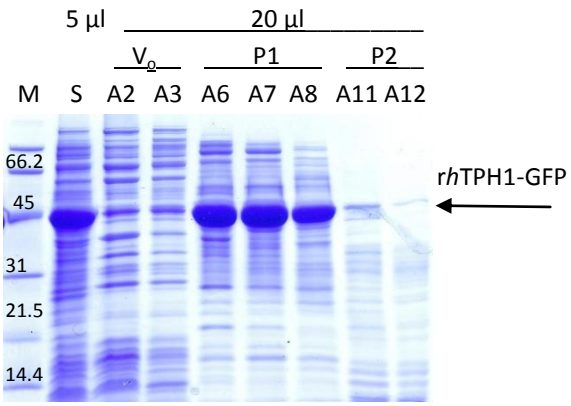

Figure 7.8. SDS-Page analysis of the samples collected during gel filtration of *rh*TPH1-GFP. S is the supernatant and peak numbers and fraction numbers refers to the chromatogram in figure 7.7. M is the molecular weight standard given in kDa.

7.3.2.3 Summary and overall discussion

From the purification of r*h*TPH1-frGFP the elution pattern of r*h*TPH1 is visualized by the green fluorescence from the frGFP and from the pictures taking during anion exchange of r*h*TPH1-frGFP it is seen that the variant binds throughout the column volume (see figure 7.5). In the anion exchange the variant exists in different oligomer forms giving rise to different overall net charges and elution at different conductivities. Formations of these oligomer forms could be due to intermolecular interactions or associations with other components present in the sample. The regulatory domain consists of a 3,4-hydrophobic repeat, which most probably creates a hydrophobic face and if this hydrophobic face is located at the outer surface of the native protein hydrophobic interaction between r*h*TPH1 and other hydrophobic molecules could be possible, as described in chapter 5. In order to see if the extent of these associations could be decreased three variants of r*h*TPH1 with different mutations in the hydrophobic face were constructed, as described in chapter 5. From expression and solubility test (chapter 6) it was concluded that changing the hydrophobic residues to positively charged residues causes the protein to be folded incorrectly in an insoluble form. Hence, the hydrophobic face is important for correctly folding of the protein.

Loading the supernatant directly onto a gel filtration column as the first step with a salt concentration of 200 mM $(NH_4)_2SO_4$ causes the protein to elute in one single chromatographic peak indication that salt stabilizes the protein. This is consistent with the gel filtration of r*h*TPH1 described in section 7.3.1 and from studies on c*gg*TPH1 [12]. Therefore, stabilizing r*h*TPH1 by high salt concentration is needed in both the preparation of the raw extract and during purification. High salt concentrations are usually used to increase the hydrophobic interactions between proteins causing them to aggregate, but if the protein has very hydrophilic areas at the surface the salt could stabilize these by electrostatic stabilization.

To scale up the purification, gel filtration as the first purification step is not the answer due to small volume capacities; therefore, r*h*TPH1 was fused to GST in order to have high salt concentration in the buffer system from the beginning of the purification.

7.3.3 Purification of GST-r*h*TPH1

It was chosen to use 300 mM $(NH_4)_2SO_4$ to make sure that there was enough salt present to stabilize the protein. The GST-r*h*TPH1 fusion protein was purified on a GSTPrep column as described in section 7.2.6.1. The chromatogram of the purification is shown on figure 7.9. As expected one peak is seen (P1) and samples from the supernatant, flow-through and P1 were analyzed by SDS-Page and shown in figure 7.10.

From the SDS-Page approximately 80 % of GST-r*h*TPH1 is in the soluble fraction (S) and comparing this amount with the amount in the flow-through (Ft) approximately 75 % binds to the column.

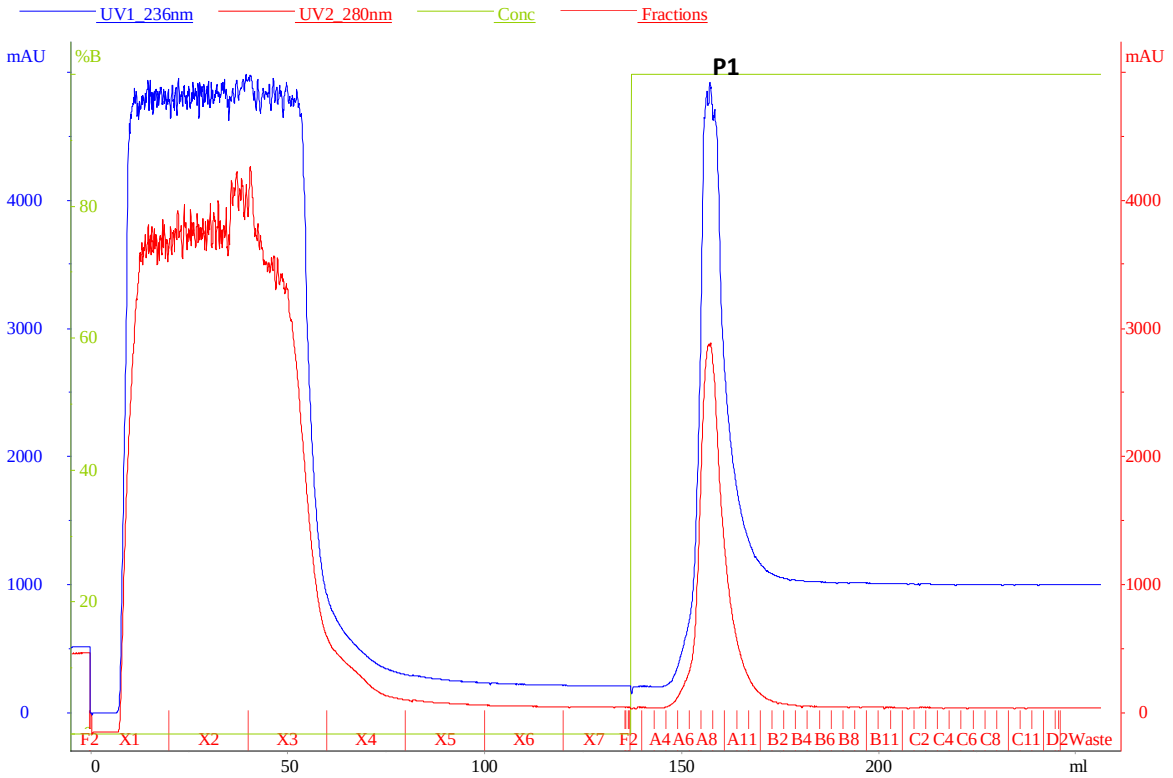

Figure 7.9. Chromatogram of the purification of GST-r*h*TPH1 on a GSTPrep 16/10 column. The blue curve is absorbance at 236 nm, the red curve is the absorbance at 280 nm and the green curve is concentration of buffer B. Fractions are shown with red lines on the x-axis.

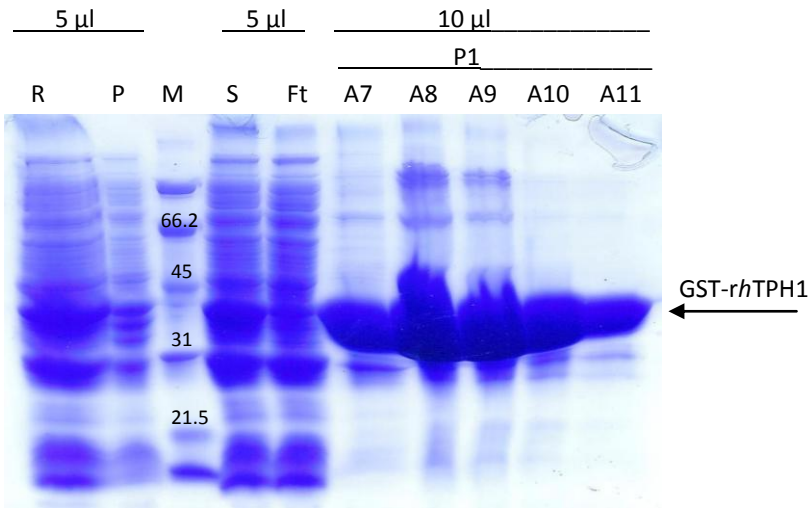

Figure 7.10. SDS-Page analysis of the solubility and purification of GST-r*h*TPH1 on a GSTPrep column. R is the raw extract, P is the resuspended pellet, S is the supernatant, Ft is the flow-through and peak number and fraction numbers refers to the chromatogram in figure 7.9. M is the molecular weight standard given in kDa.

The eluted fractions (fraction A7-A11) were collected, pooled and loaded onto the gel filtration column as described in section 7.2.6.2. The chromatogram of the gel filtration is shown on figure

7.11. Three peaks are seen; one corresponding to the void volume, V_o, and two eluting at approximately 160 ml (P1) and 184 ml (P2), respectively. Samples from the supernatant loaded onto the column and from each peak were analyzed by SDS-Page and shown on figure 7.12.

From the analysis, GST-r*h*TPH1 exists in both P1 and P2, but the amount in P1 is most probably due to a poor resolution of P1 and P2. GST-r*h*TPH1 elutes in P2 at 184 ml which corresponds to a size of 65 kDa, indicating that the fusion protein is a dimer (monomer is 38 kDa, dimer is 76 kDa). The dimerization is most probably due to GST [129]. Fraction 45 to 55 were collected and pooled and the concentration was determined to 1.2 mg/ml (approximately 40 mg/l culture). The sample was analyzed by mass spectrometric analysis on a LCT Premier as described in section 7.2.6.5. The *m/z* spectrum is shown on figure 7.13. From the spectrum a protein with the mass of 76241.9±1 Da is identified which corresponds to a dimer of GST-r*h*TPH1 (2 x 38116.37 Da).

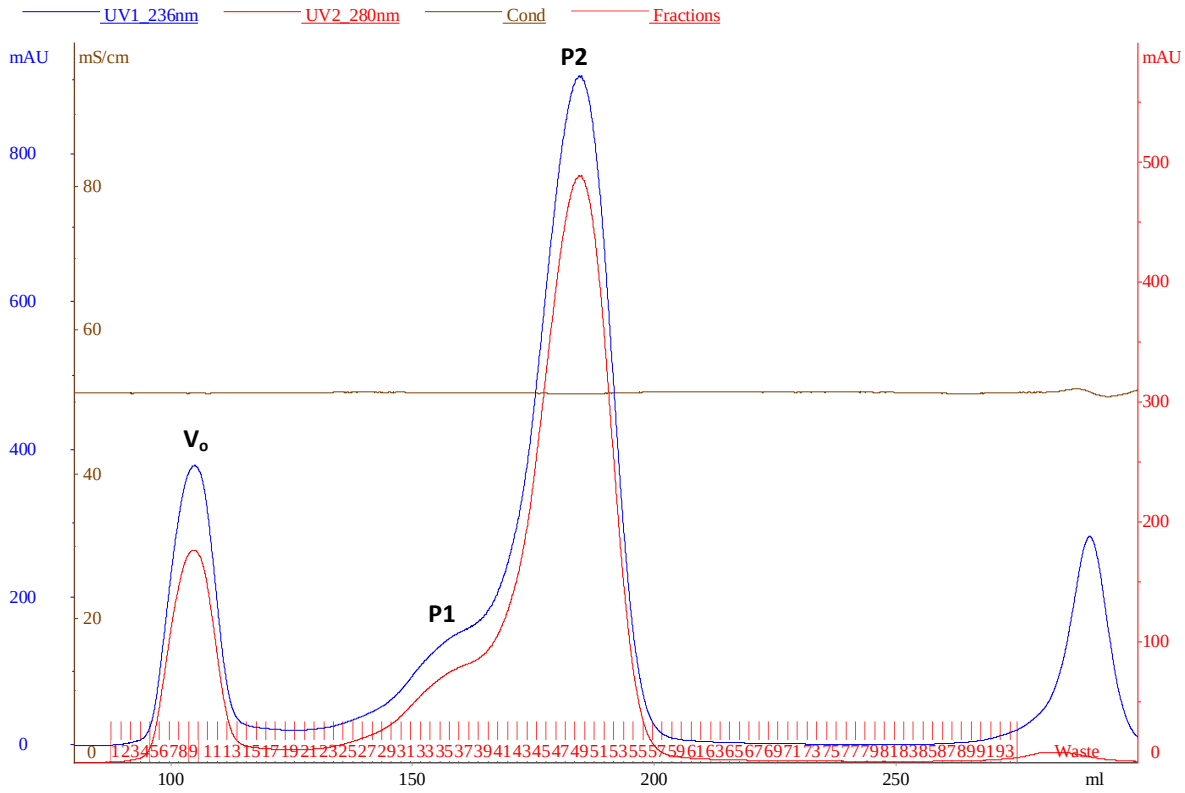

Figure 7.11. Chromatogram of the gel filtration on a Superdex200 26/60 column of samples collected and pooled from the GST purification of GST-r*h*TPH1. The blue curve is absorbance at 236 nm, the red curve is the absorbance at 280 nm and the brown curve is the conductivity in mS/cm. Fractions are shown with red lines on the x-axis.

GST was cleaved of the fusion protein by Factor Xa using different concentrations of protease as described in section 7.2.6.3. Samples were analyzed on SDS-Page analysis and shown on figure 7.14. From the analysis it is seen that the fusion protein can be cleaved given rise to bands corresponding to the size of GST and r*h*TPH1, respectively. It is also seen that the higher the concentration of Factor Xa the faster the fusion protein is cleaved. All the GST is cleaved after 21

hours at all four concentrations of Faktor Xa. A drawback of having to high concentration of Factor Xa is nonspecific cleavage of the protein, also mentioned by the manufacture [130]. This nonspecific cleavage is also seen in this case, where a band with a lower molecular size than r*h*TPH1 is present with increased intensity at higher concentration of Factor Xa. From sequence alignment shown in figure 7.15 of r*h*TPH1 and the recognition site of Factor Xa a four amino acid site in r*h*TPH1 almost corresponds to the recognition site of Factor Xa with the exception of one amino acid. It could be thought that Factor Xa would cleave at this site given rise to two truncated sequences of r*h*TPH1. Because the site is in the middle of the r*h*TPH1 sequence only one band corresponding to the truncated r*h*TPH1 is seen on the SDS-Page, which is also the case. For further use, 0.3 unit/50 µg of Factor Xa overnight due to lowest amount of degradation of r*h*TPH1 should be used (or less).

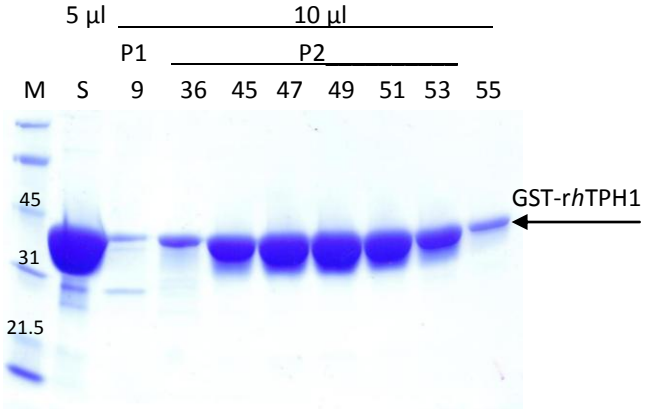

Figure 7.12. SDS-Page analysis of GST-r*h*TPH1 purified on a Superdex200 26/60 column. S is the supernatant and peak number and fraction numbers refers to the chromatogram in figure 7.11. M is the molecular weight standard given in kDa.

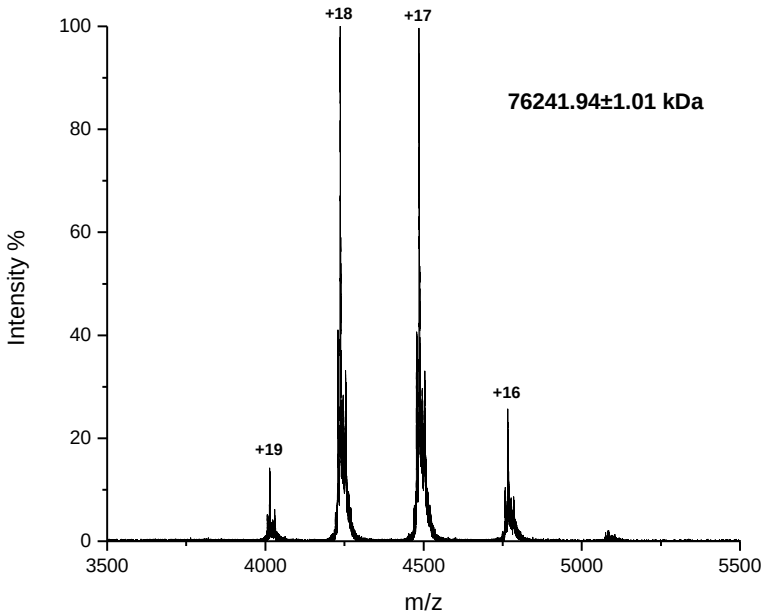

Figure 7.13. Mass spectrum of 2-4 µM of the gel filtrated GST-r*h*TPH1 analyzed on a LCT premier as described in section 7.2.6.4.

The 1 ml sample with 0.3 unit/50 µg of Factor Xa was loaded onto a 1 ml GST column as described in section 7.2.6.4. Samples of the supernatant, flow-through and elution were analyzed by SDS-Page and shown in figure 7.16. From the SDS-Page r*h*TPH1 is seen in the flow-through as expected due to cleavage of the GST affinity tag. GST is seen in the elution fractions.

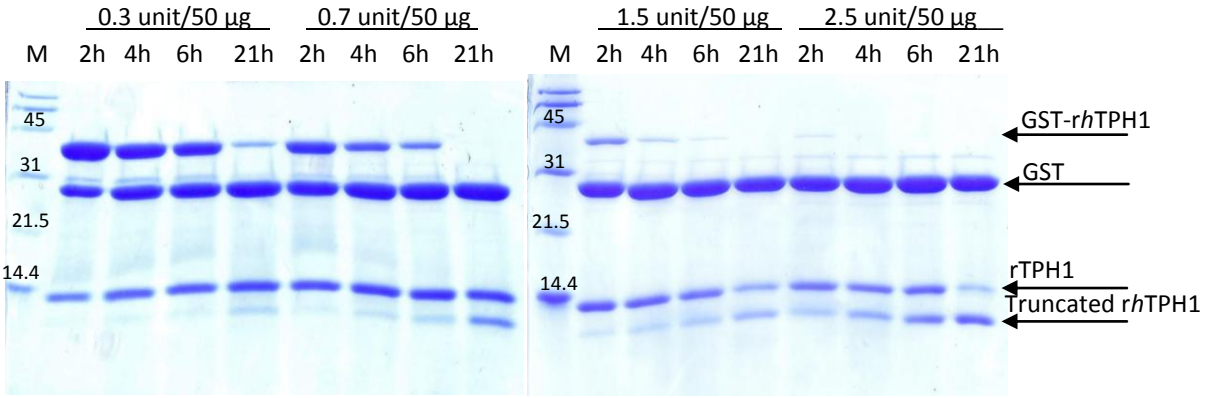

Figure 7.14. SDS-Page analysis of the cleavage of the GST-r*h*TPH1 fusion using Factor Xa at different concentrations. M is the molecular weight standard given in kDa. Samples were taken after incubation with protease after 2 hours (2h), 4 hours (4h), 6 hours (6h) and 21 hours (21h).

```
                  1                                                    60
    rhTPH1    (1) MIEDNKENKDHSLERGRASLIFSLKNEVGGLIKALKIFQEKHVNLLHIESRKSKRRNSEF
  Faktor XA   (1) ----------------------------------------------IEGR---------
3C protease   (1) ----------------------------------------------LEVLFQGP-----
  Consensus   (1)                                                IE R
                  61                                        99
    rhTPH1   (61) EIFVDCDINREQLNDIFHLLKSHTNVLSVNLPDNFTLKE
  Faktor XA   (5) ----------------------------------------
3C protease   (9) ----------------------------------------
  Consensus  (61)
```

Figure 7.15. Protein sequence alignment of r*h*TPH1 and the recognition site of Factor Xa and the 3C protease. The alignment was done using the program Vector NTI advance 11 from Invitrogen [34].

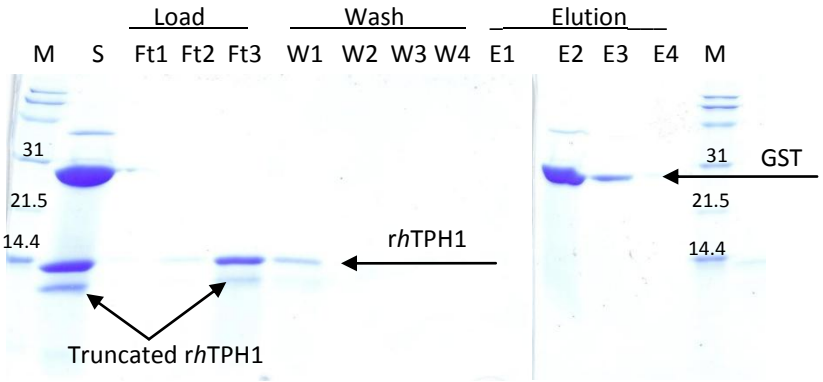

Figure 7.16. SDS-Page analysis of purification of r*h*TPH1 on a GSTrap column after cleavage of the fusion protein by Factor Xa. M is the molecular weight standard given in kDa, S is the supernatant and Ft1, Ft2, Ft3, W1, W2, W3, W4, E1, E2, E3 and E4 are fractions collected during affinity tag removal of GST.

7.3.3.1 Summary

r*h*TPH1 can be purified as a GST-r*h*TPH1 fusion protein in 300 mM $(NH_4)_2SO_4$. The fusion protein elutes as a dimer most probably due to dimerization of GST. After cleavage of GST the protein does not bind to the GST column. r*h*TPH1 can be purified by the strategy given in figure 7.17. It is a simple purification strategy consisting of three purification steps and a cleavage step. The purification can be done within two days.

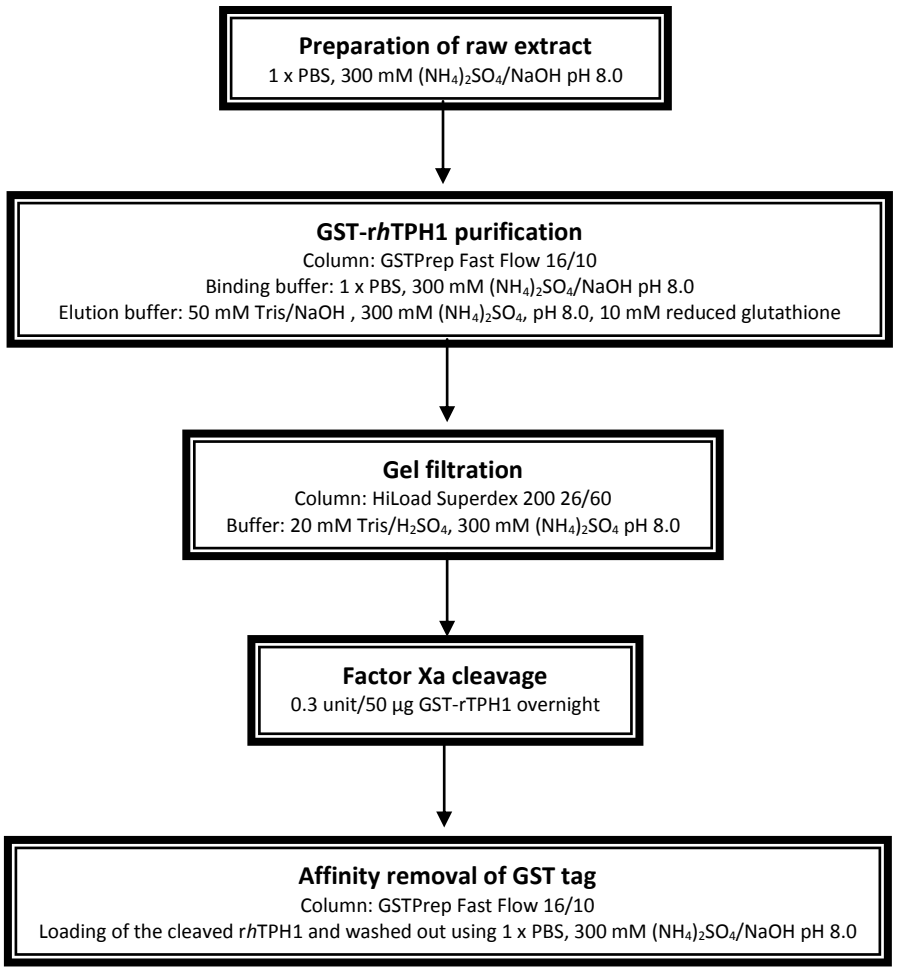

Figure 7.17. Purification steps in the purification of r*h*TPH1.

7.3.4 Overall summary and discussion

Methods for expression of r*h*TPH1 in a soluble form (chapter 5 and 6) and purification of r*h*TPH1 have been developed and documented. From the purification attempts of the three r*h*TPH1 variants described in section 7.3.1 to 7.3.3 it is seen that the presence of $(NH_4)_2SO_4$ in the preparation of the raw extract stabilizes the variant and decreases the extent of oligomerization from being trimer (without presence of salt in the raw extract) to dimer as described in section 7.3.3. This stabilization effect by salt could be due to the presence of hydrophilic areas in the protein which is stabilized by the salt. Comparing these results with the purification results of

c*gg*TPH1 it is observed that the catalytic domain is stable without the presence of salt in the raw extract but requires salt during purification [12], whereas the regulatory domain needs salt from the beginning.

The high salt purification strategy developed for r*h*TPH1 might be the key to purification of full-length *h*TPH1.

7.3.5 Future directions

Mass spectrometry results of the cleavage product of r*h*TPH1 should be performed in order to determine the oligomerization of r*h*TPH1. Additionally, it could be of interest to use a fusion protein, which does not form a dimer itself in order to determine the oligomerization of r*h*TPH1.

Due to non-specific cleavage by Factor Xa, the 3C protease [131] should be used instead. From the sequence alignment, shown in figure 7.15, r*h*TPH1 does not contain a sequence corresponding to the sequence of the recognition site of the 3C protease. An additional advantage of using the 3C protease is that it is also purified as a GST fusion protein meaning that by purification on a GST column the protease will bind to the column as well. It is therefore possible to cleave the GST-r*h*TPH1 while bound to the GST column [131].

The results obtained from purification of r*h*TPH1 with salt, should be implemented in the purification strategy of *h*TPH1. However, using GST as an affinity tag for oligomeric proteins is a problem due to its dimerization [129]. Therefore, *h*TPH1 should be fused to another affinity tag such as maltose-binding protein (MBP) and both detergent and salt should be used during purification.

7.4 Conclusion

r*h*TPH1 has successfully been purified using a high content of salt in preparation of the raw extract and during purification in order to stabilize the variant. Due to the stabilization effect of salt the r*h*TPH1 was fused to GST in order to have salt throughout the purification. The GST affinity tag was successfully removed by cleavage with Factor Xa and the r*h*TPH1 was isolated on a GST column after cleavage in high purity. This is the first time that a variant of TPH containing the regulatory domain has been documental purified. This strategy is hopefully the key to purification of full-length *h*TPH1.

8 Enzymatic characterization of the catalytic domain of *h*TPH1

Enzymatic characterization includes determination of the kinetic parameters (V_{max}, K_m and K_i) and knowledge of these parameters makes it possible to compare and differentiate isoenzymes from different tissues or organisms [132]. In order to understand the reaction and enzymatic properties of *h*TPH and to elucidate the possibility of isoform-specific inhibitors, the kinetic parameters of c*h*TPH1 is determined and compared with the kinetic parameters of c*h*TPH2 determined by Michael S. Windahl [6]. In this chapter an introduction to enzyme kinetic is presented and followed by a description of the TPH assay used to determine the kinetic parameters of c*h*TPH1. This is followed by the experimental procedures and a result and discussion section.

8.1 Enzyme kinetic

8.1.1 Michaelis-Menten equation

The initial rate of a mono substrate enzyme reaction is related to the substrate concentration by the Michaelis-Menten equation given in equation 8.1,

$$\nu_i = \frac{V_{max}[S]}{K_M + [S]} \tag{8.1}$$

where the initial rate, ν_i, is given as a function of the substrate concentration, [S]. From this equation the kinetic parameters; the maximal rate of reaction, V_{max}, and the Michaelis constant, K_m, can be determined [132,133,134]. The derivation of the equation relies on the assumptions

that the reaction is under pseudo-steady-state conditions (the concentration of the enzyme-substrate complex is constant), that the enzyme-substrate complex does not deplete the concentration of free substrate, that the reverse reaction is negligible and that the total enzyme concentration does not change over time [132,134]. To ensure these assumptions, the measured initial velocity should be linear with time (steady-state assumption) and the velocity should be linearly proportional to the enzyme concentration (enzyme does not deplete substrate concentration assumption) [132].

8.1.1.1 Substrate inhibition

Substrate inhibition is often seen at high concentration of substrate where they often act as dead-end inhibitors. Normally this kind of inhibition does not occur at physiological substrate concentrations and therefore, it gives information about the upper limit of substrate concentration *in vivo* [135]. When a substrate acts as a dead-end inhibitor the initial rate as a function of the substrate concentration does no longer follow equation 8.1. Instead equation 8.2 is applied, where K_i is the inhibition constant for the inhibitory substrate**.**

$$\nu_i = \frac{V_{max}[S]}{K_M + [S] + \frac{[S]^2}{K_i}} \tag{8.2}$$

8.1.2 Terreactant reaction

TPH is a terreactant enzyme which catalyzes the ter-bi-reaction of tryptophan, BH_4 and O_2 to give 5-hydroxytryptophan and 4a-hydroxy-BH_4, as described in chapter 2. For terreactant enzymes the kinetic mechanism is more complex due to binding of substrates in different ways and determination of the kinetic parameters is therefore not as straightforward. By using the Michaelis-Menten equation for a mono substrate reaction the parameters can be determined in a simpler manner, by changing the concentration of one substrate while saturating the enzyme with the other two substrates ([S] > 100 K_M). Even though one substrate is maintained at a constant, below-saturating concentration, the relationship of the initial rate and the substrate concentration can follow equation 8.1, but only if the enzyme-substrate complex is under steady-state conditions (i.e. the [ES] is constant and the [S] does not change significantly) [132,136].

8.1.2.1 Determining the kinetic parameters for terreactant enzymes

There are distinguished between two values of the kinetic parameters: The true and the apparent values. The true V_{max} is the maximum reaction rate of the enzyme when saturated with all substrates and the true K_M is the substrate concentration at the true $V_{max}/2$. In practice it might be difficult to saturate the enzyme ([S] > 100K_M) with all substrates and often the apparent K_m and V_{max} values are determined instead [132]. The apparent K_m and V_{max} values are often dependable on the concentration of the fixed substrates and it is therefore difficult to compare values determined at different concentrations of the fixed substrates below saturation. Comparison of kinetic parameters also requires that they are obtained under identical conditions e.g. ionic strength, pH and temperature [132].

Determination of the kinetic parameters can be done by fitting the Michaelis-Menten equation to measured values of the initial rates, v_i, at different substrate concentrations. For terreactant reactions the initial rate is determined at substrate concentrations of the varied substrate while maintaining the other substrates concentrations fixed. Different methods for fitting data sets to the Michaelis-Menten equation can be used, such as the linear double reciprocal Lineweaver-Burk plot (1/v against 1/s) where the equation is rearranged to give straight-line relationships. The problem with linear transformations is that the errors in each data set are weighted differently, and therefore they should not be used to determine the K_m and V_{max}**.** The most accurate way is to fit the Michaelis-Menten equation to the data using non-linear regression [132].

8.2 Tryptophan hydroxylase assay

The assay used in determination of the kinetic parameters of c*h*TPH1 is a non-coupled continuous fluorimetric assay developed by G. R. Moran and P. F. Fitzpatrick, where production of 5-hydroxytryptophan is monitored [137]. The assay is further optimized in the Metalloprotein Chemistry and Engineering Group by M. Storgaard [138] and A. Munch [8]. The assay is based on different spectral properties of tryptophan and 5-hydroxytryptophan as shown in figure 8.1. By using an excitation wavelength of 300 nm, excitation of 5-hydroxytryptophan is almost exclusive. Emission is measured at 330 nm where 5-hydroxytryptophan has high emission intensity [137].

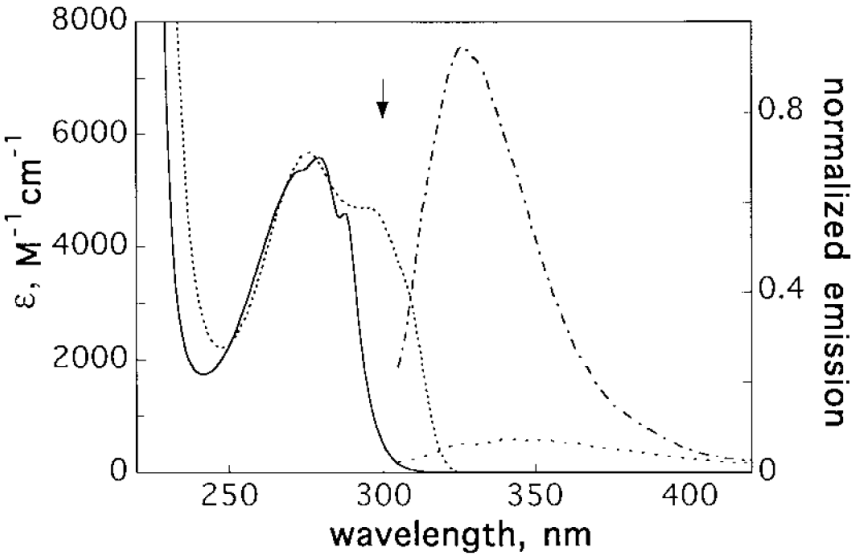

Figure 8.1. Absorbance and emission spectra of tryptophan and 5-hydroxy-tryptophan [137]. Reproduced with permission from Elsevier.

Besides the three substrates (tryptophan, BH_4 and O_2), $(NH_4)_2SO_4$, dithiothreitol (DTT), catalase, $(NH_4)_2Fe(SO_4)_2$ and Hepes buffer are also added to the assay. The addition of $(NH_4)_2Fe(SO_4)_2$ and $(NH_4)_2SO_4$ is due to TPH's requirement of ferrous iron for activity and stabilization of the enzyme by ammonium sulfate. DTT is added to prevent autooxidation of BH_4 [137] and to maintain the iron on a reduced form. Catalase is added to consume any hydrogen peroxide formed upon autooxidation. The Hepes buffer is used to maintain the assay at pH 7.0.

8.2.1 Standard curves for 5-hydroxytryptophan

Addition of BH_4 initiates the reaction and a progression curve with the emission intensity of 5-hydroxytryptophan as a function of time is produced. At pH 7.0 BH_4 absorbs at 300 nm (see figure 8.2), which is used as excitation wavelength in the assay, and therefore the fluorescence signal from 5-hydroxytryptophan is reduced by attenuation of the incoming light. Because of this, it is necessary to make 5-hydroxytryptophan standard curves for all BH_4 concentrations used for determination of the kinetic parameters. These standard curves were done by Michael S. Windahl [6] and given in appendix A2.

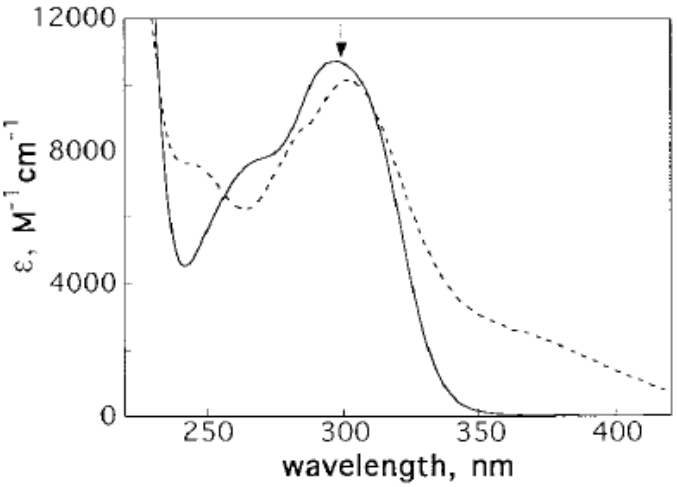

Figure 8.2. The absorption spectra of 5,6,7,8-tetrahydrobiopterin (BH_4) at pH 7.0 (full line) and quinonoid dihydropterin (q-BH_2) (dashed line) [137]. Reproduced with permission from Elsevier.

8.3 Experimental procedures

8.3.1 Materials

Ultrapure glycerol was obtained from Invitrogen. 12% Tri-HCl gels were from Bio-Rad. (6R)-5,6,7,8-tetrahydro-L-biopterin dihydrochlorid (BH_4) was from Schircks Laboratories, Jona, Switzerland. LB media and all other chemicals used were analytical grade obtained from Sigma-Aldrich. All solutions were prepared using 18.2 MΩ cm water from a Milli-Q synthesis A10 Q-Gard system (Millipore).

8.3.2 Expression and purification of c*h*TPH1

The expression and purification strategies were developed in my master project [14] and therefore, they will not be described in details. c*h*TPH1 was expressed in *E. coli* BL21 cells at 30°C, 250 rpm for approximately 5 hours. The cells were harvested using 20 mM Tris/H_2SO_4 pH 8.5, transferred to 50 ml polypropylene tubes and stored at -80°C.

The protein was purified using a method consisting of four steps: Preparation of raw extract, anion exchange, buffer exchange to the gel filtration buffer and concentration by ultrafiltration

followed by gel filtration, as given in figure 8.3. In table 8.1 the composition of the buffers used in the purification are given. After the last purification step, fraction containing c*h*TPH1 were collected and pooled, the concentration determined and the protein was stored at -80^{o}C in Eppendorf tubes.

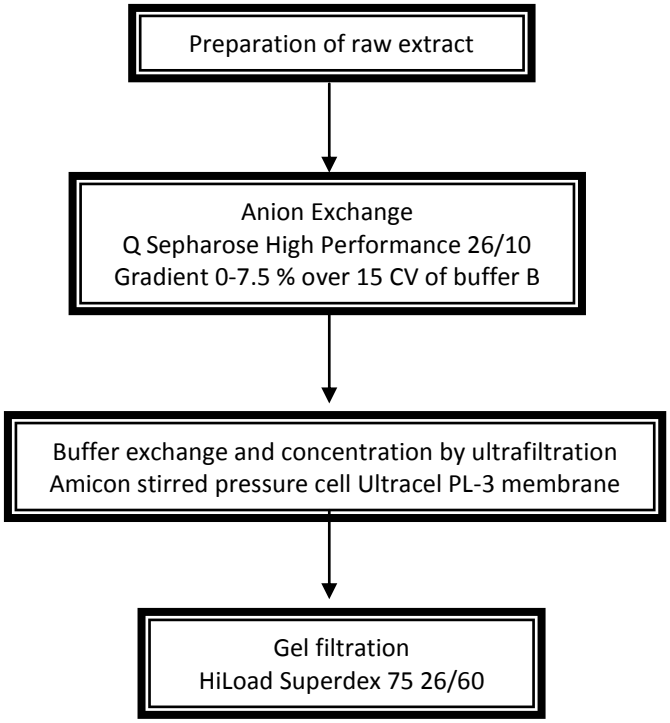

Figure 8.3. Steps involved in the purification of c*h*TPH1.

Table 8.1. Composition of the buffers used in purification of c*h*TPH1.

	Buffer A	**Buffer B**
Anion exchange	20 mM Tris/H_2SO_4 pH 8.5	20 mM Tris/NaOH, 800 mM $(NH_4)_2SO_4$ pH 8.5
Gel filtration	20 mM HEPES/NaOH, 200 mM $(NH_4)_2SO_4$ + 10 % glycerol pH 8.5	

8.3.3 The tryptophan hydroxylase assay

8.3.3.1 Instrument and instrument settings

The activity measurements were done on a Varian Cary Eclipse Fluorescence Spectrophotometer. The excitation wavelength was 300 nm and the emission was measured at 330 nm. Excitation and emission slits were 5 nm and the photomultiplicator tube (PMT) voltage was 650 V. The measurements were done in 10.00 mm x 10.00 mm QS quartz cuvettes from Helma. The fluorescence spectrophotometer was equipped with a temperature-controlled-four-cuvette holder with stirring. All measurements were done at 15 ^{o}C.

To control the O_2 concentration a MI-730 Oxygen electrode and an OM-4 Oxygen Meter from Microelectrodes, Inc., Londonderry, NH, USA were used. Different N_2/O_2 mixtures were produced by using Mass Flow controllers model 5850 TR from Brooks instruments B.V. Veenendaal, The Netherlands. The flow controllers were operated through a monitor model 0152 from Brooks Instruments.

8.3.3.2 Preparation of c*h*TPH1 samples

Stocks of the c*h*TPH1 from section 8.3.2 were thawed on ice and the concentration was determined using ε_{280} = 33350 M^{-1} cm^{-1} [126]. The samples were diluted with an equal volume of 20 mM HEPES/NaOH, 10% w/v glycerol, 200 mM $(NH_4)_2SO_4$ pH 7.2, 4 mM DTT, 0.1 g/L catalase and 0.16 mM tryptophan. The mixture was stored at 4°C in 3-6 polypropylene tubes closed under argon. This was done to prevent loss of activity. 0.221 units of c*h*TPH1 (measured at 70 μM tryptophan, 300 μM BH_4 and 500 μM O_2) were used in the measurements which equal ~1.26 μM c*h*TPH1.

8.3.3.3 Composition of the assay solution

The assay volume was 2500 μl and contained 50 mM Hepes/NaOH, 200 mM $(NH_4)_2SO_4$ pH 7.0, 7 mM DTT, 25 μg/ml catalase, 25 μM $(NH_4)_2Fe(SO_4)_2$ and standard substrate concentrations were 70 μM tryptophan, 300 μM BH_4 and 500 μM O_2. All measurements were done at 15°C.

Stock solutions of the different compounds were prepared as seen in table 8.2. Catalase was dissolved in water in larger batches and frozen at -20°C in aliquots of 1.0 ml in Eppendorf tubes until use, whereas DTT, tryptophan, BH_4 and $(NH_4)_2Fe(SO_4)_2$ were freshly prepared prior to each measuring session. DTT, tryptophan and $(NH_4)_2Fe(SO_4)_2$ were dissolved in water, while BH_4 was dissolved in 10 mM HCl in order to protonate N5 and prevent autooxidation [137]. DTT and BH_4 were kept on ice during the measurements.

Table 8.2. Concentration and amounts of the stock solutions used in the standard assay. Compounds marked with * are compounds where the concentration changes with changing in tryptophan or BH_4 concentration.

	Concentration in the stock solution	Volume in μl	Concentration in the assay
Water		Variable	
Hepes/NaOH,	125 mM Hepes	1000	50 mM
$(NH_4)_2SO_4$ pH 7.0	50 mM $(NH_4)_2SO_4$		200 mM
$(NH_4)_2Fe(SO_4)_2$	1.27 mM	50	25 μM
DTT	175 mM	100	7 mM
Tryptophan*	3 mM	50	60 μM
Catalase	1.25 g/L	50	25 mg/L
BH_4*	15 mM	50	300 μM

The concentration of tryptophan was determined in 10 mM HCl using ε_{278} = 5500 M^{-1} cm^{-1} and the concentration of BH_4 was determined in 2 M HCl using ε_{266} = 18000 M^{-1} cm^{-1} [137]. This was done using UV-Vis visible measurements on a HP Diode-array 8453 spectrophotometer.

8.3.3.4 Calibration of the oxygen electrode and controlling the O_2 flow

Controlling the O_2 concentration is not as straightforward as controlling the concentration of tryptophan or BH_4, which is determined by UV-Vis spectrophotometry. The O_2 concentration in an aqueous solution is dependent on several factors, such as temperature, the ionic strength and the partial pressure of O_2 above the solution. The solubility of O_2 in water at 15°C is 1528 µM at an O_2 partial pressure of 101.325 kPa [139]. In all following measurements the value of 1528 µM was used as equal to 100 % O_2. This is an approximation since the measurements were done in 50 mM Hepes/NaOH, 200 mM $(NH_4)_2SO_4$ pH 7.0 and not in pure water. Another complication in controlling the O_2 concentration is that the assay mixture contains 7 mM DTT which reacts with O_2 [140]. The reaction at pH 7.0 between DTT and O_2 is not fast, but it is faster than the diffusion of O_2 from the gas above the solution and fast enough to disturb the oxygen concentration in the mixture. To solve this problem it was necessary to use an O_2 sensing electrode so that the O_2 concentration could be measured at the time of the reaction. Because it was impractical to have the electrode in the cuvette during measurements two cuvettes was used: One reaction cuvette and one reference cuvette. The reference cuvette contained the same solution as the reaction cuvette except that enzyme and BH_4 was not added to the reference cuvette. The O_2 concentration was measured in the reference cuvette.

The calibration of the electrode was done by placing the electrode into the reference cuvette containing 50 mM Hepes/NaOH, 200 mM $(NH_4)_2SO_4$ pH 7.0 at 15°C. The zero set point was obtained by flushing the solution with 100 % N_2 until saturation followed by flushing with 100 % O_2 until saturation which was equal to 1528 µM O_2 in 15°C water. The flushing tube was lifted out of the solution but still keeping 100 % O_2 above the solution surface and after a few minutes the oxygen meter was set to 100 % O_2. This was done to make sure that the solution was not supersaturated with oxygen. Corrections were not made for fluctuations in the ambient air pressure. To obtain the desired O_2 concentration in the reaction solution, the solutions in the reference and the reaction cuvette were flushed with appropriate N_2/O_2 mixtures.

8.3.3.5 Procedure for measuring the initial rate of 5-hydroxytryptophan formation

From stock solutions water, buffer, tryptophan, DTT and Fe in the amount given in table 8.2 were added to the reaction cuvette containing cylindrical magnetic stir bar. Lids with three holes for gas tubes, O_2 electrode and enzyme/substrate addition were sealed to the cuvettes with parafilm. The cuvettes were placed in the temperature-controlled-cuvette holder in the fluorescence spectrophotometer and gas tubes and oxygen electrode added. The solutions were flushed with the desired gas mixture of O_2 and N_2 with magnetic stirring done as described in section 8.3.3.4. The oxygen concentration was monitored and at a desired concentration the tubes were pulled up still keeping a constant flow of the gas mixture above the solutions. Catalase and enzyme (kept on ice) was added to the reaction cuvette and an equal volume of

water (kept on ice) was added to the reference cuvette. BH_4 was added to the reaction cuvette to initiate reaction and an equal volume of 10 mM HCl was added to the reference cuvette.

8.3.3.6 Activity measurements of c*h*TPH1

The enzyme activity measurements were done using the assay described in section 8.3.3.3 and the procedure described in section 8.3.3.5. The enzyme solution was prepared as described in section 8.3.3.2. Each of the three substrate concentrations were varied while maintaining the other two substrate concentrations fixed using the standard substrate concentrations: 70 μM tryptophan, 300 μM BH_4 and 500 μM O_2. All data points were measured at least three times.

8.3.3.7 Data acquisition

The initial slope (int/min) was determined using the fluorescence spectrophotometer software. The software performs linear regression on an interval of the progression curve where the selection of the interval was done manually with an interval of minimum 0.04 min. The initial rate was converted to μM 5-hydroxytryptophan/min from the standard curves at different concentration of BH_4 as mentioned in section 8.2.1 and given in appendix A2**.** When the initial rates had been measured the appropriate equation was fitted to the data using OriginPro 7.5 from OriginLab Corp. The kinetic data for varied concentrations of BH_4 and O_2 were fitted to the Michaelis-Menten equation 8.1, whereas data for varied tryptophan concentration were fitted to equation 8.2 taking substrate dead-end inhibition into account.

For each fit to the presented in the following sections a SS/DoF is presented. This is the sum of squares (SS) divided by the number of degrees of freedom (DoF). The closer SS/DoF is to zero the better. The coefficient of determination (R^2) is also presented in the figures showing the data points and fitted equation [141].

8.4 Results

The results described in this chapter were published in 2009 [142].

8.4.1 Expression and purification

c*h*TPH1 is expressed in *E. coli* BL21(DE3) as described in section 8.3.2. A high level of c*h*TPH1 expression was achieved as seen on the SDS-Page analysis in figure 8.4 lane R. The supernatant (figure 8.4 lane S) was loaded onto a Q Sepharose High Performance column and c*h*TPH1 eluted at a conductivity of 1.5 mS/cm. A sample of the collected fractions from the anion exchange is seen in the SDS-Page in figure 8.4. c*h*TPH1 eluted from the 26/60 Superdex 75 gel filtration column at 147 ml. A sample of the collected fractions from the gel filtration is shown in figure 8.4. The c*h*TPH1 band corresponds to the expected molecular weight of 36.1 kDa. The yield was 10 mg/L culture with a specific activity of 70 μmol 5-hydroxytryptophan/(min μmol c*h*TPH1) (measured with 70 μM tryptophan, 300 μM BH_4 and 500 μM O_2).

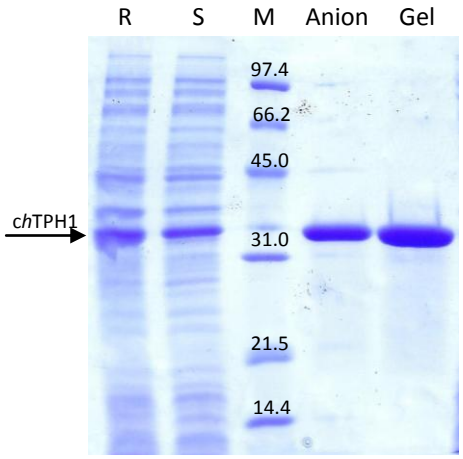

Figure 8.4. SDS-Page analysis of samples from the purification of c*h*TPH1. R is the raw extract (1 µl), S is the supernatant loaded onto the anion exchange column (2 µl), M is the molecular weight standard given in kDa, Anion is the collected fractions from the anion exchange column and Gel is the collected fractions from the gel filtration column.

8.4.2 The kinetic parameters of c*h*TPH1

After purification of the sample, the apparent kinetic parameters were determined. This was done as described in section 8.3.3. The measured initial rates with varied tryptophan concentration are shown in figure 8.5A, varied concentration of BH_4 in figure 8.5B and varied concentration of O_2 in figure 8.5C. The fitted curve is also shown in the figures. The determined kinetic parameters of both c*h*TPH1 and c*h*TPH2 (determined by Michael S. Windahl) are summarized in table 8.3.

Table 8.3. The apparent enzyme kinetic parameters of c*h*TPH1 and c*h*TPH2.[a]

Enzyme	Varied substrate	K_m ± SE (µM)	V_{max} ± SE (µM min^{-1})	K_i ± SE (µM)	k_{cat} (min^{-1})
c*h*TPH1	Tryptophan	22.8±0.9	201±11	72±7	160
c*h*TPH2	Tryptophan	15.0±0.4	151±1	-	302
c*h*TPH1	BH_4	315±37	164±10	-	130
c*h*TPH2	BH_4	26.5±1.3	137±2	-	274
c*h*TPH1	O_2	109±7	105±2	-	83
c*h*TPH2	O_2	273±9	202±3	-	404

[a] Measured at 15˚C with the fixed substrate concentration being: 70 µM tryptophan, 300 µM BH_4 and 500 µM O_2. Assay conditions were 50 mM HEPES/NaOH, 200 mM $(NH_4)_2SO_4$, pH 7.0, 7 mM dithiothreitol (DTT), 25 µM $(NH_4)_2Fe(SO_4)_2$, and 0.025 g/L catalase. Standard error (SE) at 95% confidence interval.

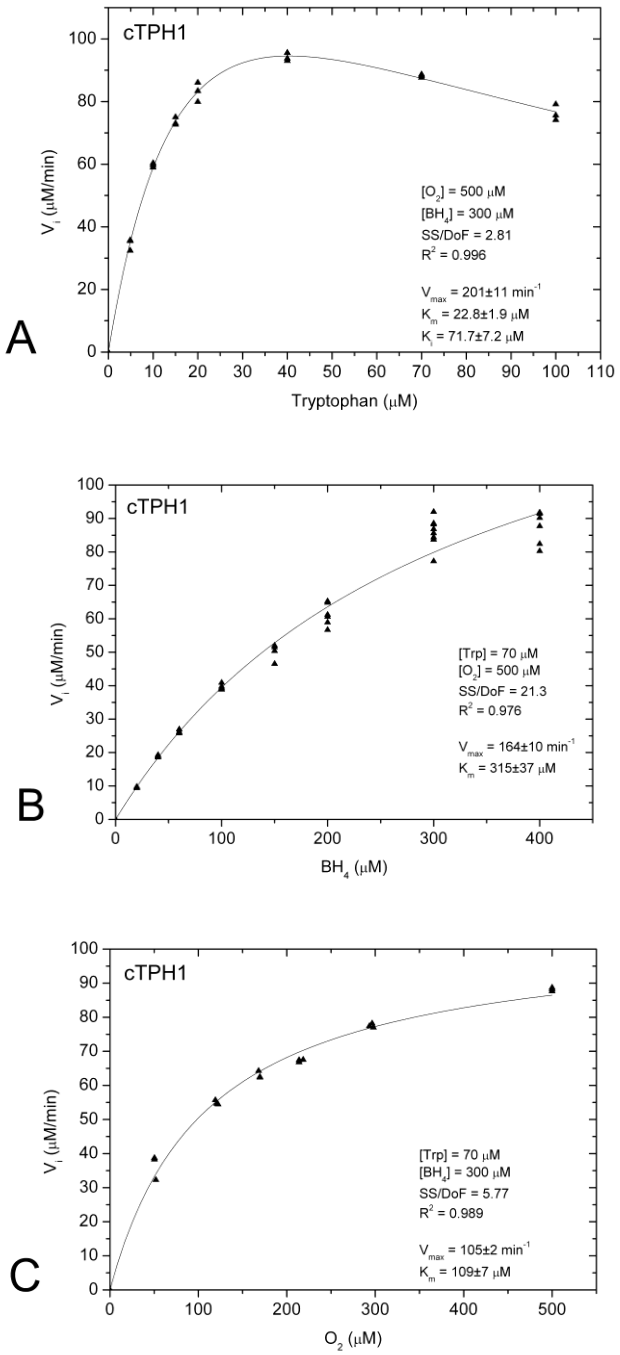

Figure 8.5. Initial rate as a function of substrate concentrations of c*h*TPH1. A) Varied concentrations of tryptophan, B) varied concentrations of BH_4 and C) varied concentrations of O_2. Equation 8.2 was fitted to the data from varied tryptophan concentrations. Equation 8.1 was fitted to the data from varied BH_4 and O_2 concentrations. The curves from the fitted equations are shown. The kinetic parameters obtained from fitting equation 8.1 and 8.2 to the data are listed in table 8.3.

8.5 Discussion

8.5.1 Expression and purification

c*h*TPH1 was expressed and purified using a method developed in my master project with a high purity without any other bands on the SDS-Page gel.

8.5.2 Activity measurements of cTPH1

The apparent K_m values for all three substrates of c*h*TPH1 and c*h*TPH2 were determined at the same conditions and the data are therefore directly comparable.

From figure 8.5A substrate inhibition by tryptophan is observed above 40 μM, which is lower than that reported for c*h*TPH1 [36,143]. The $K_{i,tryptophan}$ for c*h*TPH1 was determined to 72±7 μM. These values corresponds to values determined for c*gg*TPH1 where inhibition was observed above 15 μM and with a $K_{i,tryptophan}$ of 163±24 μM [12]. Substrate inhibition of c*h*TPH2 is not observed, see table 8.3. Substrate inhibition by tryptophan have been reported for TPH1 with a $K_{i,tryptophan}$ of 282-740 μM with assay conditions of 40 mM HEPES pH 7.0, 250 μM BH_4, 2 mM DTT, 10 μM $(NH_4)_2Fe(SO_4)_2$ and 30°C [49]. These conditions differ significantly from the ones used in these experimental procedures both in the temperature and the ionic strength of the solution and can therefore not be directly compared. At conditions similar to the one used here (50 mM MES, 100 mM (NH4)2SO4, 6 mM DTT, pH 7.0, 15°C) a $K_{i,tryptophan}$ of 146±14 μM have been reported for the catalytic domain of rabbit TPH1 [144]. This $K_{i,tryptophan}$ is in the same range as the 72±7 μM of c*h*TPH1 and 164±24 μM of c*gg*TPH1. To determine the mechanism of inhibition as well as determining why tryptophan inhibition is not observed for c*h*TPH2 (which is unexpected in view of the high sequence identity) further studies needs to be performed.

The $K_{m,tryptophan}$ values for the two isoforms are similar; 22.8±0.9 μM for c*h*TPH1 and 15.0±0.4 μM for c*h*TPH2. These values are in line with the value for c*gg*TPH1 (7.7±0.7 μM) determined at the same conditions [12]. For *h*TPH1 the reported $K_{m,tryptophan}$ values are in the range of 10.6 – 33 μM [49,143,145] while for TPH2 the reported $K_{m,tryptophan}$ values are in the range of 20.1 - 77 μM [18,49,145]. It should be noted that the assay conditions in [49,18,143] differ significantly from the ones used in this experiment by using a higher temperature and lower ionic strength Additionally, the experiments by Tenner et al. [145] were done on crude lysates and it is unclear if it is actually the initial rates that have been measured [145]. It is known that the catalytic domain is unstable at low ionic strength [12,144] and therefore 200 mM $(NH_4)_2SO_4$ have been used in this assay. No $(NH_4)_2SO_4$ was added to the assay used in [49,18,143] and this may yield an unstable catalytic domain. From the results obtained in this it is concluded that the $K_{m,tryptophan}$ values for the two isoforms are similar and within a quite narrow range.

A large difference is observed for $K_{m,BH4}$ with a $K_{m,BH4}$ of 315±37 μM for c*h*TPH1 and a $K_{m,BH4}$ of 26.5±1.3 μM for c*h*TPH2. The value for c*h*TPH1 is similar to the c*gg*TPH1 $K_{m,BH4}$ which is 324±10 μM [12] and is more than a factor 10 higher than the $K_{m,BH4}$ for c*h*TPH2. Currently, two possible explanations for this large difference between the two isoforms can be envisioned. This large

difference might be a result of the substrate inhibition by tryptophan observed for c*h*TPH1 or it might be due to some structural differences in the BH_4 binding pocket resulting in a higher affinity of c*h*TPH2 for BH_4. For TPH1 reported $K_{m,BH4}$ values are in the range of 27-50.8 μM [49,143] and for TPH2 reported $K_{m,BH4}$ values are in the range of 6.2-20.2 μM [18,49].

The $K_{m,O2}$ value of c*h*TPH1 is 109±7 μM while it is 272±9 μM for c*h*TPH2. The reported $K_{m,O2}$ for c*gg*TPH1 is 39±2 μM [12]. $K_{m,O2}$ have only been reported for partially purified TPH from natural sources (rabbit hindbrain [146], neoplastic murine mast cells [147] and human carcinoid tumor [148]). The assay conditions used in [146,147,148] differ greatly from the ones used in this assay, either by using 6-methyl-5,6,7,8-tetrahydropterin or 6,7-dimethyl-tetrahydropterin [147,148] and/or by not measuring initial rates [146,147,148]. A comparison with these values is therefore pointless.

8.5.2.1 Mass spectrometric observations

From mass spectrometric analysis of c*h*TPH1 done in this project (chapter 9) two species were present in the sample; one corresponding to c*h*TPH1 and one corresponding to either a truncated version of c*h*TPH1 or another protein. The purification method of the sample used for kinetic characterization and for mass spectrometric analysis was the same. The only difference was the gel filtration buffer used, which should not have any influence on the species present in the sample after purification. The other species present in the mass spectra does not contain iron and it does not bind the other substrates. Therefore, the only influence this species has is the determination of the concentration of c*h*TPH1 by absorbance measurements, which will only affect the specific activity and the determination of k_{cat}.

The mass spectrometric results were obtained in the last part of my Ph.D. project and after the kinetic characterization of the isoform.

8.6 Conclusion

c*h*TPH1 have been expressed and purified. The apparent K_m, V_{max} and K_i of c*h*TPH1 have been successfully determined and compared with c*h*TPH2. Overall, large differences are observed in the enzyme kinetic parameters of c*h*TPH1 and c*h*TPH2 despite the high primary sequence identity (81 %) and homology (91 %) between the catalytic domains of the two TPH isoforms (mentioned in chapter 2). Just a few amino acid substitutions probably lead to subtle structural differences causing these large differences in enzyme kinetic parameters. These differences hold promises for future identification of isoform-specific compounds that selectively can target either TPH1 or TPH2 in contrast to the recently published inhibitors which inhibits both isoforms [43,82].

9 Mass spectrometric analysis of *h*TPH variants

Mass spectrometry (MS) is an analytical tool that can be used for mass determination, verification of species in a sample as well as studying sample homogeneity, which is an important factor in crystallization of proteins, and structural analysis. In this chapter mass spectrometry of intact non-covalent proteins and protein complexes will be described. This will be followed by an experimental description of mass spectrometric characterization of TPH variants and a result and discussion section.

9.1 Mass spectrometry

In the last two decades MS has gained enormous significance in structural biology and it has been used as a major tool in investigation of intact protein complexes to study their topology, stoichiometry, secondary, tertiary and quaternary structure [149,150]. In the 1990s the first observations of specific non-covalently interactions were reported [150,151,152].

The overall principal in MS is to determine the molecular mass of charged species in a sample. It consists of three steps where the first step is to generate gas-phase ions from a sample of interest, the second step is to analyze the gas-phase ions and the third step is detection of the ions [149]. In the following sections the first two steps will be described.

9.1.1 Electrospray ionization

Different techniques have been used to generate gas-phase ions such as chemical and electron ionization (CI and EI). The problem with these ionization techniques is that they are only able to analyze volatile organic compounds and not biopolymers such as proteins and nucleic acids. The

introduction and development of the matrix-assisted laser desorption ionization (MALDI) and electrospray ionization (ESI) created a new approach to the MS in protein research, due to their ability to ionize even fragile compounds like proteins. In particular ESI has proven to be the ionization method of choice for the analysis of intact proteins and non-covalent protein complexes [153].

ESI was developed in the 1960s. In 1968 Dole *et al* [154] showed that it was possible to generate gas-phase macro-ions of definite mass-to-charge states by electrospray ionization, and in 1970 they sprayed polymers of masses from 600 to 97.200 Da [155]. 15 years later Yamashita and Fenn [156] coupled ESI to MS and five years later John B. Fenn published a study of ESI on biological macromolecules in Science [157]. His achievement was awarded in 2002 with the Nobel Prize in Chemistry.

To analyze intact non-covalent protein complexes, nanoelectropsray ionization (nanoESI) is the ionization method of choice (see section 9.1.1.2). To get a better understanding of nanoESI and the reason why it is used in intact protein complex analysis, the mechanism of ESI will be described first.

9.1.1.1 Mechanism of Electrospray ionization

The electrospray device generally consists of a needle and a counter electrode. A sample solution flows through the needle, which is maintained at voltage of 2-3 kV and atmospheric pressure, producing gas-phase ions. These ions are then sampled into a vacuum stage of the mass spectrometer through an interface region. The ESI process can be divided into three major steps: First step is production of charged droplets, second step is solvent evaporation of the droplets, which reduces the size of the charged droplets generating highly charged “daughter” droplets, and the third step is the mechanism where charged gas-phase ions are produced from highly charged droplets [157,158].

In a positive ion mode a positive voltage is applied to the needle inducing an electric field. The field causes the ions in the solution to move. Positive ions will move toward the outlet of the needle, whereas negative ions will move away from the outlet of the needle. This charge separation eventually make the positive charges, at the liquid surface, to repel each other and as the repulsion overcomes the surface tension of the liquid, the surface will begin to expand further downfield, away from the needle tip. This results in a cone-like shape, called the “Taylor cone” [159], and is illustrated on figure 9.1. If the applied field (E) is sufficiently high a fine spray of highly charged droplets will emerge from the cone tip [158,160].

Charged droplets will drift downfield through the air towards the counter electrode. Solvent from the droplets will evaporate, thus decreasing the droplet size while maintaining the charge. A decrease in size at a constant charge leads to an increase in the electrostatic repulsion of the charges at the surface and at a given radius, R, and charge, q, the repulsion force is equal to the force due to the surface tension, which holds the droplet together. This is known as the Rayleigh limit [161] and is given by equation 9.1:

$$q_R = 8\pi (\epsilon_0 \gamma R^3)^{1/2} \quad (9.1)$$

where ε_0 is the permittivity of the vacuum and γ is the surface tension of the solvent. When the radius is smaller than the Rayleigh limit the droplet becomes unstable and will undergo "coulomb explosion" or droplet fission. Droplets at the Rayleigh limit undergo fission by distorting to a teardrop shape and emitting a jet of very small droplets, as shown on figure 9.2. These small droplets can evaporate and undergo another "coulomb explosion" at their Rayleigh limit, thus producing smaller and smaller droplets [160].

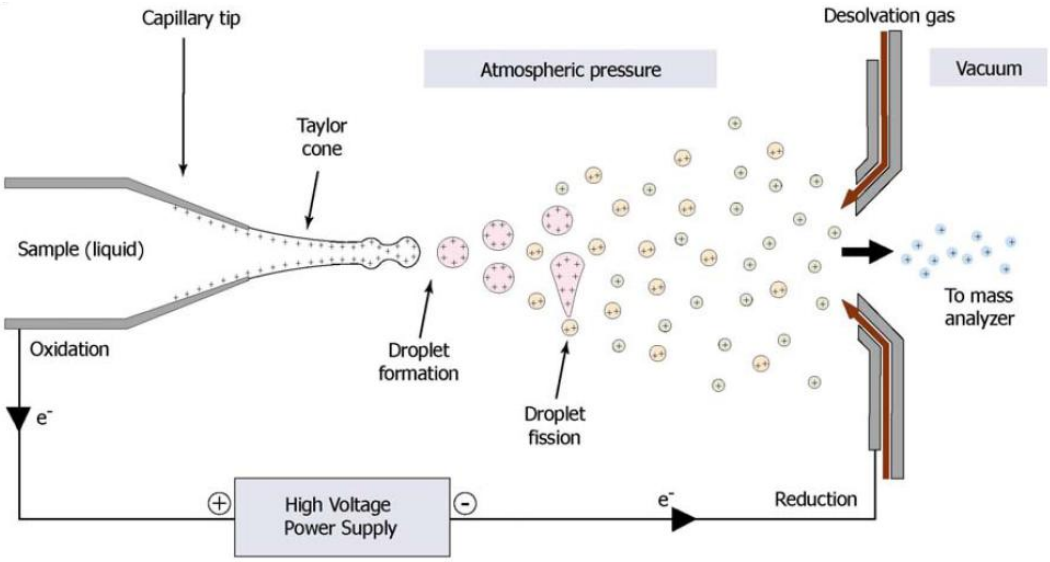

Figure 9.1. Schematic representation of the electrospray ion source and the steps involved in electrospray ionization [162]. Reproduced with permission.

Figure 9.2. Teardrop droplet [163]. Reproduced with permission from Springer.

The electrospray source functions as an electrolysis cell, where oxidation reactions, such as production of H^+ from water, occur at the liquid-metal interface of the capillary tip and reduction reactions (removal of positive ions) occur at the negative counter electrode. These electrochemical reactions, which maintain the charge balance, allow continuous production of charged droplets [164,165].

Two different mechanisms have been proposed to account for the formation of gas-phase ions from the small charged droplets: Dole's explanation, the charged residue model (CRM) [154] and Iribarne and Thomson's theory, the ion evaporation model (IEM) [166]. In CRM "coulomb explosions" is assumed to continue until only one molecule is left in each droplet, and after all

the solvent has evaporated the molecule will be left as a charged gas-phase ion by retaining the charge of the droplet, as shown in figure 9.3. However, in IEM solvent evaporation and coulomb droplet fission will continue until a certain radius (R ≈ 10-20nm) of the charged droplets. When this radius is reached, direct emission of molecular ions M^+ into the gas-phase will occur. The charge on the droplet required for this ion evaporation is lower than that required for "coulomb explosions" and therefore, it replaces "coulomb explosions" [167]. Experimental evidence suggests that formation of ions from large globular intact proteins proceed through CRM, whereas IEM is true for small molecules [167,168].

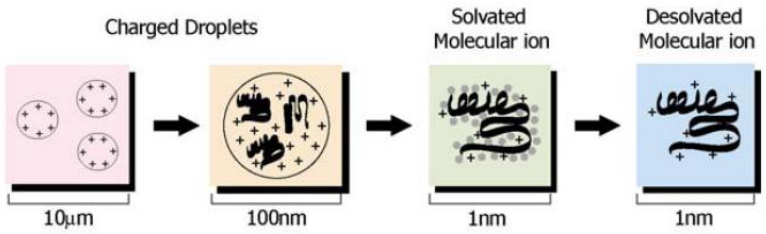

Figure 9.3. Schematic representation of the charged residue model where "coulomb explosions" continue until only one molecule is left in each droplet and after all the solvent has evaporated the molecule will be left as a charged gas-phase ion by retaining the charge of the droplet [162]. Reproduced with permission.

9.1.1.2 Nano electrospray

In conventional electrospray, the ion source typically sprays ion droplets of the size of 1-2 µm using a capillary with an inner diameter of approximately 100 µm. To evaporate the solvent from these large droplets and to achieve ion formation, volatile solvents with low surface tension were added and the solution was often heated [169,170]. The introduction of a nanoESI source in 1994 by Wilm and Mann [169] allowed the analysis of samples from water under more physiological conditions and was at the same time introduced to achieve lower flow rates [169].

In nanoESI borosilicate glass capillaries are used and are typically coated with gold to make them conductive. These capillaries have an inner tip diameter of approximately 1 µm, resulting in droplets with a diameter less than 200 nm, about 100-1000 times smaller than for conventional ESI. The smaller droplets make the evaporation more easily and facilitate stable spraying of solvents with high surface tensions such as water and aqueous buffers, allowing proteins to remain intact in their native conformation, thus preserving non-covalent interactions. The flow rate is approximately 20-50 nL/min allowing long measuring time from small amounts of sample (1 µl can last for more than 30 min), which is also a benefit in analysis of proteins due to low sample volumes [169,170,171]. Sometimes it may be necessary to apply a backing pressure to initiate the liquid flow [169,170].

9.1.1.3 Electrospray spectra and mass determination

Ions formed by electrospray are typically multiply charged ions of the form $(M + nH)^{n+}$ (in positive mode). Several peaks are observed in the spectra due to different degrees of protonation of basic sites on a protein or protein complex (in positive ion mode). These are known as 'charge states' [172]. An example of a mass spectrum is shown in figure 9.4.

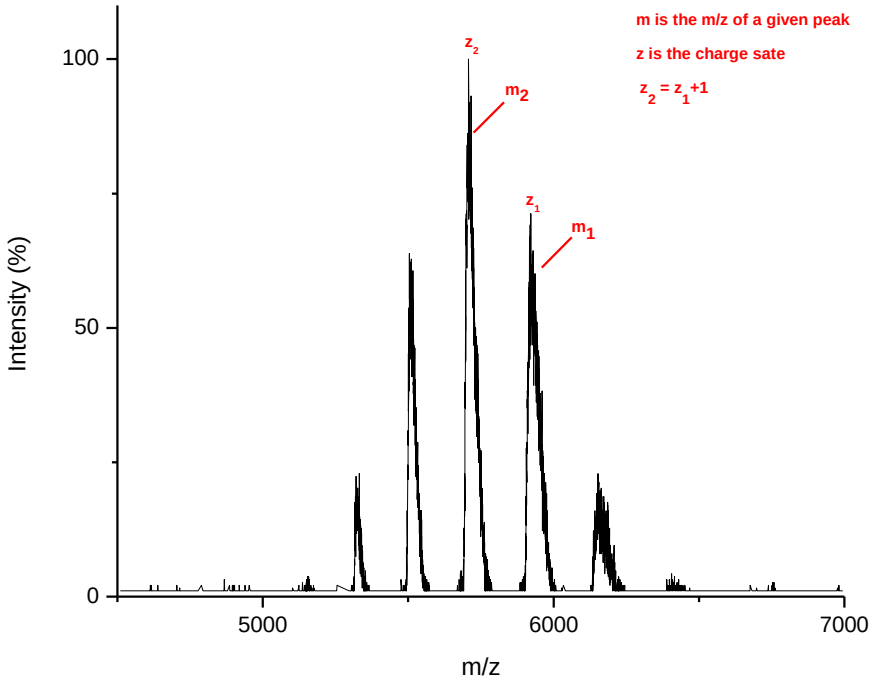

Figure 9.4. An illustration of a spectrum from ESI mass spectrometric analysis of a non-covalent protein complex composed of multiply charged ions.

To determine the molecular mass of a neutral protein and protein complex from its electrosprayed ion mass spectrum it is important to separate the individual charge states. The charge states and molecular mass can be determined by solving corresponding equations for adjacent peaks. The charge states for adjacent peaks can be calculated from the following equations 9.2 and 9.3,

$$m_1 = \frac{M + z_1 M_{H^+}}{z_1} \tag{9.2}$$

$$m_2 = \frac{M + z_2 M_{H^+}}{z_2} = \frac{M + (z_1 + 1)M_{H^+}}{z_1 + 1} \tag{9.3}$$

where M is the molecular mass, z is the number of charges (charge state) present on the ion where $z_2 = z_1 + 1$, m_1 and m_2 are the mass-to-charge (m/z) values for each peak and M_{H+} is the mass of a proton [172]. Solving these equations for z_1 gives equation 9.4, from which the charge, z_1, is determined, and substitution of this value into equation 9.2 or 9.3 allows the calculation of

the molecular mass, *M*. Calculation of the molecular mass of a protein with multiply charged ions is done by using this simple algorithm where the mass is calculated for two charge states differing by one, and subsequently repeating this calculation for the rest of the charge states. The molecular mass of a protein in this simple case is then determined by averaging these masses.

$$z_1 = \frac{m_2 - M_{H^+}}{m_1 - m_2} \tag{9.4}$$

Using this algorithm the mass-to-charge for a multiply charged ion is converted to the mass of the zero-charge molecule [172,173]. A problem with this approach is that it assumes that all charge is due to excess or deficit of protons for positive or negative ions, respectively. It does not take into account the presence of modifications such as metals and/or disulfide bonds in a protein. The metal center in metalloproteins can carry charge depending on its oxidation state and therefore, the use of equation 9.2 or 9.3 will overestimate (or underestimate) the number of protons giving a higher (or lower) molecular mass than the actual mass of the metalloprotein. It is important to take the oxidation state into account for proper determination of the molecular mass from the mass spectrometric data. The first step in determining the oxidation state is to calculate the mass of the metalloprotein from its amino acid composition plus the atomic masses of the metal center, cofactors and possible post translational modifications present in the protein. This mass is termed the calculated mass, as seen in table 9.1. The second step is to determine the apparent mass, which is the mass determined using equation 9.2 and 9.3 for a protein where all of the charge of an ion is assumed to be due to excess or deficit of protons. The apparent mass will differ to the actual mass by the number of protons equal to the charge present on e.g. the metal-centre (see table 9.1). A comparison of the apparent mass with the calculated mass allows the oxidation state in the metalloprotein to be determined from the difference between the two values [173]. For an intact disulfide bond there will be a difference between the apparent mass and the calculated mass corresponding to two protons, due to a loss of one proton from each thiol group by formation of a disulfide bond [173]. The mass which takes the oxidation state and the number of disulfide bonds into account is termed the expected molecular mass. Therefore, in mass spectrometric analysis of proteins it is important to distinguish between the following masses given in table 9.1.

When determining the molecular mass of large proteins the average mass is usually used, due to incomplete resolution of the isotopic distribution, and corresponds to the centroid of the molecular peak in the experimental mass spectral data. It is important to remember that different analyzers have different resolving power and some analyzers such as FTICR can resolve the isotope distribution for very large proteins [172,173]. In table 9.2 the average masses for the most common elements in proteins are given as well as for iron.

The experimental mass determined from the mass spectra is sometimes higher than the calculated mass from the sum of the protein components. This is due to incomplete removal of

solvent and/or buffer ions during the electrospray process, which results in broadening (tailing) of the peaks and therefore a shift in the *m/z* to a higher value [153].

Table 9.1. The masses that should be distinguish between in MS of intact proteins [173].

Masses	Definition
Calculated mass	The mass which is calculated based on the molecular formula of a neutral protein molecule plus the atomic masses of the metal center, the masses of cofactors and possible post translational modifications present in the protein; i.e., all ionizable sites in the protein are assumed to be neutral.
Expected mass	The mass which is determined from the calculated mass, but where oxidation state and number of disulfide bonds have been taken into account. This is the mass that should be compared with the apparent mass.
Apparent mass	The mass which is derived directly from the experimental data using the algorithm given in equation 9.2 and 9.3 where the mass-to-charge for a multiply charged ion is converted to the mass of the zero-charge molecule. This algorithm assumes that all charge is due to excess of protons.

Table 9.2. Masses for the most common elements.

Name	Molecular formula	Average Masses
Hydrogen	H	1.0079
Carbon	C	12.011
Nitrogen	N	14.0067
Oxygen	O	15.9994
Sulfur	S	32.06
Iron	Fe	55.847

9.1.1.4 Electrospray of non-covalent complexes

The analysis of non-covalent complexes by mass spectrometry presents several challenges. Firstly, analyzing large complexes requires a high *m/z* range. Non-covalent complexes carry relatively low charge in their native compact conformation and thus large non-covalent complexes have relatively high *m/z*, because of the inaccessibility of some of the charge state sites compared to the open (unfolded) solution conformation [150,152]. In most quadrupole analyzers this can become a major problem, because of their upper *m/z* limit (see section 9.1.2.1), but by increasing the quadrupole operation range up to 32,000 m/z this problem can be overcome [174]. Secondly, maintaining the right solution condition is important for keeping the non-covalent complex in its folded, native state and therefore the use of appropriate solvents (almost exclusively aqueous solutions), pH values and ionic strength is necessary to maintain intact complex. Generally, volatile, aqueous buffered solutions, such as ammonium acetate or ammonium bicarbonate, are used and prepared at physiological pH (6-8) [175,176]. Thirdly, solvent adducts are often observed on large multiply charged complexes and therefore, the degree of desolvation, i.e. stripping of solvent molecules from the molecular complex, is a critical

parameter in observation and correct molecular mass determination of the complex (also mentioned in section 9.1.1.3) [175]. Therefore, additional desolvation can be accomplished by heating of the capillary in the interface region and by gas phase collisions in the interface region downstream from the atmospheric pressure [177]. Non-covalent complexes are extremely fragile in the gas phase state and are easily dissociated using an excess of heat or too high collision energy. It is therefore important to maintain a balance between removing solvent molecules and keeping the complex intact [175,176,178]. Due to orders of magnitude smaller droplets produced in nanoESI than in conventional ESI, the desolvation process will be less of a problem. Fourthly, gas-phase ions are generated at atmospheric pressure, as mentioned in section 9.1.1.1**,** and introduced into the vacuum chamber by acceleration to velocities of several hundred meters per second [179]. Since energy is proportional to mass for ions having the same velocity, transmission of large ions (mass > 500 Da) into the vacuum acquire large amount of energy compared to small ions. This serves to broaden the ion beam leading to transmission loss. Using higher pressures in the initial stages of the instrument will result in more collisions with the gas molecules, which cool the large ions, effectively focus the ion beam and allowing more ions to reach the detector. This phenomenon is known as collisional cooling [179].

Non-covalent complexes are stabilized by water molecules and in the gas phase these water molecules are removed. One major issue regarding ESI is whether or not protein and protein complexes preserve their solution structure in the absence of water in the gas phase. Recent findings for protein complexes in the gas phase suggest that many features of protein structure, including compact structure, elements of secondary structure, hydrogen bonding interactions, and quaternary structure, can be retained in the absent of solvent. Although, it is important to remember that these results do not necessarily imply that the precise interactions present in the native state of a protein complex are maintained, but the overall size(s) and many of the binding interactions deduced for proteins in solution are found to persist in the gas phase [180,181,182].

One problem in ESI-MS is the tendency of proteins and protein complexes to form nonspecific interactions with other molecules or ions present in the sample resulting in complexes, which are not present in solution. These are termed nonspecific complexes. The formation of gaseous macromolecular ions in ESI proceeds through CRM, as mentioned in section 9.1.1.1, where the initial ESI droplets undergo solvent evaporation until they come close to the Rayleigh limit at which point they undergo droplet fission releasing several small multiply charged nanodroplets (offspring droplets). If these offspring droplets contain more than one analyte molecules, nonspecific interactions may be formed as the solvent evaporates to form gaseous ions [183]. The probability of a droplet to contain more than just one analyte molecule is increased by increasing the concentration of analyte. Also by lowering the potential within the instrument (e.g. the declustering potential) the presence of nonspecific interactions increases. Therefore, to eliminate these nonspecific interactions either the concentration can be lowered or the potentials within the instrument can be increased [184]. The problem with nonspecific interactions is in interpretation of the mass spectrum where they are misidentified as specific. This will obscure the binding stoichiometry [183,184].

9.1.2 Mass analyzers

Mass analyzers separate ions according to their *m/z* ratios based on ion behavior in an electrical and/or magnetic field. There exist many different analyzers and some of the most widely used are the Quadrupole (Q) and the Time-Of-Flight (TOF) analyzers.

9.1.2.1 Quadrupole

The quadrupole mass filter is a commonly used analyzer. It consists of four cylindrical electrodes (or rods), which are connected parallel to each other in opposite pairs with a fixed direct current (DC) and an alternating radio frequency (RF) potential applied to them, as shown in figure 9.5. The two opposite rods have a potential of $+(U - V\cos(2\pi\omega))$ and the other two of $-(U - V\cos(2\pi\omega))$, where *U* is the fixed DC potential and *V*cos(2$\pi\omega$) is the alternating RF potential of amplitude *V* and frequency ω [185]. This applied field causes the ions to oscillate during their time in the quadrupole and the ions are separated based on the different stabilities of their trajectories. By changing the two parameters *U* and *V* the quadrupole can operate in two different modes; in a RF only mode and in a mass filter mode. In the RF only mode *U* is set to zero and the quadrupole operates as a broad mass filter, whereas in the mass filter mode *U* and *V* are fixed and only ions with specific *m/z* values passes through the analyzer [186].

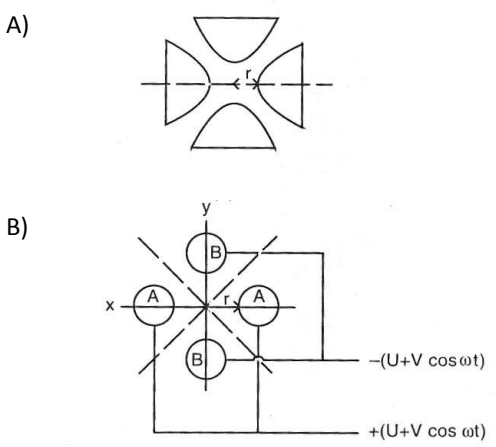

Figure 9.5. A) A cut through the quadrupole indicating the radius between the rods. B) A and B indicate rods with opposite charge. The dotted lines indicate planes of zero electrical fields [187]. Reproduced with permission from Copyright Clearance Center.

The quadrupole operates in a limited *m/z* range with a certain upper limit, that is dependent on the RF amplitude and frequency as well as the inner radius between the rods and the highest *m/z*, M_{max}, that can be transmitted is given by equation 9.5,

$$M_{max} = \frac{7 \text{ x } 10^6 \, V_m}{f^2 r_0^2} \tag{9.5}$$

with $V_m$cos(2π*ft*) as the RF voltage applied between adjacent rods ($2V_m$ is the peak-to-peak amplitude, *f* is the frequency and *t* is the time), as mentioned earlier, and r_0 as the inner radius

between the rods in meter. The upper limit for a conventional quadrupole is between 3000 and 4000 *m/z* and therefore, the analysis of large non-covalent proteins and protein complexes with much higher *m/z* ratios will become a problem in these analyzers. To increase the upper limit all three parameters in equation 9.5 (V_m, f and r_0) could be changed, but changing V_m is limited, due to possible breakdown of the high voltage between the rods. Decreasing r_0 can reduce transmission. In practice there is no lower limit to the frequency and therefore, by adjusting this parameter the mass range can be extended. Decreasing the frequency of the quadrupole reduces the resolution of the instrument, but using the quadrupole as a mass filter to isolate ions for tandem MS (mentioned in section 9.1.3) and a TOF analyzer as second analyzer, the resolution is not compromised significantly [174].

9.1.2.2 TOF analyzer

The principle of the TOF analyzers is to separate ions according to the time it takes for an ion to reach a detector in a field-free drift space. Ions, formed in the ion source, are accelerated into a field-free drift region with the same amount of kinetic energy ($E_{kin} = zeV_a$), but different velocities depending on their masses as given in equation 9.6,

$$v = \left(\frac{2zeV_a}{m}\right)^{½} \tag{9.6}$$

where z is the number of charges, e is the charge of an electron, V_a is the acceleration voltage and *m* is the mass. The time it takes an ion to travel thought the drift tube, also termed the drift time, t_D, can then be described by equation 9.7,

$$v = \frac{dx}{dt} = \frac{D}{t_D} \quad \Leftrightarrow \quad t_D = \left(\frac{m}{2zeV_a}\right)^{½} D \tag{9.7}$$

where *D* is the length of the drift region. From these equations it is seen that the *m/z* ratio is proportional to the drift time and ions with higher masses will have a longer drift time and therefore reach the detector later than ions with smaller masses [188,189]. The first TOF analyzer was built in 1948 by A. E. Cameron and D. F. Eggers [190], although at that time the resolution was still poor, due to differences in the ions initial kinetic energies and their starting point, but the introduction of the reflector has improved the resolution tremendously. It consists of an electrostatic ion mirror that can refocus and reflect the ions towards the detector. More energetic ions will penetrate deeper into the mirror and therefore spend more time in the reflector, whereas less energetic ions will leave the reflector faster and the differences in flight time for ions with same *m/z* ratios will be corrected. Another benefit using a reflector is the longer drift length, which increases the time to separate ions with different *m/z* ratios and therefore increases the resolution [188]. TOF analyzers have in theory an unlimited *m/z* range and are therefore the analyzer of choice when studying non-covalent proteins and protein complexes, but coupling a continuous-flow technique such as the ESI source to a TOF analyzer can be difficult, because TOF analyzers are pulsed devices. Using orthogonal injection, in which

ions from the ESI source enter a storage region in the TOF instrument perpendicular to the spectrometer axis, overcomes this problem [191].

Connecting quadrupoles and TOF together, results in hybrid Q-TOF mass analyzers that allow mass spectrometers to function in a tandem mass spectrometry mode, as described in section 9.1.3.

9.1.3 Tandem mass spectrometry on large protein complexes

ESI-MS can be used for studying the structure of protein complexes. By dissociation of non-covalent complexes it is possible to determine the composition, stoichiometry and oligomeric architecture of the complex. Different dissociation techniques can be used, but only collision-induced-dissociation (CID) will be described.

In CID protein complex ions are accelerated into an inert collision gas. When the ions collide with the neutral gas atoms or molecules (e.g. argon) a small portion of the ions kinetic energy is converted into internal energy and if sufficient internal energy is accumulated the protein complex ions will dissociate. These experiments can either be performed in the source region of the mass spectrometer, known as “in-source CID”, or in a specifically designed collision-cell, where ions with a specific *m/z* can be pre-selected and this is referred to as tandem-MS or MS/MS. Tandem-MS consists of two MS stages; in the first stage (typically a quadrupole) ions of a specific *m/z* value are selected and termed precursor ions. These precursor ions undergo CID in the collision-cell giving rise to product ions which in the second MS stage is subsequently analyzed (typically a TOF analyzer). The extent of dissociation is influenced by changing the pressure of the argon gas and the accelerating voltage [149,153,192,193].

The general pathway of CID is ejection of a highly charged monomer and a lowly charge “stripped” protein complex of *n*-1 components which appears at higher *m/z* values than the parent oligomers and can be described as;

$$n^q \rightarrow (n-1)^{q-x} + m^x \tag{9.8}$$

where *n* is the number of subunits in the oligomer, *q* is the number of charges on the oligomer, and *x* is the average charge carried by a monomer *m* [194]. The dissociation process has been described as being asymmetric in the charge partitioning over the CID products relative to their mass. It has showed to be a Coulombically driven process in which the monomer becomes unraveled and ejected from the oligomer with a disproportionally large share of the charge [150,181,194].

9.1.4 Instrumentation

The mass spectrometer used for MS and tandem MS analysis of the TPH variants is the Qstar XL mass spectrometer (Sciex, Toronto, Canada). This is a hybrid instrument which contains three quadrupoles and a TOF analyzer. In figure 9.6 a schematic representation of the instrument is shown. In MS mode the protein complex ions are transmitted to the TOF analyzer and their

masses are determined. In MS/MS mode protein complex ions with a certain m/z ratio are selected in the first analyzer (Q_1) and subjected to CID in the gas-filled collision cell. Product ions are then analyzed in the TOF mass analyzer. The low-frequency extended mass range of Q_1 permits the isolation of ions up to 32,000 m/z [174]. A flow-restricting sleeve has been installed in the front part of the Q_0 to increase the pressure locally and allows collisional cooling (described in section 9.1.1.4) of heavy ions [179].

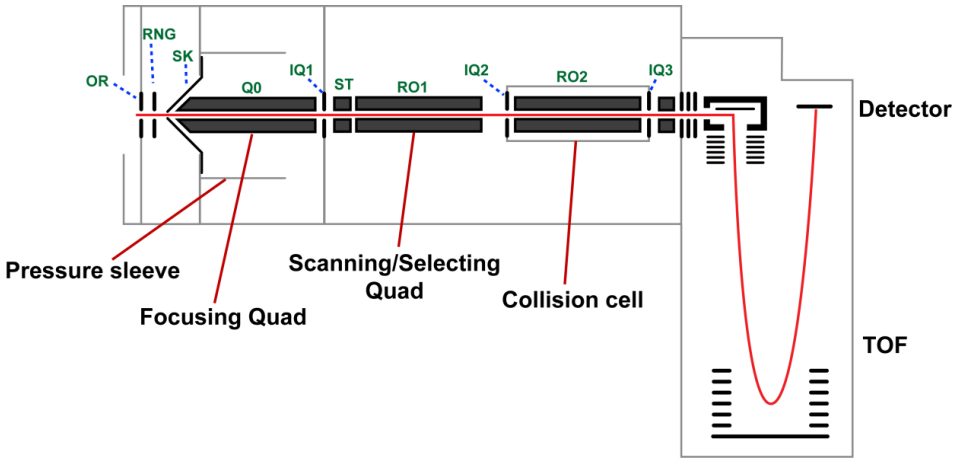

Figure 9.6. Illustration of the Qstar XL platform [179]. Reproduced with permission from the American Chemical Society.

9.2 Experimental procedures

The experiments done and results described in this chapter have been performed in Professor Carol V. Robinson Mass Spectrometry Group at the University of Cambridge, UK.

9.2.1 Materials and chemicals

Three *h*TPH variants: c*h*TPH1, c*h*TPH2 and ct*h*TPH2, were analyzed by MS and tandem MS. They were cloned and expressed in *E. coli* and purified using a simple two step procedure containing an ion exchange followed by a gel filtration. In chapter 8 the expression and purification methods of c*h*TPH1 are described, whereas expression and purification of c*h*TPH2 were done by M. S. Windahl and described in [9,142]. ct*h*TPH2 was expressed and purified by L. T. Haahr in the Metalloprotein Group [57]. After purification the variants were stored at -80°C. In table 9.3 the composition of the storage buffer solution and concentration of each variant are given.

Table 9.3. Composition of storage buffer and concentration of each *h*TPH variant analyzed by mass spectrometry.

Variant	Buffer	Concentration
c*h*TPH1	20 mM Tris/NH_3, 0.3 M CH_3COONH_4 pH 8.5	13 µM
c*h*TPH2	20mM Hepes/NaOH, 0.1 M $(NH_3)_2SO_4$, 5 % glycerol pH 7.2	25 µM
ct*h*TPH2	0.3 M CH_3COONH_4 pH 7.2	55 µM

Cesium iodide solutions, used for external calibration of the Qstar instrument, were prepared from 99 % grade CsI salt (Sigma). The ammonium acetate solutions, used for buffer exchange, were prepared from a 7.5 M stock solution obtained from Sigma. Tryptophan, Fe(II)acetate and ethylenediamine tetraacetate (EDTA) were obtained from Sigma. The two pterins (BH_2 and BH_4) were obtained from *S*chircks Laboratories.

Water from an ELGA LabWater's PURELAB Maxima system was used.

9.2.2 Sample preparation

Prior to MS analysis the three *h*TPH variants were buffer exchanged into 600 mM ammonium acetate with a pH value of either 7.0 or 8.5 depending on the sample (see table 9.4). The buffer exchange was done by using ultrafiltration devices (500 µl Vivaspin devices, Sartorius Stedim Biotech.) with molecular weight cut-off (MWCO) of either 5,000 or 10,000 Da depending on the sample. The columns were washed with 400 µl of buffer and centrifuged for 3 min at 11,000 x g and +4^{o}C. This was repeated 3 times (4 times in total). After washing, the sample was added to the device followed by addition of buffer to a total volume of 400 µl and the sample was concentrated to 50 µl by centrifugation at 11,000 x g and +4^{o}C. The buffer exchange was done 2 or 3 times depending on the sample. After buffer exchange the concentration of the sample was determined using a picodrop spectrophotometer (PicoDrop). In table 9.4 the pH value, amount of sample added to the columns, total number of buffer exchange and the final concentration for each variant are given.

Table 9.4. The pH value of the ammonium acetate buffer, the volume added of the purification product, total number buffer exchange and the final concentration for each variant.

Sample	pH value	Volume added of the purification product	MWCO	Number of buffer exchange	Final concentration
***ch*TPH1**	8.5	50 µl	5 kDa	2	~10 µM
***ch*TPH2**	7.0	5 µl	5 kDa	3	~50 µM
ct*h*TPH2	7.0	50 µl	10 kDa	2	~50 µM

9.2.3 Preparation of needles

The needles used for MS and tandem MS were prepared in-house. They were made from borosilicate glass capillaries with an inner filament (cat. no. GC100TF-10, Harvard Apparatus). The capillaries have an inner diameter (i.d.) of 0.78 mm and an outer diameter (o.d.) of 1.0 mm. They were pulled using a micropipette puller (flaming/brown P-97, Sutter Instrument Co., Novato, CA) and coated with a thin layer of gold using a SEM sputter-coater (Polaron, Newhaven, U.K.) to make them electrically conductive. The pulled end of the capillary was clipped under a stereomicroscope using a tweezer, resulting in a tip inner diameter between 1 and 5 µm. Typically 3-6 µl of protein solution, prepared as described in section 9.2.2, were loaded into the capillaries.

9.2.4 MS and tandem MS measurements

All spectra were recorded in positive ion mode using a Quadrupole Time-of-Flight (Q-ToF) instrument (Qstar XL) equipped with a nanoESI source, under conditions optimized for the transmission of high-mass non-covalent proteins and protein complexes, as described in section 9.1.4. The following instrumental parameters were used: Capillary voltage up to 1.8 kV, declustering potential (DP) 150-200 V, focusing potential (FP) 200-250 V, second declustering potential 15 V and collision energy up to 220 V, microchannel plate (MCP) 2350 V. For tandem MS argon was used as a collision gas at pressures from 3 x 10^{-2} to 12 x 10^{-2} mBar with collision energy ranging from 100 to 220 V. All spectra were calibrated externally by using a solution of cesium iodide (100 mg/ml) in water with the mass range *m/z* 350 to 10100.

9.2.4.1 Determination of the apo-protein monomer mass

To determine the exact experimental monomer mass of the apo-protein, the protein complex was denatured prior to ESI-MS. This was done using C_4 or C_{18} ZipTip columns from Millipore. The columns were washed 3 times in acetonitrile (ACN), then twice in 1% formic acid followed by one time in 5 % formic acid. 20 µl of the protein sample (prepared as described in section 9.2.2) was loaded by pipetting up and down five times. After loading the sample, the column was washed once with 1 % formic acid and eluted using 2 µl of a mixture of 1 % formic acid and 50 % ACN. The sample was immediately loaded into a capillary and introduced into the mass spectrometer. The denatured spectrum was obtained in the mass range 300-3000 m/z.

9.2.4.2 Mass spectrometry of intact *h*TPH

To obtain a mass spectrum of intact *h*TPH the sample was prepared as described in section 9.2.2. After buffer exchange the sample was diluted with 600 mM ammonium acetate pH 7.0 or 8.5 depending on the sample. This was done to decrease the amount of nonspecific interactions due to high concentration of the sample in the nanoelectrospray droplets. After dilution 3-5 µl aliquot of the samples were loaded into capillaries and analyzed immediately by the mass spectrometry.

9.2.4.3 Ligand binding

To determine the iron binding either Fe or EDTA were added to the protein sample prepared in section 9.2.2. A mixture of Fe(II)acetate:*h*TPH with a ratio of 5:1 as well as a mixture of EDTA:*h*TPH with a ratio of 4:1 were incubated for 15 minutes on ice. 3-5 µl aliquot of the samples were loaded into capillaries and immediately analyzed.

To determine the substrate binding an excess of either tryptophan, BH_2 or BH_4 were added to the variants prior to analysis. A solution of tryptophan:*h*TPH, BH_2:*h*TPH or BH_4:*h*TPH with a ratio of either 1:1, 5:1, 10:1 or 20:1 with *h*TPH variant were incubated for 15 minutes on ice. A 3-5 ul aliquot of this sample was loaded into a capillary and introduced immediately into the mass spectrometer.

9.2.4.4 Oligomerization

The stoichiometry of ct*h*TPH2 was determined by tandem-MS. The relevant *m/z* value was selected in the selecting quadrupole and argon was used as a collision gas at a pressure of 3 x 10^{-2}

mbar. In the collision cell the energy and pressure of the collision gas were increased gradually from 50 to 200 V for the energy and from 3 x 10^{-2} to 12 x 10^{-2} mbar of the pressure.

9.2.4.5 Data acquisition

Data were acquired and processed with MassLynx software (Waters). The average mass of both the expected and apparent mass (centroid of the peaks) of all three variants were used due to the size of the variants as well as the resolving power of the instrument. The apparent masses of c*h*TPH1, c*h*TPH2 and ct*h*TPH2 were calculated from the obtained spectra according to the method described previously (section 9.1.1.3) and processed with MassLynx 4.1 software.

As mentioned in section 9.1.1.3 the apparent mass calculated by using the algorithm in equation 9.2 is the molecular mass of the zero-charge molecule where all the charge assumes to be due to excess of protons. This is not true for metalloproteins as explained in section 9.1.1.3. Therefore, the mass used to compare the apparent mass obtained from the mass spectra is the expected mass, which takes into account metal binding, disulfide bonds and binding of cofactors. *h*TPH binds Fe in either oxidation state +II or +III. To determine the expected mass in positive ion mode the oxidation state is subtracted from the calculated mass. In table 9.5 and 9.6 the expected masses of apo- and holo-*h*TPH are given, where Fe has a mass of 55.847 Da, tryptophan has a mass of 204.2314 Da, BH_2 has a mass of 239.2365 Da, BH_4 has a mass of 241.2525 Da, H_2O has a mass of 18.0154 Da, CH_3COO^- has a mass of 59.0445 Da and O_2 has a mass of 31.9988 Da.

All spectra are shown with no smoothing and without background subtraction.

Table 9.5. Expected average molecular masses of the monomer of apo-c*h*TPH1, apo-c*h*TPH2 and apo-ct*h*TPH2 with Met as well as the holo-form of c*h*TPH2 with Fe, Trp, BH_2 or BH_4 and holo-c*h*TPH1-Fe. Also the expected average masses of 2mer, 3mer and 4mer of holo-ct*h*TPH2 with ligands are given.

	c*h*TPH1 (Da)	**c*h*TPH2 (Da)**
Apo-TPH	36197.4564	36316.4612
TPH-Fe(II)/(III)	36251.3034 /36250.3034	36370.3082 / 36369.3082
TPH-Fe(II)/(III)-3H_2O	36305.3496 / 36304.3496	36424.3544 / 36423.3544
TPH-Fe(II)/(III)-CH_3COO^-	36310.3475 / 36309.3475	36429.3527 / 36428.3527
TPH-Fe(II)/(III)-Trp	----------	36574.5382 / 36573.5382
TPH-Fe(II)/(III)-Trp-3H_2O	----------	36628.5842 / 36627.5842
TPH-Fe(II)/(III)-BH_2	----------	36609.5447 / 36608.5447
TPH-Fe(II)/(III)-BH_2-3H_2O	----------	36663.5909 / 36662.5909
TPH-Fe(II)/(III)-BH_4	----------	36611.5607 / 36610.5607
TPH-Fe(II)/(III)-BH_4-3H_2O	----------	36665.6069 / 36664.6069

Table 9.6. Expected average molecular masses of the monomer, dimer, trimer and tetramer of apo-ct*h*TPH2 and holo-ct*h*TPH2-Fe.

	ct*h*TPH2 (Da)			
	1mer	2mer	3mer	4mer
Apo-TPH	39822.4411	79644.8822	119467.3233	159289.7644
TPH-Fe	39876.2881	79752.5762	119628.8643	159505.1524
TPH-Fe-3H_2O	39930.3343	79860.6686	119791.0029	159721.3372
TPH-Fe-CH_3COO^-	39936.3405	79872.681	119809.215	159745.362

9.3 Results and discussion

9.3.1 c*h*TPH1

Before MS analysis of the c*h*TPH1 sample the buffer was changed to 600 mM ammonium acetate pH 8.5 as described in section 9.2.2. After buffer exchange the concentration of the c*h*TPH1 was 10 µM.

9.3.1.1 Determination of the experimental monomer mass of apo-c*h*TPH1

The experimental monomer mass of apo-c*h*TPH1 was determined as described in section 9.2.4.1. In figure 9.7 the *m/z* spectrum of the denatured c*h*TPH1 is shown.

Two proteins with different masses are present in the spectrum: One with an apparent mass of 36198.18±2.20 Da and one with an apparent mass of 33749.45±0.61 Da**.** The first protein with a mass of 36198.18±2.20 Da corresponds to the expected mass of the monomer of apo-c*h*TPH1 including its N-terminal methionine, 36197.4564 Da, as given in table 9.5. From the sequence of c*h*TPH1 (see figure 2.3) this protein is also expected to maintain methionine since the penultimate amino acid is an aspartic acid [195].

The second protein with an approximately 2450 Da lower mass could either be a truncated version of c*h*TPH1 or another protein present in the sample. The buffer exchanged sample was therefore analyzed by SDS-Page. Additionally, two other proteins with known masses of approximately 38 kDa and 41 kDa were analyzed in order to see if the resolution of the SDS-Page was high enough to distinguish between these two proteins. In figure 9.8 the SDS-Page analysis is shown. Only one band is seen for the c*h*TPH1 sample (see also figure 8.4), whereas the sample with the two proteins of known size, having the same mass difference as c*h*TPH1 and the second species, are separated. This indicates either that the sample only contains c*h*TPH1 and that the truncation most probably happens during mass spectrometric analysis or that the other protein runs through the SDS-Page as c*h*TPH1 even though the mass is different. In order to determine this, the c*h*TPH1 sample was tryptic digested and the protein was identified. The identification was done by Dr. Min Zhou and the result is given in table 9.7. Two proteins are identified: TPH1 from human and an *E. coli* protein, thiosulfate-binding protein. The *E. coli* thiosulfate-binding protein has a mass of 37615 Da and without its 25 aa signal peptide it has a mass of 35057 Da

[196]. This does not correspond to the mass of 33.7 kDa determined by MS, indicating that the second species could be due to truncation.

A)

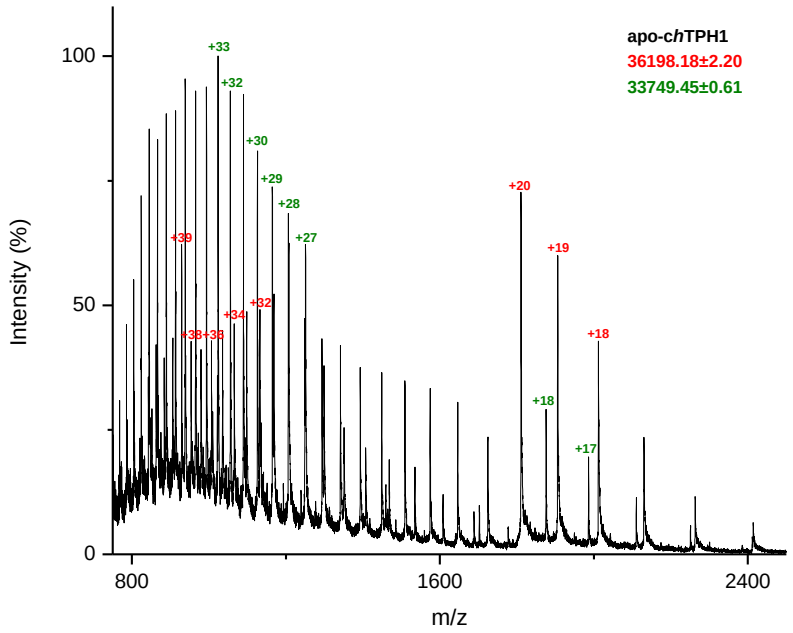

B)

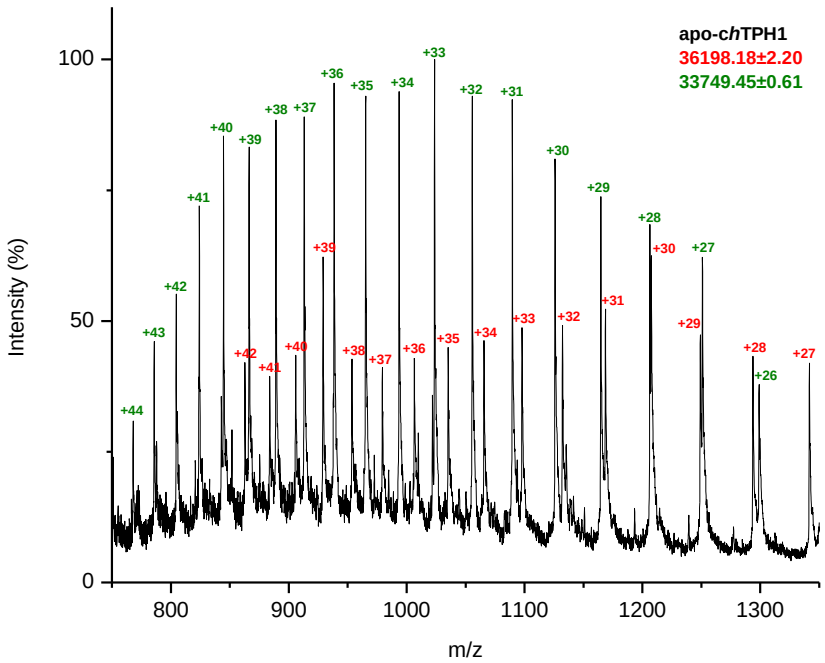

Figure 9.7. Mass spectrum of denatured *ch*TPH1. The buffer was changed to 600 mM ammonium acetate pH 8.5 using ultrafiltration devices and denatured using ZipTip (C4) and 5 % formic acid as described in section 9.2.4.1. The sample was eluted from the tip using 1 % formic acid and 50 % acetonitrile. Spectrum B) is a zoom of spectrum A) with m/z 750 to 1350. In both spectra two species are seen; one highlighted in red with a mass corresponding to *ch*TPH1 and one in green corresponding to the second species.

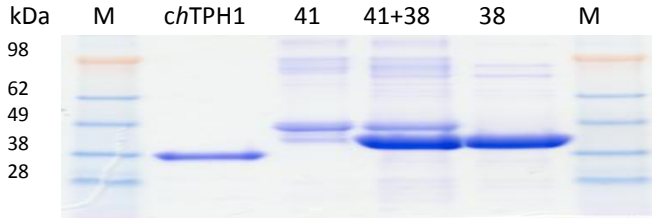

Figure 9.8. SDS-Page analysis of the c*h*TPH1 sample after transportation and buffer exchange. Lane 1 and 6 is the marker, lane 2 the c*h*TPH1 sample, lane 3 is the known protein of 41 kDa, lane 4 is a mixture of the known proteins (41 and 38 kDa) and lane 5 is the 38 kDa protein. The gel is a NuPage 4-12% gel from Invitrogen, the marker is a SeeBlue *Plus2* prestained standard (1x) invitrogen and the running buffer is a MES buffer.

The truncation of c*h*TPH1 can either be in the N-terminal, the C-terminal or in both. In figure 9.9 the sequence of c*h*TPH1 is shown. Different truncation of the sequence were tried to see if it could give masses corresponding to the apparent mass obtained from the denatured c*h*TPH1 spectrum. Three different truncations of c*h*TPH1 with a mass corresponding to 33749 Da were observed and the sequences of the three truncations are marked with green, blue and red arrows in figure 9.9. For the *E. coli* thiosulfate-binding protein only one truncation of this protein gives rise to a mass of 33751 Da. The sequence of the *E. coli* thiosulfate-binding protein with the truncation marked with green arrows is given in figure 9.10.

From these results it is difficult to determine whether or not the second species is due to another protein or due to truncation in the c*h*TPH1 sequence.

Table 9.7. Results obtained from the tryptic digested c*h*TPH1 sample.

Acession #	**Coverage**	**Peptides identified (see also figure 9.9 and 9.10)**	**#AAs**	**Description**
P17752	20.72	VLMYGSELDADHPGFK KYFADLAMNYK YFADLAMNYK EDNIPQLEDVSNFLK NLPLLSK VFGAGLLSSISELK VEFTEEEIK DFLSGLAFR TWGTVFQELNK	444	Tryptophan 5-hydroxylase 1 OS = *Homo sapiens* GN=TPH1 PE=1 SV=4 - [TPH1_HUMAN]
P16700	12.13	KQYEAQGFEVVIPK NIHDWNDLVR QALAILQGLK LIFPNPK	338	Thiosulfate-binding protein OS = *E. coli* (strain K12) GN=cysP PE=1 SV=1 - [CYSP_ECOLI]

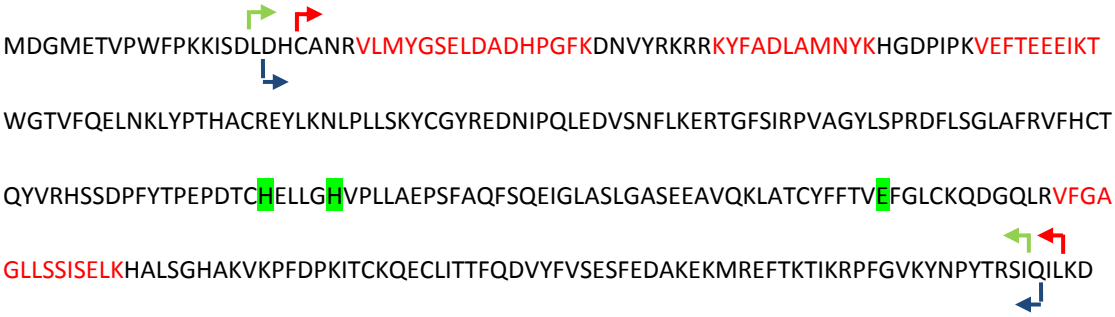

Figure 9.9. Sequence of c*h*TPH1. The peptide identified in tryptic digestion is highlighted in red. The three different truncations of cTPH1 that give rise to masses of approximately 33749 Da are marked with green arrows (33751.5261 Da), blue arrows (33749.5970 Da) and red arrows (33750.6446 Da), respecively. The three amino acids highlighted in green are the amino acids iron is coordinated to [13].

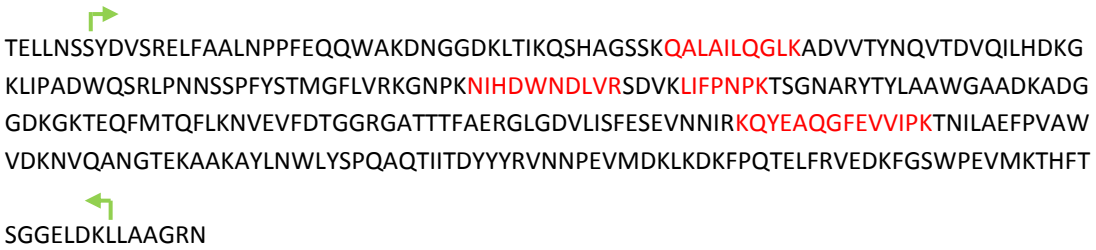

Figure 9.10. Sequence of the *E. coli* thiosulfate-binding protein without its signal peptide. The peptide identified in tryptic digestion is highlighted in red. The truncation that gives rise to a mass of 33751 Da is marked with green arrows.

9.3.1.2 Mass spectrometry of intact c*h*TPH1

The mass spectrum of intact c*h*TPH1 was obtained after determination of the experimental monomer mass of apo-c*h*TPH1 using acid denaturation. This was done as described in section 9.2.4.2 and the spectrum is shown in figure 9.11. The bottom spectrum in figure 9.11B was obtained using lower declustering and focusing potential (DP 100, FP 150) between OR and Q_0 (see figure 9.6) and the upper spectrum was obtained using higher potentials (DP 150, FP 200). By having a higher voltage in the instrument a cleaner spectrum is achieved due to elimination of nonspecific interactions with solvent molecules.

As for the denatured c*h*TPH1 two species are seen: One with a mass of approximately 36.3 kDa corresponding to c*h*TPH1 and one with a mass of approximately 33.7 kDa (figure 9.11A). This is consistent with the results obtained from the denatured sample of c*h*TPH1 (section 9.3.1.1). Comparing the two spectra of intact c*h*TPH1 from figure 9.11B obtained at low and high potential the ratio of the intensity between c*h*TPH1 and the second species is changed. The second species has the highest intensity at low potential whereas c*h*TPH1 has the highest intensity at high potential. This is most probably due to a better resolution between the two species at higher

potentials and that some of the intensity of the 33.7 kDa species comes from nonspecific interaction of solvent molecules with c*h*TPH1. These solvent molecules are removed at high potential and therefore the intensity ratio is changed.

A)

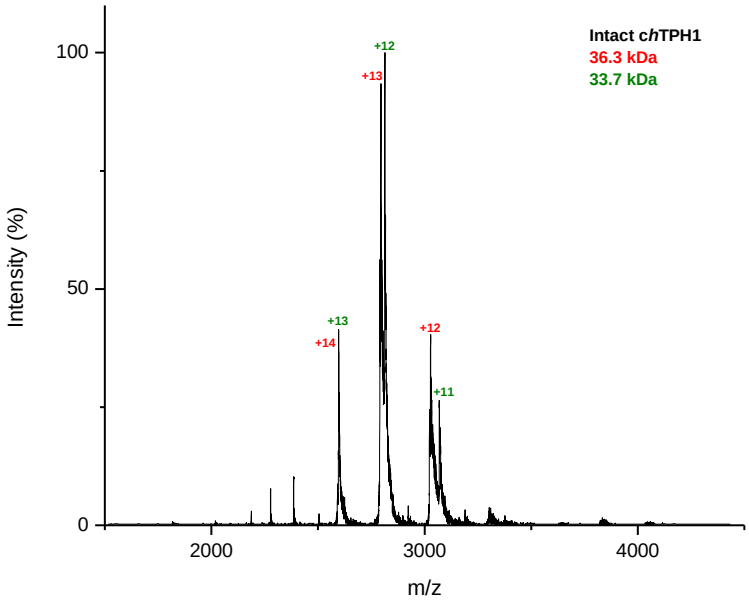

B)

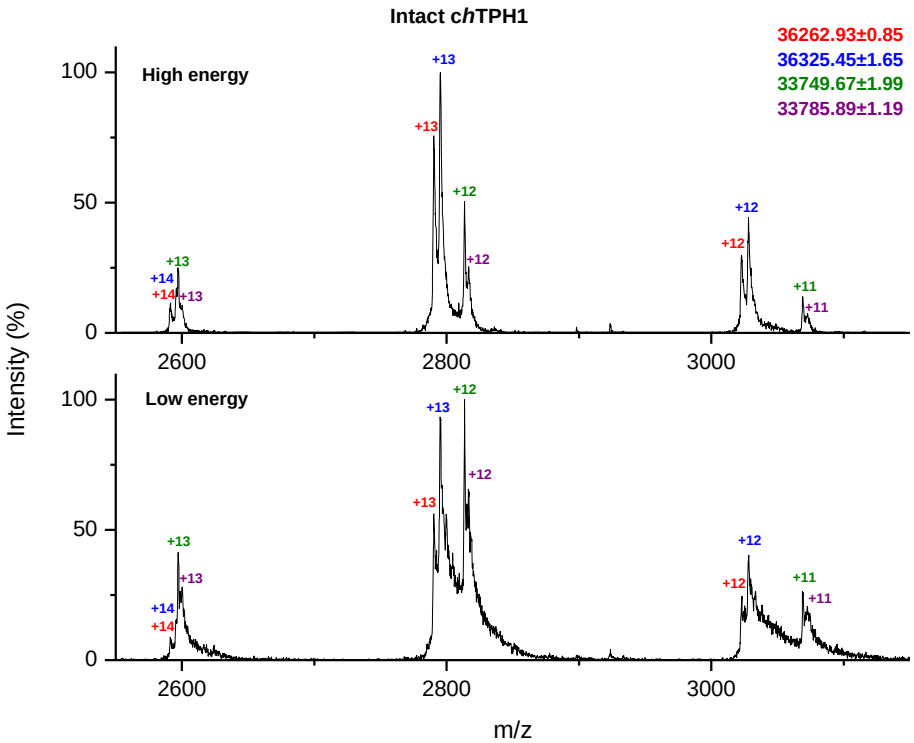

Figure 9.11. Mass spectrum of 4 µM c*h*TPH1 in 600 mM ammonium acetate pH 8.5. A) Mass spectrum with *m/z* 1500-4500. B) Mass spectrum with *m/z* 2550-3150 obtained at both low and high voltages.

The c*h*TPH1 has two charge-state series with apparent masses of 36262.93±0.85 Da (in red, see figure 9.11) and 36325.45±1.65 Da (in blue, see figure 9.11). Each charge state series has three charge states, +14, +13 and +12. The first mass corresponds to the expected mass of holo-c*h*TPH1-Fe(II)/(III) (36251.3034/36250.3034 Da) or holo-c*h*TPH1-Fe(II)/(III) with oxidation of either a methionine or cysteine residue (36267.3028/36266.3028 Da). This gives a mass difference between the apparent and the expected mass of +10/11 Da and -4/3 Da, respectively. A small difference in calibration can give day-to-day variation which most probably is the case for this minor mass difference between the apparent and expected mass. The second mass could corresponds to the expected mass of holo-c*h*TPH1-Fe(II)/(III)-$3H_2O$ (36305.3496/36304.3496 Da) or holo-c*h*TPH1-Fe(II)/(III)-CH_3COO^- (36310.3475/36309.3475 Da). The difference between the apparent mass of the two series is approximately 62.5 Da and therefore, it is most probably due to binding of acetate (CH_3COO^- has a mass of 59.0445 Da).

The second protein also contains two charge state series with masses of 33749.67±1.99 Da (in green, see figure 9.11) and 33785.89±1.19 Da (in purple, see figure 9.11), respectively, but with charge states, +13, +12 and +11. Due to lower charge states this species is observed at higher *m/z* compared to c*h*TPH1, despite the lower mass. The difference in apparent mass between the two series is approximately 36 Da which could correspond to O_2**.** By comparing the mass obtained from the denatured sample (figure 9.7) with the mass from the intact sample it is seen that the apo- and holo-form has the same mass (33.749 Da). Therefore, it can be concluded that the second species does not contain iron.

The iron in c*h*TPH1 is coordinated to His272, His277 and Glu317 [13]. From the sequence in figure 9.9 none of the three truncations miss these amino acids and it would therefore be expected to bind iron if the second species corresponds to a truncated version of c*h*TPH1. Otherwise, the interaction between truncated c*h*TPH1 and iron is too weak to be maintained in the mass spectrometer. Additionally, if the second species corresponded to a truncated form of c*h*TPH1 this truncation would be very specific, generating a species with a specific mass in every single mass spectrum obtained of both the apo- and holo-form.

9.3.1.3 Iron binding

To assign each of the two charge-state series from the intact MS analysis of c*h*TPH1 both iron and EDTA was added to the sample prior to analysis as described in section 9.1.4.2. In figure 9.12 the mass spectra of intact c*h*TPH1 and intact c*h*TPH1 with either EDTA (1:4) or added Fe (1:5) are shown. Again the same two proteins are observed in the spectrum without EDTA or Fe both with three charge states; +14, +13 and +12 for c*h*TPH1 and +13, +12 and +11 for the 33.7 kDa protein.

By comparing the spectra of c*h*TPH1 without EDTA/Fe and c*h*TPH1 with added Fe no change is observed (both having same two charge state series with the same intensity ratio), whereas a third charge state series (green in figure 9.12) with a mass of 36197.07±0.18 Da corresponding to apo-c*h*TPH1 is observed in the spectrum of c*h*TPH1 with EDTA. This indicates that the protein is fully saturated with iron.

By adding EDTA or Fe to the sample the ratio between the two charge state series for the 33.7 kDa protein does not change indicating that the protein does not bind iron and is therefore most probably not a truncated version of c*h*TPH1. This is consistent with the spectrum of intact c*h*TPH1 in section 9.3.1.2.

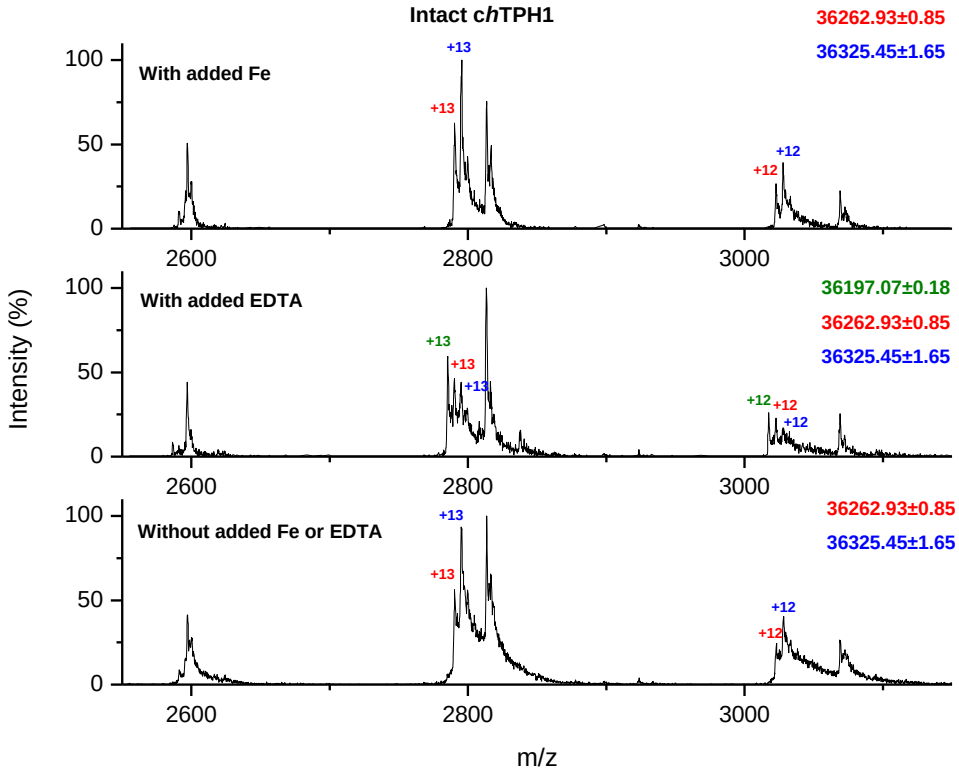

Figure 9.12. Mass spectra of 4 µM c*h*TPH1 in 600 mM ammonium acetate without added Fe or EDTA, with added EDTA and with added Fe.

9.3.1.4 Summary and overall discussion

The mass spectrometric results indicate that the c*h*TPH1 sample is heterogeneous containing two proteins: One with a mass of 36.3 kDa corresponding to the mass of c*h*TPH1 and one with a mass of 33.7 kDa. The second species could be due to truncation in the c*h*TPH1 sequence or due to the presence of an *E. coli* contaminant protein.

If the second species corresponded to a truncated form of c*h*TPH1 this truncation would be very specific, generating a species with a specific mass in every single mass spectrum obtained of both the apo- and holo-form. The other possibility is that the second species could correspond to a part of another protein which cannot be chromatographic purified from c*h*TPH1 and which migrates through the SDS-Page exactly as c*h*TPH1 even though the masses are different. From the iron binding analysis the second species does not bind iron and from the sequence of c*h*TPH1 the three amino acids which coordinate iron are still present in the sequence corresponding to the truncated version of c*h*TPH1. This suggests that the second species is a part of another

protein, which is also consistent with the fact that c*h*TPH1 can be crystallized and a structure of the protein was solved with electron density from Thr104 to Gln409 (see chapter 10). To solve this problem the purification method of c*h*TPH1 should be changed in order to obtain a sample of higher purity. This can be done by affinity tag purification where c*h*TPH1 is fused to for example GST or MBP.

9.3.2 c*h*TPH2

Before MS analysis of the c*h*TPH2 sample the buffer was changed to 600 mM ammonium acetate pH 7.0 as described in section 9.2.2. Changing the buffer was necessary because c*h*TPH2 was in a HEPES buffer with 5 % glycerol and both HEPES and glycerol, especially glycerol, are detrimental to ESI [197]. After the buffer was changed the protein concentration was approximately 50 µM.

9.3.2.1 Determination of the experimental monomer mass of apo-c*h*TPH2

The experimental monomer mass of apo-c*h*TPH2 was determined as described in section 9.2.4.1. In figure 9.13 the *m/z* spectrum of denatured sample of c*h*TPH2 is shown. From the spectrum only one species is seen with an apparent mass of 36318.67±1.33 Da which corresponds to the expected average mass of the monomer of apo-c*h*TPH2 including its N-terminal methionine, 36316.46 Da, as given in table 9.5. From the sequence of c*h*TPH2 (see figure 2.3) this protein is also expected to maintain methionine since the penultimate amino acid is a Glu [195].

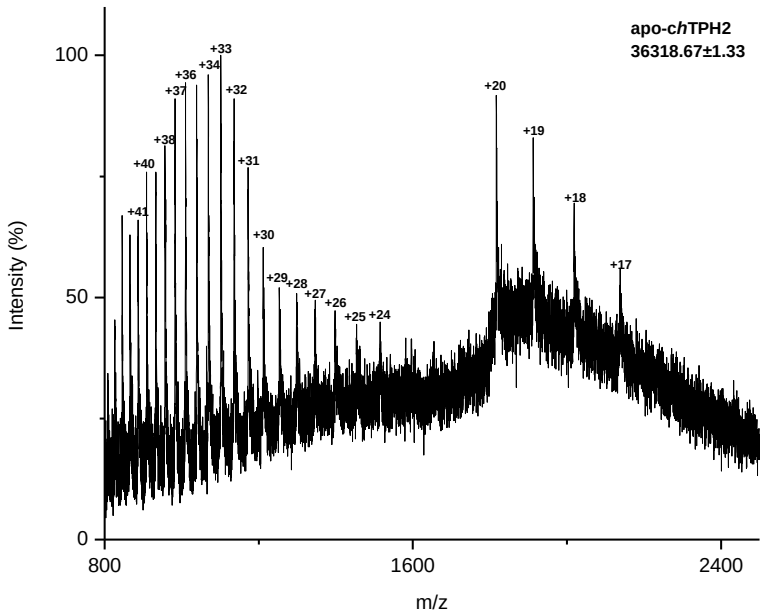

Figure 9.13. Spectrum of denatured c*h*TPH2. The buffer was changed to 600 mM ammonium acetate pH 7.0 using ultrafiltration devices and denatured using ZipTip (C18) and 5 % formic acid. The sample was eluted from the tip using 1 % formic acid and 50 % acetonitrile.

9.3.2.2 Mass spectrometry of intact c*h*TPH2

After determination of the experimental monomer mass of apo-c*h*TPH2, the mass spectrum of intact c*h*TPH2 was obtained. This was done as described in section 9.2.4.2 and the spectrum is

shown in figure 9.14, where figure 9.14A shows the spectrum with *m/z* range 1500 to 5500, whereas figure 9.14B are a zoom in with *m/z* range 2750 to 3150.

A)

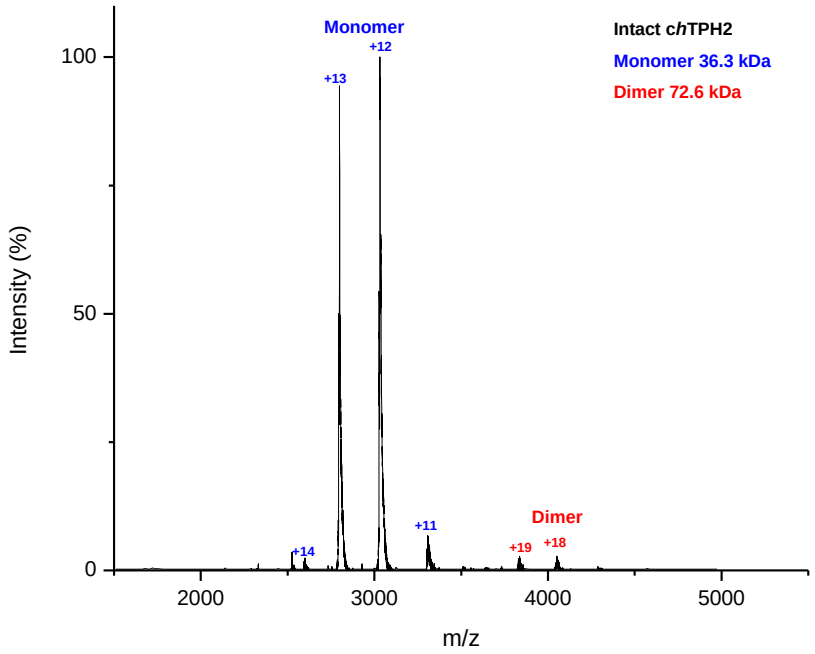

B

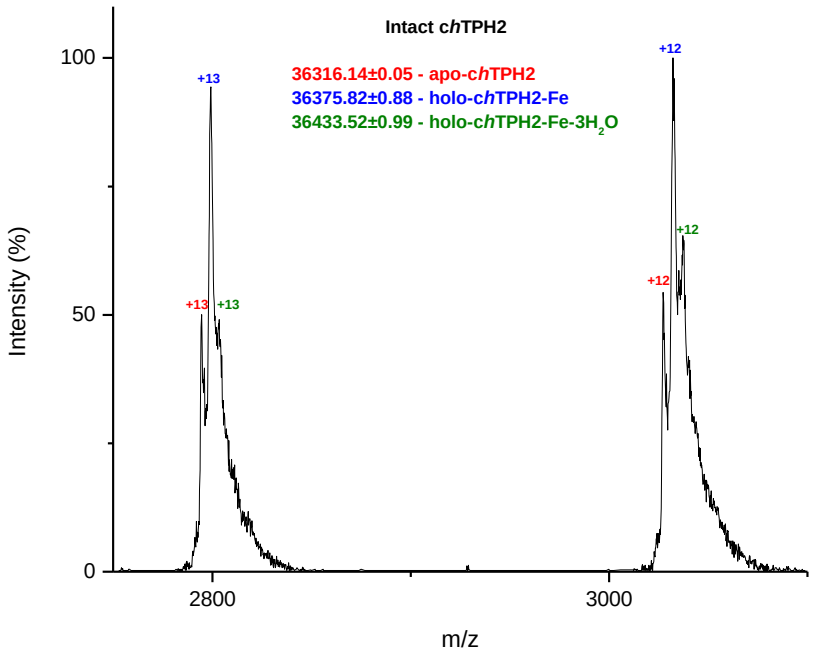

Figure 9.14. Mass spectrum of 2.4 µM intact c*h*TPH2 in 600 mM ammonium acetate pH 7.0. A) The full mass spectrum of intact c*h*TPH2 where both a monomer and a dimer are present. The dimer is due to nonspecific interactions. B) Zoom in on the monomer charge states +13 and +12.

In figure 9.14A two species are seen: One with a mass around 36.3 kDa corresponding to a monomer of c*h*TPH2 and one with a mass of around 72.6 kDa corresponding to a dimer of c*h*TPH2. By decreasing the concentration of c*h*TPH2 the relative amount of dimer decreases indicating that the interaction is a non-pecific interaction happening during the electrospray process, as described in section 9.1.1.5 (data not shown).

The monomer species has three charge state series with masses of 36316.14±0.05 Da, 36375.82±0.88 Da and 36433.52±0.99 Da, respectively, and four charge states +14, +13, +12 and +11 (figure 9.14B). The apparent mass difference between the three charge states are approximately 60 Da and 58 Da. The two first masses correspond to apo-c*h*TPH2 (36316.46 Da) and holo-c*h*TPH2-Fe(II)/Fe(III) (36370.31/36369.31 Da), whereas the latter could correspond to holo-c*h*TPH2-Fe(II)/(III)-3H_2O (36424.35/36423.35 Da) or holo-c*h*TPH2-Fe(II)/(III)-CH_3COO^- (36429.3527/36428.3527 Da).

By increasing the declustering and focusing potential in the mass spectrometer the third charge state series almost disappear, as shown in figure 9.15. This indicates that the series is either due to non-specific interaction or the binding is too weak to be maintained at high voltage. Comparing the spectra obtained at high voltage of c*h*TPH1 (figure 9.11B) and of c*h*TPH2 (figure 9.15), the charge state series, which could correspond to binding of either water or acetate to c*h*TPH, does not disappear for c*h*TPH1 but it does for c*h*TPH2. This could mean that the interaction between water/acetate and c*h*TPH1 is stronger than the interaction between water/acetate to c*h*TPH2 due to specific and nonspecific interaction, respectively.

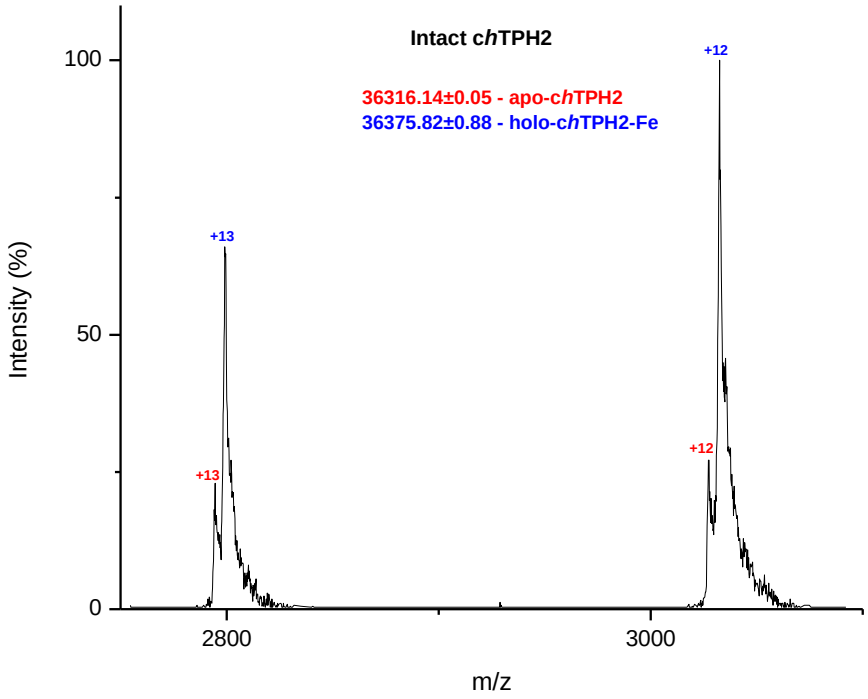

Figure 9.15. Mass spectrum of 2.4 µM intact c*h*TPH2 in 600 mM ammonium acetate pH 7.0 and obtained at higher declustering (DP 200) and focusing potential (FP 250) compared to figure 9.14 which were DP 150 and FP 200.

9.3.2.3 Iron binding

To assign each of the three charge state series from the intact MS analysis of c*h*TPH2, iron or EDTA is added to the sample prior to MS analysis as described in section 9.1.4.2. In figure 9.16 the MS spectra of intact c*h*TPH2 and intact c*h*TPH2 with either EDTA (1:4) or added Fe (1:5) are shown.

Again four charge states are present, +14, +13, +12 and +11 for each condition but only charge state +12 and +13 are shown in figure 9.16. By comparing the three spectra the ratios between the three charge state series are changing depending on the condition of the sample. By adding Fe only two charge-state series are present corresponding to masses of 36375 Da (holo-c*h*TPH2-Fe(II)/(III)) and 36434 Da (holo-c*h*TPH2-Fe(II)/(III)-$3H_2O$ or CH_3COO^-). Also, the ratio between the second and third charge state series decreases indicating that the third series binds iron. By adding EDTA the ratio of the apo-c*h*TPH2 (first series) and holo-c*h*TPH2-Fe (second series) is increasing and more of the apo-form is present. This is due to EDTA's chelating effect. The ratio of the second and third series in the sample with EDTA is approximately the same as the one in the sample without Fe or EDTA, indicating again that the third charge state series also contains iron. The charge state series are therefore assigned as being apo-c*h*TPH2, holo-c*h*TPH2-Fe(II)/(III) and holo-c*h*TPH2-Fe(II)/(III)-$3H_2O$ or maybe holo-c*h*TPH2-Fe(II)/(III)-CH_3COO^- showing that the sample is heterogeneous with respect to Fe.

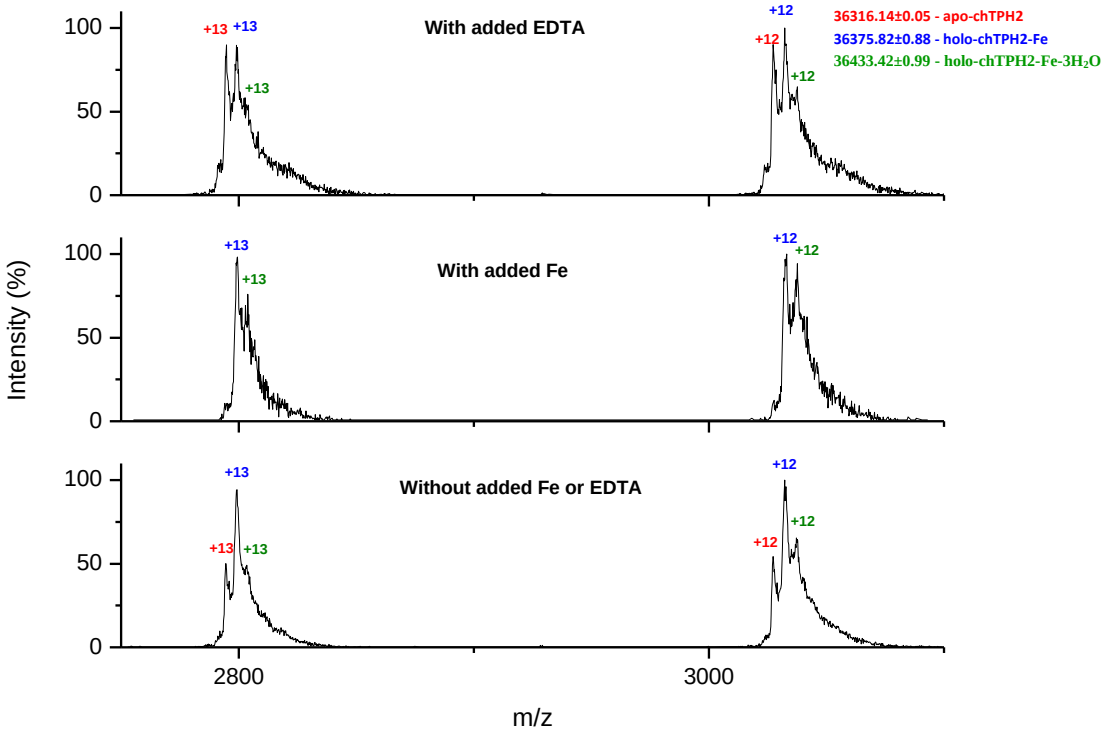

Figure 9.16. Mass spectra of 2.4 µM c*h*TPH2 and 2.4 µM c*h*TPH2 with EDTA (1:4) or Fe (1:5) in 600 mM ammonium acetate pH 7.0.

The difference seen in iron binding between c*h*TPH2 and c*h*TPH1 is due to the elution pattern observed in the anion exchange [6,14,142]. In the anion exchange both apo-c*h*TPH2 and holo-c*h*TPH2-Fe(II)/(III) elutes at the same conductivity, whereas apo-c*h*TPH1 and holo-c*h*TPH1-Fe(II)/(III) elutes at different conductivities. This is due to a much higher overall charge of c*h*TPH2 compared to c*h*TPH1 and therefore the presence of Fe(II)/(III), which change the overall charge by +II or +III, does not affect the elution pattern for c*h*TPH2 in the same way as seen for c*h*TPH1. The c*h*TPH1 is fully loaded with iron prior to MS analysis [12,6,142].

As already discussed in section 9.3.2.3 different scenarios exist for assignment of the third mass (36433.42 Da), which has an apparent mass of approximately 58 Da higher than the apparent mass of the second charge state series corresponding to holo-c*h*TPH2-Fe. This mass difference could be due to three water molecules (54.0462 Da), a second iron (55.847 Da) or a CH_3COO^- (59.0445 Da) binding to c*h*TPH2.

9.3.2.4 Substrate/ligand binding

The binding of substrates to c*h*TPH2 was investigated. This was done by adding either tryptophan, BH_2 or BH_4 to the c*h*TPH2 sample followed by incubation on ice for 15 min prior to the mass spectrometric analysis, as described in section 9.2.4.3. In order to investigate the location and specificity of substrate binding by MS, the enzyme was analyzed in the presence of different concentration of substrate.

In figure 9.17 the mass spectra of the two charge states, +13 and +12, of c*h*TPH2 without and with tryptophan in ratios of 1:5, 1:10 and 1:20 (c*h*TPH2:tryptophan) are shown. By incubation of c*h*TPH2 with tryptophan a second species is seen. This species is present in two charge state series: One with a mass of 36589.05±1.16 Da and one with a mass of 36643.89±1.85 Da. These masses could correspond to c*h*TPH2-Fe(II)/(III)-Trp (36574.5382/36573.5382 Da) and c*h*TPH2-Fe(II)/(III)-Trp-CH_3COO^- (36634.5906 Da). When the sample is incubated with tryptophan the peak corresponding to apo-c*h*TPH2 disappears, but holo-c*h*TPH2-Trp (without Fe) cannot be detected in the spectra. This could be due to a poor resolution between c*h*TPH2 and c*h*TPH2+Trp. Comparing the apparent mass of holo-c*h*TPH2-Fe and holo-c*h*TPH2-Fe-Trp there is a mass difference of 213.23 Da and the mass of Trp is 204.23 Da given a Δ10 Da. By increasing the concentration of tryptophan only one tryptophan is bound to c*h*TPH2. This indicates that the binding of Trp is specific and it binds to the active site of c*h*TPH2.

BH_4 was also added to the sample as well as the inhibitor analog, BH_2, in the ratios 1:5, 1:10 and 1:20. In figure 9.18 and 9.19 the sample with added BH_2 and BH_4 are shown, respectively. By adding either BH_2 or BH_4 a second species is seen with a mass of either 36606 Da or 36620 Da corresponding to a mass of holo-c*h*TPH2-Fe-BH_2 (36611.54 Da) or holo-c*h*TPH2-Fe-BH_4 (36613.56 Da). By increasing the amount of ligand the ratio between the two species decreases meaning that the amount of c*h*TPH2-Fe-BH_2/BH_4 is increased. By increasing the concentration of ligand only the species with one bound ligand is observed, meaning that the enzyme must bind the ligand specifically.

In the comparison of the apparent mass of holo-c*h*TPH2-Fe and holo-c*h*TPH2-Fe-BH_2/BH_4 a difference of 230 Da is due to BH_2 (239 Da) and 239 Da is due to BH_4 (241 Da). Although, a better signal-to-noise would be prepared it can be concluded that both BH_2 and BH_4 binds to c*h*TPH2.

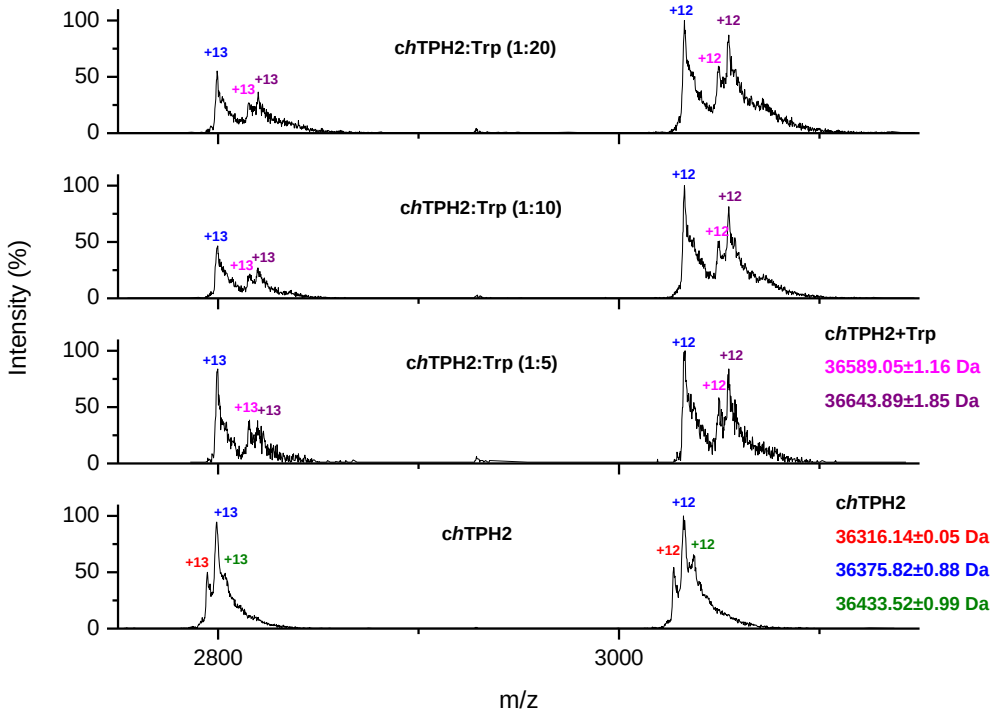

Figure 9.17. Mass spectra of c*h*TPH2 and c*h*TPH2 with tryptophan in the ratio 1:5, 1:10 and 1:20. The buffer was changed to 600 mM ammonium acetate pH 7.2 using ultrafiltration devices and the concentration determined to 24 µM. Tryptophan in ratios 1.5, 1:10, 1:20 (cTPH2:Trp) were added and the sample was incubated on ice for 15 min. Before analysis the sample was diluted to a c*h*TPH2 concentration of 2.4-3.5 µM with 600 mM ammonium acetate pH 7.0.

9.3.2.5 Summary

The MS results indicate that only c*h*TPH2 is present in the sample and that it is heterogeneous with respect to Fe, indicating that the sample is not fully saturated with iron. On the contrary, c*h*TPH1 is saturated with iron. This difference is most probably due to the elution pattern and the overall charge of the two isoforms, as described in section 9.3.2.3. These results have lead to the addition of iron during purification of c*h*TPH2 in the other project carried out in the Metalloprotein Chemistry and Engineering Group in order to obtain a homogenous sample for crystallization.

All three ligands (tryptophan, BH_2 and BH_4) can bind individually to c*h*TPH2 and their binding did not change the oligomeric state of TPH. This indicates that the binding of substrate is random. It would have been more appropriate to saturate the sample with Fe for these ligand binding studies.

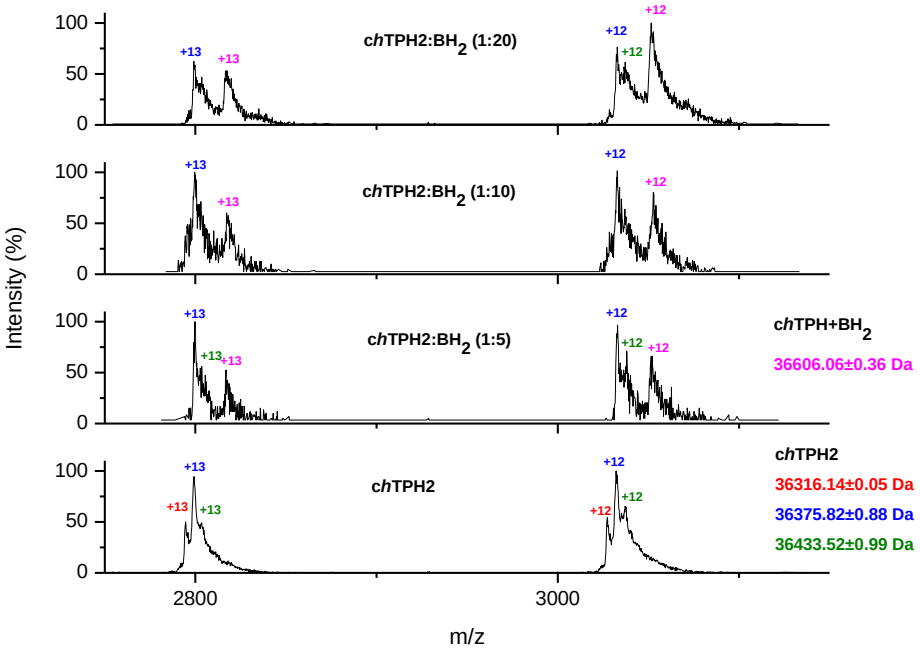

Figure 9.18. Mass spectra of c*h*TPH2 and c*h*TPH2 with BH_2 in the ratio 1:1, 1:5, 1:10 and 1:20. The buffer was changed to 600 mM ammonium acetate pH 7.2 using ultrafiltration devices and the concentration determined to 24 µM. BH_2 in ratios 1:1, 1:5, 1:10, 1:20 (c*h*TPH2:BH_2) were added and the sample was incubated on ice for 15 min. Before analysis the sample was diluted to a c*h*TPH2 concentration of 2.4-3.5 µM with 600 mM ammonium acetate pH 7.0.

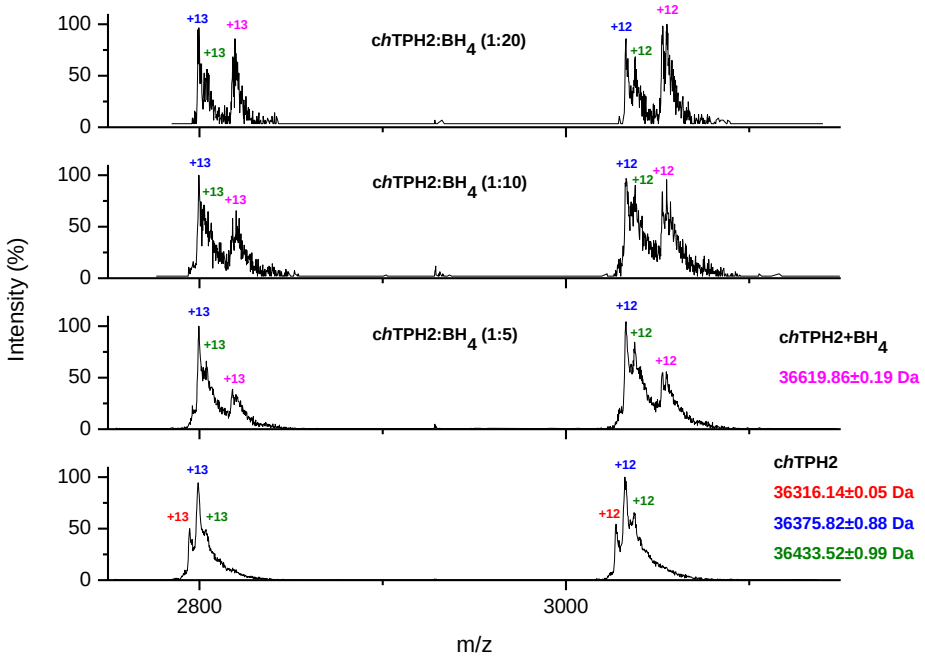

Figure 9.19. Mass spectra of c*h*TPH2 and c*h*TPH2 with BH_4 in the ratio 1:5, 1:10 and 1:20. The buffer was changed to 600 mM ammonium acetate pH 7.2 using ultrafiltration devices and the concentration determined to 24 µM. BH_2 in ratios 1:5, 1:10 and 1:20 (c*h*TPH2:BH_4) were added and the sample was incubated on ice for 15 min. Before analysis the sample was diluted to a c*h*TPH2 concentration of 2.4-3.5 µM with 600 mM ammonium acetate pH 7.0.

9.3.3 ct*h*TPH2

Prior to MS analysis of ct*h*TPH2 the buffer was changed to 600mM ammonium acetate pH 7.0 as described in section 9.2.2, and the concentration was 45-55 µM for the monomer.

9.3.3.1 Determination of the experimental monomer mass of apo-ct*h*TPH2

The experimental monomer mass of apo-ct*h*TPH2 was determined as described in section 9.1.4.1. In figure 9.20 the mass spectrum of the denatured ct*h*TPH2 is shown.

A)

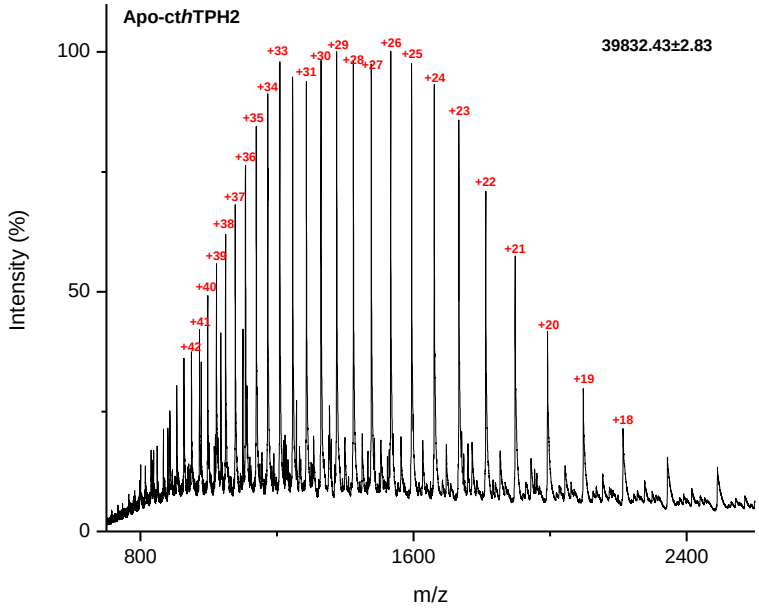

B)

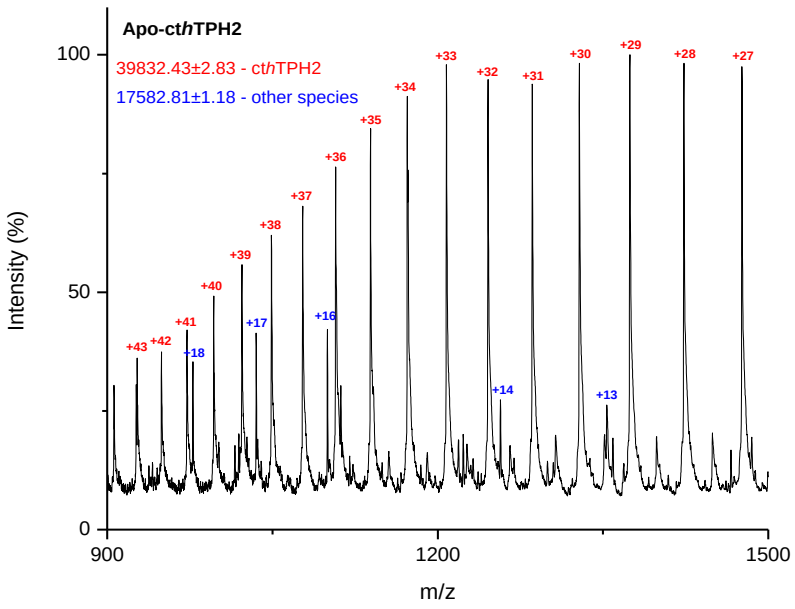

Figure 9.20. Mass spectrum of denatured ct*h*TPH2. The buffer was changed to 600 mM ammonium acetate pH 7.0 using ultrafiltration devices and denatured using ZipTip (C18) and 5 % formic acid. The sample is eluted from the tip using 1% formic acid and 50 % acetonitrile.

In the spectrum one dominant protein has an apparent average mass of 39831±2.93 Da corresponding to the expected average mass of the monomer of apo-ct*h*TPH2 including its N-terminal methionine (39822.4411 Da) as given in table 9.6. As for c*h*TPH2, ct*h*TPH2 is also expected to have the N-terminal Met presence, due to the same N-terminal sequence of the two variants.

At the low *m/z* a smaller protein with an apparent mass of 17582.81±1.18 is present (figure 9.20B). This protein is probably an impurity. By comparing the relative intensity of the two proteins ct*h*TPH2 is by far more dominant.

9.3.3.2 Determination of the oligomeric state by tandem MS

The oligomeric state of ct*h*TPH2 was determined by tandem MS. First the MS spectrum of intact ct*h*TPH2 was obtained and is shown in figure 9.21. The spectrum contains two proteins: One with a mass corresponding to the tetramer of ct*h*TPH2 and one with a mass corresponding to the octamer form (see figure 9.21A). By decreasing the concentration of ct*h*TPH2 the octamer disappears (data not shown) and is therefore assigned to be due to nonspecific interaction created in the ESI process, see section 9.1.1.4.

The tetramer shows 5 charge states, +26-30, centered on a *m/z* value of 5950 and with an apparent mass of approximately 160823.52±26.78 Da. This corresponds to the expected mass of the tetramer of ct*h*TPH2 (159.5 kDa). The increase in apparent mass compared to the expected mass could be due to non-specific binding of small molecules such as sodium and solvent/buffer molecules such as H_2O and NH_4^+, which also give rise to broader peaks. By increasing the voltage in the instrument (DP 150, FP 200), shown in figure 9.21B, the peaks get sharper and less broad indicating that some nonspecific bound molecules have been removed from the protein. The apparent mass is also lowered to 159786.30±8.44, which is close to the expected mass of holo-ct*h*TPH2-Fe(II)-$3H_2O$ (159721.33 Da) or holo-ct*h*TPH2-Fe(II)-CH_3COO^- (159745.36 Da). The different forms of ct*h*TPH2, such as apo-form and holo-Fe-forms, are more difficult to distinguish because of the overlapping of broad peaks, if compared to the mass spectrum of c*h*TPH2 (figure 9.14).

The +28 charge state of the intact ct*h*TPH2 was isolated in the quadrupole and the complex dissociated by collisions with gas molecules in an argon-filled collision cell, as described in section 9.2.4.4. In figure 9.22 the tandem mass spectrum of +28 charge state is shown. Tandem mass spectrometry of ct*h*TPH2 gives rise to two ion series: A highly charged series of peaks assigned to a monomeric subunit and a “stripped” oligomer at higher *m/z*. The monomer mass, 39.8 kDa, correspond to ¼ of the mass measured of the intact complex, 160 kDa. Stripping of this single subunit gives rise to a mass of 119 kDa corresponding to a trimer. This result confirms that the species that was isolated (+28 charge state) is a tetramer. The monomeric subunit has 6 charge states, +16-21, centered at charge state +20 with a m/z of 2000, whereas the trimer (n-1) has 6 charge states, +8-13, centered at charge state +9 with a m/z of 13300. The charge of the parent ion is divided between the product ions as expected and described in section 9.1.3. Due to dissociation into a monomer and trimer and not two dimers it can be concluded that the protein

does not contain any intermolecular disulfide bonds. It can be concluded that ct*h*TPH2 can retain its oligomeric form in the absence of solvent.

A)

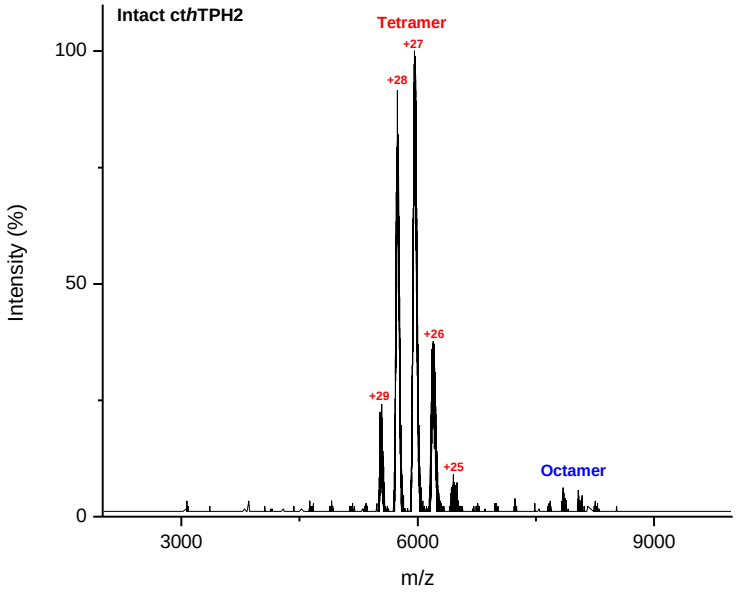

B)

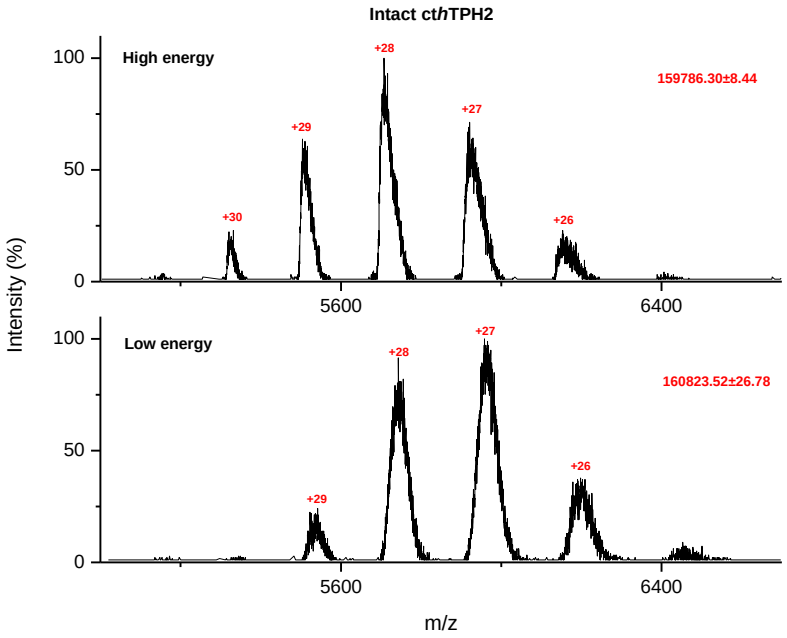

Figure 9.21. Mass spectrum of intact ct*h*TPH2 obtained using conditions that preserve non-covalent interactions and maximize the transmission of large ions. The buffer was changed to 600 mM ammonium acetate pH 7.0 using ultra filtration columns and diluted to 8 µM (monomer) before MS analysis.

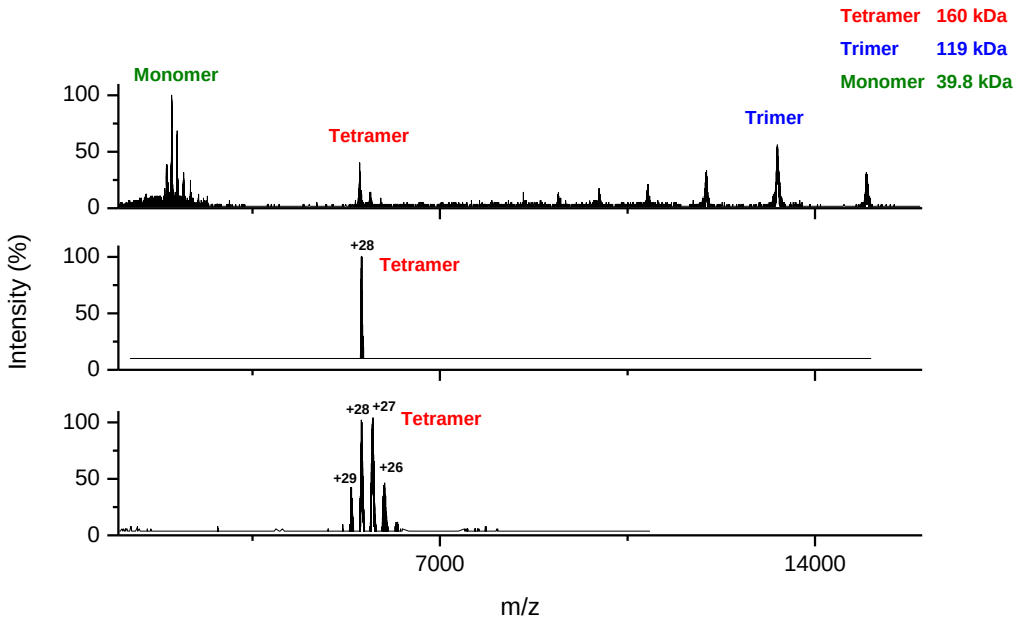

Figure 9.22. Mass spectrum of intact ct*h*TPH2 and tandem mass spectrum of the +28 charge state, which was isolated in the quadrupole and the complex dissociated by collisions with gas molecules in an argon filled collision cell. This gives rise to two ion series products; a highly charged series of peaks assigned to a monomeric subunit and a "stripped" oligomer at higher m/z. The monomer mass, 39.8 kDa, correspond to ¼ of the mass measured of the intact complex, 160 kDa. Stripping of this single subunit gives rise to a mass of 119 kDa corresponding to a trimer.

9.3.3.3 Fe binding

ct*h*TPH2 binds Fe and taking a closer look at the highly charged monomer species present in the tandem mass spectra of the +28 charge state isolated in the quadrupole, it is possible to see the apo-ct*h*TPH2 (39822.44 Da) as well as the holo-ct*h*TPH2-Fe species, as shown in figure 9.23, indicating that the energy necessary to dissociate the complex is not enough to fully remove the Fe.

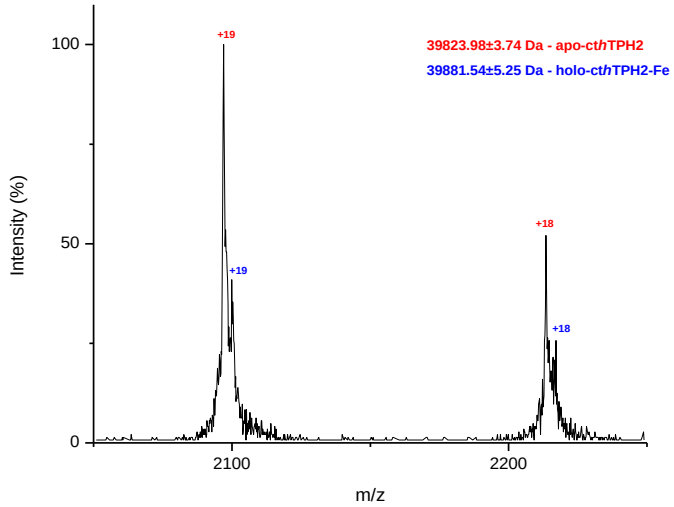

Figure 9.23. Tandem mass spectrum of the highly charged monomer of ct*h*TPH2.

9.3.3.4 Summary

The MS results indicate that the sample almost exclusively contains ct*h*TPH2. The MS/MS results show that ct*h*TPH2 is a tetramer that dissociates into a monomer and a trimer when increasing the energy in the collision cell. This also indicates that the variant does not contain any intermolecular disulfide bonds. The protein can preserve its solution structure in the gas phase.

9.4 Conclusion

Mass spectrometry is an extremely useful technique in studying non-covalent protein complexes. Both by chromatography and electrophoresis the c*h*TPH1 sample was shown to be homogenous, whereas mass spectrometric characterization of the sample showed that it was heterogeneous and contained two species. Also the heterogeneity of c*h*TPH2 has been detected by mass spectrometry, but by purification or electrophoresis this is not observed. Therefore, the use of MS gave very important results which were impossible to be obtained using other analytical techniques. These results have also been of fundamental importance to the group who has changed the purification strategies in order to obtain homogenous samples. Mass spectrometric characterization also determined that ct*h*TPH2 is a tetramer in a simple and fast way and using this technique it does not only give the right mass of the variant but also show the dissociation pattern of the protein complex.

10 Crystallization of c*h*TPH1

The determination of the three-dimensional structure of proteins can be done by using X-ray crystallography. The growth of suitable crystals is important for determination of the structure and to produce these, pure and concentrated solutions of the protein must be available. So far, only five structures of the catalytic domain of TPH have been determined: One with bound BH_2, one with tryptophan/imidazole and three with binding of different inhibitors. These structures showed different coordination of iron where a change in iron coordination from six to five upon incorporation of tryptophan/imidazole was observed as well as a change in structure (mentioned in chapter 2). It is still difficult to determine whether or not these observations are due to the substrate alone or that the imidazole mimics BH_4 and therefore, the structural change is caused by both binding of substrate and pterin (imidazole). A three-dimensional structure of the catalytic domain without substrate as well as with both substrates binding in the active site is therefore important for elucidating this iron coordination and the structural changes in the enzyme.

In this chapter a short introduction to protein crystallization with focus on the experimental parts will be given. This will be followed by description of the crystallization experiments done with c*h*TPH1 as well as the collected diffraction data and structure solution.

10.1 Crystallization of proteins

The crystallization process of proteins consists of two phases: A nucleation phase and a growth phase, in which both are driven by creation of a supersaturated state (non-equilibrium state) [198,199]. Before crystals can grow, stable nuclei must be formed. These are small aggregates of protein molecules that are formed in the supersaturated state. The probability and amount of stable nuclei formation (nucleation) are dependent on the degree of supersaturation [200].

The supersaturated state is divided into two regions: A metastable region and a labile region. In the metastabile region, which is just above saturation, nucleation cannot occur but crystal growth can continue if stable nuclei have already been formed. In the labile region, which is at higher supersaturation, nuclei can form spontaneously. Therefore, the degree of supersaturation necessary for nucleation is higher than that for crystal growth and at high supersaturation degree a large number of nucleation might occur [198,200]. When stable nuclei have been formed the protein molecules will start to order themselves into a crystal lattice with bonds that are energetically more favorable than the supersaturated state of the protein. This drives crystal growth. The crystal will continue to grow until the system regains its equilibrium where the protein concentration is decreased to the point of saturation [200]. Both the nucleation rate and growth rate are dependent on the degree of supersaturation; the higher the degree of supersaturation is the faster the growth of crystals is. A problem with too fast growth rate is that more growth defects can be seen [198,199]. Therefore, ideal crystal growth is where the degree of supersaturation is just high enough to get nucleation, which is just beyond the metastable region [199,200].

Proteins are sensitive and labile macromolecules that readily lose their native structure and the stability of crystals in aqueous media is restricted to a narrow range of pH, temperature and ionic strength. Therefore, protein crystals must be grown from a solution, which is known as the mother liquor [198,200]. Determination of the optimal crystallization conditions are not as straight forward as it might seem and usually a large range of growth conditions must be screened. This can be done by using pre-produced crystallization screens based on different solutions that have already been shown to be successful in crystallization of numerous proteins [198].

An important parameter in crystallization is the purity of the protein sample. It is not an absolute requirement but often crystals obtained from a mixture of proteins are small, not well shaped and of bad diffraction quality. By purity it is not only meant in terms of contaminants but also in terms of conformation and structural micro-heterogeneities, which often affect crystal growth. If crystallization is unsuccessful an improvement or reconsideration of the purification procedures needs to be studied first [198].

10.1.1 The vapor diffusion methods

There exist different methods to crystallize proteins and one of the most used method is the vapor diffusion method using either hanging drops or sitting drops, where only small volumes of protein are required [201].

The concept of the vapor diffusion methods is that a droplet containing the protein to be crystallized with buffer and precipitating agents is equilibrated against a reservoir containing a solution of the precipitating agents. The concentration of crystallizing agents in the drops is typically half of the concentration in the reservoir. This causes the volatile species such as water or organic solvents to vapor diffuse until the vapor pressure in the droplet equals the one of the reservoir and equilibrium has been reached. As a consequence the protein concentration, which

starts at an undersaturated state, will increase in the droplet and eventually reach the supersaturated state [201].

10.1.2 Factors influencing crystal growth

To achieve a limited degree of supersaturation, just beyond the metastabile region, the physical properties of the protein solution needs to be modified in order to reduce the solubility of the protein. This can be achieved by either changing the pH, temperature or through equilibration with precipitating agents [198,199,200].

10.1.2.1 Precipitating agents

Precipitating agents (precipitants) has two functions: One is to decrease the solubility of the protein and thereby achieve the supersaturated state faster and one is to cause vapor diffusion. In the vapor diffusion method the initial precipitant concentration in the non-equilibrated drop is half of that in the reservoir, which results in water diffusion until equilibrium is reached increasing the protein concentration. Different types of precipitants are used and these are typically categorized into four groups: Salts, organic solvents, long-chain polymers and low-molecular-mass polymers/non-volatile organic compounds. Examples of salts and organic solvents are ammonium sulfate and ethanol, respectively, whereas long-chain polymers are polyethylene glycol (PEG) 4000. The latter group are typically compounds such as methylpentanediol and PEG of molecular weight less than 1000 [199,200]. PEGs and salts are the most used and only these will be described in the following.

The solubility of proteins is highly affected by the ionic strength of the solutions. At very low ionic strength no ions are available to satisfy the electrostatic requirements of the protein and therefore, protein molecules seek to interact with one another to satisfy their electrostatic requirements, thus leading to aggregation or crystal formation. This process is known as “salting-in” and can be achieved by removing salt ions from the solution [200]. In the opposite process, known as “salting-out”, where salt ions are used as precipitant, the salt ions will “dehydrate” the protein by competition for water molecules. Proteins bind water molecules on their surface to maintain their solubility and in highly concentrated salt solutions there is a competition between the salt ions and the protein for the binding of water molecules. At sufficiently high concentrations the amount of water molecules available for the protein will be decreased causing the protein to associate with one another in order to satisfy their electrostatic requirements. In this environment ordered crystals as well as disordered amorphous precipitate may form [199,200]. Multivalent ions, particularly anions, are the most efficient precipitants and sulfates, phosphates and citrates have been used with success [200].

PEGs dehydrate proteins in solution by the volume exclusion effect [199,200]. They are randomly and flexible in structure and occupies a large volume. By adding PEGs to a protein solution it reduces the solvent available space for the protein molecules resulting in aggregation of protein molecules [199]. PEG is produced in various lengths and molecular sizes from 400 to 20,000 [200].

10.1.2.2 pH and temperature

A solutions pH value affects the solubility of a protein due to change in the proteins net charge. At the pI value, where the net charge of the protein is zero, the solubility of the protein is at its minimum. By increasing the net charge of the protein the solubility increases [202]. The temperature is also an important factor that affects the solubility of a protein where the solubility varies as a function of temperature. Usually the solubility increases with increasing temperature in low ionic strength conditions such as PEG solutions. At high ionic strength proteins are generally less soluble at high temperatures. If the protein is unstable at high temperatures, crystallization at low temperatures will be of choice, due to stabilization of the protein, which increases the probability of crystal growth [203].

10.2 Experimental procedures

10.2.1 Materials

The Solubility screen and the Structure screen 1 and 2 (appendix A.3) were both obtained from Molecular Dimensions. Tryptophan was obtained from Sigma and BH_2 was obtained from Schirks Laboratories. The trays used were either CombiClover sitting drop trays from Jena Biosciences with four satellite drop chambers connected to a central reservoir or VDX greased plates hanging drop trays from Hampton Research.

10.2.2 Preparation of sample

The c*h*TPH1 for the crystallization experiments was purified as described in chapter 8 except that 20 mM Tris/NaOH, 100 mM $(NH_4)_2SO_4$ pH 8.5 was used as gel filtration buffer. The concentration of the sample was 2.5 mg/ml. The concentrated sample was frozen in 100 µl aliquots using liquid N_2 and stored at -80^{o}C until use.

For crystallization stock solutions of c*h*TPH1 was thawed on ice. Four different samples were prepared: One with only c*h*TPH1, one with c*h*TPH1 and tryptophan, one with c*h*TPH1 and BH_2 and one with c*h*TPH1 and both tryptophan and BH_2. The samples were prepared by diluting the c*h*TPH1 from the stock solutions to the desired concentration with 20 mM Tris/NaOH, 100 mM $(NH_4)_2SO_4$ pH 8.5 after addition of ligand, if needed. The ligands were added in 2 fold molar excess from 7 mM stock solutions.

10.2.3 Crystallization trials using crystal screens

The Solubility screen and the Structure screen 1 and 2 were used and the crystallization trials were conducted using vapor diffusion method with sitting drop. The screens were set up with four drops, one drop from each sample prepared as described in section 10.2.2, per reservoir. 250 µl of reservoir solution was added to the each reservoir. The c*h*TPH1 concentration in the non-equilibrated drops was 2 mg/ml with 2 time's molar excess of tryptophan, BH_2 or both. The drops were set up with 2 µl reservoir solution + 2 µl of the protein solution. The trays were stored at room temperature.

10.2.4 Crystallization trials using c*gg*TPH1 conditions

c*h*TPH1 was also set up using the same condition where c*gg*TPH1 showed to crystallize [13]. 250 µl of 22.5 % PEG10,000, 0.2M imidazole malat pH 8.5 was added to the reservoir of a sitting drop vapor tray. Four drops were added, one drop from each sample prepared as described in section 10.2.2, per reservoir using 2 µl reservoir solution + 2 µl of the protein solution. The trays were stored at room temperature.

10.2.5 Optimization trials

Results obtained from section 10.2.3 and 10.2.4 were further optimized using different concentration of precipitant, different concentration of protein and different temperatures. The different optimization screens were prepared as described in section 10.2.5.1, 10.2.5.2 and 10.2.5.3 and given in appendix A.3.

10.2.5.1 Optimization screen 1

Three screens of the optimization screen 1 were set up using 1 mg/ml, 1.5 mg/ml or 2 mg/ml of c*h*TPH1, respectively. These optimization trials were conducted using vapor diffusion method with sitting drop. The screens were set up with four drops, one drop from each sample prepared as described in section 10.2.2, per reservoir. 250 µl of reservoir solution was added to the each reservoir. The drops were set up with 2 µl reservoir solution + 2 µl of the protein solution. The trays were stored at room temperature.

10.2.5.2 Optimization screen 2

The best conditions (precipitant concentration, protein concentration) for crystal growth of c*h*TPH1 seen from the optimization screen 1 (section 10.2.5.1) were used and conducted using hanging drop vapor diffusion. The drops were set up with 2 µl reservoir solution + 2 µl of the protein solution and having 500 µl in the reservoir. Two screens with these conditions were set up: One stored at room temperature and one stored at +4^{o}C.

10.2.5.3 Optimization screen 3

The optimization screen 3 contained the most suitable condition of the reservoir solution obtained from section 10.2.5.1 and 10.2.5.2 at different pH values. One drop of c*h*TPH1 with or without ligands (sample prepared as described in section 10.2.2) were set up per reservoir solution using the hanging drop vapor diffusion method. The drops were set up with 2 µl reservoir solution + 2 µl of the protein solution and having 500 µl in the reservoir using the hanging drop vapor diffusion method. The trays were stored at room temperature.

10.2.6 Data collection

Several crystals were tested on Beamline I911-3 and I911-2 at the MaxLab synchrotron in Lund. The crystals were transferred to a cryo-buffer (see appendix A.3), mounted in loops (from Molecular Dimensions) and cryo-cooled immediately. For testing the crystals the loop was centered in the x-ray beam. If the crystal gave a good diffraction a data set of the full diffraction pattern was collected.

10.2.7 Data processing, structure solution and refinement

Data processing and structure solution was done using the program CCP4 and molecular replacement using the structure of c*h*TPH1 (1MLW) and Phaser in CCP4 [204]. The refinement was done in WinCoot using Refmac [205].

10.3 Results and discussion

10.3.1 Crystallization trials

Crystallization trials of c*h*TPH1 were done using two pre-produced crystal screens as described in section 10.2.3 and using the same condition where c*gg*TPH1 crystallized as described in section 10.2.4. Crystals were observed within a week in several drops both with and without ligands. Approximately half of these drops contained calcium which could form $CaSO_4$ with the sulfate from the c*h*TPH1 buffer and from the shape of the crystals these where concluded to be $CaSO_4$ crystals.

From the Solubility screen it was seen that c*h*TPH1 crystallized with or without ligands in ammonium citrate pH 9, ammonium sulfate pH 9 and sodium acetate pH 4.5. The crystals from sodium acetate pH 4.5 showed to be salt crystals of most probably $NaSO_4$. c*h*TPH1 also crystallized without ligands and with BH_2 at the same conditions were c*gg*TPH1 crystallized. Even though imidazole was present in the precipitant and the structure of c*gg*TPH1 shows to contain an imidazole (see chapter 2) it was still decided to go further with these crystals, see section 10.3.1.1. From the Structure screen 1 and 2 crystals were observed in several drops and marked with a red arrow in appendix A.3.

The size, shape and amount of crystals were compared from all screens to find the most suitable condition for further optimization trials. By comparing the crystals obtained using the solubility screen it was seen that the amount of crystals increased whereas the size decreased by increasing the concentration of either ammonium citrate pH 9 or ammonium sulfate pH 9.0. Therefore, it was chosen to use the two lowest concentrations in the optimization screen 1 (see section 10.2.5.1) as well as concentrations lower than these. From the structure screens only solution number 15 and 32 from screen 1 and number 14 and 28 from screen 2 were used.

10.3.1.1 Data collection on crystallization trials

Crystals obtained from the same condition where c*gg*TPH1 crystallized (22.5 % PEG10,000, 0.2 M imidazol malat pH 8.5) without ligands as well as the condition in solubility screen box 1 set N nr. 3a (1.1 M ammonium citrate pH 9.0) with tryptophan were tested on Beamline I911-3 at the MaxLab synchrotron in Lund as described in section 10.2.6. In figure 10.1 pictures of these crystals are shown. Crystals obtained from 1.1 M ammonium citrate pH 9.0 diffracted to a 7-8 Å resolution, whereas crystals obtained from the solubility screen diffracted to 4 Å resolution. A dataset of the latter crystal was collected. The testing on the synchrotron was done immediately after mounting and cryo-cooling of the crystals (the crystals were not stored).

A) B)

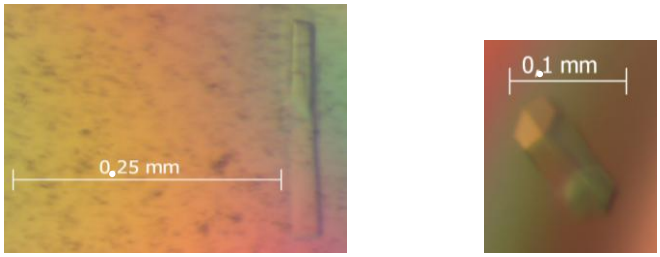

Figure 10.1. A) Crystal of c*h*TPH1 crystallized with 22.5 % PEG10.000, 0.2 M imidazole malat pH 8.5, c*h*TPH1 concentration was 2.0 mg/ml and the drops were stored at room temperature. B) Crystal of c*h*TPH1 and tryptophan crystallized with 1.1 M ammonium citrate pH 9.0, c*h*TPH1 concentration was 2.0 mg/ml and the drops were stored at room temperature.

10.3.1.2 Data processing, structure solution and refinement

Data collection (section 10.3.1.1), data processing, structure solution and refinement were done with help from Associate Professor Ole Kristensen from Department of Medicinal Chemistry, Faculty of Pharmaceutical Sciences, University of Denmark. The structure was determined by molecular replacement using c*h*TPH1 (PDB entry 1MLW) as search model. The refinement was carried out using Refmac in WinCoot, as described in section 10.2.7. In table 10.1 the data statistics for the space group is given.

Table 10.1. Data collection and processing statistics for the c*h*TPH1 crystal.

Space group	**P222**
Crystallization conditions	22.5 % PEG10,000, 0.2 M imidazole malat pH 8.5 Sitting drop, room temperature
X-ray source	I911-3, MAXII, MaxLab Lund
Detector	Marmosaic 225
Wavelength	1.00
Data collection temperature (K)	100 K
Resolution limit (Å)	50.7 – 4.0
No. reflections	46647
Unique reflections	12486
Redundancy	3.7
Completeness (%)	92.6
R_{merge}	0.236
<I/σ(I)>	4.8
Unit cell parameters	
a (Å), b (Å), c (Å)	84.1, 123.6, 148.4
α (°), β (°), γ (°)	90.0, 90.0, 90.0
Solvent content (%)	53.8
Matthews coefficient ($Å^3Da^{-1}$)	2.66
Nmol/assym.	4

10.3.1.3 Summary

From the crystallization trials of c*h*TPH1 (see section 10.3.1), c*h*TPH1 could crystallize with and without ligands at several conditions. Two crystals of c*h*TPH1 without and with tryptophan were tested on the synchrotron to resolution of 4 Å and 7-8 Å, respectively. A dataset of the c*h*TPH1 without ligands was obtained. Further optimizations needed to be done to obtain bigger and better crystals. The crystals of especially c*h*TPH1 with tryptophan and BH_2 were very small and the amount of crystals were high (many nucleation sites).

10.3.2 Optimization trials

To obtain bigger crystals and to get crystals with a higher resolution, different optimization screens with a change in protein concentration, precipitant concentration, pH values and temperature were performed as described in section 10.2.5.1, 10.2.5.2 and 10.2.5.3 and given in appendix A.3.

After 6 weeks no crystals were observed in the optimization screen 2, which was stored at +4^{o}C, whereas crystals were observed in several drops within the 1-2 weeks in the two other optimization screens, but no change in size, shape or amount of crystals were observed. Most of the crystals of c*h*TPH with and without ligands from the crystallization trials (described in section 10.3.1) could be reproduced, but not all of them. Crystals of c*h*TPH1 with tryptophan crystallized with 1.1 M ammonium citrate pH 9.0 obtained from the crystallization trials described in section 10.3.1 could not be reproduced. In table 10.2 the most suitable conditions for crystallization of c*h*TPH1 with and without ligands are given.

Table 10.2. The different conditions for crystallization of c*h*TPH1 with and without ligands.

Sample	Conditions
c*h*TPH1 and tryptophan	1 mg/ml protein 1.4 M ammonium citrate pH 9.0
c*h*TPH1 and tryptophan	2 mg/ml protein 1.75 M $(NH_4)_2SO_4$ pH 9.0
c*h*TPH1 and tryptophan+BH_2	1.5 mg/ml protein 2 M $(NH_4)_2SO_4$ pH 9.0
c*h*TPH1	2 mg/ml protein 22.5 % PEG10,000, 0.2 M imidazole malat pH 8.5
c*h*TPH1 and BH_2	2 mg/ml protein 22.5 % PEG10,000, 0.2 M imidazole malat pH 8.5
c*h*TPH1	2 mg/ml protein 0.1 M Na HEPES, 20 % w/v PEG 10,000 pH 7.5
c*h*TPH1 and BH_2	2 mg/ml protein 0.1 M Na HEPES, 20 % w/v PEG 10,000 pH 7.5

10.3.3 Overall structure of c*h*TPH1

The structure of c*h*TPH1 determined from the dataset described in section 10.3.1.2 could be refined to R_{free} = 33.5 %. Due to the low resolution only a "rough" refinement was done and water molecules were not included in the structure. The structure contained 4 molecules in the asymmetric unit. All four molecules have a well defined electron density from Thr104 to Lys400. For molecule A the last visible residue in the c*h*TPH1 structure is Gln409. The overall structure is shown in figure 10.2 with the residues Thr104 to Gln409. Electron density is observed for the iron coordinated by His272, His277 and Glu317 (see figure 10.3).

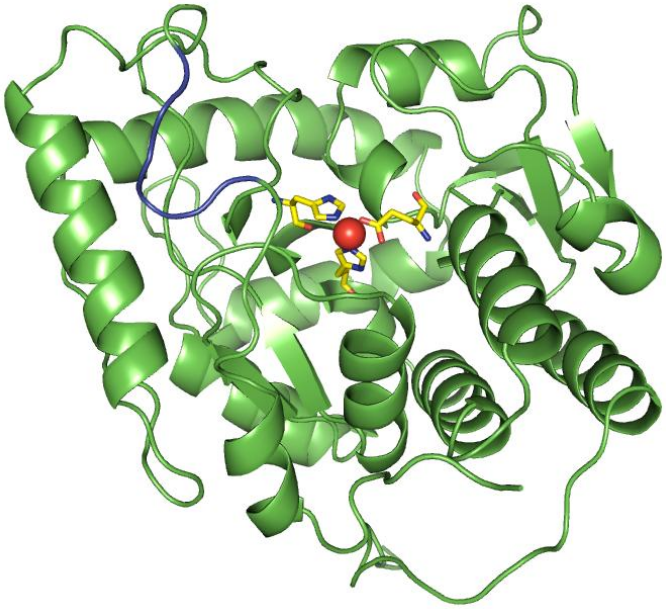

Figure 10.2. Overall structure of c*h*TPH1 determined at 4 Å resolution. His272, His273 and Glu317 are shown with sticks and the iron as a brick red sphere. The amino acid from 125 to 130 is highlighted in blue and the electron density map for this region is shown in figure 10.4. The figure was made using pymol [47].

The largest differences between this structure and the c*h*TPH1 crystallized with BH_2 are observed at residue Tyr125 to Asp130, as shown in figure 10.4, where the electron density of c*h*TPH1 is changed and has another conformation. The density observed is continuous and it is tempting to model the residues, so they are located in this density, but they are not able to fit. From the crystal structure of the catalytic domains described in chapter 2 it is known that this loop change conformation upon tryptophan binding indicating that it is flexible. This could be the reason why some of the electron density is "missing".

The precipitant contained imidazole, which coordinates to the iron in the c*gg*TPH1, but from the electron density of c*h*TPH1 no density is observed for imidazole. Therefore, it can be speculated that it does not bind to the active site, but it is difficult to conclude due to the low resolution.

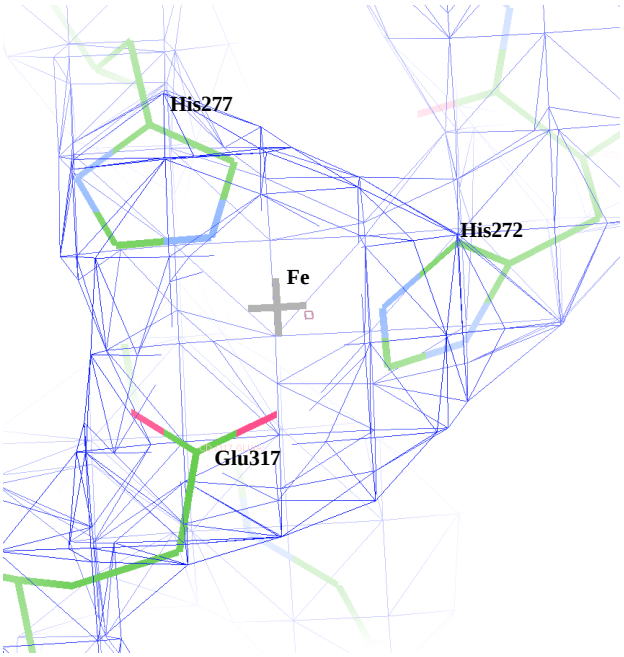

Figure 10.3. Electron density (1.08 σ) of the iron coordinated by His272, His277 and Glu317.

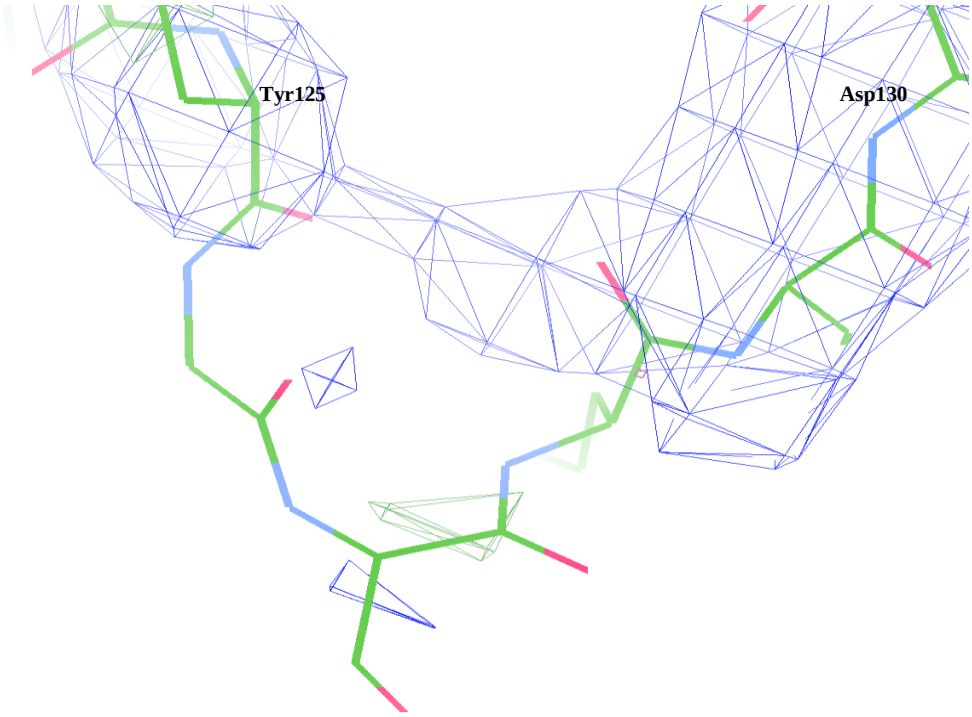

Figure 10.4. Electron density (1.08 σ) of amino acid Tyr125 to Asp130.

10.3.4 Future experiments

From the mass spectrometric analysis of c*h*TPH1 (chapter 9), a second species is observed in the sample. This species could not be observed with any other technique used. As mentioned in

section 10.1 an important parameter in crystallization is the purity of the protein sample and crystals obtained from a mixture of proteins are often small, not well shaped and of bad diffraction quality. Therefore an improvement of the purification method of c*h*TPH1 should be considered in order to obtain a more pure sample.

Additionally, to achieve better and bigger crystals of c*h*TPH1 without ligands it could be tried to decrease the growth rate. +4^{o}C has been tried with no success, but using a temperature of 15^{o}C could be enough to slow down the process and still get nucleation and crystal growth. For crystallization of c*h*TPH1 with tryptophan and tryptophan+BH_2 streak seeding should be tried where a concentration of the precipitant corresponding to the metastable zone is used.

10.4 Conclusion

Crystals of c*h*TPH1 crystallized with and without ligands were produced and a dataset of the crystals of c*h*TPH1 without ligands were collected to 4 Å. The structure could be solved in space group P222 by molecular replacement. The structure was refined to R_{free} of 33.5 %. It was possible to build most of the protein chain and some overall structural differences are observed compared to the structure of c*h*TPH1 with BH_2. This is the first structure of c*h*TPH1 without any substrates or inhibitors present in the active site and only the six structure of human TPH.

11 Overall conclusion

The main goal of this project was to purify full-length *h*TPH1. The purification strategy was based on results obtained during my master project. These results showed that *h*TPH1 most probably exists as a membrane-associated complex which can not bind to any of the ion exchange columns applied. Therefore, it was necessary to develop a method which could eliminate these interactions in order to get it to bind to the ion exchange columns. This was done by incubating the protein solution with detergent. The incubation with detergent showed to successfully solubilize the membrane-associated *h*TPH1, thus decreasing the size of *h*TPH1, causing it to bind to the column. This was the first time full-length *h*TPH1 could bind to an ion exchange column. Difficulties in understanding the behavior of full-length *h*TPH1 were still observed during purification and from the elution pattern the protein was still present in different oligomer forms. From earlier solubility test of c*h*TPH2, ct*h*TPH2 and full-length *h*TPH2 performed in this group it was observed that presence of the regulatory domain caused the protein to be insoluble [6,57,104]. Due to these observations and the difficulties during purification of full-length *h*TPH1 as well as the fact that c*h*TPH1, c*h*TPH2 and ct*h*TPH2 can be purified in a simple way [6,14,57], it was speculated that the problems with purifying full-length *h*TPH1 could be due to the regulatory domain. In order to understand and elucidate the properties of full-length TPH, a "divide-and-conquer" strategy was applied where different variants of *h*TPH containing the regulatory domain or parts of the domain were constructed.

From expression and solubility test of the constructed variants it was observed that mutations in the 3,4-hydrophobic repeat of the regulatory domain as well as truncations in N-terminal had a negative influence on the solubility and caused the protein to be insoluble. Despite this, the r*h*TPH1 as well as the two fusion proteins: r*h*TPH1-GFP and GST-r*h*TPH1, respectively showed to be soluble and therefore these variants were used for further studies and purification attempts

were performed. From these results the same elution pattern, as observed for full-length *h*TPH1 solubilized with detergent, was seen indicating that the variant was present in different oligomer forms. By having a high concentration of salt in the raw cell extract r*h*TPH1 elutes in one oligomeric form. From these results it was concluded that salt stabilizes the variant and a purification strategy based on this was designed and r*h*TPH1 was therefore fused to GST. The GST-r*h*TPH1 fusion protein was successfully purified with a high concentration of salt in the buffer system and the GST was successfully cleaved. The high salt purification strategy developed for r*h*TPH1 might be the key to purification of full-length *h*TPH1. r*h*TPH1 could be successfully purified.

In my master project a method for expression and purification of c*h*TPH1 was successfully developed and other members of the group had developed methods for purifying both c*h*TPH2 and ct*h*TPH2 [6,57]. Characterization of these three variants was therefore performed. The apparent K_m values for all three substrates of c*h*TPH1 were determined. These were compared with the values of c*h*TPH2 determined by Michael S. Windahl [6]. Substrate inhibition by tryptophan is observed for c*h*TPH1 above 40 μM but was not observed for c*h*TPH2 at concentrations up to 100 μM. Large differences are observed between the K_m values of the two isoforms especially the $K_{m,BH4}$ which is more than a factor 10 higher for c*h*TPH1 than for c*h*TPH2. This large difference might be a result of the substrate inhibition by tryptophan.

Mass spectrometric analysis of c*h*TPH1, c*h*TPH2 and ct*h*TPH2 showed that the purified c*h*TPH1 was heterogenous and contained two species. Both by chromatography and electrophoresis the c*h*TPH1 sample was shown to be homogenous. c*h*TPH2 showed to be heterogeneous with respect to Fe, indicating that the sample is not fully saturated with iron. This could not be observed either by purification or electrophoresis. Therefore, the use of MS gave very important results which were impossible to observe using other analytical techniques and these results have also been of fundamental importance to the group who has changed the purification strategies in order to obtain homogenous samples. Additionally, the mass spectrometric results showed that all three ligands (tryptophan, BH_2 and BH_4) can bind individually to c*h*TPH2 and their binding did not change the oligomeric state of TPH. Mass spectrometric analysis also determined that ct*h*TPH2 is a tetramer indicating that it preserves its solution structure in the gas phase. Mass spectrometry can therefore be used in the analysis of TPH variants in a simple and fast way.

Despite the fact that the c*h*TPH1 sample showed to be heterogeneous it was possible to crystallize the variant. Crystallization conditions of c*h*TPH1 with and without ligands were found and several crystals were grown. The best crystal diffracted to 4 Å and a data set was collected. The structure was solved by molecular replacement and refined to a R_{free} of 33.5 %. Structural differences were observed between c*h*THP1 without bound ligands and c*h*TPH1 with bound BH_2.

Further research on both isoforms is necessary to fully understand the enzymes and knowledge on these will aid to the understanding of the two serotonergic systems as well as the biochemical role of serotonin.

12 Bibliography

[1] A. Martinez, P. M. Knappskog and J. Haavik, A structural approach into human tryptophan hydroxylase and its implications for the regulation of serotonin biosynthesis, Curr. Med. Chem., 8, 2001, 1077-1091

[2] S. M. Mockus and K. E. Vrana, Advances in the molecular characterization of tryptophan hydroxylase, J. Mol. Neurosci., 10, 1998, 163-179

[3] I. Lucki, The spectrum of behaviors influenced by serotonin, Biol. Psychiatry., 44, 1998, 151-162

[4] http://www.psykiatrifonden.dk/Forside/Psykiske+sygdomme (29.06.2010)

[5] K. M. Fisher and P. G. Nielsen, Cloning and expression of tryptophan hydroxylase, Department of Chemistry, Technical University of Denmark, Kgs. Lyngby, 2002, B.Sc. thesis

[6] M. S. Nielsen, Expression, purification and characterization of tryptophan hydroxylase, Department of Chemistry, Technical University of Denmark, Kgs. Lyngby, 2007, Ph.D. dissertation

[7] C. R. Petersen, Production, chromatographic purification and crystallization of the catalytic domain from *Gallus gallus* tryptophan hydroxylase isoform 1, Department of Chemistry, Technical University of Denmark, Kgs. Lyngby, 2006, M.Sc. thesis

[8] A. Munch, Chromatographic purification and stability studies of the catalytic domain of tryptophan hydroxylase isoform 1, Department of Chemistry, Technical University of Denmark, Kgs. Lyngby, 2006, M.Sc. thesis

[9] M. S. Nielsen, Purification of tryptophan hydroxylase variants and the crystal structure of *Pyrococcus furiosus* $[Fe_3S_4]$-ferredoxin, Department of Chemistry, Technical University of Denmark, Kgs. Lyngby, 2004, M.Sc. thesis

[10] C. R. Petersen and T. V. Rasmussen, Purification and stabilization of the catalytic domain of tryptophan hydroxylase, Department of Chemistry, Technical University of Denmark, Kgs. Lyngby, 2004, B.Sc. thesis

[11] J. Boesen and M-J. K. Klitgaard, Cloning and chromatographic purification of full-length tryptophan hydroxylase (in Danish), Department of Chemistry, Technical University of Denmark, Kgs. Lyngby, 2004, B.Sc. thesis

[12] M. S. Nielsen, C. R. Petersen, A. Munch, T. V. Vendelboe, J. Boesen, P. Harris and H. E. M. Christensen, A simple two step procedure for purification of the catalytic domain of chicken tryptophan hydroxylase 1 in a form suitable for crystallization, Protein Expression Purif., 57, 2008, 116-126

[13] M. S. Windahl, C. R. Petersen, H. E. M. Christensen and P. Harris, Crystal structure of tryptophan hydroxylase with bound amino acid substrate, Biochemistry, 47, 2008, 12087-12094

[14] J. Boesen, Cloning, production and chromatographic purification of human tryptophan hydroxylase isoform 1 variants and initial kinetic studies (in Danish), Department of Chemistry, Technical University of Denmark, Kgs. Lyngby, 2007, M.Sc. thesis

[15] P. F. Fitzpatrick, Mechanism of aromatic amino acid hydroxylation, Biochemistry, 41, 2003, 14083-14091

[16] P. F. Fitzpatrick, Tetrahydrobiopterin-dependent amino acid hydroxylases, Annu. Rev. Biochem., 68, 1999, 355-381

[17] P. F. Fitzpatrick, The aromatic amino acid hydroxylases, in: Advances in enzymology and related areas of molecular biology, 74, Editor Purich, John Wiley & Sons, Inc. New York, 2000, 235-294

[18] N. Carkaci-Salli, J. M. Flanagan, M. K. Martz, U. Salli, D. J. Walther, M. Bader and K. E. Vrana, Functional domains of human tryptophan hydroxylase 2 (hTPH2), J. Biol. Chem., 281, 2006, 28105-28112

[19] K. E. Vrana, S. J. Walker, P. Rucker and X. Liu, A Carboxyl terminal leucine zipper is required for tyrosine hydroxylase tetramer formation, J. Neurochem., 63, 2014-2020

[20] M. Thórólfsson, B. Ibarra-Molero, P. Fojan, S. B. Petersen, J. M. Sanchez-Ruiz and A. Martínez, L-Phenylalanine binding and domain organization in human phenylalanine hydroxylase: a differential scanning calorimetry study, Biochemistry, 41, 2002, 7573-7585

[21] S. Kaufman, The enzymatic conversion of phenylalanine to tyrosine, J. Biol. Chem., 226, 1957, 511-524

[22] T. Flatmark and R. C. Stevens, Structural insight into the aromatic amino acid hydroxylases and their disease-related mutant forms, Chem. Rev., 99, 1999, 2137-2160

[23] T. Nagatsu, M. Levitt and S. Udenfriend, Tyrosine hydroxylase, the first step in norepinephrine biosynthesis, J. Biol. Chem., 239, 1964, 2910-2917

[24] P. M. Knappshog, T. Flatmark, J. Mallet, B. Lüdecke and K. Bartholomé, Recessively inherited L-DOPA-responsive dystonia caused by a point mutation (Q381K) in the tyrosine hydroxylase gene, Hum. Mol. Genet., 4, 1995, 1209-1212

[25] B. Lüdecke, P. M. Knappshog, p. T. Clayton, R. A. H. Surtees, J. D. Clelland, S. J. R. Heales, M. P. Brand, K. Bartholomé and T. Flatmark, Recessively inherited L-DOPA-responsive parkinsonism in infancy caused by a point mutation (L205P) in the tyrosine hydroxylase gene, Hum. Mol. Genet., 5, 1996, 1023-1028

[26] D. J. Walther, J.-U. Peter, S. Bashammakh, H. Hörtnagl, M. Voits, H. Fink and M. Bader, Synthesis of serotonin by a second tryptophan hydroxylase isoform, Science, 299, 2003, 76

[27] W. Lovenberg, E. Jequier and A. Sjoerdsma, Tryptophan hydroxylase: measurement in pineal gland, brainstem, and carcinoid tumor, Science, 155, 1967, 217-219

[28] P. D. Patel, C. Pontrello and S. Burke, Robust and tissue-specific expression of TPH2 versus TPH1 in rat raphe and pineal gland, Biol. Psychiatry, 55, 2004, 428-433

[29] A. Slominski, A. Pisarchik, O. Johansson, C. Jing, I. Semak, G. Slugocki and J. Wortsman, Tryptophan hydroxylase expression in human skin cells, Biochem. Biophys. Acta, 1639, 2003, 80-86

[30] H. Hasegawa, M. Yanagisawa, F. Inoue, N. Yanaihara and A. Ichiyama, Demonstration of non-neural tryptophan 5-mono-oxygenase in mouse intestinal mucosa, Biochem. J. 248, 1987, 501-509

[31] P. Zill, A. Büttner, W. Eisenmenger, H.-Jürgen Möller, M. Ackenheil and B. Bondy, Analysis of tryptophan hydroxylase I and II mRNA expression in the human brain: a post-mortem study, Journal of Psychiatric Research, 41, 2007, 168-173

[32] X. Zhang, J.-M. Beaulieu, T. D. Sotnikova, R. R. Gainetdinov and M. G. Caron, Tryptophan hydroxylase-2 controls brain serotonin synthesis, Science, 305, 2004, 217

[33] D. J. Walther and M. Bader, A unique central tryptophan hydroxylase isoform, Biochem. Pharmacol., 66, 2003, 1673-1680

[34] http://www.invitrogen.com/site/us/en/home/Products-and-services/Applications/Cloning/Vector-Design-Software/Vector-NTI-Software.html (25.06.10)

[35] Gasteiger E., Gattiker A., Hoogland C., Ivanyi I., Appel R.D., Bairoch A., ExPASy: the proteomics server for in-depth protein knowledge and analysis, Nucleic Acids Res. 31, 2003, 3784-3788

[36] L. Wang, H. Erlandsen, J. Haavik, P. M. Knappskog and R. C. Stevens, Three-dimensional structure of human tryptophan hydroxylase and its implications for the biosynthesis of the neurotransmitters serotonin and melatonin, Biochemistry, 41, 2002, 12569-12574

[37] H. Erlandsen, F. Fusetti, A. Martinez, E. Hough, T. Flatmark and R. C. Stevens, Crystal structure of the catalytic domain of human phenylalanine hydroxylase reveals the structural basis for phenylketonuria, Nat. Struct. Biol., 4, 1997, 995-1000

[38] K. E. Goodwill, C. Sabatier, C. Marks, R. Raag, P. F. Fitzpatrick and R. C. Stevens, Crystal structure of tyrosine hydroxylase at 2.3 Å and its implications for inherited neurodegenerative diseases, Nat. Struct. Biol., 4, 1997, 578-585

[39] E. L. Hegg and L. Que Jr., The 2-his-1-carboxylate facial triad, Eur. J. Biochem., 250, 1997, 625-629

[40] P. C. A. Bruijnincx, G. von Koten and R. J. M. K. Gebbink, Mononuclear non-heme iron enzymes with the 2-his-1-carboxylate facial triad: recent developments in enzymology and modeling studies,Chem. Soc. Rev., 37, 2008, 2716-2744

[41] O. A. Andersen, T. Flatmark and E. Hough, Crystal structure of the ternary complex of the catalytic domain of human phenylalanine hydroxylase with tetrahydrobiopterin and 3-(2-thienyl)-L-alanine, and its implications for the mechanism of catalysis and substrate activation, J. Mol. Biol., 320, 2002, 1095-1108

[42] O. A. Andersen, A. J. Stokka, T. Flatmark and E. Hough, 2.0 Å resolution crystal structure of the ternary complexes of human phenylalanine hydroxylase catalytic domain with tetrahydrobiopterin and 3-(2-thienyl)-L-alanine or L-norleucine: substrate specificity and molecular motions related to substrate binding, J. Mol. Biol., 333, 2003, 747-757

[43] G. Cianchetta, T. Stouch, W. Yu, Z.-C. Shi, L. W. Tari, R. V. Swanson, M. J. Hunter, I. D. Hoffman and Q. Liu, Current Chemical Genomics, 4, 2010, 19-26

[44] J. N. Kemsley, N. Mitic, K. L. Zaleski, J. P. Caradonna and E. I. Solomon, Circular dichroism and magnetic circular dichroism spectroscopy of the catalytically ferrous active site of phenylalanine hydroxylase and its interaction with pterin cofactor, J. Am. Chem. Soc., 121, 1999, 1528-1536

[45] M. S. Chow, B. E. Eser, S. A. Wilson, K. O. Hodgson, B. Hedman, P. F. Fitzpatrick and E. I. Solomon, Spectroscopy and kinetics of wild-type and mutant tyrosine hydroxylase: mechanistic insights into O_2 activation, J. Am. Soc. Chem., 131, 2009, 7685-7698

[46] B. Kobe, I. G. Jennings, C. M. House, B. J. Michell, K. E. Goodwill, B. D. Santarsiero, R. C. Stevens, R. G. H. Cotton and B. E. Kemp, Structural basis of autoregulation of phenylalanine hydroxylase, Nat. Struct. Biol., 6, 1999, 442-448

[47] The programme can be obtained at http://www.pymol.org/ (26.06.2010)

[48] G. J. Yohrling, IV, S. M. Mockus and K. E. Vrana, Identification of amino-terminal sequences contributing to tryptophan hydroxylase tetramer, J. Mol. Neuroscience, 12, 1999, 23-34

[49] J. McKinney, P. M. Knappskog and J. Haavik, Different properties of the central and peripheral forms of human tryptophan hydroxylase, J. Neurochem., 92, 2005, 311-320

[50] G. C.-T. Jiang, G. J. Yohrling, I. V. J. D. Schmitt and K. E. Vrana, Identification of substrate orienting and phosphorylation sites within tryptophan hydroxylase using homology-based molecular modeling, J. Mol. Biol., 302, 2000, 1005-1017

[51] P. A. Johansen, I. Jennings, R. G. H. Cotton and D. M. Kuhn, Tryptophan hydroxylase is phosphorylated by protein kinase A, J. Neurochem., 65, 1995, 882-888

[52] I. Winge, J. A. McKinney, M. Ying, C. S. D'Santos, R. Kleppe, P. M. Knappskog and J. Haavik, Activation and stabilization of human tryptophan hydroxylase 2 by phosphorylation and 14-3-3 binding, Biochem. J., 410, 2008, 195-204

[53] D. M. Kuhn, S. A. Sakowski, T. J. Geddes, C. Wilkerson and J. W. Haycock, Phosphorylation and activation of tryptophan hydroxylase 2: identification of serine-19 as the substrate site for calcium, calmodulin-dependent protein kinase II, J. Neurochem., 103. 2007, 1567-1573

[54] U. Banik, G.-A. Wang, P. D. Wagner and S. Kaufman, Interaction of phosphorylated tryptophan hydroxylase with 14-3-3 proteins, J. Biol. Chem., 272, 1997,26219-26225

[55] Y. Furukawa, N. Ikuta, S. Omata, T. Yamauchi, T. Isobe and T. Ichimura, Demonstration of the phosphorylation-dependent interaction of tryptophan hydroxylase with the 14-3-3 protein, Biochem. Biophys. Res. Commun., 194, 1993, 144-149

[56] F. Fusetti, H. Erlandsen, T. Flatmark and R. C. Stevens, Structure of tetrameric human phenylalanine hydroxylase and its implications for phenylketonuria, J. Biol. Chem., 273, 1998, 16962-16967

[57] L. T. Haahr, Expression, purification and structural studies of tetrameric variants of tryptophan hydroxylase isoform 2, Department of Chemistry, Technical University of Denmark, Kgs. Lyngby, 2008, M.Sc. thesis

[58] M. M. Abu-Omar, A. Loaiza and N. Hontzeas, Reaction mechanisms of mononuclear non-heme iron oxygenases, Chem. Rev., 105, 2005, 2227-2252

[59] A. J. Ramsey, P. J. Hillas and P. F. Fitzpatrick, Characterization of the active site iron in tyrosine hydroxylase, J. Biol. Chem., 271, 1996, 24395-24400

[60] T. A. Dix, G. E. Bollag, P. L. Domanico and S. J. Benkovic, Biochemistry, 24, 1985, 2955-2958

[61] A. Bassan, M. R. A. Blomberg and P. E. M. Siegbahn, Mechanism of dioxygen cleavage in tetrahydrobiopterin-dependent amino acid hydroxylases, Chem. Eur. J., 9, 2003, 106-115

[62] A. Bassan, T. Borowski and P. E. M. Siegbahn, Quantum chemical studies of dioxygen activation by mononuclear non-heme iron enzymes with the 2-his-1-carboxylate facial triad, Dalton Trans., 20, 2004, 3153-3162

[63] L. T. Haahr, K. P. Jensen, J. Boesen and H. E. M. Christensen, Experimentally calibrated computational chemistry of tryptophan hydroxylase: trans influence, hydrogen-bonding and 18-electron rule govern O_2-activation, J. Inorg. Biochem., 104, 2010, 136-145

[64] B. E. Eser, E. W. Barr, P. A. Frantom, L. Saleh, J. M. Bollinger, Jr., C. Krebs and P. F. Fitzpatrick, J. Am. Chem. Soc., 129, 2007, 11334-11335

[65] C. Krebs, D. G. Fujimori, C. T. Walsh and J. M. Bollinger, Jr., Non-heme Fe(IV)-oxo intermediates, Acc. Chem. Res., 40, 2007, 484-492

[66] J. N. Kemsley, E. C. Wasinger, S. Datta, N. Mitic, T. Acharya, B. Hedman, J. P. Caradonna, K. O. Hodgson and E. I. Solomon, Spectroscopic and kinetic studies of PKU-inducing mutants of phenylalanine hydroxylase: Arg158Gln and Glu280Lys, J. Am. Chem. Soc., 125, 2003, 5677-5686

[67] P. J. Hillas and P. F. Fitzpatrick, A mechanism for hydroxylation by tyrosine hydroxylase based on pertitioning of substituted phenylalanines, Biochemistry, 35, 1996, 6969-6975

[68] J. Renson, F. Goodwin, H. Weissbach and S. Udenfriend, Enzymatic conversion of 5-tritiotryptophan to 4-tritio-5-hydroxytryptophan, Biochem. Biophys. Res. Commun., 25, 1966, 504-513

[69] G. Guroff and J. Daly, Quantitative studies on the hydroxylation induced migration of deuterium and tritium during phenylalanine hydroxylation, Arch. Biochem. Biophys., 122, 1967, 212-217

[70] J. Daly, M. Levitt, G. Guroff and S. Udenfriend, Isotope studies on the mechanism of action of adrenal tyrosine hydroxylase, Arch. Biochem. Biophys., 126, 1968, 593-598

[71] J. A. Pavon and P. F. Fitzpatrick, Insights into the catalytic mechanisms of phenylalanine and tryptophan hydroxylase from kinetic isotope effects on aromatic hydroxylation, Biochemistry, 45, 2006, 11030-11037

[72] G. R. Moran, A. Derecskei-Kovacs, P. J. Hillas and P. F. Fitzpatrick, On the catalytic mechanism of tryptophan hydroxylase, J. Am. Chem. Soc., 122, 2000, 4535-4541

[73] B. Thöny, G. Auerbach and N. Blau, Tetrahydrobiopterin biosynthesis, regeneration and functions, Biochem. J., 347, 2000, 1-16

[74] M. Kirsch, H.-G. Korth, V. Stenert, R. Sustmann and H. de Groot, The autoxidation of tetrahydroniopterin revisited, J. Biol. Chem., 278, 2003, 24481-24490

[75] A. Volner, J. Zoidakis and M. M. Abu-Omar, Order of substrate binding in bacterial phenylalanine hydroxylase and its implication for pterin-dependent oxygenases, J. Biol. Inorg. Chem., 8, 2003, 121-128

[76] S. O. Pember, K. A. Johnson, J. J. Villafranca and S. J. Benkovic, Mechanistic studies on phenylalanine hydroxylase from *Chromobacterium violaceum*. Evidence for the formation of an enzyme-oxygen complex, Biochemistry, 28, 1989, 2124-2130

[77] J. Veenstra-VanderWeele, G. M. Anderson and E. H. Cook Jr., Pharmacogenetics and the serotonin system: initial studies and future directions, Eur. J. Pharmacol., 410, 2000, 165-181

[78] M. Lesurtel, R. Graf, B. Aleil, D. J. Walther, Y. Tian, W. Jochum, C. Gachet, M. Bader and P.-A. Clavien, Platelet-derived serotonin mediates liver regeneration, Science, 312, 2006, 104-107

[79] M. Berger, J. A. Grey and B. L. Roth, The expanded biology of serotonin, Annu. Rev. Med., 60, 2009, 355-366

[80] S. Ganguly, S. L. Coon and D. C. Klein, Control of melatonin synthesis in the mammalian pineal gland: the critical role of serotonin acetylation, Cell Tissue Res., 309, 2002, 127-137

[81] M. D. Coates, C. R. Mahoney, D. R. Linden, J. E. Sampson, J. Chen, H. Blaszyk, M. D. Crowell, K. A. Sharkey, M. D. Gershon, G. M. Mawe and P. L. Moses, Molecular defects in mucosal serotonin content and decreased serotonin reuptake transporter in ulcerative colitis and irritable bowel syndrome, Gastroenterology, 126, 2004, 1657-1664

[82] Z.-C. Shi, A. Devasagayaraj, K. Gu, H. Jin, B. Marinelli, L. Samala, S. Scott, T. Stouch, A. Tunoori, Y. Wang, Y. Zang, C. Zhang, S. D. Kimball, A. J. Main, W. Sun, Q. Yang, A. Nouraldeen, X.-Q. Yu, E. Buxton, S. Patel, N. Nguyen, J. Swaffield, D. R. Powell, A. Wilson and Q. Liu, Modulation of peripheral serotonin levels by novel tryptophan hydroxylase inhibitors for the potential treatment of functional gastrointestinal disorders, J. Med. Chem., 51, 2008, 3684-3687

[83] S. Walitza, T. J. Renner, A. Dempfle, K. Konrad, C. Wewetzer, A. Halbach, B. Herpertz-Dahlmann, H. Remschmidt, J. Smidt, M. Linder, L. Flierl, U. Knölker, S. Friedel, H. Schäfer, C. Gross, J. Hebebrand, A. Warnke and K. P. Lesch, Transmission disequilibrium of polymorphic variants in the tryptophan hydroxylase-2 gene in attention-deficit/hyperactive disorder, Mol. Psychiatry, 10, 2005, 1126-1132

[84] J. J. Mann, K. M. Malone, D. J. Diehl, J. Perel, T. B. Cooper, and M. A. Mintun, Demonstration in vivo of reduced serotonin responsivity in the brain of untreated depressed patients, Am. J. Psychiatry, 153, 1996, 174-182

[85] S. Matthes, V. Mosienko, S. Bashammakh, N. Alenina and M. Bader, Tryptophan hydroxylase as novel target for the treatment of depressive disorders, Pharmacology, 85, 2010, 95-109

[86] K. Nakamura and H. Hasegawa, Developmental role of tryptophan hydroxylase in the nervous system, Mol. Neurobiol., 35, 2007, 45-53

[87] Q. Liu, Q. Yang, W. Sun, P. Vogel, W. Heydorn, X-Q. Yu, Z. Hu, W. Yu, B. Jonas, R. Pineda, V. Calderon-Gay, M. Germann, E. O'neill, R. Brammage, E. Cullinan, K. Platt, A. Wilson, D. Powell, A. Sands, B. Zambrowicz and Z.-C. Shi, Discovery and characterization of novel tryptophan hydroxylase inhibitors that selectively inhibit serotonin synthesis in the gastrointestinal tract, J. Pharmacol. Exp. Ther., 325, 2008,47-55

[88] J. McKinney, P. M. Knappskog, J. Pereira, T. Ekern, K. Toska, B. B. Kuitert, D. Levine, A. M. Gronenborn, A. Martinez and J. Haavik, Expression and purification of human tryptophan hydroxylase from *Escherichia coli* and *Pichia pastoris*, Protein Expression Purif., 33, 2004, 185-194

[89] D. Kowlessur and S. Kaufmann, Cloning and expression of recombinant human pineal tryptophan hydroxylase in *Escherichia coli*: purification and characterization of the cloned enzyme, Biochim. Biophys. Acta, 1434, 1999, 317-330

[90] A. Munch, Affinity ligands for purification of tryptophan hydroxylase (in Danish), Department of Chemistry, Technical University of Denmark, Kgs. Lyngby, 2004

[91] R. G. H. Cotton and I. G. Jennings, Affinity chromatography of phenylalanine hydroxylase, Eur. J. Biochem., 85, 1978, 357-363

[92] E. P. Carpenter, K. Beis, A. D. Cameron and S. Iwata, Overcoming the challenges of membrane protein crystallography, Curr. Opin. Struct. Biol., 18, 2008, 581-586

[93] M. le Maire, P. Champeil and J. V. Møller, Interaction of membrane proteins and lipids with solubilizing detergents, Biochim. Biophys. Acta, 1508, 2000, 86-111

[94] S. Kalipatnapu and A. Chattopadhyay, Membrane protein solubilization: recent advances and challenges in solubilization of serotonin$_{1A}$ receptors, Life, 57, 2005, 505-512

[95] A. M. Seddon, P. Curnow and P. J. Booth, Membrane proteins, lipids and detergents: not just a soap opera, Biochim. Biophys. Acta, 1666, 2004, 105-117

[96] D. Drew, M. Lerch, E. Kunji, D-J. Slotboom and J-W. de Gier, Monitoring expression of an *E. coli* membrane protein GFP-(His)$_8$ fusion and purification using a combination of IMAC and gel filtration, Discovery Matters, Issue 5, 2007, GE Healthcare

[97] E. Layne, Spectrophotometric and turbidimetric methods for measuring proteins, Methods Enzymol., 3, 1957, 447–454.

[98] J. H. Kleinschmidt, M. C. Wiener and L. K. Tamm, Outer membrane protein A of *E. coli* folds into detergent micelles but not in the presence of monomeric detergent, Protein Sci., 8, 1999, 2065-2071

[99] www.bio-rad.com (22.06.2010)

[100] R. G. H., Cotton, W. McAdam, I. Jennings and F. J. Morgan, A monoclonal antibody to aromatic amino acid hydroxylases, Biochem. J., 255, 1988, 193-196

[101] http://www.bio-rad.com/LifeScience/pdf/Bulletin_9281.pdf (22.06.2010)

[102] http://www.pick-n-post.com/default.asp?ID=50010300067 (22.06.2010)

[103] http://www.epc.bio.dtu.dk/Proteinanalyse-service.aspx (22.06.2010)

[104] P. E. Karlsen, Expression and purification of the metal-containing monooxygenases tryptophan hydroxylase and dopamine β-hydroxylase, Department of Chemistry, Technical University of Denmark, Kgs. Lyngby, 2010, Ph.D. dissertation

[105] F. W. Studier, A. H. Rosenberg, J. J. Dunn and J. W. Dubendorff, Use of T7 RNA polymerase to direct expression of cloned genes, Methods in Enzymology, 185, 1990, 60-89

[106] J. W. Dubenhorff and F. W. Studier, Controlling basal expression in an inducible T7 expression system by blocking the target T7 promoter with lac respressor, J. Mol. Biol., 219, 1991, 45-59

[107] pET System Manual, 11th edition: http://kirschner.med.harvard.edu/files/protocols/Novagen_petsystem.pdf (22.06.2010)

[108] J. Arnau, C. Lauritzen, G. E. Petersen and J. Pedersen, Current strategies for the use of affinity tags and tag removal for the purification of recombinant proteins, Protein Expr. Purif., 48, 2006, 1-13

[109] A. Crameri, E. A. Whitehorn, E. Tate and W. P. C. Stemmer, Improved green fluorescent protein by molecular evolution using DNA shuffling, Nature Biotechnology, 14, 1996, 315-319

[110] B. P. Cormack, R. H. Valdivia and S. Falkow, FACS-optimized mutants of the green fluorescent protein (GFP), Gene, 173, 1996, 33-38

[111] G. S. Waldo, B. M. Standish, J. Berendzen and T. C. Terwilliger, Rapid protein-folding assay using green fluorescent protein, Nature Biotechnology, 17, 1999, 691-695

[112] D. E. Drew, G. von Heijne, P. Nordlund and J.-W. L. de Gier, Green fluorescent protein as an indicator to monitor membrane protein overexpression in *Escherichia coli*, FEBS letters, 507, 2001, 220-224

[113] D. Drew, M. Lerch, E. Kunji, D.-J. Slotboom and J.-W. de Gier, Optimization of membrane protein overexpression and purification using GFP fusions, Nature Methods, 3, 2006, 303-313

[114] D. B. Smith and K. S. Johnson, Single-step purification of polypeptides expressed in *Escherichia coli* as fusions with glutathione S-transferase, Gene, 67, 1988, 31-40

[115] C. Zurek, Y. Berghöfer-Hochheimer and T. Munder, Expression and purification of myoglobin using glutathione S-transferase gene fusion system, Science Tools from Pharmacia Biotech., 2, 1997, 18-19

[116] http://www.gelifesciences.com (08.04.2010)

[117] T. Nishikubo, N. Nakagawa, S. Kuramitsu and R. Masui, Improved heterologous gene expression in *Escherichia coli* by optimization of the AT-content of codons immediately downstream of the initiation codon, J. Biotechnol., 120, 2005, 341-346

[118] S. C. Makrides, Strategies for achieving high-level expression of genes in *Escherichia coli*, Micobiological reviews, 60, 1996, 512-538

[119] D. V. K. Rao, J. V. Rao, M. L. Narasu and A. K. S. B. Rao, Optimization of the AT-content of codons immediately downstream of the initiation codon and evaluation of culture conditions for high-level expression of recombinant human G-CSF in *Escherichia coli*, Mol. Biotechnol., 38, 2008, 221-232

[120] http://www.viogene.com/files/show_case/Protocol/EG-PF_p.pdf (08.04.2010)

[121] http://www.stratagene.com/manuals/211190.pdf (08.04.2010)

[122] http://www.sigmaaldrich.com/etc/medialib/docs/Sigma/Bulletin/pln70bul.Par.0001.File.tmp /pln70bul.pdf (08.04.2010)

[123] http://www.neb.com/nebecomm/tech_reference/restriction_enzymes/buffer _activity_restriction_enzymes.asp? (09.04.10)

[124] http://www.usbweb.com/brief_proto/78400b.pdf (09.04.10)

[125] K. Marcher, Optimization of the expression yield of tryptophan hydroxylase i *E. coli*, Department of Chemistry, Technical University of Denmark, Kgs. Lyngby, 2008, Laboratory Technician project

[126] C. N. Pace, F. Vajdos, L. Fee, G. Grimsley and T. Gray, How to measure and predict the molar absorption coefficient of a protein, Protein Science, 4, 1995, 2411-2423

[127] www.gelifesciences.com (27.06.2010)

[128] J.-D. Pédelacq, S. Cabantous, T. Tran, T. C. Twillinger and G. S. Waldo, Engineering and characterization of a superfolder green fluorescent protein, Nature Biotechnology, 24, 2006, 79-88

[129] D. S. Waugh, Making the most of affinity tags, Trends Biotechnol., 23, 2005, 316-320

[130] http://www.qiagen.com/literature/handbooks/literature.aspx?id=1000081 (27.06.2010)

[131] http://www.gelifesciences.com/aptrix/upp01077.nsf/Content/Products?Open Document&parented=390399&moduleid=166490 (27.06.2010)

[132] P. J. Henderson, Statistical analysis of enzyme kinetic data, Chapter 10, Enzyme Assays, A practical approach, Editors R. Eisenthal and M. J. Danson, Oxford University Press, Oxford, 1992

[133] V. Leskovac, Kinetics of monosubstrate reactions, Chapter 3, Comprehensive enzyme kinetics, Kluwer Academic/Plenum Press, New York, 2003

[134] D. Jukíc, K. Sabo and R. Scitovski, A review of existence criteria for parameter estimation of the Michaelis-Menten regression model, Ann. Univ. Ferrara, 53, 2007, 281-291

[135] W. W. Cleland, Steady state kinetics, Chapter 1, The enzymes, kinetics and mechanism, vol. 2, 3rd edition, Editor P. D. Boyer, Academic Press, New York, 1970

[136] V. Leskovac, Kinetics of monosubstrate reactions, Chapter 12, Comprehensive enzyme kinetics, Kluwer Academic/Plenum Press, New York, 2003

[137] G. R. Moran and P. F. Fitzpatrick, A continuous fluorescence assay for tryptophan hydroxylase, Anal. Biochem., 266, 1999, 148-152

[138] M. Storgaard, Activity assay for tryptophan hydroxylase (in Danish), Department of Chemistry, Technical University of Denmark, Kgs. Lyngby, 2005

[139] R. Battino, Editor, IUPAC solubility data series, vol. 7, Oxygen and ozone, Pergamon Press, Oxford, 1981

[140] W. W. Cleland, Dithiothreitol, a new protective reagent for SH groups, Biochemistry, 3, 1964, 480-482

[141] H. Motulsky and A. Christopoulos, Fitting models to biological data using linear and nonlinear regression, a practical guide to curve fitting, Oxford University Press, Oxford 2004

[142] M. S. Windahl, J. Boesen, P. E. Karlsen and H. E. M. Christensen, Expression, purification and enzymatic characterization of the catalytic domains of human tryptophan hydroxylase isoforms, Protein J., 28, 2009, 400-406

[143] J. McKinney, K. Teigen, N. Å. Frøystein, C. Salaün, P. M. Knappskog, J. Haavik and A. Martinéz, Conformation of the substrate and pterin cofactor bound to human tryptophan hydroxylase. Important role of Phe313 in substrate specificity, Biochemistry, 40, 2001, 15591-15601

[144] G. R. Moran, S. C. Daubner and F. P. Fitzpatrick, Expression and characterization of the catalytic core of tryptophan hydroxylase, J. Biol. Chem., 273, 1998, 12259-12266

[145] K. Tenner, D. Walther and M. Bader, Influence of human tryptophan hdroxylase 2 N- and C-terminus on enzymatic activity and oligomerization, J. Neurochem., 102, 2007, 1887-1894

[146] P. A. Friedman, A. H. Kappelman and S. Kaufman, Partial purification and characterization of tryptophan hydroxylase from rabbit hindbrain, J. Biol. Chem., 247, 1972, 4165-4173

[147] S. Hosoda, Further studies on tryptophan hydroxylase from neoplastic murine mast cells, Biochem. Biophys. Acta, 397, 1975, 58-68

[148] S. Hosoda, W. Nakamura and K. Takatsuki, Properties of tryptophan hydroxylase from human carcinoid tumor, 482, 1977, 27-34

[149] J. L. P. Benesch, B. T. Ruotolo, D. A. Simmons and C. V. Robinsin, Protein complexes in the gas phase: Technology for structural genomics and proteomics, Chem. Rev., 107, 2007, 3544-3567

[150] K. J. Light-Wahl, B. L. Schwartz and R. D: Smith, Observations of the noncovalent quaternary associations of proteins by electrospray ionization mass spectrometry, J. Am. Chem. Soc., 116, 1994, 5271-5278

[151] M. Baca and S. B. H. Kent, Direct observation of a ternary complex between the dimeric enzyme HIV-1 protease and a substrate-based inhibitor, J. Am. Chem. Soc., 114, 1992, 3992-3993

[152] K. J. Light-Wahl, B. E. Winger and R. D. Smith, Observation of the multimeric forms of concanavalin A by electrospray ionization mass spectrometry, J. Am. Chem. Soc., 115, 1993, 5869-5870

[153] M. Sharon and C. V. Robinson, The role of mass spectrometry in structure elucidation of dynamic protein complexes, Annu. Rev. Biochem., 76, 2007, 167-193

[154] M. Dole, L. L. Mack and R. L. Hines, Molecular beams of macroions, J. Chem. Phys., 49, 1968, 2240-2249

[155] L. L. Mack, P. Kralik, A. Rheude and M. Dole, Molecular beams of macroions. II, J. Chem. Phys., 52, 1970, 4977-4986

[156] M. Yamashita and J. B. Fenn, Electrospray ion source. Another variation on the free-jet theme, J. Phys. Chem., 88, 1984, 4451-4459

[157] J. B. Fenn, M. Mann, C. K. Meng, S. F. Wong and C. M. Whitehouse, Science, 246, 1989, 64-71

[158] P. Kebarle and L. Tang, From ions in solution to ions in the gas phase, The mechanism of electrospray mass spectrometry, Anal. Chem., 65, 1993, 972-986

[159] Sir G. Taylor, Disintegration of water drops in an electric field, Proc. Roy. Soc. (London) Series A, 280, 1964, 383-385

[160] P. Kebarle and M. Peschke, On the mechanisms by which the charged droplets produced by electrospray lead to gas phase ions, Analytica Chemica Acta, 406, 2000, 11-35

[161] L. Rayleigh, On the equilibrium of liquid conducting masses charged with electricity, London Philisophical Magazine 5th Series, 14, 1882, 184-186

[162] A. R.C. McKay, A mass spectrometry study of noncovalent interactions: from single proteins to intact ribosomes, Clare Hall, University of Cambridge, Cambridge, 2006, Ph.D. thesis

[163] J. H. Gross, Mass Spectrometry – A textbook, Springer, 2004

[164] A. T. Blades, M. G. Ikonomou and P. Kebarle, Mechanism of electrospray mass spectrometry. Electrospray as an electrolysis cell, Anal. Chem., 63, 1991, 2109-2114

[165] R. B. Cole, Some tenets pertaining to electrospray ionization mass spectrometry, J. Mass Spectrom., 35, 2000, 763-772

[166] J. V. Iribarne and B. A. Thomson, On the evaporation of small ions from charged droplets, J. CHem. Phys., 64, 1976, 2287-2294

[167] P. Kebarle, A brief overview of the present status of the mechanisms involved in electrospray mass spectrometry, J. Mass Spectrom., 35, 2000, 804-817

[168] J. F. de la Mora, Electrospray ionization of large multiply charged species proceeds via Dole's charged residue mechanism, Analytica Chimica Acta, 406, 2000, 93-104

[169] M. S. Wilm and M. Mann, Electrospray and Taylor-cone theory, Dole's beam of macromolecules at last?, Int. J. Mass Spectrom. Ion Processes, 136, 1994, 167-180

[170] M. Wilm and M. Mann, Analytical properties of the nanoelectrospray ion source, Anal. Chem., 68, 1996, 1-8

[171] M. Karas, U. Bahr and T. Dülcks, Nano-electrospray ionization mass spectrometry: addressing analytical problems beyond routine, Fresenius J. Anal. Chem., 366, 2000, 669-676

[172] A. G. Marshall, M. W. Senko, W. Li, M. Li, S. Dillon, S. Guan and T. M. Logan, Protein molecular mass to 1 Da by ^{13}C, ^{15}N double-depletion and FT-ICR mass spectrometry, J. Am. Chem. Soc., 119, 1997, 433-434

[173] K.A. Johnson, M. F. J. M. Verhagen, P. S. Brereton, M. W. W. Adams and I. J. Amster, Probing the stoichiometry and oxidation states of metal centers in iron-sulfur proteins using electrospray FTICR mass spectrometry, Anal. Chem., 72, 2000, 1410-1418

[174] F. Sobott, H. Hernández, M. G. McCammon, M. A. Tito and C. V. Robinson, A tandem mass spectrometer for improved transmission and analysis of large macromolecular assemblies, Anal. Chem., 74, 2002, 1402-1407

[175] J. A. Loo, Electrospray ionization mass spectrometry: a technology for studying noncovalent macromolecular complexes, Int. J. Mass Spectrom., 200, 2000, 175-186

[176] S. Yin and J. A. Loo, Mass spectrometry detection and characterization of noncovalent protein complexes, Mass spectrometry of proteins and peptides, 492, 2009, 273-282

[177] A. R. McKay, B. T. Ruotolo, L. L. Ilag and C. V. Robinson, Mass Measurements of Increased Accuracy Resolve, Heterogeneous Populations of Intact Ribosomes, J. Am. Chem. Soc., 128, 2006, 11433-11442

[178] J. A. Loo, Studying noncovalent protein complexes by electrospray ionization mass spectrometry, Mass Spectrom. Rev., 16, 1997, 1-23

[179] I. V. Chernushevich and B. A. Thomson, Collisional cooling of large ions in electrospray mass spectrometry, Anal. Chem., 76, 2004, 1754-1760

[180] B. T. Ruotolo, K. Giles, I. Campuzano, A. M. Sandercock, R. H. Bateman and C. V. Robinson, Evidence for macromolecular protein rings in the absence of bulk water, Science, 310, 2005, 1658-1661

[181] B. T. Ruotolo and C. V. Robinson, Aspects of native proteins are retained in vacuum, Current Opinion in Chemical Biology, 10, 2006, 402-408

[182] K. Breuker and F. W. McLafferty, Stepwise evolution of protein native structure with electrospray into the gas phase, 10^{-12} to 10^{2} s, Proc. Natl. Acad. Sci., 105, 2008, 18145-18152

[183] W. Wang, E. N. Kitova and J. S. Klassen, Nonspecific protein-carbohydrate complexes produced by nanoelectrospray ionization. Factors influencing their formation and stability, Anal. Chem., 77, 2005, 3060-3071

[184] J. Sun, E. N. Kitova, N. Sun and J. S. Klassen, Method for identifying nonspecific protein-protein interactions in nanoelectrospray ionization mass spectrometry, Anal. Chem., 79, 2007, 8301-8311

[185] P. E. Miller and M. B. Denton, The quadrupole mass filter: basic operating concepts, J. Chem. Edu., 63, 1986, 617-622

[186] I. V. Chernushevich, A. V. Loboda and B. A. Thomson, An introduction to quadrupole-time-of-flight mass spectrometry, J. Mass Spectrom., 36, 2001, 849-865

[187] C. G. Herbert and R. A. W. Johnstone, Mass spectrometry basics, 2003, CRC Press LLC

[188] R. J. Cotter, Time-of-flight mass spectrometry for the structural analysis of biological moleculesI, Anal. Chem., 64, 1992, 1027-1039 A

[189] M. Guilhaus, Principles and instrumentation in time-of-flight mass spectrometry, J. Mass Spectrom., 30, 1995, 1519-1532

[190] A. E. Cameron and D. F. Eggers, Laboratory and shop notes, Rev. Sci. Instrum., 19, 1948, 605-607

[191] A.N. Krutchinsky, I.V. Chernushevich, V. L. Spicer, W. Ens and K. G. Standing, Collisional damping interface for an electrospray ionization time-of-flight mass spectrometer, J. Am. Soc. Mass Spectrom., 9, 1998, 569-579

[192] J. L. P. Benesch and C. V. Robinson, Mass spectrometry of macromolecular assemblies: preservation and dissociation, Current Opinion in Structural Biology, 16, 2006, 245-251

[193] J. L. P. Benesch, Collisional activation of protein complexes: picking up the pieces, Am. Soc. Mass Spectrom., 20, 2009, 341-348

[194] J. L. P. Benesch, J. A. Aquilina, B. T. Ruotolo, F. Sobott and C. V. Robinson, Tandem mass spectrometry reveals the quaternary organization of macromolecular assemblies, Chemistry and Biology, 13, 2006, 597-605

[195] P. H. Hirel, J.-M. Schmitter, P. Dessen, G. Fayat and S. Blanquet, Proc. Natl. Acad. Sci. USA, 86, 1989, 8247-8251

[196] http://www.uniprot.org/uniprot/P16700 (04.05.10)

[197] H. Hernández and C. V. Robinson, Determining the stoichiometry and interactions of macromolecular assemblies from mass spectrometry, Nature protocols, Vol. 2 No. 3, 2007, 715-726

[198] R. Giegé and A. Ducruix, An introduction to the crystallogenesis of biological macromolecules, Chapter 1 in Crystallization of nucleic acids and proteins, A practical approach, Editors A. Ducruix and R. Giegé, 2nd edition, Oxford University Press, Oxford, 1999

[199] A. McPherson, Introduction to protein crystallization, Methods, 34, 2004, 254-265

[200] A. McPherson, Current approaches to macromolecular crystallization, Eur. J. Biochem., 189, 1990, 1-23

[201] R. Giegé and A. Ducruix, Methods of crystallization, Chapter 5 in Crystallization of nucleic acids and proteins, A practical approach, Editors A. Ducruix and R. Giegé, 2nd edition, Oxford University Press, Oxford, 1999

[202] C. W. Carter, Jr. and M. Riés-Kautt, Improving marginal crystals, Methods Mol. Biol., 363, 2007, 153-174

[203] T. M. Bergfors, Protein crystallization: Techniques, strategies, and tips. A Laboratory manual, Edited by T. M. Bergfors, International University Line, 1999

[204] Collaborative Computational Project, Number 4, "The CCP4 Suite: Programs for Protein Crystallography", Acta Cryst. D50, 1994, 760-763

[205] Emsley P, Cowtan K (2004). Coot: model-building tools for molecular graphics. Acta Crystallogr. D60, 2126-2132.

Appendix 1

A.1 Primer sequences

Primer sequences of the *h*TPH1 gene variants.

Table A1.1. Primer sequence for amplification of TPH1 genes as either *Nde*I/*Xho*I-fragments or *Nde*I/*Bam*HI-fragments.

Gene	Primer		Sequence	Product size
c*h*TPH1	5'-end	HCP596	*Nde*I Annealing sequence 5'-AAAACATATGGATGGCATGGAAACCGTGC-3'	~950bp
	3'-end	HCP593	*Xho*I Stop Annealing sequence 5'-AAAACTCGAGTTAATCTTTCAGAATTTGAATACTGC-3'	
ct*h*TPH1	5'-end	HCP596	*Nde*I Annealing sequence 5'-AAAACATATGGATGGCATGGAAACCGTGC-3'	~1000bp
	3'-end	HCP655	*Xho*I Stop 5'-AAAACTCGAGTTAGATCGAAGGTTT-3' Annealing sequence	
rc*h*TPH1	5'-end	HCP641	*Nde*I 5'-AAAACATATGATTGAAGACAACAAAGA-3' Annealing sequence	~1300bp
	3'-end	HCP593	*Xho*I Stop Annealing sequence 5'-AAAACTCGAGTTAATCTTTCAGAATTTGAATACTGC-3'	
r*h*TPH1	5'-end	HCP641	*Nde*I 5'-AAAACATATGATTGAAGACAACAAAGA-3' Annealing sequence	~300bp
	3'-end	HCP643	*Xho*I Stop Annealing sequence 5'-AAAACTCGAGTTACTCTTTCAGGGTAAAATTGTC-3'	

Primer sequences of *h*TPH1 fusion genes.

Table A1.2. Primer sequence for amplification of *h*TPH1 genes as either *Nde*I/*Xho*I-fragments or *Nde*I/*Bam*HI-fragments.

r*h*TPH1-GFP	5'-end	HCP641	*Nde*I Annealing 5'-AAAACATATGATTGAAGACAACAAAGA-3'	~300bp
	3'-end	HCP642	*Bam*HI Annealing sequence 5'-AAAAGGATCCCTCTTTCAGGGTAAAATTGTC-3'	
L24R/V28R-r*h*TPH1 -GFP	5'-end	HCP683	5'-GCCTGATTTTTAGCCGCAAGAACGAACGCGGCGGACTGATCAAAGC-3'	~300bp
	3'-end	HCP684	3'-CGGACTAAAAATCGGCGTTCTTGCTTGCGCCGCCTGACTAGTTTCG-5'	
L31R/L35R-r*h*TPH1 –GFP	5'-end	HCP685	5'-GAAGTGGGCGGACGCATCAAAGCGCGCAAGATTTTTCAGGAG-3'	~300bp
	3'-end	HCP686	3'-CTTCACCCGCCTGCGTAGTTTCGCGCGTTCTAAAAAGTCCTC-5'	
V28R/L31R-r*h*TPH1 -GFP	5'-end	HCP687	5'-GCCTGAAGAACGAACGCGGCGGACGCATCAAAGCGCTGAAG-3'	~300bp
	3'-end	HCP688	3'-CGGACTTCTTGCTTGCGCCGCCTGCGTAGTTTCGCGACTTC-5'	
GST-r*h*TPH1	5'-end	HCP702	*Bam*HI Annealing sequence 5'-AAAAGGATCCCCATGATTGAAGACAACAAAGAGA-3'	~300bp
	3'-end	HCP643	*Xho*I Stop Annealing sequence 5'-AAAACTCGAGTTACTCTTTCAGGGTAAAATTGTC-3'	

Primer sequences of *h*TPH2 gene variants.

Table A1.3. Primer sequence for amplification of TPH2 genes.

Gene	Primer		Sequence	Product size
$TPH2_{59-490}$	5'-end	HCP631	*Nde*I Annealing 5'-AAAACATATGACCGAAAGCGGCAAAACCG-3'	~1300bp
	3'-end	HCP632	Annealing *Dra*I 5'-TTACTTTAAAGCCCGGATGAT-3'	
$TPH2_{90-490}$	5'-end	HCP697	*Nde*I Annealing 5'-AAAACATATGAACATGGTGCATATTGAAAGC-3'	~1200bp
	3'-end	HCP632	Annealing *Dra*I 5'-TTACTTTAAAGCCCGGATGAT-3'	

Appendix 2

A.2 Standard curves of 5-hydroxytryptophan

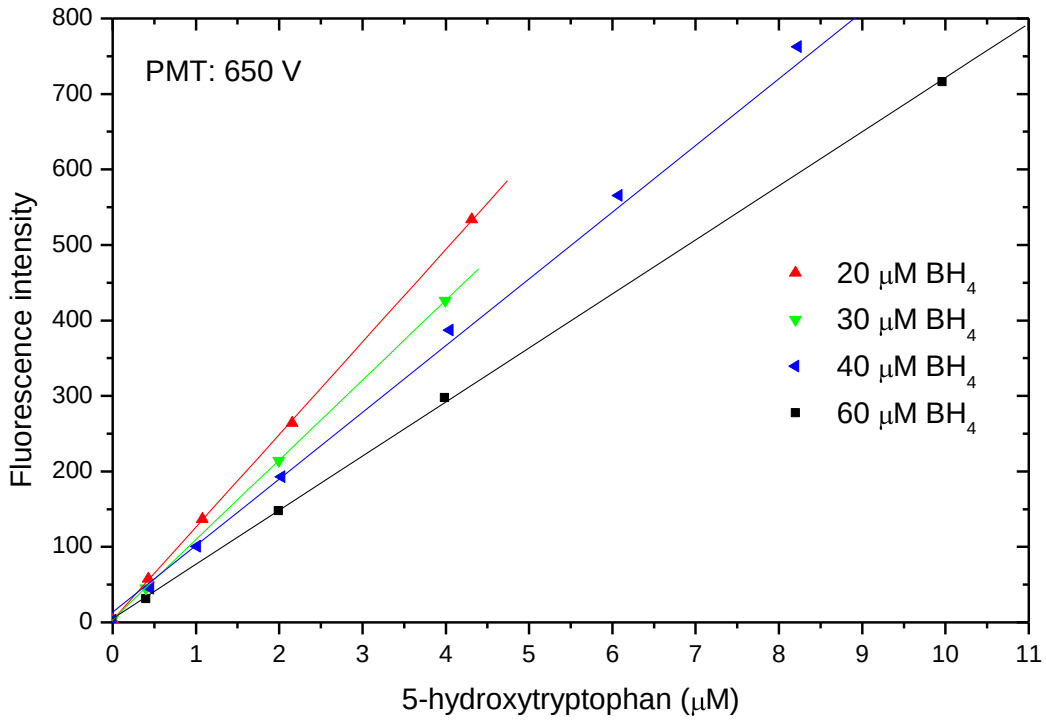

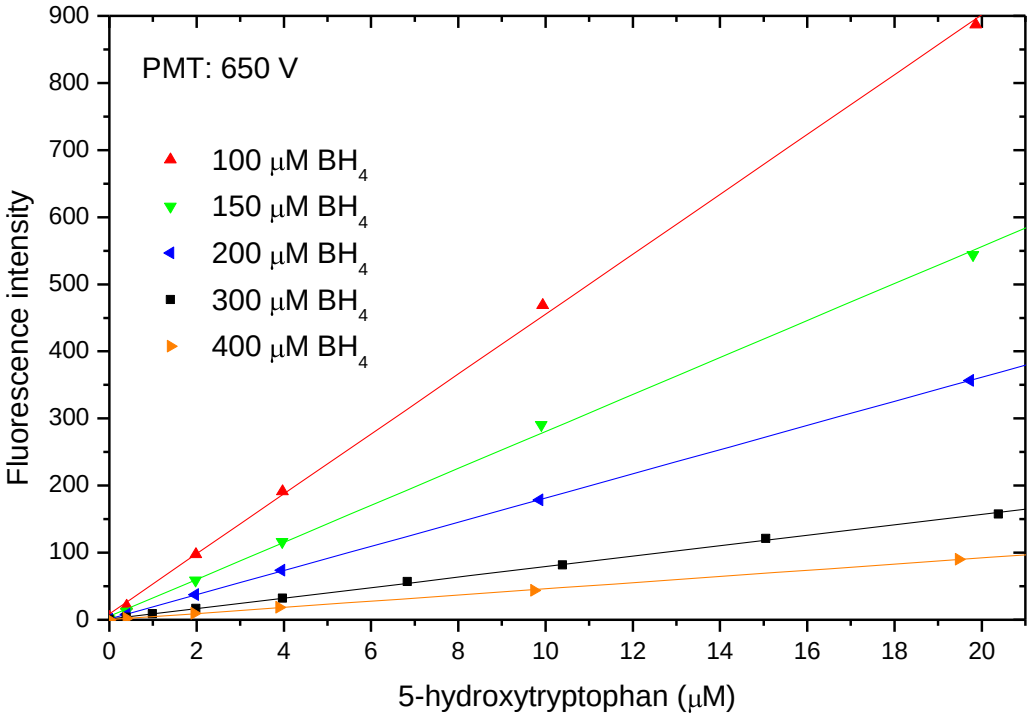

Slopes of the standard curves for 5-hydroxytryptophan at different concentrations of BH_4.

BH_4 (μM)	Slope (f.i./ μM 5-hydroxytryptophan)	R^2
20	122.65±0.7	0.9999
30	105.81±0.2	0.9999
40	88.36±1.8	0.9987
60	71.625±0.6	0.9999
100	44.635±0.6	0.9996
150	27.552±0.5	0.9995
200	18.015±0.05	0.9999
300	7.7749±0.08	0.9996
400	4.5998±0.04	0.9999

Appendix 3

A.3 – Crystallization screens

Solubility screen

Set contents – Box 1 set P – pH 4.5

P	1	2	3	4	5	6
	Potassium Thiocyanate	Sodium chloride	Sodium acetate	Ammonium dihydrogen phosphate	Ammonium citrate	Ammonium Sulfate
A	0.05 M	0.5 M	1.0 M	1.5 M	1.1 M	1.5 M
B	0.10 M	1.0 M	1.5 M	2.0 M	1.4 M	2.0 M
C	0.25 M	1.5 M	2.0 M	2.5 M	1.7 M	2.5 M
D	0.50 M	2.0 M	3.0M	3.0 M	2.0 M	3.0M

Set contents – Box 1 set N – pH 9.0

N	1	2	3	4	5	6
	Ammonium sulfate	Di-ammonium hydrogen phosphate	Ammonium citrate	Sodium acetate	Magnesium sulfate	Calcium chloride
A	1.0 M	1.0 M	1.1 M	1.0 M	0.05 M	0.21 M
B	1.5 M	1.5 M	1.4 M	1.5 M	1.00 M	0.49 M
C	2.0 M	2.0 M	1.7 M	2.0 M	1.50 M	1.00 M
D	2.5 M	2.5 M	2.0 M	3.0M	1.80 M	1.50 M

Set contents – Box 2 set Z – pH = pI = 6.0

Z		1	2	3	4	5	6
A	PEG 400 (v/v%)	4.8	9.6	14.4	19.2	33.6	48
B	PEG 4000 (%)	6.0	12.0	18.0	24.0	30.0	45
C	PEG 8000 (%)	3.6	7.2	10.8	14.4	18.0	27
D	MDP (% v/v)	4.8	9.6	14.4	19.2	33.6	48

Structure screen 1 and 2

Red arrows indicate the solution conditions where crystals were observed.

Structure Screen 1 — MD1-01

Tube #	Salt	Buffer	pH	Precipitant
1	0.02 M calcium chloride	0.1 M sodium acetate	4.6	30 % v/v MPD
2	0.2 M ammonium acetate	0.1 M sodium acetate	4.6	30 % w/v PEG 4K
3	0.2 M ammonium sulfate	0.1 M sodium acetate	4.6	25 % w/v PEG 4K
4	None	0.1 M sodium acetate	4.6	2.0 M sodium formate
5	None	0.1 M sodium acetate	4.6	2.0 M ammonium sulfate
6	None	0.1 M sodium acetate	4.6	8 % w/v PEG 4K
7	0.2 M ammonium acetate	0.1 M tri-sodium citrate	5.6	30 % w/v PEG 4K
8	0.2 M ammonium acetate	0.1 M tri-sodium citrate	5.6	30 % v/v MPD
→ 9	None	0.1 M tri-sodium citrate	5.6	20 % v/v 2-propanol, 20%w/v PEG 4K
10	None	0.1 M tri-sodium citrate	5.6	1.0 M ammonium dihydrogen phosphate
11	0.2 M calcium chloride	0.1 M sodium acetate	4.6	20 % v/v 2-propanol
12	None	0.1 M sodium cacodylate	6.5	1.4 M sodium acetate
13	0.2 M tri-sodium citrate	0.1 M sodium cacodylate	6.5	30 % v/v 2-propanol
→ 14	0.2 M ammonium sulfate	0.1 M sodium cacodylate	6.5	30 % w/v PEG 8K
→ 15	0.2 M magnesium acetate	0.1 M sodium cacodylate	6.5	20 % w/v PEG 8K
16	0.2 M magnesium acetate	0.1 M sodium cacodylate	6.5	30 % v/v MPD
17	None	0.1 M imidazole	6.5	1.0 M sodium acetate
→ 18	0.2 M sodium acetate	0.1 M sodium cacodylate	6.5	30 % w/v PEG 8K
19	0.2 M zinc acetate	0.1 M sodium cacodylate	6.5	18 % w/v PEG 8K
20	0.2 M calcium acetate	0.1 M sodium cacodylate	6.5	18 % w/v PEG 8K
21	0.2 M tri-sodium citrate	0.1 M Na HEPES	7.5	30 % v/v MPD
22	0.2 M magnesium chloride	0.1 M Na HEPES	7.5	30 % v/ v 2-propanol
23	0.2 M calcium chloride	0.1 M Na HEPES	7.5	28 % v/v PEG 400
24	0.2 M magnesium chloride	0.1 M Na HEPES	7.5	30 % v/v PEG 400
→ 25	0.2 M tri-sodium citrate	0.1 M Na HEPES	7.5	20 % v/v 2-propanol
26	None	0.1 M Na HEPES	7.5	0.8 M K/Na tartrate
27	None	0.1 M Na HEPES	7.5	1.5 M lithium sulfate
28	None	0.1 M Na HEPES	7.5	0.8 M sodium dihydrogen phosphate/ 0.8 M K dihydrogen phosphate
→ 29	None	0.1 M Na HEPES	7.5	1.4 M tri-sodium citrate
30	None	0.1 M Na HEPES	7.5	2 % v/v PEG 400, 2.0 M ammonium sulfate
31	None	0.1 M Na HEPES	7.5	10 % v/v 2-propanol, 20% w/v PEG 4K
→ 32	None	0.1 M Tris	8.5	2.0 M ammonium sulfate
→ 33	0.2 M magnesium chloride	0.1 M Tris	8.5	30 % w/v PEG 4K
34	0.2 M tri-sodium citrate	0.1 M Tris	8.5	30 % v/v PEG 400
35	0.2 M lithium sulfate	0.1 M Tris	8.5	30 % w/v PEG 4K
36	0.2 M ammonium acetate	0.1 M Tris	8.5	30 % v/v 2-Propanol
→ 37	0.2 M sodium acetate	0.1 M Tris	8.5	30 % w/v PEG 4K
→ 38	None	0.1 M Tris	8.5	8 % w/v PEG 8K
39	None	0.1 M Tris	8.5	2.0 M ammonium dihydrogen phosphate
40	None	None	-	0.4 M K/Na Tartrate
41	None	None	-	0.4 M ammonium dihydrogen phosphate
42	0.2 M ammonium sulfate	None	-	30 % w/v PEG 8K
43	0.2 M ammonium sulfate	None	-	30 % w/v PEG 4K
44	None	None	-	2.0 M ammonium sulfate
45	None	None	-	4.0 M sodium formate
46	0.05 M potassium dihydrogen phosphate	None	-	20 % w/v PEG 8K
47	None	None	-	30 % w/v PEG 1.5K
48	None	None	-	0.2 M magnesium formate
49	1.0 M lithium sulfate	None	-	2 % w/v PEG 8K
50	0.5 M lithium sulfate	None	-	15 % w/v PEG 8K

Abbreviations: Na HEPES; 2-(4-(2-Hydroxyethyl)-1-piperazinyl)ethanesulfonic Acid Sodium Salt, **MPD**; 2,4-methyl pentanediol, **PEG**; Polyethylene glycol (1.5K, 4K and 8K correspond to the molecular weight, in thousands of Daltons, of PEG), **Tris**; 2-Amino-2-(hydroxymethyl)propane-1,3-diol.

Structure Screen 2 — MD1-02

Tube No.	Salt	Buffer	pH	Precipitant
1	0.1 M sodium chloride	0.1 M Bicine	9.0	30 % v/v PEG 550 MME
2	None	0.1 M Bicine	9.0	2.0 M magnesium chloride
3	None	0.1 M Bicine	9.0	2 % v/v 1,4-Dioxane/10 % w/v PEG 20,000
4	0.2 M magnesium chloride	0.1 M Tris	8.5	3.4 M 1,6-hexanediol
5	None	0.1 M Tris	8.5	25 % v/v tert-butanol
6	0.01 M nickel chloride	0.1 M Tris	8.5	1.0 M lithium sulfate
7	1.5 M ammonium sulfate	0.1 M Tris	8.5	12 % v/v glycerol
8	0.2 M ammonium dihydrogen phosphate	0.1 M Tris	8.5	50 % v/v MPD
9	None	0.1 M Tris	8.5	20 % v/v ethanol
10	0.01 M nickel chloride	0.1 M Tris	8.5	20 % w/v PEG 2000 MME
11	0.5 M ammonium sulfate	0.1 M Na HEPES	7.5	30 % v/v MPD
12	None	0.1 M Na HEPES	7.5	10 % w/v PEG 6000, 5% v/v MPD
13	None	0.1 M Na HEPES	7.5	20 % v/v Jeffamine M-600
14	0.1 M sodium chloride	0.1 M Na HEPES	7.5	1.6 M ammonium sulfate
15	None	0.1 M Na HEPES	7.5	2.0 M ammonium formate
16	0.05 M cadmium sulfate	0.1 M Na HEPES	7.5	1.0 M sodium acetate
17	None	0.1 M Na HEPES	7.5	70 % v/v MPD
18	None	0.1 M Na HEPES	7.5	4.3 M sodium chloride
19	None	0.1 M Na HEPES	7.5	10 % w/v PEG 8000, 8 % v/v ethylene glycol
20	None	0.1 M MES	6.5	1.6 M magnesium sulfate
21	0.1 M potassium phosphate + 0.1 M sodium phosphate	0.1 M MES	6.5	2.0 M sodium chloride
22	None	0.1 M MES	6.5	12 % w/v PEG 20,000
23	1.6 M ammonium sulfate	0.1 M MES	6.5	10 % v/v Dioxane
24	0.05 M caesium chloride	0.1 M MES	6.5	30 % v/v Jeffamine M-600
25	0.01 M cobalt chloride	0.1 M MES	6.5	1.8 M ammonium sulfate
26	0.2 M ammonium sulfate	0.1 M MES	6.5	30 % w/v PEG 5000 MME
27	0.01 M zinc sulfate	0.1 M MES	6.5	25 % v/v PEG 550 MME
28	None	0.1 M Na HEPES	7.5	20 % w/v PEG 10,000
29	0.2 M potassium sodium tartrate	0.1 M Na citrate	5.6	2.0 M ammonium sulfate
30	0.5 M ammonium sulfate	0.1 M Na citrate	5.6	1.0 M lithium sulfate
31	0.5 M sodium chloride	0.1 M Na citrate	5.6	4 % v/v polyethyleneimine
32	None	0.1 M Na citrate	5.6	35 % v/v tert-butanol
33	0.01 M ferric chloride	0.1 M Na citrate	5.6	10 % v/v Jeffamine M-600
34	0.01 M manganese chloride	0.1 M Na citrate	5.6	2.5 M 1,6-hexanediol
35	None	0.1 M Na acetate	4.6	2.0 M sodium chloride
36	0.2 M sodium chloride	0.1 M Na acetate	4.6	30 % v/v MPD
37	0.01 M cobalt chloride	0.1 M Na acetate	4.6	1.0 M 1,6-hexanediol
38	0.1 M cadmium chloride	0.1 M Na acetate	4.6	30 % v/v PEG 400
39	0.2 M ammonium sulfate	0.1 M Na acetate	4.6	30 % w/v PEG 2000 MME
40	2.0 M sodium chloride	None	None	10 % w/v PEG 6000
41	0.01 M CTAB	None	None	0.5 M sodium chloride, 0.1 M magnesium chloride
42	None	None	None	25 % v/v ethylene glycol
43	None	None	None	35 % v/v dioxane
44	2.0 M ammonium sulfate	None	None	5 % v/v 2-propanol
45	None	None	None	1.0 M imidazole pH 7.0
46	None	None	None	10 % w/v PEG 1000, 10 % w/v PEG 8000
47	1.5 M sodium chloride	None	None	10 % v/v ethanol
48	None	None	None	1.6 M sodium citrate pH 6.5
49	15 % w/v polyvinylpyrrolidone	None	None	None
50	2.0 M urea	None	None	None

Optimization screen 1

The optimization screen 1 was set up using 1 mg/ml, 1.5 mg/ml or 2 mg/ml of c*h*TPH1.

	1 2	3 4	5 6	7 8	9 10	11 12
A	1.4M (NH_4) citrate pH 9.0	2.0M $(NH_4)_2SO_4$ pH 9.0	3.0M Na acetate pH 4.5	K_M 22.5% PEG10.000 0.2M imidazole malate pH 8.5	Structure2 – nr.28 0.1M Na HEPES 20% w/v PEG 10.000 pH 7.5	Structure1 – nr.32 0.1M Tris 2.M $(NH_4)_2SO_4$ pH 8.5
B						
C	1.1M (NH_4) citrate pH 9.0	1.75M $(NH_4)_2SO_4$ pH 9.0	2.75M Na acetate pH 4.5		½*Structure2 – nr. 28 0.05M Na HEPES 10% w/v PEG 10.000 pH 7.5	½*Structure1 – nr. 32 0.05M Tris 1.0M $(NH_4)_2SO_4$ pH 8.5
D						
E	0.8M (NH_4) citrate pH 9.0	1.5M $(NH_4)_2SO_4$ pH 9.0	2.5M Na acetate pH 4.5		Structure2 – nr.14 0.1M NaCl 0.1M Na HEPES 1.6M $(NH_4)_2SO_4$ pH 7.5	Structure1 – nr.15 0.2M Mg acetate 0.1M Na cacodylate 20% w/v PEG 8K pH 6.5
F						
G	0.5M (NH_4) citrate pH 9.0	1.25M $(NH_4)_2SO_4$ pH 9.0	2.25M Na acetate pH 4.5		½*Structure2 – nr. 14 0.05M NaCl 0.05M Na HEPES 0.8M $(NH_4)_2SO_4$ pH 7.5	½*Structure1 – nr. 15 0.1M Mg acetate 0.05M Na cacodylate 10% w/v PEG 8K pH 6.5
H						

Optimization screen 2

The optimization screen 2 was stored at +4^{o}C and at room temperature.

	1	2	3	4	5	6
A	**Solution 1** 1mg/ml, Trp 1.4M (NH_4) citrate pH 9.0	**Solution 2** 2mg/ml, Trp 1.75M $(NH_4)_2SO_4$ pH 9.0	**Solution 3** 1.5mg/ml, Trp+BH2 2M $(NH_4)_2SO_4$ pH 9.0	**Solution 4** 2mg/ml, without ligand K_M 22.5% PEG10.000 0.2M imidazole malate pH 8.5	**Solution 5** 2mg/ml, BH2 K_M 22.5% PEG10.000 0.2M imidazole malate pH 8.5	**Solution 6** 2mg/ml, without ligand Structure2 – nr.28 0.1M Na HEPES 20% w/v PEG 10.000 pH 7.5
B	**Solution 1** 1mg/ml, Trp 1.4M (NH_4) citrate pH 9.0	**Solution 2** 2mg/ml, Trp 1.75M $(NH_4)_2SO_4$ pH 9.0	**Solution 3** 1.5mg/ml, Trp+BH2 2M $(NH_4)_2SO_4$ pH 9.0	**Solution 4** 2mg/ml, without ligand K_M 22.5% PEG10.000 0.2M imidazole malate pH 8.5	**Solution 5** 2mg/ml, BH2 K_M 22.5% PEG10.000 0.2M imidazole malate pH 8.5	**Solution 6** 2mg/ml, without ligand Structure2 – nr.28 0.1M Na HEPES 20% w/v PEG 10.000 pH 7.5
C	**Solution 1** 1mg/ml, Trp 1.4M (NH_4) citrate pH 9.0	**Solution 2** 2mg/ml, Trp 1.75M $(NH_4)_2SO_4$ pH 9.0	**Solution 3** 1.5mg/ml, Trp+BH2 2M $(NH_4)_2SO_4$ pH 9.0	**Solution 4** 2mg/ml, without ligand K_M 22.5% PEG10.000 0.2M imidazole malate pH 8.5	**Solution 5** 2mg/ml, BH2 K_M 22.5% PEG10.000 0.2M imidazole malate pH 8.5	**Solution 6** 2mg/ml, without ligand Structure2 – nr.28 0.1M Na HEPES 20% w/v PEG 10.000 pH 7.5
D	**Solution 7** 2mg/ml, BH_2 Structure2 – nr.28 0.1M Na HEPES 20% w/v PEG 10.000 pH 7.5	**Solution 7** 2mg/ml, BH_2 Structure2 – nr.28 0.1M Na HEPES 20% w/v PEG 10.000 pH 7.5	**Solution 7** 2mg/ml, BH_2 Structure2 – nr.28 0.1M Na HEPES 20% w/v PEG 10.000 pH 7.5			

Optimization screen 3

	1 1 mg/ml, Trp	2 2 mg/ml, Trp	3 2 mg/ml, Trp+BH2
A	1.4M Ammonium citrate pH 9.5	1.75M Ammonium sulfate pH 9.5	2M Ammonium sulfate pH 9.5
B	1.4M Ammonium citrate pH 9.0	1.75M Ammonium sulfate pH 9.0	2M Ammonium sulfate pH 9.0
C	1.4M Ammonium citrate pH 8.5	1.75M Ammonium sulfate pH 8.5	2M Ammonium sulfate pH 8.5
D	1.4M Ammonium citrate pH 8.0	1.75M Ammonium sulfate pH 8.0	2M Ammonium sulfate pH 8.0

Cryo-buffer solutions

	Conditions	**Cryo-buffer solution**
1	1 mg/ml, tryptophan 1.4 M (NH_4) citrate pH 9.0	1 mg/ml, tryptophan 1.4 M (NH_4) citrate pH 9.0
2	2 mg/ml, tryptophan 1.75 M $(NH_4)_2SO_4$ pH 9.0	2 mg/ml, tryptophan 1.75M $(NH_4)_2SO_4$ pH 9.0
3	1.5 mg/ml, tryptophan +BH2 2 M $(NH_4)_2SO_4$ pH 9.0	1.5 mg/ml, tryptophan +BH2 2 M $(NH_4)_2SO_4$ pH 9.0
4	2 mg/ml, without ligand 22.5 % PEG10.000, 0.2 M imidazole malate pH 8.5	2 mg/ml, without ligand 22.5 % PEG10.000, 0.2 M imidazole malate pH 8.5
5	2mg/ml, BH2 22.5 % PEG10.000, 0.2M imidazole malate pH 8.5	2emg/ml, BH2 22.5 % PEG10.000, 0.2M imidazole malate pH 8.5
6	2 mg/ml, without ligand 0.1 M Na HEPES, 20 % w/v PEG10.000 pH 7.5	2 mg/ml, without ligand 0.1 M Na HEPES, 20 % w/v PEG10.000 pH 7.5
7	2 mg/ml, BH_2 0.1 M Na HEPES, 20 % w/v PEG10.000 pH 7.5	2 mg/ml, BH_2 0.1 M Na HEPES, 20 % w/v PEG10.000 pH 7.5